

# **Electrochemical and Thermodynamic Investigations on Th<sup>4+</sup> and Cd-Th Alloys in LiCl-KCl Eutectic Melt**

*By*

**Gurudas Pakhui**

**Enrolment No: CHEM02201304006**

**Indira Gandhi Centre for Atomic Research, Kalpakkam**

*A thesis submitted to the  
Board of Studies in Chemical Sciences*

*In partial fulfillment of requirements*

*for the Degree of*

**DOCTOR OF PHILOSOPHY**

*of*

**HOMI BHABHA NATIONAL INSTITUTE**



**July, 2019**

**Homi Bhabha National Institute**  
**Recommendations of the Viva Voce Committee**

As members of the Viva Voce Committee, we certify that we have read the dissertation prepared by Mr. Gurudas Pakhui entitled "Electrochemical and Thermodynamic Investigations on Th<sup>4+</sup> and Cd-Th alloys in LiCl-KCl Eutectic Melt" and recommend that it may be accepted as fulfilling the thesis requirement for the award of Degree of Doctor of Philosophy.

Chairman - Dr. S. Rangarajan



Date: 04.12.2019

Guide / Convener - Dr. B. Prabhakara Reddy



Date: 04.12.2019

Examiner – Prof. Arindam Sarkar



Date: 4<sup>th</sup> Dec. 2019

Member 1 - Dr. V. Jayaraman



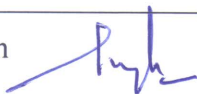
Date: 04.12.2019

Member 2 - Dr. Rajesh Ganesan



Date: 04/12/19

Member 3 – Dr. S. Ningshen



Date: 04/12/2019

Final approval and acceptance of this thesis is contingent upon the candidate's submission of the final copies of the thesis to HBNI.

I/We hereby certify that I/we have read this thesis prepared under my/our direction and recommend that it may be accepted as fulfilling the thesis requirement.

Date: 04.12.2019

Place: Kalpakam



**Dr. B. Prabhakara Reddy**  
(Guide)

## **STATEMENT BY AUTHOR**

This dissertation has been submitted in partial fulfillment of requirements for an advanced degree at Homi Bhabha National Institute (HBNI) and is deposited in the Library to be made available to borrowers under rules of the HBNI.

Brief quotations from this dissertation are allowable without special permission, provided that accurate acknowledgement of source is made. Requests for permission for extended quotation from or reproduction of this manuscript in whole or in part may be granted by the Competent Authority of HBNI when in his or her judgment the proposed use of the material is in the interests of scholarship. In all other instances, however, permission must be obtained from the author.

Gurudas Pakhui

## **DECLARATION**

I, hereby declare that the investigation presented in the thesis has been carried out by me. The work is original and has not been submitted earlier as a whole or in part for a degree / diploma at this or any other Institution / University.

Gurudas Pakhui

## List of Publications arising from the thesis

### Journal

#### a. Published

1. “Electrochemical studies on the reduction behaviour of  $\text{Th}^{4+}$  in molten LiCl-KCl eutectic”, **Gurudas Pakhui**, Manish Chandra, Suddhasattwa Ghosh, B. Prabhakara Reddy, K. Nagarajan, *Electrochim. Acta.* **2015**, 155, 372-382.
2. “Exchange current density of thorium in molten LiCl-KCl eutectic”, **Gurudas Pakhui**, Suddhasattwa Ghosh, B. Prabhakara Reddy, *Electrochim. Acta.* **2016**, 222, 92-99.
3. “ $\text{Th}^{4+}|\text{Th}$  couple in LiCl-KCl eutectic: Anodic polarization of thorium and electrochemical impedance spectroscopy study at tungsten, cadmium and thorium electrodes”, **Gurudas Pakhui**, Suddhasattwa Ghosh, B. Prabhakara Reddy, *Electrochim. Acta.* **2019**, 295, 354-366.

#### b. Communicated

1. “A thermochemical evaluation of standard electrode potential, Gibbs energy of formation and activity coefficient of  $\text{Th}^{4+}$  in LiCl-KCl eutectic melt”, **Gurudas Pakhui**, Suddhasattwa Ghosh, B. Prabhakara Reddy, under review in the journal *Electrochimica Acta*.

#### c. Manuscript under preparation

1. Electromotive force measurements on Cd-Th intermetallic compounds in LiCl-KCl eutectic melt.

### Conferences

1. “Electrochemistry of  $\text{Th}^{4+}|\text{Th}$  couple in molten LiCl-KCl eutectic”, **Gurudas Pakhui**, Suddhasattwa Ghosh, B. Prabhakara Reddy, Theme meeting on Chemistry in Nuclear Technology (CHEMNUT), July 30-31, 2015, 32, IGCAR, Kalpakkam, India.
2. “Electrochemical and thermodynamic properties of Th and Th-Cd alloys using transient electrochemical techniques”, **Gurudas Pakhui**, Suddhasattwa Ghosh, B. Prabhakara Reddy, Symposium on thermal analysis (THERMANS), January 18-20, 2016, T040, IIT BHU, Varanasi, India.
3. “Redox behavior of  $\text{Th}^{4+}|\text{Th}$  couple at tungsten and cadmium electrodes in LiCl-KCl eutectic”, **Gurudas Pakhui**, Suddhasattwa Ghosh, B. Prabhakara Reddy, Symposium on Nuclear and Radiochemistry (NUCAR), February 6-10, 2017, C-146, KIIT University, Bhubaneswar, India.
4. “Determination of partial excess Gibbs energy of  $\text{ThCl}_4$  in LiCl-KCl eutectic using electromotive force measurements”, **Gurudas Pakhui**, Suddhasattwa Ghosh, B.

Prabhakara Reddy, International Conference on Electrochemical Science & Technology (ICONEST), August 10-12, 2017, PP-EC-23, IISc Bengaluru, India.

5. “Molten salt electromotive force measurements on Th-Cd alloys”, **Gurudas Pakhui**, Suddhasattwa Ghosh, B. Prabhakara Reddy, Symposium on Nuclear and Radiochemistry (NUCAR), January 15-19, 2019, C-27, BARC, Mumbai, India.

Gurudas Pakhui

**DEDICATED TO MY PARENTS**

## ACKNOWLEDGEMENTS

It is a genuine pleasure to convey my deep sense of thanks and gratitude to all of those, whose support and encouragement assisted me in preparing this Ph.D. thesis. My humble acknowledgement is as follows:

I express my sincere thanks and gratitude to my research guide Dr. B. Prabhakara Reddy, Associate Director, Metal Fuel Recycle Group, Materials Chemistry and Metal Fuel Cycle Group, IGCAR for his invaluable guidance, inspiration and support throughout this project.

I am extremely grateful to Dr. Suddhasattwa Ghosh, Head, Pyro-chemical Process Studies Section, whose persistent guidance and indispensable technical support assisted me in the completion of my Ph.D. work. I am thankful to him for his critical corrections that make this thesis worth reading. I am grateful to Dr. K. Nagarajan, my former guide and formerly Director, Chemistry Group, IGCAR for his continuous support, encouragement and value addition to my thesis.

I express my sincere thanks to Dr. S. Rangarajan, Head, WSCD, BARCF and chairman of the doctoral committee for giving me valuable ideas and suggestions during the course of my research. I also express my sincere thanks to the members of doctoral committee Dr. V. Jayaraman (Head, MCD), Dr. Rajesh Ganesan (Head, LMCS, MCD) and Dr. S. Ningshen (Head, ACPS, CSTD) for their insightful suggestions for the progress of the research work at various DC meetings. I am grateful to Dr. Manish Chandra for his support and encouragement during the course of my research work.

I express my sincere thanks to my colleagues Mr. S. Nedumaran, Smt. Suriya Kumari K, Mrs. Nibedita Samanta and Ms. Litun Swain, SRF for their timely help in the laboratory works and useful discussions. I thank Dr. K. C. Pitchaiah and Mr. Ujjwal Kumar Maity for the analytical support. I thank Dr. Raja Madhavan, Dr. Binoy Kumar Maji and Mr. Shyam Kumar for characterization of the samples by XRD analysis.

I express my sincere gratitude to my parents and my wife Riya Maji for their constant support and encouragement.

Gurudas Pakhui

# CONTENTS

Sl. No.	Title	Page No.
<b>SYNOPSIS</b>		xiii
<b>NOMENCLATURE</b>		xxvii
<b>LIST OF FIGURES</b>		xxx
<b>LIST OF TABLES</b>		xxxviii
<b>CHAPTER 1 Introduction</b>		1
1.1	Objective of present thesis	1
1.2	Electrochemical and thermodynamic studies on thorium in molten salts: Literature survey	2
1.3	Thermodynamic studies on Cd-Th alloys: Literature survey	6
1.4	Scope of present thesis	8
<b>CHAPTER 2 Experimental</b>		10
2.1	Argon atmosphere glove box set-up	10
2.2	Chemicals and preparation of electrolytes	13
2.2.1	Chemicals	13
2.2.2	Preparation and purification of LiCl-KCl eutectic melt	13
2.2.3	Preparation of LiCl-KCl-ThCl <sub>4</sub> electrolyte	15
2.2.4	Preparation of LiCl-KCl-AgCl electrolyte	16
2.2.5	Estimation of Th, Cd and Ag in LiCl-KCl eutectic melt	16
2.3	Cd-Th alloys	17
2.3.1	Preparation of Cd-Th alloys	17
2.3.2	Phase characterization of Cd-Th alloys	19
2.4	Electrodes and cell assembly	20

2.4.1	Electrodes for transient electrochemical measurements	20
2.4.2	Electrodes for electromotive force measurements	21
2.5	Measurement methodology	23
2.5.1	Transient techniques and EIS study	23
2.5.2	Polarization technique	25
2.5.3	Electrochemical impedance spectroscopy	27
2.5.4	Electromotive force measurements	29
2.5.4.1	emf measurement of ThCl <sub>4</sub> in LiCl-KCl eutectic melt	29
2.5.4.2	emf measurement of Cd-Th alloys	32
<b>CHAPTER 3 Redox behaviour of Th<sup>4+</sup> in LiCl-KCl eutectic melt using transient methods</b>		<b>35</b>
3.1	Cyclic voltammetry (CV) at inert tungsten electrode	35
3.2	Chronopotentiometry (CP) at inert tungsten electrode	42
3.3	Square wave voltammetry (SWV) at inert tungsten electrode	45
3.4	Semi-integral voltammetry (SIV)	47
3.5	Estimation of diffusion coefficient of Th <sup>4+</sup>	51
3.6	Estimation of $E_{\text{Th}^{4+} \text{Th}}^{\circ*}$ from CP and SIV	55
3.7	Anodic dissolution of Th electrode: Estimation of theoretical equilibrium potential of Th <sup>4+</sup>  Th couple	58
3.8	Cyclic voltammetry of Th <sup>4+</sup> at liquid cadmium electrode: Underpotential deposition of Th	64
3.9	Influence of CdCl <sub>2</sub> on redox behaviour of Th <sup>4+</sup> and investigation of disproportionation of Th <sup>4+</sup>	65
3.10	Corrosion study of alumina crucible during electrochemical measurement	67

3.11	Conclusions	71
<hr/>		
<b>CHAPTER 4</b>	<b>Exchange current density of Th<sup>4+</sup> Th couple in LiCl-KCl eutectic melt</b>	73
4.1	Estimation of $i_o$ at inert tungsten electrode	73
4.1.1	Estimation of $i_o$ from polarization curves	73
4.1.2	Estimation of $i_o$ at inert tungsten electrode by cyclic voltammetry	76
4.1.3	Dependence of $i_o$ on $C_{\text{ThCl}_4}$ at inert tungsten electrode	78
4.2	Estimation of $i_o$ at liquid cadmium cathode	79
4.3	Estimation of $i_o$ for anodic polarization of Th electrode	80
4.4	Temperature dependence of $i_o$	81
4.5	Conclusions	83
<hr/>		
<b>CHAPTER 5</b>	<b>Anodic dissolution of Th and cathodic deposition of Th<sup>4+</sup> at inert tungsten and cadmium electrodes by electrochemical impedance spectroscopy</b>	85
5.1	Cathodic: at inert tungsten electrode	85
5.2	Cathodic: at liquid cadmium electrode	91
5.3	Anodic dissolution of Th electrode	96
5.4	Validation of complex impedance data by Kramers-Kronig transforms	103
5.5	Reversibility of Th <sup>4+</sup>  Th couple	111
5.6	Conclusions	113
<hr/>		
<b>CHAPTER 6</b>	<b>Thermochemical evaluation of <math>E_{\text{Th}^{4+} \text{Th}}^\circ</math> and <math>\Delta_f G_{\text{ThCl}_4}^\circ</math> in LiCl-KCl eutectic melt</b>	115
6.1	Analysis of electromotive force data	117
6.2	Data analysis and recommendations	121
<hr/>		

6.3	Estimation of $\gamma_{\text{ThCl}_4}^{liq.}$	124
6.4	Conclusions	128
<b>CHAPTER 7 Electromotive force measurements on Cd-Th intermetallic compounds in LiCl-KCl eutectic melt</b>		130
7.1	Electromotive force measurements of Cd-Th intermetallics	130
7.2	Estimation of $\Delta_f G_{\text{Cd}_m\text{Th}_n}^\circ$ of Cd-Th intermetallics	132
7.3	Comparison of $\Delta_f H_{\text{Th}_m\text{Cd}_n}^\circ$ data with estimation using Miedema's model	135
7.4	Conclusions	136
<b>CHAPTER 8 Conclusions and future outlook</b>		138
8.1	Conclusions	138
8.2	Challenges during experimentation	139
8.3	Impact of present work	141
8.4	Future outlook	142
	<b>List of errata in journal publications</b>	143
	<b>References</b>	144



# Homi Bhabha National Institute

## SYNOPSIS OF Ph.D. THESIS

- 1. Name of the Student:** Gurudas Pakhui
- 2. Name of the Constituent Institution:** HBNI, IGCAR Campus
- 3. Enrolment No.:** CHEM02201304006
- 4. Title of the Thesis:** Electrochemical and Thermodynamic Investigations on  $\text{Th}^{4+}$  and Cd-Th Alloys in LiCl-KCl Eutectic Melt
- 5. Board of Studies:** Chemical Sciences

### SYNOPSIS

High temperature molten salts have found applications in several industrial processes such as Down's process for production of sodium, Hall-Heroult process for production of aluminium, and also in nuclear industry for the reprocessing of nuclear fuels, most notably the RIAR's (Russian Institute of Atomic Reactors, Dimitrovgrad) process for spent uranium-plutonium oxide fuels and IFR (Integral Fast Reactor) process of ANL (Argonne National Laboratory) for spent metal fuels. In all the above industrial processes, apart from purity of the melt, electrochemical properties of ions of interest are of paramount significance. In the field of nuclear fuel reprocessing, electrochemistry of actinides in various melts is an active area of research where efforts have been put by several groups, sometimes in collaboration with each other over the last five decades to investigate the redox behavior of electroactive species in molten salts thus creating an electrochemical database of estimated properties in a particular melt. In a similar manner, electrochemical series of LiCl-KCl eutectic melt was also

developed covering actinides, lanthanides, transition elements *etc.* These properties include stability of various oxidation states, electron transfer reactions, standard electrode potential, diffusion coefficient *etc.* In the context of pyroprocessing of spent metal fuels, redox behavior of uranium and plutonium in LiCl-KCl eutectic melt is well known although there are few research groups currently involved in further understanding electrode kinetic aspects of uranium and plutonium behavior at different electrodes under different experimental conditions. Electrochemistry of thorium in LiCl-KCl eutectic melt has also been studied in detail in the last four decades mostly in fluoride melts in the context of molten salt reactors and as well in chloride and chloride-fluoride melts for investigating the presence of multiple oxidation states of thorium. There are reports available in the literature that clearly states that both  $\text{Th}^{4+}$  and  $\text{Th}^{2+}$  exist in chloride melts. The reduction of  $\text{Th}^{4+}$  should be therefore a two-step process,  $\text{Th}^{4+}$  to  $\text{Th}^{2+}$  and  $\text{Th}^{2+}$  to metallic Th. Although this was observed in binary chloride melts at high temperature, it was in this perspective that the current study was taken up in LiCl-KCl eutectic melt. Based on literature survey, it was soon realized that exhaustive experimental work on  $\text{Th}^{4+}$  was required to completely understand its reduction behavior in the eutectic melt. The present work, tries to meet this objective by focusing on electrochemical investigations on reduction behavior of  $\text{Th}^{4+}$  in LiCl-KCl eutectic melt at various working electrodes and thermodynamic investigations by electromotive force measurements for determination of Gibbs energy of formation of Cd-Th intermetallics.

## **Chapter 1: Introduction**

Chapter 1 describes the importance of electrochemistry of thorium species in high temperature melts carried out in the past as part of development of molten salt reactors with thorium fuel cycle employing fluoride based melts. Motivation and objectives of electrochemical and thermodynamic measurements on thorium in LiCl-KCl eutectic melt have been highlighted. One of the primary aims of present work was to elucidate the

mechanism of anodic dissolution of Th and cathodic deposition of  $\text{Th}^{4+}$  in LiCl-KCl eutectic melt at various working electrodes (inert tungsten, cadmium and thorium) using transient techniques and AC impedance methods. In order to achieve this objective, an exhaustive literature survey on electrochemical studies carried out in various alkali halide melts such as NaCl, KCl, CsCl, LiCl-KCl, NaCl-KCl, LiF-NaF-KF, LiF-CaF<sub>2</sub> *etc.* is described. This is followed by literature survey on Cd-Th binary system and its similarity with Cd-U and Cd-Pu has been highlighted. Phase diagram data and characterization of Cd-Th alloys, solubility data of Th in Cd and crystallographic data of different Cd-Th intermetallics are described. Based on literature data, scope of present work is discussed emphasizing on experimental work necessary to address the limitations in literature data and fill the gap areas on electrochemistry of  $\text{Th}^{4+}$  in LiCl-KCl eutectic melt and thermodynamics of Cd-Th alloys.

## **Chapter 2: Experimental**

This chapter gives a brief overview of all experimental facilities, equipments, chemicals, electrochemical cell assembly etc. used in the present work. An argon atmosphere glove box pressure controlled between +20 to +40 mm of water column (positive *wrt* ambient) is first described that was used for storage of hygroscopic LiCl-KCl eutectic mixture post chlorination step for purification of melt [1]. The glove box was also used for the preparation of LiCl-KCl-ThCl<sub>4</sub> electrolyte and loading of electrodes in electrochemical cells. The electrolyte was prepared by equilibrating Th chips with CdCl<sub>2</sub> in chlorinated LiCl-KCl eutectic melt, and the procedure is described in detail. Preparation of LiCl-KCl-AgCl electrolyte used in Ag<sup>+</sup>|Ag reference electrode is also described in detail. Analytical methods for estimating Th and Ag in electrolytes are also discussed. Subsequently, preparation and characterization of Cd-Th alloys are described. Design, fabrication and preparation of electrodes for transient measurements and electromotive force measurements are then discussed. Measurement principles and methodology adopted for transient techniques,

polarization methods, electrochemical impedance spectroscopy and electromotive force measurements for estimating  $\gamma_{\text{ThCl}_4}$  and Gibbs energy of formation of Cd-Th alloys are described.

### **Chapter 3: Redox behavior of Th<sup>4+</sup> in LiCl-KCl eutectic melt using transient methods**

Chapter 3 describes in detail the reduction of Th<sup>4+</sup> in LiCl-KCl eutectic at inert tungsten electrode investigated using cyclic voltammetry, chronopotentiometry, square wave voltammetry and semi-integral voltammetry studies. This is followed up by general sections on the estimation of diffusion coefficient and  $E_{\text{Th}^{4+}|\text{Th}}^{*o}$ . The existence of multiple oxidation states of thorium is also addressed in this chapter. Temperature dependence of diffusion coefficient using cyclic voltammetry and chronopotentiometry were respectively given by

$$\ln D = -3.63 - \frac{5659}{T} \quad [1]$$

$$\ln D = -3.20 - \frac{5665}{T} \quad [2]$$

Temperature dependence of  $E_{\text{Th}^{4+}|\text{Th}}^{*o}$  (by chronopotentiometry) was expressed as

$$E_{\text{Th}^{4+}|\text{Th}}^{*o} \text{ vs. } \text{Cl}_2/\text{Cl}^- (\text{V}) = -3.289 + 1.2 \times 10^{-3} T (\text{K}) \quad [3]$$

The chapter further discusses anodic dissolution of thorium electrode investigated by cyclic voltammetry and estimation of theoretical equilibrium potential of Th<sup>4+</sup>|Th couple. Finally, underpotential deposition of thorium at liquid cadmium electrode is described. Formation of intermetallics of Cd-Th is explained on the basis of features observed in cyclic voltammograms.

### **Chapter 4: Exchange current density of Th<sup>4+</sup>|Th couple in LiCl-KCl eutectic melt**

This chapter deals with the estimation of exchange current density  $i_0$  of thorium at inert tungsten, liq. cadmium and Th working electrodes in LiCl-KCl eutectic melt in the temperature range of 698-798 K. Polarization experiments were carried out using DC

amperometry technique, where current was sampled at each applied cathodic potential and were subsequently plotted logarithm of current density *versus* overpotential, and further analyzing them using Tafel and Allen-Hickling methods  $i_0$  was estimated [4]. In all cases, a good agreement in  $i_0$  from both the plot analysis methods was observed with fairly strong temperature dependence. At inert tungsten electrode,  $i_0$  was found to be in the range 19-50 mA cm<sup>-2</sup> in the temperature range 698-798 K, whereas it varied from 11-16 mA cm<sup>-2</sup> at cadmium electrode in the temperature range 723-773 K. For anodic dissolution of thorium,  $i_0$  varied from 24-34 mA cm<sup>-2</sup> in the temperature range 698-798 K. From the cyclic voltammetry data discussed in Chapter 3,  $i_0$  of Th<sup>4+</sup>|Th couple was estimated and compared with that obtained from polarization methods. Concentration ( $x_{\text{ThCl}_4}$ ) dependence of  $i_0$  was also addressed, and it was found that although  $i_0$  linearly increased with  $\ln x_{\text{ThCl}_4}$  at any given temperature, the variation could not be extrapolated beyond the concentration range studied. Temperature dependence of  $i_0$  for cathodic and anodic cases is given by the following expressions:

$$\text{Cathodic: } \ln i_0 = (1.50 \pm 0.67) - \frac{3821 \pm 502}{T} \quad [4]$$

$$\text{Anodic: } \ln i_0 = -(0.82 \pm 0.13) - \frac{2066 \pm 118}{T} \quad [5]$$

### **Chapter 5: Anodic dissolution of Th and cathodic deposition of Th<sup>4+</sup> at inert tungsten and cadmium electrodes by electrochemical impedance spectroscopy**

Chapter 5 describes electrochemical impedance spectroscopic investigations on Th<sup>4+</sup>|Th couple in LiCl-KCl eutectic melt at inert tungsten, liquid cadmium and Th electrodes. Complex impedance spectra at these electrodes were recorded at different applied potentials in the frequency range 10-5000 Hz using an AC perturbation amplitude of 10 mV and

temperature range 698-798 K. The complex impedance data were validated by Kramers-Kronig transforms [5-7]. These were subsequently fitted to equivalent circuit consisting of melt resistance, charge transfer resistance and constant phase element for modelling Warburg impedance and double layer capacitance effects. The complex impedance plots recorded at inert tungsten electrode were characterized by a flattened semi-circle at higher frequencies and a linear region at lower frequencies at lower cathodic applied potentials. The flattened semicircle suggested a very fast charge transfer process whereas the linear part was related to the mass transfer of  $\text{Th}^{4+}$  ions or Warburg impedance. Impedance spectra recorded at lower cathodic potentials (-0.9, -1.0 V) had a higher span of linear region that indicated the process was controlled by mass transfer at these potentials. Impedance spectra recorded at applied potentials -1.1 to -1.2 V had a more prominent semicircle indicating the process was mainly kinetically controlled. Charge transfer resistance at different applied potential was estimated from equivalent circuit fitting of complex impedance data. It was observed that variation of  $R_{ct}$  versus applied potential had a single minimum for inert tungsten electrode but two minima for cadmium electrode. Each minimum point corresponded to a redox couple, and in case of inert tungsten electrode, it was attributed to reduction of  $\text{Th}^{4+}$  to Th, whereas in case of cadmium electrode, it was due to the formation of  $\text{Cd}_{11}\text{Th}$  and  $\text{Cd}_5\text{Th}$  intermetallics due to underpotential deposition of Th. Complex impedance plots of anodic polarization of thorium electrode were characterized by a very prominent semicircle at higher frequencies and a comparatively smaller linear region at lower frequencies. The charge transfer process at higher frequencies was associated with a large capacitive contribution due to continuous accumulation of  $\text{Th}^{4+}$  ions near the electrode|melt interface. Mechanism of anodic dissolution of thorium was elucidated based on impedance characteristics due to Warburg diffusion and double layer capacitance. Heterogeneous rate constant ( $k_s$ ) of  $\text{Th}^{4+}|\text{Th}$  couple was calculated from  $R_{ct}$  at inert tungsten, liq. Cd and thorium working electrodes. Temperature dependence

of  $k_s$  for cathodic (inert tungsten) and anodic polarization (thorium electrode) cases are given by the following relationships:

$$\text{Cathodic: } \ln k_s = (2.491 \pm 1.181) - \frac{(6.27 \pm 0.88) \times 10^3}{T} \quad [6]$$

$$\text{Anodic: } \ln k_s = (3.939 \pm 0.992) - \frac{(6.53 \pm 0.74) \times 10^3}{T} \quad [7]$$

From which activation energy of charge transfer process was subsequently calculated. Finally, the reversibility of  $\text{Th}^{4+}|\text{Th}$  couple was addressed by Matsuda-Ayabe criterion [8].

### Chapter 6: Thermochemical evaluation of $E_{\text{Th}^{4+}|\text{Th}}^\circ$ and $\Delta_f G_{\text{ThCl}_4}^\circ$ in LiCl-KCl eutectic melt

Chapter 6 describes molten salt emf measurements on  $\text{Th}^{4+}$  in LiCl-KCl eutectic melt for estimating Gibbs energy of formation of  $\text{ThCl}_4$ . Primary aim of this chapter was to carry out a thermochemical evaluation of  $E_{\text{Th}^{4+}|\text{Th}}^\circ$  and  $\Delta_f G_{\text{ThCl}_4}^\circ$  using statistical data fitting. In this context, emf measurements were carried out in the temperature range 673-798 K at different compositions of  $\text{ThCl}_4$  in the eutectic melt using the following cell configuration:



for measuring equilibrium potential  $E_{\text{Th}^{4+}|\text{Th}}^{eq}$  between  $\text{Th}^{4+}|\text{Th}$  couple and  $\text{Ag}^+|\text{Ag}$  reference electrode at various  $x_{\text{ThCl}_4}$  in LiCl-KCl eutectic melt. Electromotive force data were subsequently analyzed by the method of Roy *et al.* [9] and Lantelme *et al.* [10] for estimating  $E_{\text{Th}^{4+}|\text{Th}}^\circ$ . It was then compared with those estimated from cyclic voltammetry and chronopotentiometry measurements (discussed in Chapter 3) and data taken from literature after critical review. From linear least squares fitting, standard expressions of temperature dependence of  $E_{\text{Th}^{4+}|\text{Th}}^\circ$  and  $\Delta_f G_{\text{ThCl}_4}^\circ$  arrived at and are given by

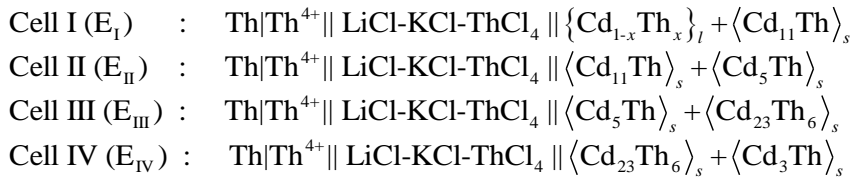
$$E_{\text{Th}^{4+}|\text{Th}}^\circ / \text{V vs. Cl}^-|\text{Cl}_2 = -(3.059 \pm 0.213) + (6.076 \pm 2.875) \times 10^{-4} T \quad [8]$$

$$\Delta_f G_{\text{ThCl}_4}^\circ (\text{kJ/mol}) = -(1180.44 \pm 23.62) + (0.234 \pm 0.033)T \quad [9]$$

Finally,  $\gamma_{\text{ThCl}_4}$  was estimated from  $\Delta_f G_{\text{ThCl}_4, \text{liq.}}^\circ$  as reference state obtained from various thermochemical data compilations [11-15]. Few conclusions were drawn on the choice of reference state data and its influence on the range of  $\gamma_{\text{ThCl}_4}$

### Chapter 7: Electromotive force measurements on Cd-Th alloys in LiCl-KCl eutectic melt

Chapter 7 discusses about emf measurements for on Cd-Th binary system. This work was taken primarily because it was seen from literature survey that no thermodynamic data were available on Cd-Th intermetallics. Electromotive force method of estimating  $\Delta_f G^\circ$  was chosen as it was a superior method than open-circuit chronopotentiometry technique. Following galvanic cells were constructed for determining  $\Delta_f G^\circ$  of Cd-Th intermetallics that comprises of  $\text{Th}^{4+}|\text{Th}$  as ref. electrode and Cd-Th biphasic alloy as the other electrode:



emf of the above cell configurations represented by  $E_I$ ,  $E_{II}$ ,  $E_{III}$  and  $E_{IV}$  was measured in the temperature range 673-800 K. From the derived relationships among  $E_I$ ,  $E_{II}$ ,  $E_{III}$  and  $E_{IV}$ ,  $\Delta_f G_{\text{Cd}_{11}\text{Th}}^\circ$ ,  $\Delta_f G_{\text{Cd}_5\text{Th}}^\circ$ ,  $\Delta_f G_{\text{Cd}_{23}\text{Th}_6}^\circ$  and  $\Delta_f G_{\text{Cd}_3\text{Th}}^\circ$  were determined. The temperature dependence of these quantities were established and are given by

$$\Delta_f G_{\text{Cd}_{11}\text{Th}}^\circ (\text{J. mol-atom}^{-1}) = -(13885.35 \pm 269.87) + (9.44 \pm 0.37)T \quad [10]$$

$$\Delta_f G_{\text{Cd}_5\text{Th}}^\circ (\text{J. mol-atom}^{-1}) = -(32638.69 \pm 145.98) + (25.94 \pm 0.19)T \quad [11]$$

$$\Delta_f G_{\text{Cd}_{23}\text{Th}_6}^\circ (\text{J. mol-atom}^{-1}) = -(41219.89 \pm 68.27) + (33.83 \pm 0.09)T \quad [12]$$

$$\Delta_f G_{\text{Cd}_3\text{Th}}^\circ (\text{J. mol-atom}^{-1}) = -(44636.91 \pm 44.92) + (34.87 \pm 0.06)T \quad [13]$$

From the fitted expressions,  $\Delta_f H^\circ$  of each intermetallic was derived and compared with that calculated using Miedema model; the agreement between them was found to be reasonable [16].  $\Delta_f G^\circ$  of Cd-Th intermetallics were also compared with that of Fe-Th, Ni-Th and Co-Th intermetallics as the nature of those phases and crystal structures were similar [17-19]. Phase stability of Cd-Th intermetallics was finally explained on the basis of emf measurements.

## Chapter 8: Conclusions and Future Outlook

This chapter briefly discusses the major highlights of the present work, and difficulties faced during experimental works. Possibility of employing electrochemical data of  $\text{Th}^{4+}$  and Cd-Th in the separation of uranium from thorium matrix at either inert tungsten or cadmium electrode is described. Difficulties faced during electromotive force measurements on Th-rich Cd-Th alloys are explained. Finally, the chapter focuses on future work that can be taken up to further understand the thermodynamics of LiCl-KCl-ThCl<sub>4</sub> system, and influence of various electroactive impurities on the reduction behavior of  $\text{Th}^{4+}$ .

## Nomenclature

$E_{\text{Th}^{4+}|\text{Th}}^{\text{app}}$  : Apparent standard electrode potential of  $\text{Th}^{4+}|\text{Th}$  couple in LiCl-KCl eutectic melt

$D$ : Diffusion coefficient

$i_0$  : Exchange current density

$x_{\text{ThCl}_4}$  : Mole fraction of  $\text{ThCl}_4$  in LiCl-KCl eutectic melt

$R_{ct}$  : Charge transfer resistance

$k_s$  : Heterogeneous rate constant

$E_{\text{Th}^{4+}|\text{Th}}^{\text{eq}}$  : Equilibrium potential of  $\text{Th}^{4+}|\text{Th}$  couple (*versus*  $\text{Ag}^+|\text{Ag}$ )

$E_{\text{Th}^{4+}|\text{Th}}^\circ$  : Standard electrode potential of  $\text{Th}^{4+}|\text{Th}$  couple in LiCl-KCl eutectic melt

$\Delta_f G_{\text{ThCl}_4}^\circ$  : Standard Gibbs energy of formation of  $\text{ThCl}_4$  in LiCl-KCl eutectic melt

$\Delta_f G_{\text{ThCl}_4, \text{liq.}}^\circ$  : Gibbs energy of formation of pure ThCl<sub>4</sub> in supercooled liquid state

$\gamma_{\text{ThCl}_4}$  : Activity coefficient of ThCl<sub>4</sub>

## References

- [1] D.L. Maricle, D.N. Hume, "A new method for preparing hydroxide-free alkali chloride melts", *J. Electrochem. Soc.*, **107** (1960) 354-356.
- [2] L. Martinot, "Electrochemical behaviour of tetravalent thorium in molten (Li-K)Cl eutectic", *J. Radioanal. Nucl. Chem. Lett.*, **103** (1986) 357-363.
- [3] L. Cassayre, J. Serp, P. Soucek, R. Malmbeck, J. Rebizant, J.P. Glatz, "Electrochemistry of thorium in LiCl-KCl eutectic melts", *Electrochim. Acta.*, **52** (2007) 7432-7437.
- [4] A.J. Bard, L.R. Faulkner, "Electrochemical Methods-Fundamentals and Applications", John Wiley and Sons, 1980.
- [5] B.A. Boukamp, "Kramers-Kronig test for Windows", accessed: April, <https://www.utwente.nl/en/tnw/ims/publications/downloads/>, 2018.
- [6] B. Boukamp, "A linear Kronig-Kramers transform test for immittance data validation" *J. Electrochem. Soc.*, **142** (1995) 1885-1894.
- [7] B.A. Boukamp, "Electrochemical impedance spectroscopy in solid state ionics: recent advances", *Solid State Ionics*, **169** (2004) 65-73.
- [8] H. Matsuda, Y. Ayabe, "Zur Theorie der Randles -Sevcikschen Kathodenstrahl-Polarographie", *Z. Elektrochem.*, **59** (1955) 494-503.
- [9] J.J. Roy, L.F. Grantham, D.L. Grimmett, S.P. Fusselman, C.L. Krueger, T.S. Storvick, "Thermodynamic Properties of U, Np, Pu, and Am in Molten LiCl-KCl Eutectic and Liquid Cadmium", *J. Electrochem. Soc.*, **143** (1996) 2487-2492.
- [10] F. Lantelme, Y. Berghoute, "Electrochemical studies of LaCl<sub>3</sub> and GdCl<sub>3</sub> dissolved in fused LiCl-KCl", *J. Electrochem. Soc.*, **146** (1999) 4137-4144.

- [11] L. Martinot, J. Bohet, G. Duyckaerts, W. Muller, "Thermodynamic properties of dilute solutions of ThCl<sub>4</sub> in (Li-K)Cl and (Na-K)Cl eutectics", *Inorg. Nucl. Chem. Lett.*, **13** (1977) 315-319.
- [12] A. Glassner, "The thermochemical properties of the oxides, fluorides and chlorides to 2500 K", Argonne National Lab., ANL-5750, Lemont, 1957, pp. 201-274.
- [13] J. Fuger, V.B. Parker, W.N. Hubbard, F.L. Oetting, "The Chemical Thermodynamics of Actinide Elements and Compounds, Part 8", "The Actinide Halides", IAEA, Vienna, 1983.
- [14] C. Bale, E. Belisle, P. Chartrand, S. Decterov, G. Eriksson, A. Gheribi, K. Hack, I.H. Jung, Y.B. Kang, J. Melancon, A. Pelton, S. Petersen, C. Robelin, J. Sangster, P. Spencer, M.A.V. Ende, Factsage thermochemical software and databases 2010-2016, *Calphad*, **54** (2016) 35-53.
- [15] J. Fuger, D. Brown, "Thermodynamics of the actinide elements. Part IV. Heats and free energies of formation of the tetrachlorides, tetrabromides, and tetraiodides of thorium, uranium, and neptunium", *J. Chem. Soc., Dalton Trans.*, **0** (1973) 428-434.
- [16] A. Dębski, R. Dębski, W. Gasior, "New features of Entall database: Comparison of experimental and model formation enthalpies", *Archives of Metallurgy and Materials*, **59** (2015) 1337-1343.
- [17] W.H. Skelton, N.J. Magnani, J.F. Smith, "Thermodynamics of formation of Th-Ni alloys", *Metall. Mater. Trans.*, **1** (1970) 1833-1837.
- [18] W.H. Skelton, N.J. Magnani, J.F. Smith, "Thermodynamics of formation of Th-Co alloys", *Metall. Mater. Trans.*, **2** (1971) 473-476.
- [19] W.H. Skelton, N.J. Magnani, J.F. Smith, "Thermodynamics of formation of Th-Fe alloys", *Metall. Mater. Trans.*, **4** (1973) 917-920.

## **Publications in Refereed Journal:**

### **a. Published**

1. **Gurudas Pakhui**, Manish Chandra, Suddhasattwa Ghosh, B. Prabhakara Reddy, K. Nagarajan, “Electrochemical studies on the reduction behaviour of  $\text{Th}^{4+}$  in molten LiCl-KCl eutectic”, *Electrochim. Acta.*, **155** (2015) 372-382.
2. **Gurudas Pakhui**, Suddhasattwa Ghosh, B. Prabhakara Reddy, “Exchange current density of thorium in molten LiCl-KCl eutectic”, *Electrochim. Acta.*, **222** (2016) 92-99.
3. **Gurudas Pakhui**, Suddhasattwa Ghosh, B. Prabhakara Reddy, “ $\text{Th}^{4+}|\text{Th}$  couple in LiCl-KCl eutectic: Anodic polarization of thorium and electrochemical impedance spectroscopy study at tungsten, cadmium and thorium electrodes”, *Electrochim. Acta.*, **295** (2019) 354-366.

### **b. To be communicated:**

1. **Gurudas Pakhui**, Suddhasattwa Ghosh, B. Prabhakara Reddy, “Thermochemical Evaluation of  $E_{\text{Th}^{4+}|\text{Th}}^{\circ}$  and  $\Delta_f G_{\text{ThCl}_4}^{\circ}$  in LiCl-KCl eutectic melt”.
2. **Gurudas Pakhui**, Suddhasattwa Ghosh, B. Prabhakara Reddy, “Gibbs energy of formation of Cd-Th intermetallics by electromotive force measurements”.

## **Other Publications:**

### **c. Conference/Symposium**

1. **Gurudas Pakhui**, Suddhasattwa Ghosh, B. Prabhakara Reddy, “Electrochemical behavior of  $\text{Th}^{4+}$  in molten LiCl-KCl eutectic”, Theme meeting on Recent Trends in Materials Chemistry (RTMC), July 25-27, 2013, VIT University, Vellore, India.

2. **Gurudas Pakhui**, Suddhasattwa Ghosh, B. Prabhakara Reddy, “Electrochemistry of  $\text{Th}^{4+}|\text{Th}$  couple in molten LiCl-KCl eutectic”, Theme meeting on Chemistry in Nuclear Technology (CHEMNUT), July 30-31, 2015, 32, IGCAR, Kalpakkam, India.
3. **Gurudas Pakhui**, Suddhasattwa Ghosh, B. Prabhakara Reddy, “Electrochemical and thermodynamic properties of Th and Th-Cd alloys using transient electrochemical techniques”, Symposium on thermal analysis (THERMANS), January 18-20, 2016, T040, IIT BHU, Varanasi, India.
4. **Gurudas Pakhui**, Suddhasattwa Ghosh, B. Prabhakara Reddy, “Redox behaviour of  $\text{Th}^{4+}|\text{Th}$  couple at tungsten and cadmium electrodes in LiCl-KCl eutectic”, Symposium on Nuclear and Radiochemistry (NUCAR), February 6-10, 2017, C-146, KIIT University, Bhubaneswar, India.
5. **Gurudas Pakhui**, Suddhasattwa Ghosh, B. Prabhakara Reddy, “Determination of partial excess Gibbs energy of  $\text{ThCl}_4$  in LiCl-KCl eutectic using electromotive force measurements”, International Conference on Electrochemical Science & Technology (ICONEST), August 10-12, 2017, PP-EC-23, IISc Bengaluru, India.
6. **Gurudas Pakhui**, Suddhasattwa Ghosh, B. Prabhakara Reddy, “Molten salt electromotive force measurements on Th-Cd alloys”, Symposium on Nuclear and Radiochemistry (NUCAR), January 15-19, 2019, C27, BARC, Mumbai, India.

Signature of Student:

Date:

**Doctoral Committee:**

<b>S. No.</b>	<b>Name</b>	<b>Designation</b>	<b>Signature</b>	<b>Date</b>
1.	Dr. S. Rangarajan	Chairman		
2.	Dr. B. Prabhakara Reddy	Guide & Convener		
3.	Dr. V. Jayaraman	Member		
4.	Dr. Rajesh Ganesan	Member		
5.	Dr. S. Ningshen	Member		

## NOMENCLATURE

---

$T$	Temperature (K)
$R$	Universal gas constant ( $8.314 \text{ J mol}^{-1} \text{ K}^{-1}$ )
$F$	Faraday constant ( $96500 \text{ C/mol}$ )
$i_{pc}$	Cathodic peak current (A)
$E_{pc}$	Cathodic peak potential (V)
$(E_p - E_{p/2})_c$	Magnitude of peak width (V)
$n$	No of electrons transferred in redox reaction
$W_{1/2}$	Peak width at half height
$\Delta E$	Amplitude of square wave potential (V)
$A$	Electrode area ( $\text{cm}^2$ )
$C_{\text{ThCl}_4}$	Concentration of $\text{ThCl}_4$ in LiCl-KCl eutectic melt ( $\text{mol cm}^{-3}$ )
$C_{\text{CdCl}_2}$	Concentration of $\text{CdCl}_2$ in LiCl-KCl eutectic melt ( $\text{mol cm}^{-3}$ )
$D_{\text{Th}^{4+}}$	Diffusion coefficient of $\text{Th}^{4+}$ in LiCl-KCl eutectic melt ( $\text{cm}^2 \text{ s}^{-1}$ )
$E_a$	Activation energy of $\text{Th}^{4+} \text{Th}$ couple ( $\text{kJ mol}^{-1}$ )
$m(t)$	Semi-integral current ( $\text{A s}^{1/2}$ )
$m_c(\infty)$	Limiting semi-integral current ( $\text{A s}^{1/2}$ )
$E(t)$	Time dependent applied potential (V)
$i$	Current density ( $\text{mA cm}^{-2}$ )
$i_0$	Exchange current density ( $\text{mA cm}^{-2}$ )
$\nu$	Scan rate ( $\text{mV s}^{-1}$ )
$\tau$	Transition time (s)
$\eta$	Overpotential (V)
$\alpha$	Charge transfer coefficient
$\omega$	Angular frequency (Hz)
$Z_{\text{Re}}(\omega)$	Real impedance ( $\Omega$ )
$Z_{\text{Im}}(\omega)$	Imaginary impedance ( $\Omega$ )
$Y_Q$	Admittance (mho)
$R_{ct}$	Charge transfer resistance ( $\Omega$ )

---

---

$k_s$	Heterogeneous rate constant ( $\text{cm s}^{-1}$ )
$E_{\text{Th}^{4+} \text{Th}}^{\text{app}}$	Apparent equilibrium potential of $\text{Th}^{4+} \text{Th}$ in LiCl-KCl eutectic melt (V)
$E_{\text{Th}^{4+} \text{Th}}^{\circ*}$	Apparent standard electrode potential of $\text{Th}^{4+} \text{Th}$ couple in LiCl-KCl eutectic melt (V)
$E_{\text{Th}^{4+} \text{Th}}^{\text{eq}}$	Equilibrium potential of $\text{Th}^{4+} \text{Th}$ couple in LiCl-KCl eutectic melt (V)
$E_{\text{Th}^{4+} \text{Th}}^{\circ}$	Standard electrode potential of $\text{Th}^{4+} \text{Th}$ couple in LiCl-KCl eutectic melt ( <i>versus</i> $\text{Cl}^-/\text{Cl}_2$ ) (V)
$E_{\text{AgCl}}^{\circ}$	Standard electrode potential of AgCl in LiCl-KCl eutectic melt ( <i>versus</i> $\text{Cl}^-/\text{Cl}_2$ ) (V)
$\Delta_f G_{\text{ThCl}_4, \text{liq.}}^{\circ}$	Standard Gibbs energy of formation of pure liq. $\text{ThCl}_4$ ( $\text{kJ mol}^{-1}$ )
$\Delta_f G_{\text{ThCl}_4, \text{LiCl-KCl}}$	Gibbs energy of formation of $\text{ThCl}_4$ in LiCl-KCl eutectic melt ( $\text{kJ mol}^{-1}$ )
$\Delta_f G_{\text{ThCl}_4}^{\circ}$	Standard Gibbs energy of formation of $\text{ThCl}_4$ in LiCl-KCl eutectic melt ( $\text{kJ mol}^{-1}$ )
$\Delta \bar{G}_{\text{ThCl}_4}^{\text{ex}}$	Partial excess Gibbs energy of formation of $\text{ThCl}_4$ in LiCl-KCl eutectic melt ( $\text{kJ mol}^{-1}$ )
$\Delta_f G_{\text{AgCl}}$	Gibbs energy of formation of AgCl in LiCl-KCl eutectic melt ( $\text{kJ mol}^{-1}$ )
$\Delta_f G_{\text{AgCl}}^{\circ}$	Standard Gibbs energy of formation of pure AgCl ( $\text{kJ mol}^{-1}$ )
$\Delta_{\text{fus}} H_{\text{ThCl}_4}$	Enthalpy of fusion of pure $\text{ThCl}_4$ ( $\text{kJ mol}^{-1}$ )
$a_{\text{ThCl}_4, \text{liq.}}$	Activity of $\text{ThCl}_4$ in LiCl-KCl eutectic melt ( $\text{kJ mol}^{-1}$ )
$a_{\text{AgCl}}$	Activity of AgCl in LiCl-KCl eutectic melt
$\gamma_{\text{ThCl}_4}, \gamma_{\text{ThCl}_4}^{\text{s}}, \gamma_{\text{ThCl}_4}^{\text{liq.}}$	Activity coefficient of $\text{ThCl}_4$ in LiCl-KCl eutectic melt. Second and third term refer to $\gamma_{\text{ThCl}_4}$ in solid and liquid reference states
$\gamma_{\text{AgCl}}$	Activity coefficient of AgCl in LiCl-KCl eutectic melt
$x_{\text{ThCl}_4}$	Mole fraction of $\text{ThCl}_4$ in LiCl-KCl eutectic melt
$x_{\text{AgCl}}$	Mole fraction of AgCl in LiCl-KCl eutectic melt
$x_{\text{Th}}$	Mole fraction of Th in Cd
$a_{\text{Th}}$	Activity of Th in Cd
$a_{\text{Cd}}$	Activity of Cd saturated by Th

---

---

$G_{\text{Th}}^{\circ}$	Gibbs energy of thorium in reference state of $\alpha$ -Th ( $\text{kJ mol}^{-1}$ )
$\bar{G}_{\text{Th}}$	Partial Gibbs energy of thorium in liq. Cd ( $\text{kJ mol}^{-1}$ )
$\Delta_{\text{f}}G_{\text{Cd}_m\text{Th}_n}^{\circ}$	General term to express standard Gibbs energy of formation of all Cd-Th intermetallics ( $\text{J mol-atom}^{-1}$ )
$\Delta_{\text{f}}G_{\text{Cd}_{11}\text{Th}}^{\circ}$	Standard Gibbs energy of formation of $\text{Cd}_{11}\text{Th}$ ( $\text{J mol-atom}^{-1}$ )
$\Delta_{\text{f}}G_{\text{Cd}_5\text{Th}}^{\circ}$	Standard Gibbs energy of formation of $\text{Cd}_5\text{Th}$ ( $\text{J mol-atom}^{-1}$ )
$\Delta_{\text{f}}G_{\text{Cd}_{23}\text{Th}_6}^{\circ}$	Standard Gibbs energy of formation of $\text{Cd}_{23}\text{Th}_6$ ( $\text{J mol-atom}^{-1}$ )
$\Delta_{\text{f}}G_{\text{Cd}_3\text{Th}}^{\circ}$	Standard Gibbs energy of formation of $\text{Cd}_3\text{Th}$ ( $\text{J mol-atom}^{-1}$ )
$\Delta_{\text{f}}H_{\text{Cd}_m\text{Th}_n}^{\circ}$	General term to express standard enthalpy of formation of all Cd-Th intermetallics ( $\text{J mol-atom}^{-1}$ )
$\bar{\Delta}H_{\text{Th}}$	Partial molar enthalpy of Th in Cd-Th intermetallic ( $\text{J mol}^{-1}$ )
$\bar{\Delta}S_{\text{Th}}$	partial molar entropy of Th in Cd-Th intermetallic ( $\text{J mol}^{-1}$ )
$\bar{\Delta}H_{\text{Cd}}$	Partial molar enthalpy of Cd in Cd-Th intermetallic ( $\text{J mol}^{-1}$ )
$\bar{\Delta}S_{\text{Cd}}$	partial molar entropy of Cd in Cd-Th intermetallic ( $\text{J mol}^{-1}$ )
$\phi^*$	Electronegativity
$n_{\text{ws}}$	Electron density at the boundary of the Wigner-Seitz atomic cell

---

## LIST OF FIGURES

Figure No	Figure caption	Page No
Figure 1.1	Graph of publications <i>versus</i> year on studies carried out on thorium in molten salts across the world, Reference: Scopus database, search words: thorium and molten, thorium and fused.	2
Figure 1.2	Cd-Th binary phase diagram given by Palenzona <i>et al.</i> [52].	7
Figure 1.3	Flowchart of scope of work in current PhD thesis.	9
Figure 2.1	The layout of argon atmosphere glove box [53].	11
Figure 2.2	Photograph of argon atmosphere glove box.	12
Figure 2.3	Chlorination set-up made of quartz vessel and teflon flanges.	14
Figure 2.4	XRD pattern of LiCl-KCl-ThCl <sub>4</sub> electrolyte (Numbers in parenthesis correspond to miller indices).	16
Figure 2.5	XRD pattern of (a) Th and (b) Cd metals.	18
Figure 2.6	Photographs of (a) iron vessel before and after loading with Th and Cd, (b) Cd-Th alloy after cleaning by diamond filing.	18
Figure 2.7	Powder XRD patterns of (a) Cd <sub>Th</sub> + Cd <sub>11</sub> Th, (b) Cd <sub>11</sub> Th + Cd <sub>5</sub> Th, (c) Cd <sub>5</sub> Th + Cd <sub>23</sub> Th <sub>6</sub> , (d) Cd <sub>23</sub> Th <sub>6</sub> + Cd <sub>3</sub> Th two-phase alloys, Step size: 0.05°, (Numbers in parenthesis correspond to miller indices).	19
Figure 2.8	Thorium electrode used in the present work.	20
Figure 2.9	Liquid cadmium electrode.	21
Figure 2.10	Electrode assembly used in emf study of ThCl <sub>4</sub> in LiCl-KCl eutectic melt.	22
Figure 2.11	Electrode assembly used in emf study of Cd-Th alloys.	23
Figure 2.12	Schematic of electrochemical cell assembly.	24
Figure 2.13	Photograph of top flange loaded with electrodes in electrochemical cell.	25

Figure 2.14	Equivalent circuit used for fitting complex impedance data for cathodic polarization of thorium at inert tungsten and cadmium electrodes and anodic polarization of metallic thorium electrode	29
Figure 2.15	Schematic diagram of emf cell set-up.	32
Figure 3.1	Cyclic voltammograms of blank LiCl-KCl eutectic melt and LiCl-KCl-ThCl <sub>4</sub> at tungsten electrode, $T = 723$ K, $C_{\text{ThCl}_4} = 9.53 \times 10^{-5} \text{ mol cm}^{-3}$ , $A = 0.25 \text{ cm}^2$ .	36
Figure 3.2	Cyclic voltammogram of Th <sup>4+</sup>  Th couple at inert tungsten electrode in LiCl-KCl eutectic melt for scan rates 3-10 mV s <sup>-1</sup> , $T = 698$ K, $C_{\text{ThCl}_4} = 9.53 \times 10^{-5} \text{ mol cm}^{-3}$ , $A = 0.25 \text{ cm}^2$ .	36
Figure 3.3	Cyclic voltammograms of Th <sup>4+</sup>  Th couple at inert tungsten electrode in LiCl-KCl eutectic melt, $T = 723$ K, $C_{\text{ThCl}_4} = 2.04 \times 10^{-5} \text{ mol cm}^{-3}$ , $A = 0.25 \text{ cm}^2$ .	37
Figure 3.4	$E_{pc}$ vs. $\log \nu$ for Th <sup>4+</sup>  Th couple at inert tungsten electrode in LiCl-KCl eutectic melt, (a) $C_{\text{ThCl}_4} = 2.04 \times 10^{-5} \text{ mol cm}^{-3}$ , (b) $C_{\text{ThCl}_4} = 2.72 \times 10^{-5} \text{ mol cm}^{-3}$ , (c) $C_{\text{ThCl}_4} = 9.53 \times 10^{-5} \text{ mol cm}^{-3}$ , $T = 698-803$ K, $A = 0.25 \text{ cm}^2$ .	41
Figure 3.5	Variation of $i_{pc}$ vs. $\nu^{1/2}$ of Th <sup>4+</sup>  Th couple at inert tungsten electrode in molten LiCl-KCl eutectic melt, (a) $C_{\text{ThCl}_4} = 2.04 \times 10^{-5} \text{ mol cm}^{-3}$ , (b) $C_{\text{ThCl}_4} = 2.72 \times 10^{-5} \text{ mol cm}^{-3}$ , (c) $C_{\text{ThCl}_4} = 9.53 \times 10^{-5} \text{ mol cm}^{-3}$ , $T = 698-803$ K, $A = 0.25 \text{ cm}^2$ .	42
Figure 3.6	a) Chronopotentiograms of Th <sup>4+</sup>  Th couple at tungsten electrode in molten LiCl-KCl eutectic melt, (b) Variation of $it^{1/2}$ versus current density, $T = 723$ K, $C_{\text{ThCl}_4} = 2.04 \times 10^{-5} \text{ mol cm}^{-3}$ , $A = 0.25 \text{ cm}^2$ .	43
Figure 3.7	Plot of $i$ versus $\tau^{-1/2}$ , (a) $C_{\text{ThCl}_4} = 2.04 \times 10^{-5} \text{ mol cm}^{-3}$ , (b) $C_{\text{ThCl}_4} = 2.72 \times 10^{-5} \text{ mol cm}^{-3}$ , (c) $C_{\text{ThCl}_4} = 9.53 \times 10^{-5} \text{ mol cm}^{-3}$ , $T = 698-803$ K, $A = 0.25 \text{ cm}^2$ .	45

Figure 3.8	(a) Square wave voltammograms of $\text{Th}^{4+} \text{Th}$ couple at inert tungsten electrode in LiCl-KCl eutectic melt, $T = 723$ K, $C_{\text{ThCl}_4} = 2.04 \times 10^{-5} \text{ mol cm}^{-3}$ , $f = 25$ Hz, $\Delta E = 20, 25, 30, 35$ mV, $A = 0.25 \text{ cm}^2$ . (b) Linear relationship of $i_{pc}$ (left axis) and $E_{pc}$ (right axis) versus $f^{1/2}$ , $T = 723$ K, $\Delta E = 25$ mV.	46
Figure 3.9	Semi-integral curve of voltammogram for $\text{Th}^{4+} \text{Th}$ couple at inert tungsten electrode in LiCl-KCl eutectic melt, $T = 723$ K, $C_{\text{ThCl}_4} = 2.04 \times 10^{-5} \text{ mol cm}^{-3}$ , $A = 0.25 \text{ cm}^2$ .	47
Figure 3.10	Logarithmic analysis of semi-integral curve of $\text{Th}^{4+} \text{Th}$ couple as per (a) Reversible, (b) quasireversible and (c) irreversible hypothesis, $C_{\text{ThCl}_4} = 2.04 \times 10^{-5} \text{ mol cm}^{-3}$ , $T = 723$ K, $A = 0.25 \text{ cm}^2$ .	50
Figure 3.11	Variation of $\ln D_{\text{Th}^{4+}}$ versus $1/T$ for $\text{ThCl}_4$ in LiCl-KCl eutectic melt.	54
Figure 3.12	Concentration and temperature dependence of $D_{\text{Th}^{4+}}$ of $\text{Th}^{4+}$ in LiCl-KCl eutectic melt.	54
Figure 3.13	Logarithmic analysis of chronopotentiogram of $\text{Th}^{4+} \text{Th}$ couple for tungsten electrode in LiCl-KCl eutectic melt, (a) $C_{\text{ThCl}_4} = 2.04 \times 10^{-5} \text{ mol cm}^{-3}$ , (b) $C_{\text{ThCl}_4} = 2.72 \times 10^{-5} \text{ mol cm}^{-3}$ , (c) $C_{\text{ThCl}_4} = 9.53 \times 10^{-5} \text{ mol cm}^{-3}$ , $T = 698-803$ K, $A = 0.25 \text{ cm}^2$ .	56
Figure 3.14	Plot of $E_{\text{Th}^{4+} \text{Th}}^{o*}$ versus $T$ (K).	58
Figure 3.15	Cyclic voltammogram of Th electrode in LiCl-KCl eutectic melt, $C_{\text{ThCl}_4} = 1.02 \times 10^{-4} \text{ mol cm}^{-3}$ , $T = 773$ K, Scan rate: $25 \text{ mV s}^{-1}$ , $A = 1.50 \text{ cm}^2$ .	59
Figure 3.16	Cyclic voltammograms of LiCl-KCl- $\text{ThCl}_4$ at inert tungsten and liquid cadmium electrodes. $C_{\text{ThCl}_4} = 3.55 \times 10^{-5} \text{ mol cm}^{-3}$ , $A = 0.25 \text{ cm}^2$ at inert tungsten electrode. $C_{\text{ThCl}_4} = 1.08 \times 10^{-4} \text{ mol cm}^{-3}$ , $A = 1.48 \text{ cm}^2$ at liquid cadmium electrode, scan rate for both the voltammograms is $25 \text{ mV s}^{-1}$ , $T = 773$ K.	65

Figure 3.17	Cyclic voltammograms of LiCl-KCl-ThCl <sub>4</sub> at liquid cadmium electrode at various scan rates, $T = 698$ K, $C_{\text{ThCl}_4} = 1.08 \times 10^{-4}$ mol cm <sup>-3</sup> .	65
Figure 3.18	Cyclic voltammograms of LiCl-KCl-ThCl <sub>4</sub> at inert tungsten electrode over period of 30 h, $T = 773$ K.	66
Figure 3.19	Cyclic voltammogram of LiCl-KCl eutectic containing ThCl <sub>4</sub> and CdCl <sub>2</sub> at inert tungsten electrode, $T = 773$ K, $C_{\text{ThCl}_4} = 1.08 \times 10^{-4}$ mol cm <sup>-3</sup> , $C_{\text{CdCl}_2} = 5.20 \times 10^{-5}$ mol cm <sup>-3</sup> .	67
Figure 3.20	(a) Recrystallized alumina crucible before experiments, (b) LiCl-KCl-ThCl <sub>4</sub> electrolyte used for the present measurements before experiment.	68
Figure 3.21	Th electrode prepared for experiment (a) before immersion in the melt, (b) after immersion in the melt.	69
Figure 3.22	Alumina crucible after experiment (a) when Th electrode was not immersed, (b) when Th electrode was immersed in the melt.	69
Figure 3.23	LiCl-KCl-ThCl <sub>4</sub> electrolyte after experiment (a) when Th electrode was not immersed and (b) when Th electrode was immersed in the melt.	70
Figure 3.24	Cyclic voltammograms of LiCl-KCl-ThCl <sub>4</sub> at inert tungsten electrode over period of 30 h, $T = 773$ K, thorium electrode was kept immersed into the melt during cyclic voltammetric measurements.	71
Figure 4.1	$i$ vs. $t$ profile for cathodic polarization of thorium at inert tungsten electrode at various potentials, $T = 773$ K.	74
Figure 4.2	$i$ vs. $E$ profile for cathodic and anodic polarization of thorium at inert tungsten, liq. Cd and Th electrodes at various potentials, $T = 773$ K.	74
Figure 4.3	Tafel plots for anodic and cathodic polarization of thorium at inert tungsten and liquid cadmium cathodes in LiCl-KCl eutectic melt.	75
Figure 4.4	Allen-Hickling plots of anodic and cathodic polarization of thorium at inert tungsten and liquid cadmium cathode in LiCl-KCl eutectic melt.	75

Figure 4.5	$i_0$ versus $\ln C_{\text{ThCl}_4}$ ( $\text{mol cm}^{-3}$ ) profile for cathodic polarization data at tungsten electrode at various temperatures. $i_0$ estimated from both polarization and cyclic voltammetric data are shown.	78
Figure 4.6	$i$ vs. $t$ profile for cathodic polarization of thorium at liquid Cd electrode at various potentials, $T = 773$ K.	80
Figure 4.7	$i$ vs. $t$ profile for anodic polarization of thorium electrode at various potentials, $T = 773$ K.	81
Figure 4.8	$\ln i_0$ versus $\frac{1}{T}$ curve for tungsten electrode (cathodic polarization). Fits of only polarization data and polarization+voltammetry data (Chapter 3) are shown	82
Figure 4.9	$i_0$ versus $\frac{1}{T}$ curve for liquid cadmium (cathodic polarization) and anodic dissolution of thorium in LiCl-KCl eutectic melt.	83
Figure 5.1	Equivalent circuit used for fitting complex impedance data for cathodic polarization of thorium at inert tungsten and cadmium electrodes and anodic polarization of metallic thorium electrode.	85
Figure 5.2	Nyquist plots of $\text{ThCl}_4$ at inert tungsten electrode in LiCl-KCl eutectic melt, $C_{\text{ThCl}_4} = 1.02 \times 10^{-4} \text{ mol cm}^{-3}$ , $T = 773$ K, Frequency range of measurement: 10 Hz to 10 kHz.	87
Figure 5.3	Nyquist plots of $\text{ThCl}_4$ at inert tungsten electrode in LiCl-KCl eutectic melt at $E_{\text{Th}^{4+} \text{Th}}^{\text{eq}}$ versus $\text{Ag}^+ \text{Ag}$ reference, $C_{\text{ThCl}_4} = 1.02 \times 10^{-4} \text{ mol cm}^{-3}$ , $T = 698-773$ K. Frequency range of measurement: 10 Hz to 10 kHz.	88
Figure 5.4	Variation of $R_{ct}$ versus applied potential at tungsten electrode (cathodic), $C_{\text{ThCl}_4} = 1.02 \times 10^{-4} \text{ mol cm}^{-3}$ , $T = 773$ K.	89
Figure 5.5	Nyquist plots of $\text{ThCl}_4$ at liquid cadmium electrode in LiCl-KCl eutectic melt, $C_{\text{ThCl}_4} = 1.02 \times 10^{-4} \text{ mol cm}^{-3}$ , $T = 773$ K, Frequency range of measurement: 10 Hz-10 kHz.	92

Figure 5.6	Variation of $R_{ct}$ versus applied potential at liquid cadmium electrode (cathodic), $C_{ThCl_4} = 1.02 \times 10^{-4} \text{ mol cm}^{-3}$ , $T = 773 \text{ K}$ .	94
Figure 5.7	Nyquist plots of thorium electrode (anodic) in LiCl-KCl-ThCl <sub>4</sub> , $C_{ThCl_4} = 1.02 \times 10^{-4} \text{ mol cm}^{-3}$ , $T = 698-798 \text{ K}$ , Frequency range of measurement: 10Hz-10 kHz.	99
Figure 5.8	Diagrammatic representation of anodic dissolution of thorium in LiCl-KCl eutectic melt. Distinct features of complex impedance plots include large capacitive response at higher frequencies and slope of linear region at lower frequencies greater than 1.0. -1.435 V is the equilibrium potential for thorium dissolution.	101
Figure 5.9	Variation of $R_{ct}$ versus applied potential for Th electrode (anodic), $C_{ThCl_4} = 1.02 \times 10^{-4} \text{ mol cm}^{-3}$ , $T = 773 \text{ K}$ .	102
Figure 5.10	Validation of complex impedance data recorded at inert tungsten electrode using Kramers-Kronig transforms, K-K compliance fit, fit residuals $\Delta_{Re,i}$ and $\Delta_{Im,i}$ are shown for cathodic potentials of -0.8 to -1.57 V, $T = 773 \text{ K}$ , $A = 0.25 \text{ cm}^2$ .	106
Figure 5.11	Validation of complex impedance data recorded at liquid cadmium electrode using Kramers-Kronig transforms. K-K compliance fit and fit residuals $\Delta_{Re,i}$ and $\Delta_{Im,i}$ are shown for cathodic potential of -0.90 to -1.47 V, $T = 773 \text{ K}$ , $A = 1.48 \text{ cm}^2$ .	109
Figure 5.12	Validation of complex impedance data recorded at metallic thorium electrode using Kramers-Kronig transforms. K-K compliance fit and fit residuals $\Delta_{Re,i}$ and $\Delta_{Im,i}$ are shown for anodic potentials of -1.35 to -1.43 V, $T = 773 \text{ K}$ , $A = 1.5 \text{ cm}^2$ .	110
Figure 5.13	Temperature dependence of $\ln k_s$ for cathodic (inert tungsten) and anodic (thorium) polarization cases.	112
Figure 6.1	Equilibrium potential $E_{Th^{4+} Th}^{eq}$ measured against $Ag^+ Ag$ reference electrode at various $x_{ThCl_4}$ and temperatures in LiCl-KCl eutectic melt.	118

---

Figure 6.2	Variation of $E_{\text{Th}^{4+} \text{Th}}^{eq} + E_{\text{AgCl}}^{\circ} + \frac{RT}{F} \ln x_{\text{AgCl}}$ (vs. $\text{Cl}^- \text{Cl}_2$ ) vs. $\ln x_{\text{ThCl}_4}$ (Method of Roy <i>et al.</i> [70,71]) in LiCl-KCl eutectic melt.	119
Figure 6.3	Variation of $E_{\text{Th}^{4+} \text{Th}}^{eq} + E_{\text{AgCl}}^{\circ} + \frac{RT}{F} \ln x_{\text{AgCl}} - \frac{RT}{4F} \ln x_{\text{ThCl}_4}$ (vs. $\text{Cl}^- \text{Cl}_2$ ) vs. $x_{\text{ThCl}_4}$ (Method of Lantelme <i>et al.</i> [72,73]) in LiCl-KCl eutectic melt.	119
Figure 6.4	Temperature dependence of $E_{\text{Th}^{4+} \text{Th}}^{\circ}$ in LiCl-KCl eutectic melt reported by various authors and in the present work. $E_{\text{Th}^{4+} \text{Th}}^{\circ}$ of Martinot <i>et al.</i> [106] re-calculated using the method of Roy <i>et al.</i> and Lantelme <i>et al.</i> are also shown. Individual linear fitting of electromotive force and transient data along with the overall fit are also shown.	122
Figure 6.5	Variation of $\Delta_f G_{\text{ThCl}_4,liq.}^{\circ}$ of pure $\text{ThCl}_4$ liquid (hypothetically supercooled) as reference state <i>versus</i> $T$ taken from different thermochemical data compilations [105–107,109,116] . $\Delta_f G_{\text{ThCl}_4,s}^{\circ}$ of pure solid $\text{ThCl}_4$ from Glassner [105] is also shown.	125
Figure 6.6	Variation of $\gamma_{\text{ThCl}_4}^{liq.}$ in LiCl-KCl eutectic melt <i>versus</i> $T$ estimated from various thermochemical compilations. The recommended linear least square fit is also shown.	126
Figure 7.1	Emf data for cells I-IV, respective linear least square fits are also shown.	132
Figure 7.2	Temperature dependence of $\Delta_f G_{\text{Cd}_m\text{Th}_n}^{\circ}$ of Cd-Th intermetallics.	133
Figure 7.3	Comparison of $\Delta_f G^{\circ}$ as a function of Th composition for intermetallics of Cd-Th, Fe-Th, Co-Th, Ni-Th, Cu-Th and Zn-Th systems [32,35–37,39].	133

---

---

Figure 7.4	Comparison of experimental values of $\Delta_f H_{\text{Cd}_m\text{Th}_n}^\circ$ with that of Miedema estimation and with experimental values of Cu-Th system[32], Ni-Th, Co-Th, Fe-Th systems, reported by Skelton <i>et al.</i> [35–37] and Th-Zn system [39].	136
Figure 8.1	Cyclic voltammogram of LiCl-KCl-ThCl <sub>4</sub> at inert tungsten electrode, $T = 773 \text{ K}$ , $A = 0.25 \text{ cm}^2$ .	140

---

## LIST OF TABLES

Table No	Table caption	Page No
Table 1.1	Literature survey on electrochemical studies of thorium in molten salts.	4
Table 1.2	Literature survey on Cd-Th system.	7
Table 2.1	Impurity analysis in chlorinated LiCl-KCl (sample weight: 475.5 mg) eutectic by ICP-AES and LiCl-KCl-ThCl <sub>4</sub> salt by ICP-MS technique (sample weight: 70 mg).	16
Table 2.2	Impurity analysis of Cd by ICP-OES and AAS techniques (sample weight: 220.22 mg) [59].	17
Table 2.3	Weight balance of Cd-Th alloys before and after equilibration	18
Table 3.1	Cathodic peak analysis of Th <sup>4+</sup>  Th couple for $C_{\text{ThCl}_4} = 2.72 \times 10^{-5} \text{ mol cm}^{-3}$ in LiCl-KCl eutectic melt.	38
Table 3.2	Calculated $\alpha n$ value for Th <sup>4+</sup>  Th couple by cyclic voltammetry	40
Table 3.3	$n$ of Th <sup>4+</sup>  Th couple calculated by squarewave voltammogram, $C_{\text{ThCl}_4} = 2.72 \times 10^{-5} \text{ mol cm}^{-3}$ .	46
Table 3.4	$n$ , $\alpha$ , $\alpha n$ values for Th <sup>4+</sup>  Th couple using reversible, quasireversible and irreversible hypothesis in semi-integral voltammetry.	50
Table 3.5	$D_{\text{Th}^{4+}}$ of Th <sup>4+</sup> in LiCl-KCl eutectic melt obtained from CV, CP, SIV, SWV.	53
Table 3.6	Estimated $E_{\text{Th}^{4+} \text{Th}}^{\circ*}$ of Th <sup>4+</sup>  Th couple and comparison with literature data.	56
Table 3.7	Estimated $E_{\text{Th}^{4+} \text{Th}}^{\circ*}$ values at different $C_{\text{ThCl}_4}$ .	57
Table 3.8	$E_{\text{Th}^{4+} \text{Th}}^{\text{app}}$ of Th dissolution in LiCl-KCl-ThCl <sub>4</sub> ( $x_{\text{ThCl}_4} = 3.86 \times 10^{-3}$ ) electrolyte measured using cyclic voltammetry at 50 mV s <sup>-1</sup> and 100 mV s <sup>-1</sup> .	60

Table 3.9	Summary of calculated equilibrium potential of thorium dissolution in LiCl-KCl eutectic melt at $T = 773$ K from various literature sources. Data of Yang <i>et al.</i> [74] are at 772 K and 774 K. $x_{\text{ThCl}_4} = 3.86 \times 10^{-3}$ is assumed for all calculations.	63
Table 4.1	$i_0$ , $a_{\text{Tafel}}$ , $b_{\text{Tafel}}$ and $b_{\text{Allen-Hickling}}$ of thorium at inert tungsten electrode in LiCl-KCl eutectic melt.	76
Table 4.2	$i_0$ of $\text{Th}^{4+} \text{Th}$ couple at inert tungsten electrode from cyclic voltammetric data (Chapter 3).	77
Table 4.3	$i_0$ of $\text{Th}^{4+} \text{Th}$ couple at liquid cadmium electrode at various temperatures	80
Table 4.4	$i_0$ of thorium in LiCl-KCl eutectic melt in temperature range 698-798 K	81
Table 4.5	Fit parameters of $\ln i_0$ versus $1/T$ plot for cathodic and anodic polarization data.	83
Table 5.1	EIS data of cathodic polarization of thorium in LiCl-KCl- $\text{ThCl}_4$ electrolyte at tungsten electrode, $C_{\text{ThCl}_4} = 1.02 \times 10^{-4} \text{ mol cm}^{-3}$ , $A = 0.25 \text{ cm}^2$ .	90
Table 5.2	EIS data of cathodic polarization of thorium in liquid cadmium, $C_{\text{ThCl}_4} = 1.02 \times 10^{-4} \text{ mol cm}^{-3}$ , $A = 1.48 \text{ cm}^2$ .	94
Table 5.3	EIS data of anodic polarization of thorium electrode in LiCl-KCl- $\text{ThCl}_4$ electrolyte, $C_{\text{ThCl}_4} = 1.02 \times 10^{-4} \text{ mol cm}^{-3}$ , $A = 1.5 \text{ cm}^2$ .	102
Table 5.4	$k_s$ estimated for cathodic and anodic polarization of thorium in LiCl-KCl eutectic melt.	111
Table 5.5	Matsuda-Ayabe criteria applied to $\text{Th}^{4+} \text{Th}$ couple for cathodic and anodic polarization cases in LiCl-KCl eutectic melt, $10^{-2(1+\alpha)} = 3.98 \times 10^{-4}$ for all cases.	113

---

Table 6.1	Literature survey on thermodynamic behaviour of ThCl <sub>4</sub> in LiCl-KCl eutectic melt.	116
Table 6.2	Equilibrium potential of Th <sup>4+</sup> /Th couple measured against Ag <sup>+</sup> /Ag reference electrode ( $x_{\text{AgCl}} = 4.6 \times 10^{-3}$ ).	118
Table 6.3	Comparison of standard electrode potential of Th <sup>4+</sup> /Th couple <i>versus</i> Cl <sup>-</sup> /Cl <sub>2</sub> estimated in the present work with literature data	120
Table 7.1	Electromotive force data of cells I, II, III and IV, superscription h and c refer to measurements in heating and cooling cycles, respectively.	131
Table 7.2	Table of thermodynamic functions for the formation of Cd-Th intermetallics at 773 K.	134
Table 7.3	Partial molar quantities for Cd-Th intermetallics relative to $\alpha$ -Th (fcc) and liquid cadmium (hcp) at 723 K.	135
Table 8.1	Electromotive force data of the cell Th Th <sup>4+</sup>    LiCl-KCl-ThCl <sub>4</sub>    $\langle \text{Cd}_3\text{Th} \rangle_s + \langle \text{Cd}_2\text{Th} \rangle_s$ .	141

---

# CHAPTER 1

## Introduction

### 1.1 Objectives of present thesis

Investigations on thorium based systems either related to preparation and characterization of condensed phases or electrochemistry pertaining to its redox behavior in high temperature melts had been initiated in 1950s in several countries to address issues on nuclear power generation using breeder reactors based on molten salts, preparation, characterization and performance of thorium based fuels or as a general area of research involving preparation of complex phases and measurement of their thermodynamic properties. These studies were extended in different directions that led to preparation of standard thermochemical databases of thermodynamic data, solution calorimetric studies on complex halides of thorium with alkali metals, generation of phase diagrams of halides, carbides, oxides etc. In so far as redox investigations on thorium in high temperature melts are concerned, the following graph (Figure 1.1) generated using Scopus database will suggest the importance of such studies in the last 7 decades.

There has been an upsurge in these investigations during the early 2000s and it continues this day. One of the reasons for this could be a renewed interest on thorium based reactor fuels, re-looking at thermodynamic data of thorium based molten salts and phase diagrams. The present work on electrochemical and thermodynamic investigations on thorium in LiCl-KCl eutectic melt was taken up to address certain issues that mainly pertained to electrochemistry of  $\text{Th}^{4+}$ , electrode kinetics and thermodynamics using combination of electromotive force and transient technique measurements. Present thesis is restricted to electrochemical investigations and thermodynamic investigations and making certain recommendations on specific thermodynamic data.

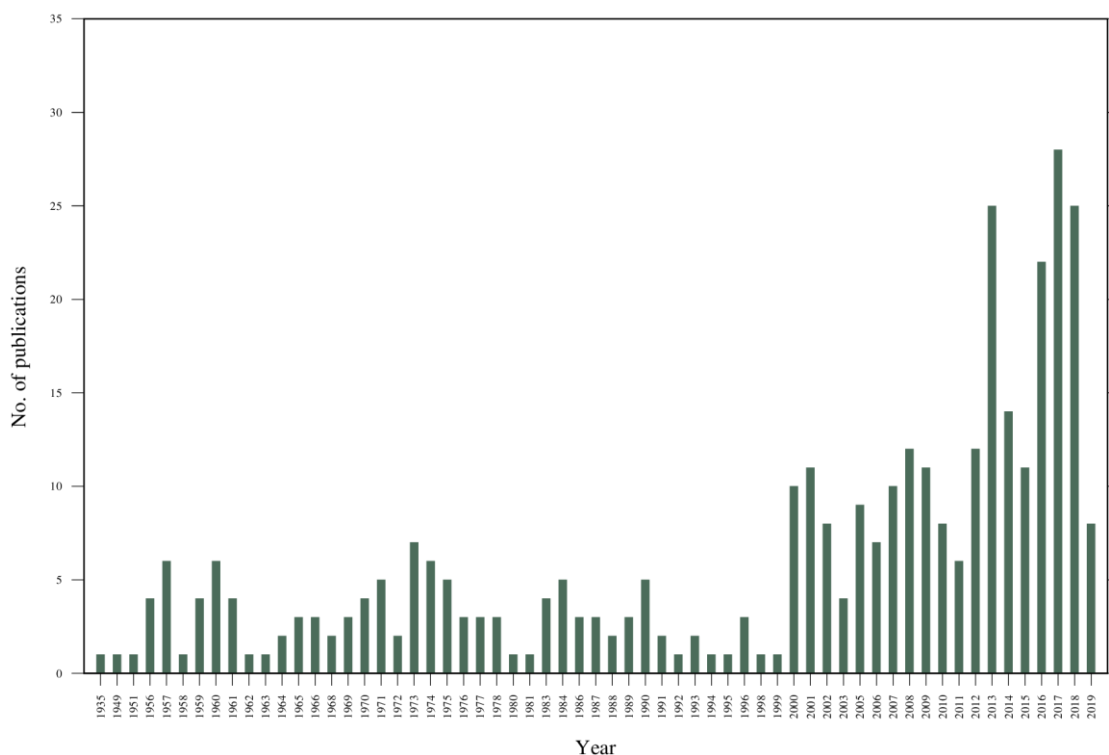


Figure 1.1 Graph of publications versus year on studies carried out on thorium in molten salts in the span of 1929-2019 across the world, Ref.: Scopus database, search words: Th and molten; Th and fused.

## 1.2 Electrochemical and thermodynamic studies on thorium in molten salts: Literature survey

With a large body of work pertaining to studies on thorium with respect to its redox behaviour in molten salts, the present thesis focuses on investigations of electrochemical and thermodynamic behaviour of  $\text{ThCl}_4$  in  $\text{LiCl-KCl}$  eutectic melt and  $\text{Cd-Th}$  alloys. Electrochemical behavior of thorium in  $\text{LiCl-KCl}$  eutectic melt has been studied exhaustively in the last five decades by various research groups across the world.

In late 50s, Smirnov *et al.* [1-4], and few other groups [5-7] in recent past have studied basic electrochemical behavior of thorium in  $\text{LiCl-KCl}$  eutectic melt. Electrochemical and thermodynamic studies on thorium in  $\text{LiCl-KCl}$  eutectic melt was also carried out by Chiotti *et al.*[8-13]. Inman *et al.*[14], Yang *et al.* [15] and Gruen *et al.* [16] investigated on oxidation state of thorium in  $\text{LiCl-KCl}$  eutectic melt. There was huge debate on the stable oxidation

state of thorium in molten halide medium and it continues to this day. Some authors concluded that +4 is the only stable oxidation state of thorium in molten halide medium, while few other groups reported the existence of more than one valence states in molten halide mediums. Smirnov *et al.* [1-4] and Chiotti *et al.* [8-10] have observed formation of Th<sup>2+</sup> and Th<sup>3+</sup> ions at very high temperature and low thorium concentration and summary of experiments are described in Table 1.1. They postulated that thorium tetrachloride would be reduced almost quantitatively by thorium metal according to the reaction:



However it was shown by several groups [5-7, 11-16] that +4 was the only stable valence state of thorium in LiCl-KCl eutectic melt. Attempts to prepare ThCl<sub>3</sub> and ThCl<sub>2</sub> were unsuccessful by Chiotti *et al.* [11, 13]. They didn't find any evidence of formation of lower valent thorium chlorides and concluded that both ThCl<sub>3</sub> and ThCl<sub>2</sub> must be metastable relative to ThCl<sub>4</sub>. Smirnov *et al.* [17-21] and few other groups [22-24] carried out investigations on valence state, complexation behaviour, electrochemical and thermodynamic properties of thorium in various chloride melts. Studies by Smirnov *et al.* [17-21] reported the existence of +2 and +3 valence states of thorium along with +4, whereas, Kanashin *et al.* [23], Srinivasan *et al.* [24] and Tumidajski *et al.* [25] reported +4 is the only stable valence state of thorium in various chloride melts as discussed in Table 1.1. Smirnov *et al.* [20] reported that disproportionation of ThCl<sub>2</sub> to Th metal and ThCl<sub>4</sub> began above 923 K which was supported by Hayek *et al.* [22], who observed that ThCl<sub>2</sub> disproportionate when heated above 943 K. Clayton *et al.* [26] and Chamelot *et al.* [27, 28] have studied electrochemical behaviour of thorium in alkali fluoride melts and reported +4 as the only stable valence state of thorium. Delpech *et al.* [29] have studied electrochemical behaviour of ThF<sub>4</sub> in LiCl-KCl eutectic melt and reported +4 as the only stable valence state of thorium. There is thus little or no

conclusive evidence for the formation of any stable lower valent thorium chlorides other than ThCl<sub>4</sub> in LiCl-KCl eutectic melt.

According to Martinot *et al.* [5] reduction of Th<sup>4+</sup> was quasi-reversible process. Liu *et al.* [6] observed reversible behaviour of Th<sup>4+</sup>|Th couple. They observed nucleation controlled deposition phenomena during reduction of Th<sup>4+</sup> at tungsten working electrode. Cassayre *et al.* [7] found it difficult to conclude about the reversibility of Th<sup>4+</sup>|Th redox couple. Different electrochemical properties like  $E_{\text{Th}^{4+}|\text{Th}}^{\text{app}}$ ,  $D_{\text{Th}^{4+}}$  and  $E_a$  of Th<sup>4+</sup>|Th couple in LiCl-KCl eutectic melt were estimated using transient electrochemical techniques by several groups [5-7]. A summary of the literature reports on the electrochemical studies on thorium in molten salts is given in Table 1.1.

Table 1.1 Literature survey on electrochemical studies of thorium in molten salts.

System	Reference(s)	Summary
ThCl <sub>4</sub> in LiCl-KCl eutectic melt	Smirnov <i>et al.</i> [1, 2]	The polarization of Mo cathode was studied in LiCl-KCl eutectic melt containing ThCl <sub>4</sub> at 873, 973, 1073 K and at relatively low current density reduction of Th <sup>4+</sup> to Th <sup>2+</sup> was observed. Temperature and concentration dependence of equilibrium potential of Th <sup>4+</sup>  Th couple was studied.
	Smirnov <i>et al.</i> [3, 4]	Metallic Thorium reduces ThCl <sub>4</sub> to ThCl <sub>2</sub> in LiCl-KCl eutectic melt. Reversible potential of Th <sup>4+</sup>  Th was estimated.
	Martinot [5]	Electrochemical studies of Th <sup>4+</sup> in LiCl-KCl eutectic melt was carried out by transient techniques in temperature range 673-773K; reduction was observed as single step four electrons transfer process without any intermediate step.
	Liu <i>et al.</i> [6]	Electrochemical behavior of Th <sup>4+</sup> was studied at tungsten, aluminum and bismuth electrodes in LiCl-KCl eutectic melt, using transient techniques. Valence of Th was estimated to be +4.
	Cassayre <i>et al.</i> [7]	Electrochemical properties of Th in LiCl-KCl eutectic melt was studied using transient techniques. It was observed that +4 is the stable valence state of Th.
	Chiotti <i>et al.</i> [8]	Experimental evidence for a valence state of three for thorium chloride was investigated by oxidation-

		reduction reaction in molten LiCl-KCl/Zn system.
	Chiotti <i>et al.</i> [9], Dock [10]	Formation of lower valent states $\text{Th}^{2+}$ and $\text{Th}^{3+}$ of thorium was proved in dilute solution of $\text{ThCl}_4$ in LiCl-KCl eutectic melt at 973 K by reaction given in Equation 1.1. Standard electrode potential and activity coefficient of $\text{ThCl}_4$ in LiCl-KCl eutectic melt were estimated by emf technique.
	Chiotti <i>et al.</i> [11], Fuller [12]	$\text{ThCl}_4$ -Th phase diagram was established and only Th and $\text{ThCl}_4$ phases were detected by XRD. No evidence was found for either $\text{ThCl}_2$ or $\text{ThCl}_3$ .
	Chiotti <i>et al.</i> [13]	No evidence for presence of lower valent thorium was found from the experiment conducted in LiCl-KCl eutectic melt. $\text{Th}^{4+}$ was observed to be the only stable ion in the melt.
	Inman <i>et al.</i> [14]	Number of electron exchanged for anodic dissolution of Th was estimated 3.7-4.5 which corresponds to a valence of +4.
	Yang <i>et al.</i> [15]	Valence of Th was estimated to be very close to +4 using emf technique.
	Gruen <i>et al.</i> [16]	No evidence of formation of $\text{Th}^{2+}$ in LiCl-KCl- $\text{ThCl}_4$ melt was found. There was no weight change of Th metal by immersing it in the melt at 773 K for 4 h.
ThCl <sub>4</sub> in molten alkali chlorides MCl (M = Li, Na, K, Cs), NaCl-KCl, NaBr-KBr, NaI-KI	Smirnov <i>et al.</i> [17]	Th valence was estimated to be non-integral values between 4 and 2 at higher temperature.
	Kudyakov <i>et al.</i> [18]	It was established that metallic thorium interacts with $\text{Th}^{4+}$ to form $\text{Th}^{2+}$ in NaCl and NaCl-KCl melt, <i>via</i> the reaction given in Equation 1.1. Temperature dependence of apparent standard electrode potentials of $\text{Th}^{4+} \text{Th}$ and $\text{Th}^{2+} \text{Th}$ was determined.
	Smirnov <i>et al.</i> [19]	Complexing behaviour of Th was studied by potentiometry technique of dilute $\text{ThCl}_4$ and $\text{ThCl}_2$ solutions in alkali chloride melt.
	Smirnov <i>et al.</i> [20]	Electrode potentials of $\text{ThCl}_4$ measured at various concentrations of thorium chloride in temperature range 943-1123 K using direct gravimetric method in NaCl-KCl eutectic melt. Disproportionation of $\text{ThCl}_2$ to Th metal and $\text{ThCl}_4$ begins above 923 K.
	Smirnov <i>et al.</i> [21]	Standard electrode potential of $\text{Th}^{4+} \text{Th}$ and $\text{Th}^{4+} \text{Th}^{2+}$ couples were estimated in the temperature range of 950-1100 K in NaCl-KCl eutectic melt.
	Hayek <i>et al.</i> [22]	$\text{ThCl}_2$ disproportionate to Th metal and $\text{ThCl}_4$ at 943 K.

	Kanashin <i>et al.</i> [23]	Chronopotentiometric reduction of Th <sup>4+</sup> to Th metal proved existence of only +4 as stable oxidation state of thorium in NaCl-KCl eutectic melt.
	Srinivasan <i>et al.</i> [24]	Standard electrode potential of Th <sup>4+</sup>  Th in NaCl-KCl eutectic melt was measured by emf technique in the temperature range 943-1123 K. Analysis of emf data indicated +4 valence state of thorium.
ThCl <sub>4</sub> in molten alkali chlorides MCl (M=Na, K, Cs), NaCl-KCl, NaCl-CsCl, KCl-CsCl	Tumidajski <i>et al.</i> [25]	Standard electrode potential of Th <sup>4+</sup>  Th was measured by emf technique. Slope of linear regression analysis for the concentration term against the cell potential proved a four electron electrode reaction.
Th <sup>4+</sup> in molten LiF-NaF-KF and LiF-CaF <sub>2</sub> medium	Clayton <i>et al.</i> [26]	Reduction of Th <sup>4+</sup> in LiF-NaF-KF at 773K was observed to be four electron transfer reversible process.
	Chamelot <i>et al.</i> [27]	The electrochemical behaviour of the Th <sup>4+</sup>  Th system was examined in molten LiF-CaF <sub>2</sub> medium on Mo, Ni and liq. Cd electrodes. Experimental result showed that ThF <sub>4</sub> was reduced in a single step exchanging 4 electrons.
	Chamelot <i>et al.</i> [28]	At Mo electrode, thorium ions are reduced at a potential of around -1.6 V versus the quasi-reference electrode (QRE) in a single step exchanging four electrons, yielding thorium metal in LiF-CaF <sub>2</sub> eutectic melt.
ThF <sub>4</sub> in LiCl-KCl eutectic melt	Delpéch <i>et al.</i> [29]	Studied electrochemical behaviour of ThF <sub>4</sub> in LiCl-KCl eutectic melt and reported +4 as the only stable oxidation state of thorium.

### 1.3. Thermodynamic studies on Cd-Th alloys: Literature survey

Thermodynamic properties like activity and partial thermodynamic properties of Th in Cd-Th alloys are of interest to understand the stability of these alloys in order to compare with Cd-U and Cd-Pu systems as well as binary systems of Th with some elements such as Co, Fe, Ni etc. Thermodynamic properties of Th alloys have been investigated by various groups [30-43]. So far there is no thermodynamic data reported on Cd-Th intermetallics. This forms one of the objectives of the present thesis described in detail in the next section. Preparation and characterization of different Cd-Th intermediate phases were carried out by various groups

[44-52] and described in Table 1.2. Phase relationship of Cd-Th system investigated by Palenzona [52] is shown in Figure 1.2.

Table 1.2 Literature survey on Cd-Th system.

Reference(s)	Summary
Bates <i>et al.</i> [44]	Solubility of Th in liquid Cd was measured in temperature range of 599-1021 K. Established phase relations and partial phase diagram of Cd-Th system.
Johnson <i>et al.</i> [45]	Solubility of Th in liquid Cd was measured over a temperature range of 598-873 K.
Brown [46]	Investigated crystal structure of $Cd_2Th$ and determined its lattice parameters.
Bruzzone <i>et al.</i> [47]	Determined crystal structure of $Cd_{11}Th$ .
Dutkiewicz <i>et al.</i> [48, 49]	Investigated Cd-Th phase diagram of Cd-rich region.
Fornasini <i>et al.</i> [50]	Investigated crystal structure of $Cd_5Th$ and determined its lattice parameters.
Fornasini <i>et al.</i> [51]	Investigated crystal structure of $Cd_7Th_6$ and determined its lattice parameters.
Palenzona <i>et al.</i> [52]	Characterized six intermetallics (namely, $Cd_{11}Th$ , $Cd_5Th$ , $Cd_{23}Th_6$ , $Cd_3Th$ , $Cd_2Th$ and $CdTh$ ) of Cd-Th system and investigated their crystal structures and lattice constant values. Established Cd-Th phase diagram.

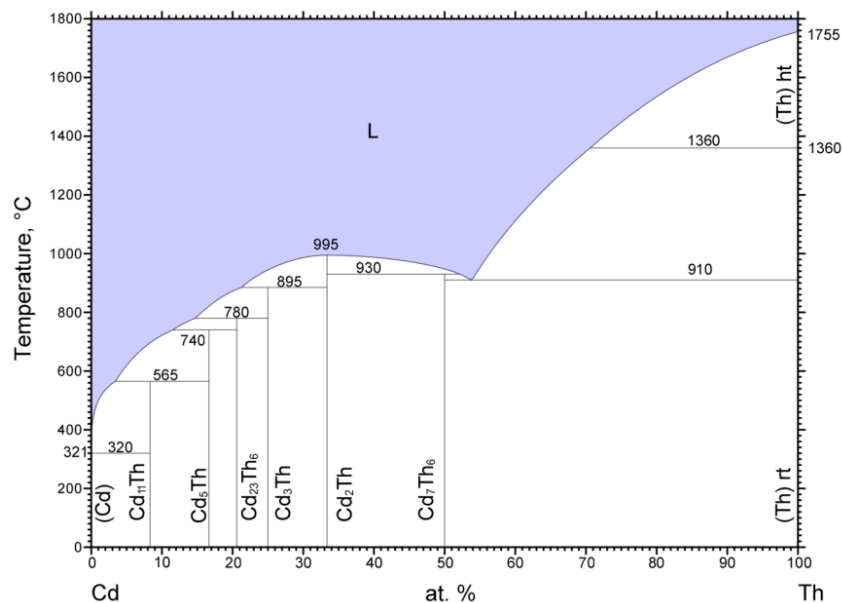


Figure 1.2 Cd-Th binary phase diagram given by Palenzona *et al.*[52].

#### 1.4. Scope of present thesis

Flowchart of scope of work in the present thesis is shown in Figure 1.3. Three major works were taken up which are described below

a) Redox behaviour of  $\text{Th}^{4+}|\text{Th}$  couple in LiCl-KCl eutectic melt using various electrochemical transient techniques and electrochemical impedance spectroscopy (EIS):

Different electrochemical transient techniques such as cyclic voltammetry, chronopotentiometry, square wave voltammetry etc. were employed to estimate electrochemical and thermodynamic properties of  $\text{Th}^{4+}|\text{Th}$  couple. This work is described in detail in Chapter 3. Studies were then extended to anodic dissolution of thorium electrode for calculating theoretical equilibrium potential of  $\text{Th}^{4+}|\text{Th}$  couple, and further its mechanism was investigated by EIS, in which complex impedance data was validated by Kramers-Kronig transforms and fitted using equivalent circuit models. Anodic dissolution of thorium and investigations on EIS are discussed in Chapter 5. Electromotive force measurements were also carried out in LiCl-KCl- $\text{ThCl}_4$  for estimating  $E_{\text{Th}^{4+}|\text{Th}}^\circ$  and  $\Delta_f G_{\text{ThCl}_4}^\circ$ . This data was then compared with literature data as well as those obtained from cyclic voltammetric and chronopotentiometric measurements in the present work and suitable recommendations on  $E_{\text{Th}^{4+}|\text{Th}}^\circ$ ,  $\Delta_f G_{\text{ThCl}_4}^\circ$  and  $\ln \gamma_{\text{ThCl}_4}$  were made. This work is discussed in Chapter 6.

b) Estimation of  $i_0$  of  $\text{Th}^{4+}|\text{Th}$  couple at inert, cadmium and thorium electrodes in LiCl-KCl eutectic melt:  $i_0$  of  $\text{Th}^{4+}|\text{Th}$  couple was estimated at different electrodes employing cathodic and anodic polarization using Tafel and Allen-Hickling methods.  $i_0$  estimated at inert tungsten electrode was compared with that obtained from cyclic voltammograms of LiCl-KCl- $\text{ThCl}_4$ . Conclusions were derived from studying the temperature and composition dependence of  $i_0$  at various electrodes. Similar investigations were carried out at liquid cadmium electrode as well. These investigations are described in Chapter 4.

c) Electromotive force measurements in LiCl-KCl-ThCl<sub>4</sub> electrolyte for determination of  $\Delta_f G_{\text{Cd}_m\text{Th}_n}^\circ$  of Cd-Th intermetallics: Electromotive force measurements were carried out for determining  $\Delta_f G_{\text{Cd}_m\text{Th}_n}^\circ$  of Cd-Th intermetallics and compared with estimations using Miedema model. This work is discussed in Chapter 7.

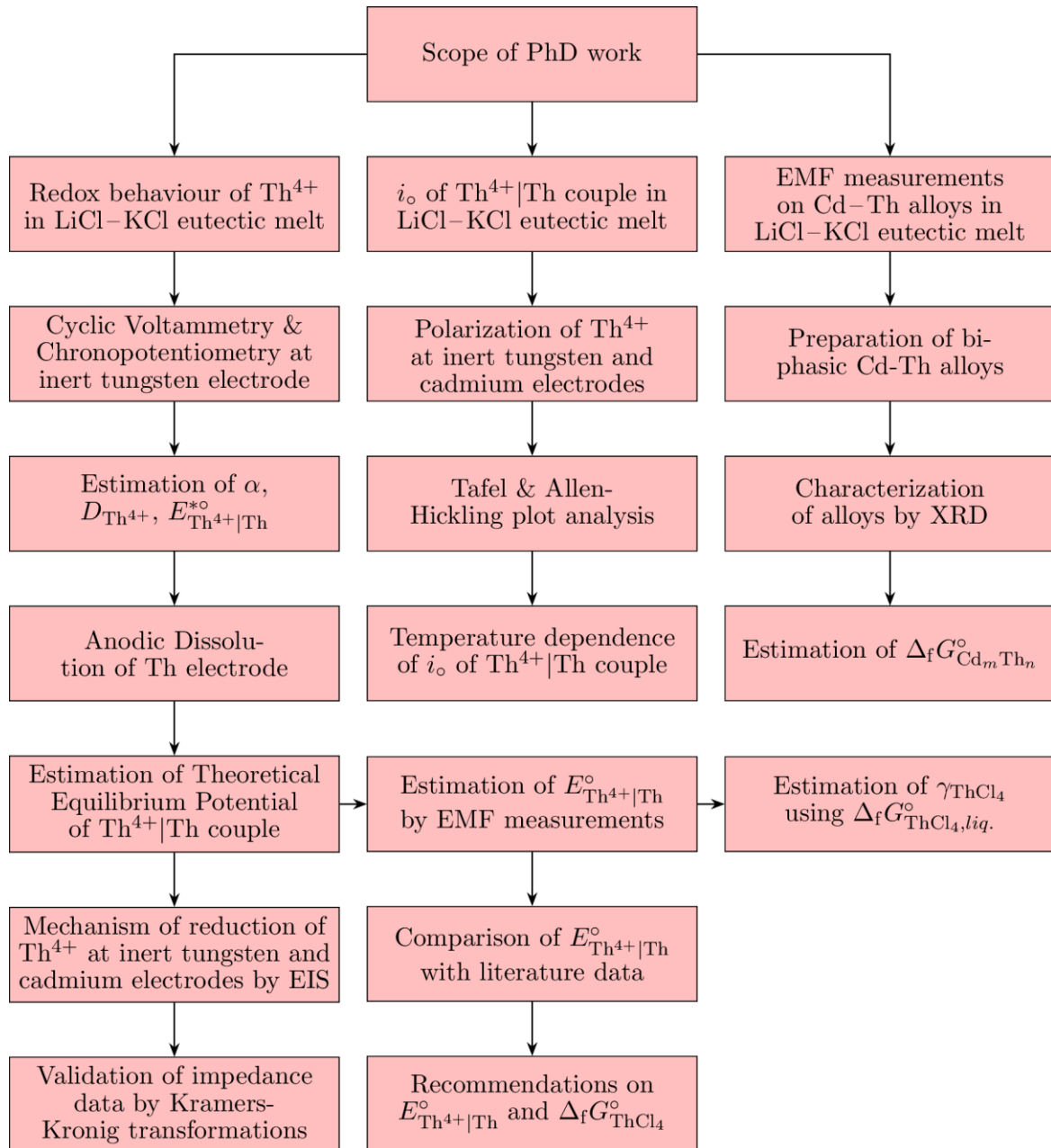


Figure 1.3 Flowchart of scope of work in current PhD thesis.

## CHAPTER 2

### Experimental

This chapter provides brief descriptions of experimental set-up for handling moisture sensitive salts, preparation and purification of LiCl-KCl eutectic mixture, preparation of LiCl-KCl-ThCl<sub>4</sub> electrolyte and fabrication of various types of electrodes for electrochemical studies. Preparation and characterization of Cd-Th alloys are then discussed, and followed by description of cell assembly of electrodes for transient and electromotive force measurements. A brief description of electrochemical methods with relevant governing equations is then provided. The chapter concludes with derivation of governing equations for estimating  $\Delta_f G_{\text{ThCl}_4}^\circ$  and  $\Delta_f G_{\text{Cd}_m\text{Th}_n}^\circ$  intermetallics by electromotive force measurements.

#### 2.1 Argon atmosphere glove box set-up

An argon atmosphere glove box operated between +20 to +40 mm of water column (*wrt* ambient) installed in our radioactive laboratory was used to handle moisture sensitive LiCl salt and high pure metals such as Th and Cd and Cd-Th alloys. A layout and photograph of the argon atmosphere glove box used for carrying out all experiments presented in the thesis are shown by Figs. 2.1 and 2.2, respectively [53].

Glove box set up consisted of pressure control system comprising of photohelic gauge and normally closed solenoid valves, recirculation system comprising of purification tower (molecular sieves + copper de-oxo catalyst) and side-channel recirculation blower, and gas analyzer system comprising of argon sampling pump and multi-trace gas analyzer for measuring oxygen and dew point in recirculating argon. It was supported by an independent feed and bleed system for controlling pressure between +20 to +40 mm of water column (positive *wrt* ambient).

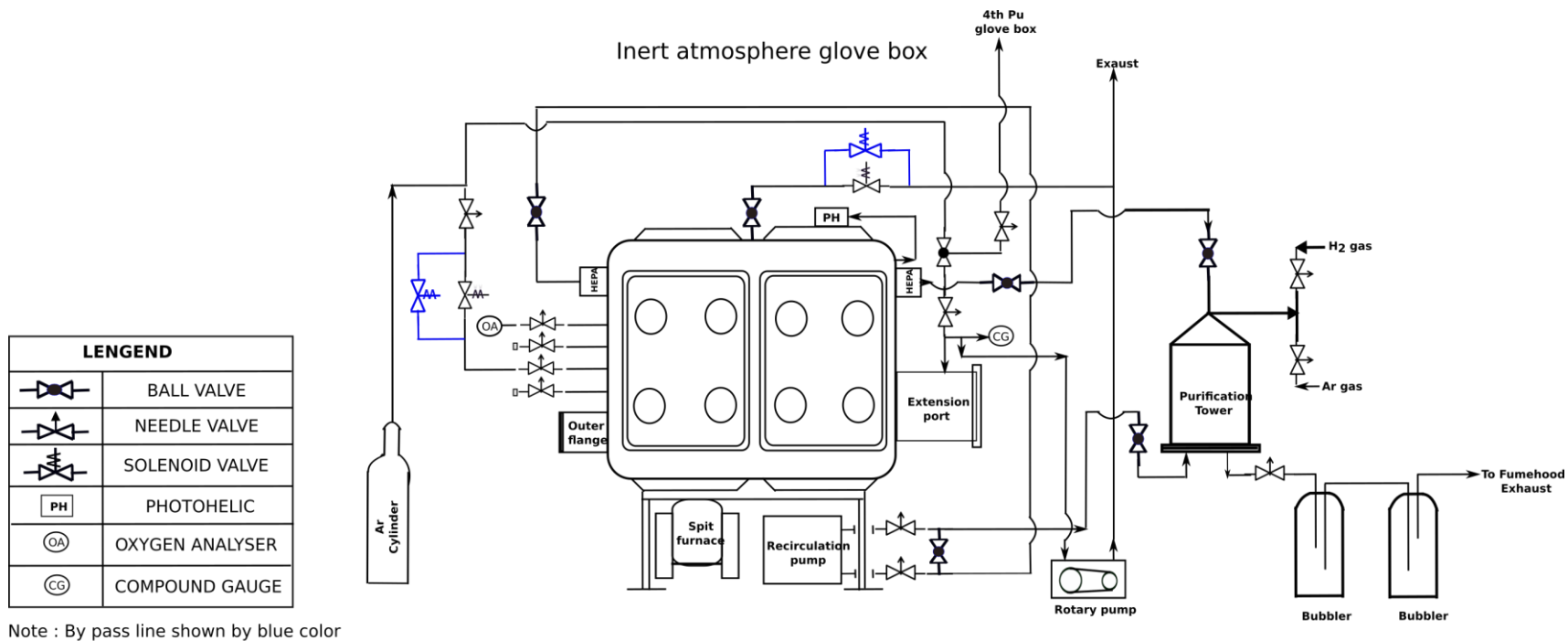


Figure 2.1 The layout of argon atmosphere glove box [53].



*Figure 2.2 Photograph of argon atmosphere glove box used for carrying out experiments.*

Internal peripherals of glove box consisted of storage vessels, electrode racks, chemical storage units, pit-type furnace and electrical feedthroughs for connecting weighing module, stirrer unit and furnace. The furnace was controlled by PID (proportional integral derivative) temperature controller kept outside glove box. All operations inside the glove box were carried out by butyl-rubber gauntlets on 6-inch glove port sealed by tightly fitted over it by neoprene o-ring. The glove box was also supported with an extension port assembly for taking materials in and out of the glove box. Since no plutonium based materials were handled in this box, it was not necessary to take the materials out in sealed PVC bags. The transfer port door was always kept in sealed condition irrespective of whether any material transfer was done. Before it was opened for any transfer in operation, the extension port was closed and alternately pressurized and evacuated multiple times to improve purity of volume of air locked inside the extension port. A similar procedure was followed for material transfer out operation. At no stage during the transfer in/out operation was the argon atmosphere of glove box was in direct contact with the ambient.

## **2.2 Chemicals and preparation of electrolytes**

### **2.2.1 Chemicals**

All chemicals used in the present measurements were of analytical grade. Anhydrous lithium chloride (>98%) was obtained from Sigma-Aldrich (CAS 7447-41-8) and anhydrous potassium chloride was obtained from Alfa-Aesar (CAS 7447-40-7).  $\text{CdCl}_2$  was obtained from Acros Organics (99%). Cadmium (>99.95 %) shots ( $\approx 3$  mm dia.) were obtained from Arora Matthey, Kolkata. Anhydrous  $\text{AgCl}$  was obtained from Sigma-Aldrich (>99.9%). The ingot (>99.5%) was obtained from BARC, Mumbai, purity of which was checked by ICP-MS, discussed later in this chapter. It was polished by sand paper and diamond coated file and cleaned by dilute acid and acetone before use.

### **2.2.2 Preparation and purification of LiCl-KCl eutectic melt**

Measurements reported in this work were carried out in LiCl-KCl eutectic melt. As per the phase diagram of LiCl-KCl binary system, the eutectic composition and temperature are known at 58.5 mol% LiCl and 625 K, respectively. Anhydrous LiCl (Sigma-Aldrich) and KCl (Alfa-Aesar) were mixed in eutectic ratio and vacuum dried at 420 K for about 120 h. It was then taken in 100 g batches and loaded in recrystallized alumina crucible that was then placed into a bottom-end closed quartz vessel with a PTFE Teflon flange. The vessel was sealed from the top by another teflon flange with neoprene O-ring gasket. The top flange had provision for inserting  $\frac{1}{4}$ " quartz tubes through veeco couplings also made of teflon. One veeco was used for connecting it to inlet chlorine gas line, and the other was used for the outlet stream. The third veeco was sealed by another quartz tube closed by glass stopper in order to use it in cases when either of the inlet and outlet tubes was choked. The outlet tube was connected to NaOH scrubber for neutralization of excess chlorine gas. The complete set-up was made inside a FRP fume hood having an exhaust system for chlorine. A chlorine

detector with an alarm system was installed near the set-up to display chlorine level near and around the set-up. Photograph of chlorination set-up is shown in Figure 2.3.



*Figure 2.3 Photograph of chlorination set-up made of quartz vessel and teflon flanges.*

Presence of moisture in melt deteriorates its purity, and may lead to formation of electroactive species such as hydroxides and oxides that may chemically react with other chlorides. LiCl undergoes high temperature hydrolysis to form LiOH and leads to large residual current in the potential range within which electrorefining operation is carried out. In order to remove such impurities, HCl or chlorine gas has been used in the past to purify the eutectic melt [54]. In pyroprocessing laboratory, purification of eutectic mixture is carried out by chlorine gas. The process of chlorination involved heating the eutectic mixture and melting it under argon atmosphere and bubbling chlorine gas (Specification of chlorine: as per IS: 646-1986) at a flow rate 10-25 ml/min into it at 773 K for 1 h to drive off any residual moisture present in the melt. The eutectic melt after chlorine bubbling was cooled to room temperature under argon atmosphere, and then taken inside glove box and stored. In a similar manner, several batches of chlorinated LiCl-KCl eutectic melt were prepared. Impurity analysis in chlorinated LiCl-KCl eutectic was carried out by inductively coupled plasma atomic emission spectrometry (ICP-AES), which is shown in Table 2.1.

### 2.2.3 Preparation of LiCl-KCl-ThCl<sub>4</sub> electrolyte

LiCl-KCl-ThCl<sub>4</sub> electrolyte was prepared by equilibration of cadmium chloride (CdCl<sub>2</sub>) and thorium slices in LiCl-KCl eutectic melt at 773 K (Equation 2.1) in argon atmosphere glove box. Standard Gibbs energy of the reaction at 773 K with ThCl<sub>4</sub> in solid reference state is -413.2 kJ mol<sup>-1</sup>, when ThCl<sub>4</sub> is in liquid reference state, Gibbs energy of reaction is -403.3 kJ mol<sup>-1</sup>.



Equilibration was carried out for about 30 h at 773 K. After completion of equilibrium step, LiCl-KCl-ThCl<sub>4</sub> was poured into a fused silica rectangular dish and stored in glove box as stock solution. From the stock solution prepared, dilute solutions of ThCl<sub>4</sub> in LiCl-KCl eutectic melt were prepared for different studies. Concentration of ThCl<sub>4</sub> ranged from 0.3 to 1.55 wt%. LiCl-KCl-ThCl<sub>4</sub> salt was characterized by XRD. Sample for XRD characterization was prepared by grinding the salt in a mortar-pestle and a one-end closed capillary tube (Borokapillaren, BGCT 1.0, I.D.: 1.0 mm, thickness: 0.01 mm) was filled with salt powder upto 25mm height. Top of the capillary was broken and sealed with molten wax. XRD pattern of LiCl-KCl-ThCl<sub>4</sub> electrolyte recorded by X-ray powder diffraction (XRD) using Cu K<sub>α</sub> radiation (Panalytical X'Pert Pro) is shown in Figure 2.4. Bragg peaks were identified to be LiCl, KCl and ThCl<sub>4</sub> phases present in the salt [55, 56]. Appearance of broad peak in 2θ region of 10-30° may be due to capillary glass used in recording XRD. Impurity analysis in LiCl-KCl-ThCl<sub>4</sub> salt was carried out by ICP-MS technique and values are tabulated in Table 2.1.

Table 2.1 Impurity analysis in chlorinated LiCl-KCl (sample weight: 475.5 mg) eutectic by ICP-AES and LiCl-KCl-ThCl<sub>4</sub> salt by ICP-MS technique (sample weight: 70 mg).

LiCl-KCl (μg/g)	Cr	Cu	Fe	Mo	Ni	Zn	Sn			
	42	42	42	42	63	84	42			
LiCl-KCl-ThCl <sub>4</sub> (μg/g)	Mo	Zr	Cd	Sn	Pb	Y	La	Ce	U	
	22	1	5	14	2	<1	<1	<1	<1	

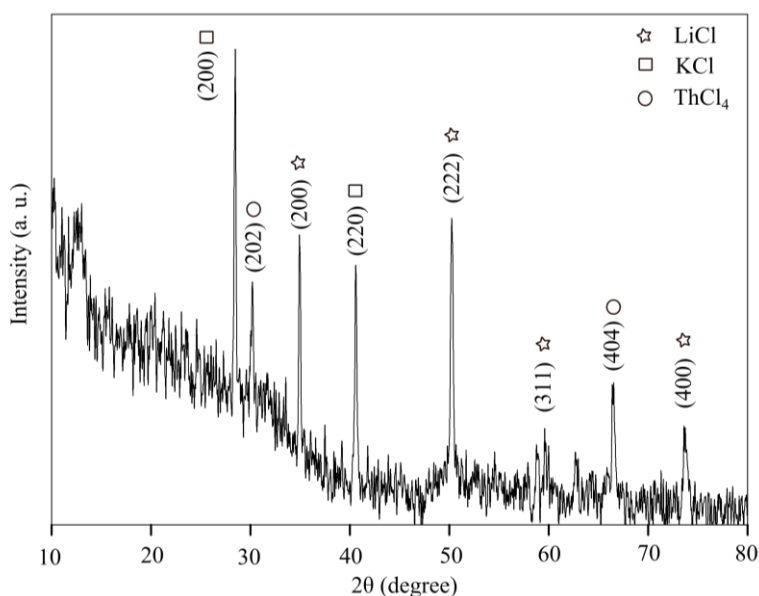


Figure 2.4 XRD pattern of LiCl-KCl-ThCl<sub>4</sub> electrolyte (Numbers in parenthesis correspond to miller indices).

## 2.2.4 Preparation of LiCl-KCl-AgCl electrolyte

LiCl-KCl-AgCl electrolyte for Ag<sup>+</sup>|Ag reference electrode was prepared by dissolving 1 g of AgCl in 100 g of chlorinated LiCl-KCl eutectic melt by bubbling Cl<sub>2</sub> at 773 K for 3 h. The salt was cooled to room temperature under Argon cover and stored in glove box.

## 2.2.5 Estimation of Th, Cd and Ag in LiCl-KCl eutectic melt

Th in LiCl-KCl-ThCl<sub>4</sub> electrolyte was estimated using HPLC [57]. Concentration of cadmium in the salt was estimated by inductively coupled plasma-mass spectrometry (ICP-MS) (Spectro MS, MSS001). Cadmium was estimated to be 29 μg/g of LiCl-KCl eutectic. Estimation of silver in LiCl-KCl-AgCl electrolyte was carried out by ICP-AES [58]. Ag concentration in salt was estimated to be 0.89 wt%.

## 2.3 Cd-Th alloys

### 2.3.1 Preparation of Cd-Th alloys

Cd-Th alloys were prepared by equilibration of thin Th slices and Cd shots at 773 K for 300 h in argon atmosphere. Impurity analysis in Th and Cd were carried out by inductively coupled plasma optical emission spectrometry (ICP-OES), inductively coupled plasma mass spectrometry (ICP-MS) and atomic emission spectrometry (AAS) techniques before preparation of Cd-Th alloys. Results of impurity analysis are given in Table 2.2. Impurity level in Th metal (Table 2.2) is similar to impurity values reported by Skelton *et al.* [36] for thermodynamic studies of Co-Th alloys. XRD patterns of Th and Cd recorded by X-ray diffraction (XRD) using Cu  $K_{\alpha}$  radiation (Panalytical X'Pert Pro) are shown in Figure 2.5. Very small intensity Bragg peak of  $\text{ThO}_2$  was appeared in XRD pattern of Th (Figure 2.5a), due to partially oxidized Th surface. All Bragg peaks in Figure 2.5b were found to be due to Cd phase. Stoichiometric amount of Th slices and Cd shots were loaded in recrystallized alumina crucible which was kept inside a specially designed leak tight high pure iron vessel. Iron vessel was then loaded into an electrochemical cell and heated to 773 K for 300 h. Weight loss of alloys after equilibration process was <5wt%. This weight loss of Cd-Th alloys was attributed to vaporization of Cd inside iron vessel during equilibration. Weight loss during melting, after polishing of alloy surface by diamond filing for each alloy is tabulated in Table 2.3. Pure iron vessel and a Cd-Th alloy are shown in Figure 2.6.

Table 2.2 Impurity analysis of Cd by ICP-OES and AAS techniques (sample weight: 220.22 mg) [59] and of Th by ICP-MS (sample weight: 27 mg).

Cd	Impurities	Cr	Cu	Fe	Ni	Mo	Sn	Zn	
	AAS + ICP-OES ( $\mu\text{g/g}$ )	11	11	11	57	45	45	91	
Th	Impurities	Mg	Al	Zn	Pb	Ba	Sr	Ag	U
	ICP-MS ( $\mu\text{g/g}$ )	382	73	1382	31	117	64	1	61

Table 2.3 Weight balance of Cd-Th alloys before and after equilibration.

Alloy	Wt. of Th (g)	Wt. of Cd (g)	Total wt. (g)		Wt. loss (%)	Wt. after polishing (g)	Final Wt. loss (%)
			Before equilibration	After equilibration			
Cd+Cd <sub>11</sub> Th	0.756	4.379	5.135	4.913	4.3	4.620	5.9
Cd <sub>11</sub> Th+Cd <sub>5</sub> Th	1.895	5.205	7.100	6.800	4.2	6.400	5.9
Cd <sub>5</sub> Th+Cd <sub>23</sub> Th <sub>6</sub>	2.520	5.205	7.725	7.563	2.1	7.218	4.5
Cd <sub>23</sub> Th+Cd <sub>3</sub> Th	2.781	4.511	7.292	7.143	2.0	6.881	3.7

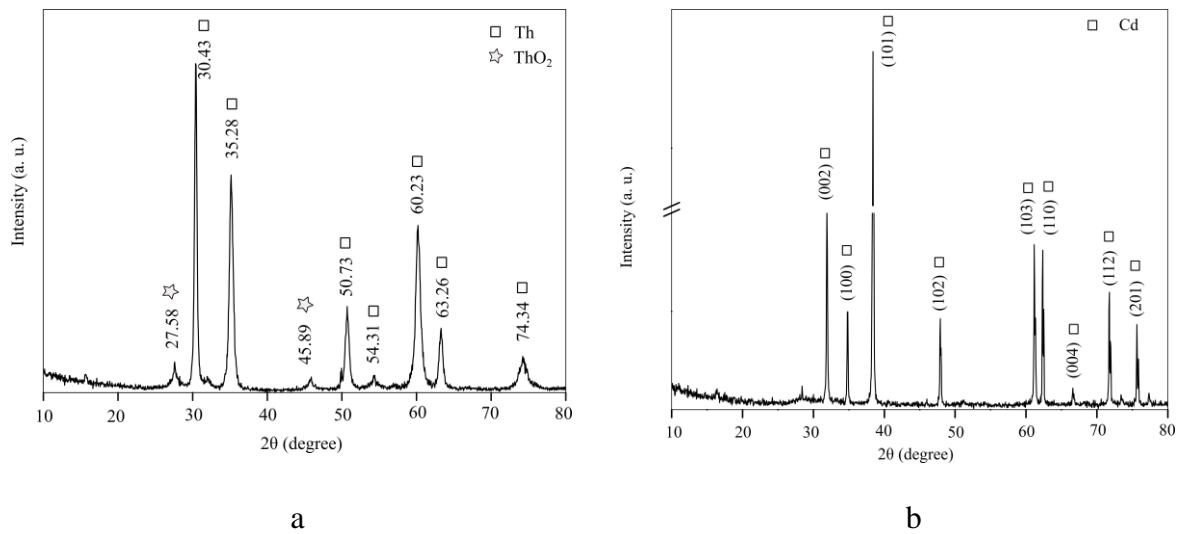


Figure 2.5 XRD pattern of (a) Th and (b) Cd metals (Numbers in parenthesis correspond to miller indices).

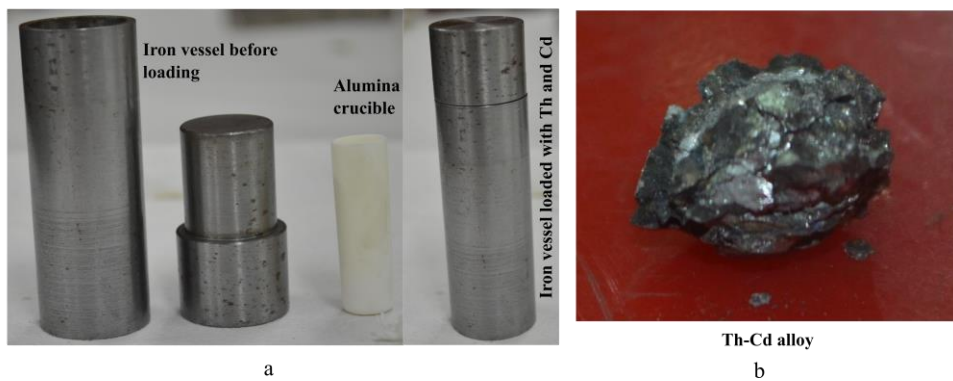


Figure 2.6 Photographs of (a) iron vessel before and after loading with Th and Cd, (b) Cd-Th alloy after cleaning by diamond filing.

### 2.3.2 Phase characterization of Cd-Th alloys

Phase characterization of Cd-Th alloys were carried out using X-ray powder diffractometer (M/s Inel, France) with Cu  $K_{\alpha}$  radiation and XRD patterns are shown in Figure 2.7. Samples of Cd-Th alloys for XRD characterization were prepared by making fine powder of alloys by grinding them in mortar-pestle inside argon atmosphere glove box and then filled in one-end closed capillary tube (Borokapillaren, BGCT 1.0, I.D.: 1.0 mm, thickness: 0.01 mm) upto 25mm height. Top of the capillary was broken and sealed with molten wax. Respective Bragg peaks for  $Cd_{11}Th$ ,  $Cd_5Th$ ,  $Cd_{23}Th_6$  and  $Cd_3Th$  phases are shown in the figures [52]

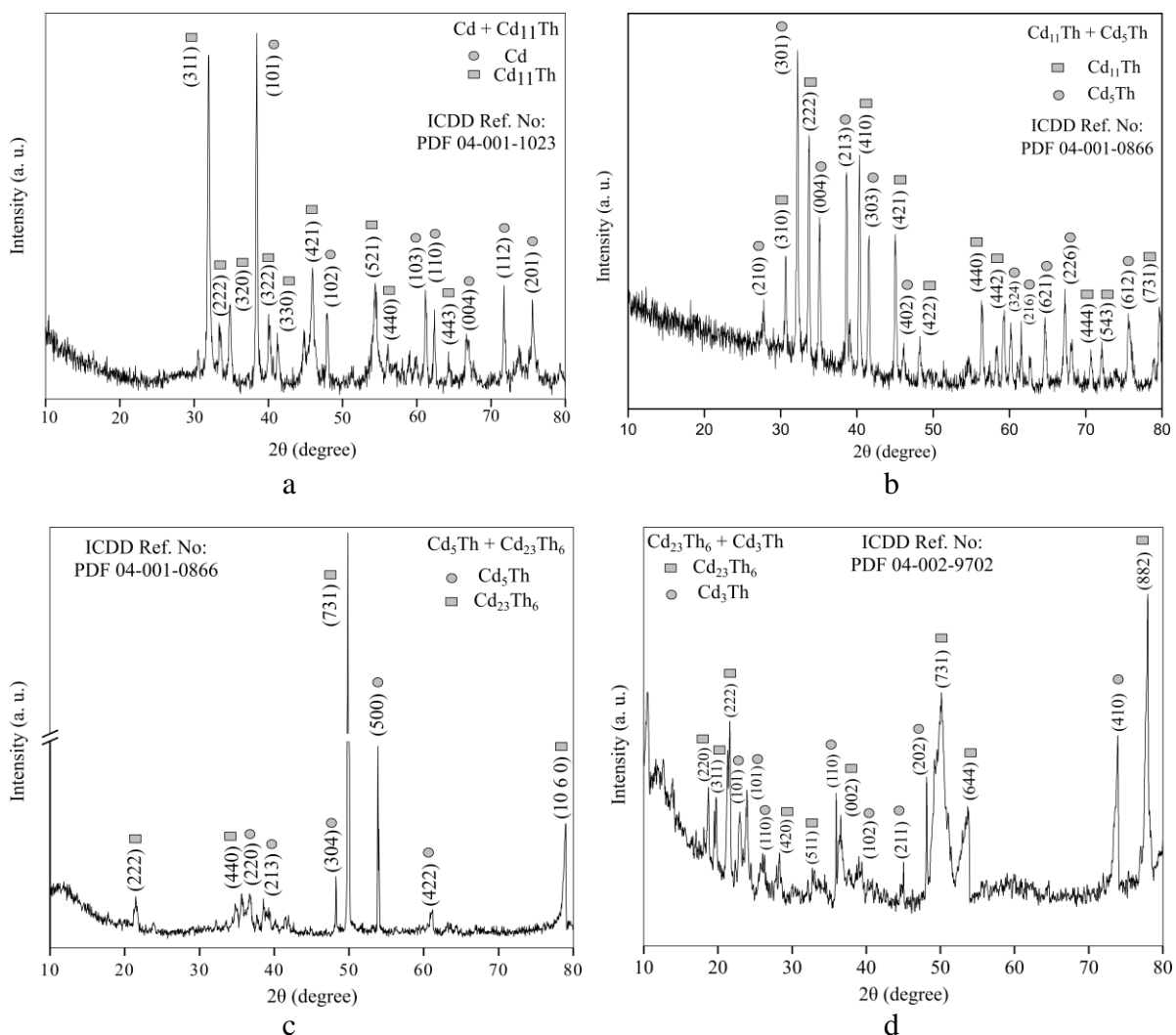


Figure 2.7 Powder XRD patterns of (a) Cd +  $Cd_{11}Th$ , (b)  $Cd_{11}Th$  +  $Cd_5Th$ , (c)  $Cd_5Th$  +  $Cd_{23}Th_6$ , (d)  $Cd_{23}Th_6$  +  $Cd_3Th$  two-phase alloys, Step size:  $0.05^\circ$  (Numbers in parenthesis correspond to miller indices).

## 2.4 Electrodes and cell assembly

### 2.4.1 Electrodes for transient electrochemical measurements

1.5 mm dia. inert tungsten wire, liquid cadmium and thorium were used as working electrodes in transient electrochemical measurements. The electrode (shown in Figure 2.8) was prepared by winding 0.5 mm dia. Ta (>99.95%) wire around Th slice and crimping the wire to a SS-304L rod for electrical connections.



*Figure 2.8 Thorium electrode used in the present work.*

Liquid cadmium electrode was designed and fabricated in our laboratory and shown in Figure 2.9. It consisted of a SS-430 perforated basket (OD: 22 mm, ID: 19 mm, Height: 23 mm) with an alumina crucible (OD: 16 mm, ID: 14 mm, Height: 20 mm, Tempsens Instruments make) inside it. A 2 mm dia. SS-430 wire was welded to the perforated basket at diametrically opposite ends. The other end of the wires was welded to a SS-304 tube (OD: 6 mm, ID: 4 mm). 1 mm dia. Mo wire (> 99.9 %) was insulated with an alumina sleeve (OD: 3 mm, ID: 2 mm, Ants Ceramics make) leaving 2-4 mm at the bottom for electrical connection in Cadmium. The top end was sealed with a teflon plug. The top end of Mo wire was left uninsulated for electrical connection. The cadmium pool of the electrode was prepared as given below. About 500 mg of cadmium shots was initially taken in the alumina crucible of the electrode assembly. The perforated basket containing the alumina crucible was then immersed in blank LiCl-KCl eutectic at 773 K. Cadmium shots were regularly added in the

alumina crucible after the electrode assembly was taken out from the molten salt, which was repeated several times until a shining cadmium surface was seen at the top of the alumina crucible as shown in Figure 2.9. The electrode area of the cadmium surface was calculated from the area of the annular gap between the alumina sleeve and the alumina crucible. This was found to be  $1.47 \text{ cm}^2$ .

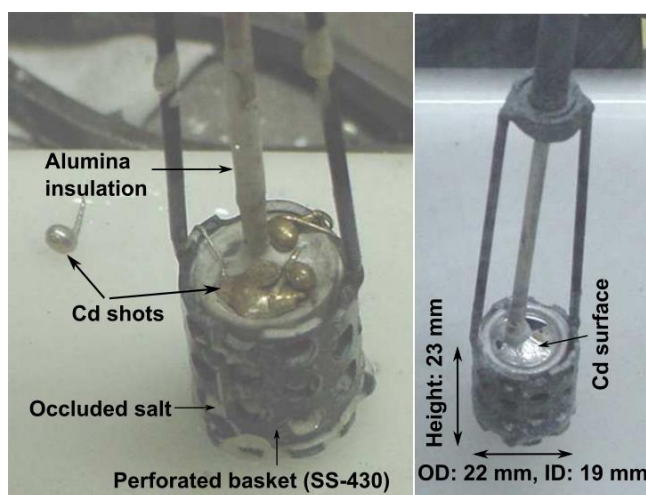


Figure 2.9 Liquid cadmium electrode.

8 mm dia. high density graphite rod was used as a counter electrode.  $\text{Ag}^+|\text{Ag}$  was used as the reference electrode. Reference electrode was prepared using a one end closed 6.0 mm diameter quartz tube with a thin walled bulb at the bottom. Top end of the quartz tube was sealed by PTFE teflon plug and a high purity Ag wire ( $>99.9\%$ , 1.5 mm diameter) was inserted inside the quartz tube for electrical connection through the hole in the teflon plug which was then sealed by adhesive (Araldite). This quartz tube with Ag wire was taken inside glove box where LiCl-KCl-AgCl salt powder was loaded inside it. All potential reported in this thesis were recorded with respect to this reference electrode.

#### 2.4.2 Electrodes for electromotive force measurements

Th as working electrode and  $\text{Ag}^+|\text{Ag}$  as reference electrode were used for galvanic cell emf measurements on  $\text{ThCl}_4$  in LiCl-KCl eutectic melt. Photographs of electrodes used for measurements are shown in Figure 2.10. Th and Cd-Th two-phase alloy were used as

electrodes for estimation of Gibbs energy of formation Cd-Th alloys by galvanic cell emf measurements. These electrodes were prepared by loading Th metal and Cd-Th two phase alloy into two tantalum cups (dimension: 6 mm dia. and 15 mm height) separately and these tantalum cups were crimped with tantalum wire of 1.5 mm dia. One tantalum crucible was loaded with 1 g of thorium slice and other with 1g of Cd-Th two-phase alloy. Tantalum wire was insulated from electrochemical cell by alumina sleeve. Electrode assembly used in the emf measurements is shown in Figure 2.11.



*Figure 2.10 Electrode assembly used in emf study of ThCl<sub>4</sub> in LiCl-KCl eutectic melt.*



*Figure 2.11 Electrode assembly used in emf study of Cd-Th alloys.*

## **2.5 Measurement methodology**

### **2.5.1 Transient techniques and EIS study**

Electrochemical measurements of  $\text{LiCl-KCl-ThCl}_4$  were carried out using a three electrode cell assembly consisted of an SS-304 electrochemical vessel and a top knife-edge flange (CF-63, M.S. Enterprises, Secunderabad) having veeco couplings used for inserting electrodes and thermocouple. The bottom vessel (SS-304, 2" dia, Sch 10) consisted of a knife-edge flange welded at the top and closed at the bottom end using a bottom-end cup (SS-304). Schematic of the electrochemical cell assembly is shown in Figure 2.12. Vacuum degassing of the cell was done to remove moisture inside the cell prior to electrochemical measurements. High density graphite ( $1.85 \text{ g cm}^{-3}$ ) electrodes were loaded inside electrochemical cell through three 1/8" veecos and 1/4" veecos were closed by 6 mm dia. teflon rod. Then the electrochemical cell was placed inside a pit type resistance heating furnace and was connected to a rotary vacuum pump. After vacuum degassing of the cell it was cooled and taken inside glove box.

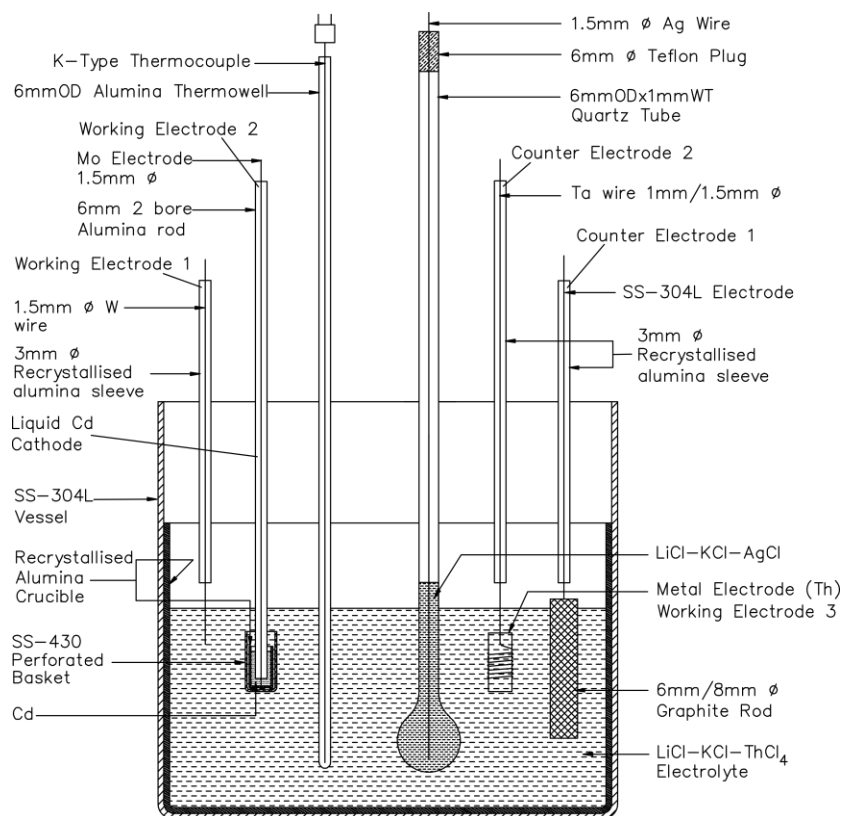


Figure 2.12 Schematic of electrochemical cell assembly.

Electrochemical cell was loaded with electrolyte salt, reference electrode; counter electrode and working electrode inside argon atmosphere glove box. A K-type thermocouple (3 mm dia., Precision Scientific, Chennai) in an alumina thermowell (OD: 6 mm, Wall thickness:1 mm, Ants Ceramics make) was used to monitor temperature of melt, the uncertainty in temperature measurement was  $\pm 1$  K. Electrochemical cell was then taken out from the glove box and placed inside a pit-type muffle furnace. The cell was heated in a vertical furnace to desired temperature. Temperature was controlled by a PID (proportional integral derivative) temperature controller (make-Bonics Systems, Chennai). Argon gas was passed through a calcium getter at 823 K before purging through electrochemical cell. A photograph of the cell used in present is shown in Figure 2.13.



*Figure 2.13 Photograph of electrochemical cell loaded with electrodes.*

Transient electrochemical techniques like cyclic voltammetry, chronopotentiometry, squarewave voltammetry and polarization measurements were carried out using PGSTAT AUTOLAB302N (Eco Chemie, Netherlands) with IF030 interface. Data were processed using GPES 4.9 software and FRA 4.9 software.

### **2.5.2 Polarization technique**

Polarization phenomena typically results in a change in the potential of an electrode during electrolysis. Polarization can occur in three ways: Concentration polarization, Resistance polarization and Activation polarization. At equilibrium potential net flow of current is zero because rate of oxidation and reduction processes of any electrochemical system are equal at this potential. When the electrode potential is shifted to either side of equilibrium potential, there is a net flow of current, because one of the two processes dominating the other. If the electrochemical system is facile in kinetics (Reversible) then there is large flow of current in negligible change of potential. For electrochemical systems with slow electrode kinetics minimum flow of current is observed for appreciable quantity of potential change. The extra potential applied over equilibrium potential is called overpotential ( $\eta$ ). When applied overpotential is due to slow electrode kinetics of the system, it is called activation overpotential. Polarization experiments are carried out by applying overpotential in the range

of 0-200mV for a specific time. For each polarization scan resulting current at that specific time is recorded. Current-overpotential relationship in polarisation study is given by Butler-Volmer Equation 2.2 [60].

$$i = i_o \left[ e^{\frac{n\alpha F\eta}{RT}} - e^{-\frac{n(1-\alpha)F\eta}{RT}} \right] \quad (2.2)$$

At large cathodic and anodic overpotentials ( $\eta$ ), Butler-Volmer Equation can be simplified to Equations 2.3 and 2.4 respectively, which are called Tafel Equations.

$$\eta = \frac{RT}{n\alpha F} \ln i_o - \frac{RT}{n\alpha F} \ln i \quad (2.3)$$

$$\eta = -\frac{RT}{(1-\alpha)nF} \ln i_o + \frac{RT}{(1-\alpha)nF} \ln i \quad (2.4)$$

Plot of  $\eta$  versus  $\ln i$  is called Tafel Plot. Intercept and slope values are called Tafel constants.

Tafel constants  $a_{\text{Tafel}}$  and  $b_{\text{Tafel}}$  for cathodic overpotentials are given by,

$$a_{\text{Tafel}} = \frac{RT}{n\alpha F} \ln i_o \quad \text{and} \quad b_{\text{Tafel}} = -\frac{RT}{n\alpha F}$$

Tafel constants  $a_{\text{Tafel}}$  and  $b_{\text{Tafel}}$  for anodic overpotentials are given by,

$$a_{\text{Tafel}} = -\frac{RT}{(1-\alpha)nF} \ln i_o \quad \text{and} \quad b_{\text{Tafel}} = \frac{RT}{(1-\alpha)nF}$$

Good Tafel relationship is observed when electrode kinetics is sluggish and significant activation over potential is required. For electrode reactions that are not totally irreversible polarization data at lower overpotential values are best fitted using Allen-Hickling Equation 2.5 [60]. The slope of Equation 2.5 is represented as  $b_{\text{Allen-Hickling}}$  in present work.

$$\ln \left( \frac{i}{1 - e^{-\frac{nF}{RT}\eta}} \right) = \ln i_o - \frac{n\alpha F}{RT} \eta \quad (2.5)$$

Errors in the Tafel and Allen-Hickling constants were obtained from linear fit of experimental data using Equations 2.3, 2.4 and 2.5. Error in  $\ln i_0$  was estimated from standard error propagation methods discussed by Taylor [61]. For example, using the expression for Tafel constant  $a_{\text{Tafel}}$ , error in  $\ln i_0$  is given by,

$$\delta \ln i_0 = C \delta a_{\text{Tafel}} \quad (2.6)$$

Where,  $C$  is a constant given by  $\frac{n\alpha F}{RT}$  and  $\frac{(1-\alpha)nF}{RT}$  for cathodic and anodic polarization data, respectively. In case of Allen-Hickling equation (Equation 2.5), error in  $\ln i_0$  was

directly obtained from the linear fit of  $\ln \left( \frac{i}{1 - e^{-\frac{nF}{RT}\eta}} \right)$  vs.  $\eta$  profile.

Polarization measurements were carried out to estimate the exchange current density of thorium at inert and liquid cadmium (cathodic polarization) and for thorium electrode (anodic polarization). In all these measurements, graphite rod was chosen as the counter electrode. Cathodic or anodic polarization of working electrode consisted of applying a constant applied potential  $E_{i=1}$  for  $t=30$  s and recording  $i$  versus  $t$  curve.  $i$  at  $t=30$  s was recorded against applied potential  $E_{i=1}$ . This procedure was repeated for other applied potentials,  $E_{i=2}, E_{i=3}$ ;  $i$  versus  $E$  was then plotted to obtain the polarization curve for a particular working electrode. It was ensured that the open-circuit potential of the working electrode remained constant for every polarization run. This was achieved by having a waiting period between the polarization runs or by carrying out several cyclic voltammetric runs at high scan rates to clean the inert electrode of any electrodeposited thorium. Similar electrochemical cell as shown in Figure 2.12 was used for polarization experiments.

### 2.5.3 Electrochemical impedance spectroscopy

EIS was carried out by applying various DC potentials at inert tungsten, liquid cadmium and metallic thorium electrodes using a perturbation signal of amplitude 10 mV in the frequency

range 10 Hz-10 kHz. Complex impedance plots were recorded in the temperature range 698-798 K. Complex impedance data were also validated by Kramers-Kronig transforms using Boukamp's freely available KK-Windows program [62] based on his earlier works [63, 64]. Validation is performed by calculating the imaginary part of the impedance from experimentally measured real part and then comparing it with experimentally measured imaginary part. Similarly, real part of impedance can be calculated from imaginary part and comparing it with real part that is experimentally measured. This dependence between the real  $Z_{\text{Re}}(\omega)$  and imaginary  $Z_{\text{Im}}(\omega)$  parts of impedance are given by Kramers-Kronig transform integrals and are given by Equation 2.7 and 2.8.

$$Z_{\text{Re}}(\omega) = R_{\infty} + \frac{2}{\pi} \int_0^{\infty} \frac{xZ_{\text{Im}}(x) - \omega Z_{\text{Im}}(\omega)}{x^2 - \omega^2} dx \quad (2.7)$$

$$Z_{\text{Im}}(\omega) = \frac{2\omega}{\pi} \int_0^{\infty} \frac{Z_{\text{Re}}(x) - Z_{\text{Re}}(\omega)}{x^2 - \omega^2} dx \quad (2.8)$$

Deviation from Kramers-Kronig compliance can be examined from the plot of real and imaginary residuals ( $\Delta_{\text{Re},i}$  and  $\Delta_{\text{Im},i}$ ) *versus* logarithm of angular frequency given by Equations 2.9 and 2.10.

$$\Delta_{\text{Re},i} = \frac{Z_{\text{Re},i} - Z_{\text{Re}}(\omega_i)}{|Z(\omega_i)|} \quad (2.9)$$

$$\Delta_{\text{Im},i} = \frac{Z_{\text{Im},i} - Z_{\text{Im}}(\omega_i)}{|Z(\omega_i)|} \quad (2.10)$$

A random distribution along frequency axis and low pseudo  $\chi^2$  value are indicative of compliance of K-K transforms. Complex impedance plots were also fitted using non-linear least squares method to an equivalent circuit model comprising of electrolyte resistance  $R_s$ , charge transfer resistance  $R_{ct}$  and constant phase elements  $Q_1$  and  $Q_2$  as shown in Figure 2.14. The frequency range of fitting was 10 Hz-10 kHz for inert tungsten and 10 Hz-5 kHz for

liquid cadmium and thorium electrodes. Admittance  $Y$  of constant phase element is given by the following expression [65]:

$$Y = Y_Q \omega^m \cos \frac{m\pi}{2} + j Y_Q \omega^m \sin \frac{m\pi}{2} \quad (2.11)$$

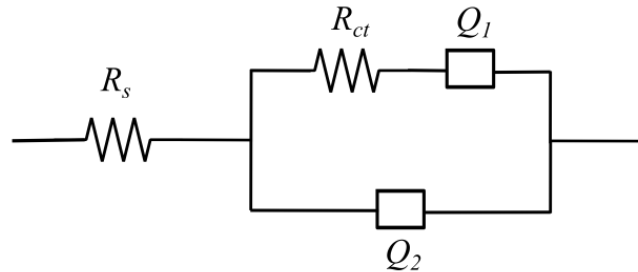


Figure 2.14 Equivalent circuit used for fitting complex impedance data for cathodic polarization of thorium at inert tungsten and cadmium electrodes and anodic polarization of metallic thorium electrode.

CPE is a general equivalent circuit component that can represent a resistor, capacitor or Warburg diffusion based on the value of  $m$ . For  $m=0$  and 1, it represents a resistor and capacitor, respectively whereas, it represents Warburg diffusion for  $m=0.5$ . For  $m=-1$ , it represents an inductance. EIS measurements were carried out in electrochemical cell as shown in Figure 2.12.

## 2.5.4 Electromotive force measurements

### 2.5.4.1 emf measurement of $\text{ThCl}_4$ in LiCl-KCl eutectic melt

Electromotive force measurement study was carried out on  $\text{ThCl}_4$  in LiCl-KCl eutectic melt in the temperature range 673-798 K using molten salt galvanic cell. Schematic of the galvanic cell is given in Figure 2.15. Standard electrode potential and partial molar Gibbs energy of formation of  $\text{ThCl}_4$  in LiCl-KCl eutectic melt was calculated from emf data. Equilibrium potential  $E_{\text{Th}^{4+}|\text{Th}}^{\text{eq}}$  between  $\text{Th}^{4+}|\text{Th}$  and  $\text{Ag}^+|\text{Ag}$  reference electrode in LiCl-KCl- $\text{ThCl}_4$  electrolyte was measured by constructing the following galvanic cell:



The half-cell reactions are given by:



Overall cell reaction is given by,



Equilibrium potential  $E_{\text{Th}^{4+}|\text{Th}}^{\text{eq}}$  of  $\text{Th}^{4+}|\text{Th}$  versus  $\text{Ag}^+|\text{Ag}$  is related to Gibbs energy of formation of  $\text{ThCl}_4$  and  $\text{AgCl}$  by Equation 2.15 and is given by,

$$\begin{aligned} \Delta G_{\text{reaction}} &= \Delta_f G_{\text{ThCl}_4} - 4\Delta_f G_{\text{AgCl}} \\ 4FE_{\text{Th}^{4+}|\text{Th}}^{\text{eq}} &= \Delta_f G_{\text{ThCl}_4, \text{LiCl-KCl}}^\circ + RT \ln a_{\text{ThCl}_4} - 4(\Delta_f G_{\text{AgCl}}^\circ + RT \ln a_{\text{AgCl}}) \\ 4FE_{\text{Th}^{4+}|\text{Th}}^{\text{eq}} &= 4FE_{\text{Th}^{4+}|\text{Th}}^\circ + RT \ln x_{\text{ThCl}_4} \gamma_{\text{ThCl}_4} - 4(FE_{\text{AgCl}}^\circ + RT \ln x_{\text{AgCl}} + RT \ln \gamma_{\text{AgCl}}) \end{aligned} \quad (2.15)$$

Equation 2.15 may be further simplified by substituting the value of  $\gamma_{\text{AgCl}} = 1$  assuming ideal behaviour of  $\text{AgCl}$  in  $\text{LiCl-KCl}$  eutectic melt, as discussed by several authors [66-69] and incorporating negative sign within  $E_{\text{Th}^{4+}|\text{Th}}^{\text{eq}}$  and  $E_{\text{Th}^{4+}|\text{Th}}^\circ$ .

$$E_{\text{Th}^{4+}|\text{Th}}^{\text{eq}} + E_{\text{AgCl}}^\circ + \frac{RT}{F} \ln x_{\text{AgCl}} = E_{\text{Th}^{4+}|\text{Th}}^\circ + \frac{RT}{4F} \ln \gamma_{\text{ThCl}_4} + \frac{RT}{4F} \ln x_{\text{ThCl}_4} \quad (2.16)$$

Therefore,  $E_{\text{Th}^{4+}|\text{Th}}^\circ$  can be estimated from the linear least squares fit of

$$E_{\text{Th}^{4+}|\text{Th}}^{\text{eq}} + E_{\text{AgCl}}^\circ + \frac{RT}{F} \ln x_{\text{AgCl}} \text{ versus } \ln x_{\text{ThCl}_4} \text{ and is extrapolated to } \ln x_{\text{ThCl}_4} = 1. \text{ This method is}$$

based on the work of Roy *et al.* [70, 71]. From the linear fits at various temperatures, we can obtain the temperature dependence in  $E_{\text{Th}^{4+}|\text{Th}}^\circ$  given by

$$E_{\text{Th}^{4+}|\text{Th}}^\circ = a_{11} + b_{11}T \quad (2.17)$$

We can again re-write Equation 2.16 as follows,

$$E_{\text{Th}^{4+}|\text{Th}}^{\text{eq}} + E_{\text{AgCl}}^{\circ} + \frac{RT}{F} \ln x_{\text{AgCl}} - \frac{RT}{4F} \ln x_{\text{ThCl}_4} = E_{\text{Th}^{4+}|\text{Th}}^{\circ} + \frac{RT}{4F} \ln \gamma_{\text{ThCl}_4} \quad (2.18)$$

From linear least square fit of  $E_{\text{Th}^{4+}|\text{Th}}^{\text{eq}} + E_{\text{AgCl}}^{\circ} + \frac{RT}{F} \ln x_{\text{AgCl}} - \frac{RT}{4F} \ln x_{\text{ThCl}_4}$  versus  $x_{\text{ThCl}_4}$  and extrapolating to  $x_{\text{ThCl}_4} = 0$ , we can estimate  $E_{\text{Th}^{4+}|\text{Th}}^{\circ}$  that can be referred to be for  $\text{ThCl}_4$  at infinite dilution in LiCl-KCl eutectic melt. Equation 2.18 is based on the work of Lantelme *et al.* [72-74]. Similar to that described above, linear fits at different temperatures can be used to estimate the temperature dependence in  $E_{\text{Th}^{4+}|\text{Th}}^{\circ}$  given by,

$$E_{\text{Th}^{4+}|\text{Th}}^{\circ} = a_{21} + b_{21}T \quad (2.19)$$

In order to convert  $E_{\text{Th}^{4+}|\text{Th}}^{\circ}$  versus  $\text{Ag}^+|\text{Ag}$  to  $\text{Cl}^-|\text{Cl}_2$ , following expressions for  $E_{\text{AgCl}}$  and  $E_{\text{AgCl}}^{\circ}$  by Yang *et al.* were used [69, 75]:

$$E_{\text{AgCl}} / \text{V vs. Cl}_2|\text{Cl}^- = E_{\text{AgCl}}^{\circ} + \frac{RT}{F} \ln x_{\text{AgCl}} \quad (2.20)$$

$$E_{\text{AgCl}}^{\circ} = -1.0931 + 2.924 \cdot 10^{-4}T(\text{K}) \quad (2.21)$$

Choosing a hypothetical supercooled liquid  $\text{ThCl}_4$  as reference state,  $\gamma_{\text{ThCl}_4}$  can be estimated from following expression for partial excess Gibbs energy of  $\text{ThCl}_4$ ,

$$\Delta \bar{G}_{\text{ThCl}_4}^{\text{ex}} = RT \ln \gamma_{\text{ThCl}_4} = \Delta_{\text{f}} G_{\text{ThCl}_4, \text{LiCl-KCl}}^{\circ} - \Delta_{\text{f}} G_{\text{ThCl}_4, \text{liq.}}^{\circ} \quad (2.22)$$

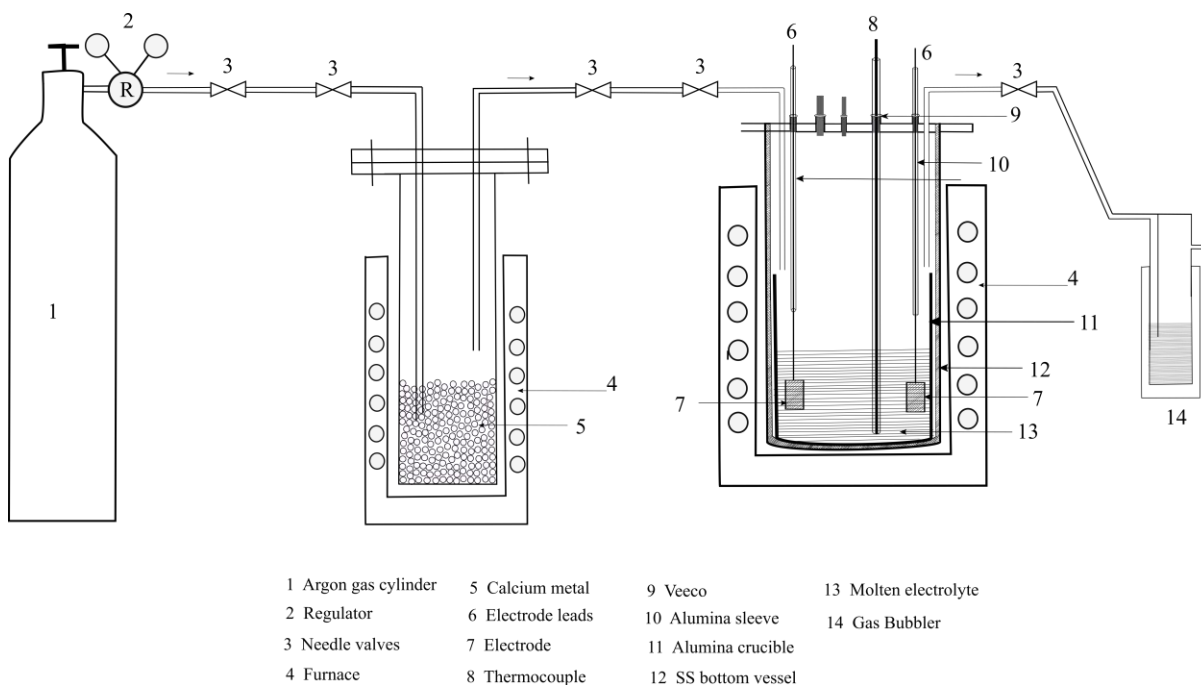


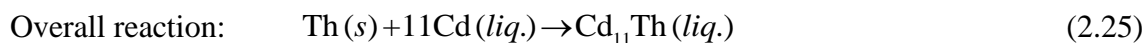
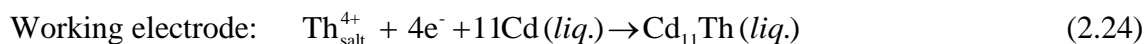
Figure 2.15 Schematic diagram of emf cell set-up.

### 2.5.4.2 emf measurements on Cd-Th alloy

Measurement of Gibbs free energy of formation of  $\text{Cd}_{11}\text{Th}$ ,  $\text{Cd}_5\text{Th}$ ,  $\text{Cd}_{23}\text{Th}_6$ ,  $\text{Cd}_3\text{Th}$  alloys were carried out by constructing four different galvanic cells, configurations of which are given below by cell I, II, III and IV respectively,



Equilibrium reaction at cell I can be established as follows:



$\Delta_f G_{\text{Cd}_{11}\text{Th}}^\circ$  of  $\text{Cd}_{11}\text{Th}$  from  $\alpha$ -thorium and liquid cadmium is related to cell emf,  $E_I$ ,  $a_{\text{Th}}$  and  $\bar{G}_{\text{Th}}$  by Equations 2.26 – 2.28.

$$\Delta \bar{G}_{\text{Th}} = \bar{G}_{\text{Th}} - G_{\text{Th}}^\circ = -nFE_I \quad (2.26)$$

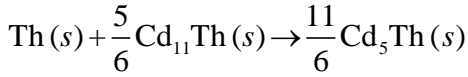
$$\Delta \bar{G}_{\text{Th}} = RT \ln a_{\text{Th}} \quad (2.27)$$

$$\Delta_f G_{\text{Cd}_{11}\text{Th}}^\circ = -nFE_I + 11RT \ln a_{\text{Cd}} \quad (2.28)$$

Saturated solution of Cd-Th system is so dilute that the solution can be assumed ideal with respect to cadmium and Equation 2.28 can be re-written as Equation 2.29 by replacing  $RT \ln a_{\text{Cd}}$  with  $RT \ln x_{\text{Cd}}$ . From solubility data of thorium in liquid cadmium available in literature [44] was used to compute concentration of cadmium in equilibrium with  $\text{Cd}_{11}\text{Th}$ .

$$\Delta_f G_{\text{Cd}_{11}\text{Th}}^\circ = -nFE_I + 11RT \ln x_{\text{Cd}} \quad (2.29)$$

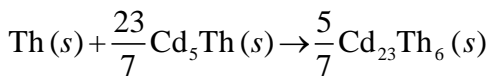
Cell reaction at equilibrium condition for Cell II can be represented as,



Equation for calculation of standard Gibbs energy of formation ( $\Delta_f G_{\text{ThCd}_5}^\circ$ ) of  $\text{Cd}_5\text{Th}$  alloy is given by Equation 2.30, which can be derived as follows:

$$\begin{aligned} \Delta G_{\text{reaction}} &= \frac{11}{6} \Delta_f G_{\text{Cd}_5\text{Th}}^\circ - \frac{5}{6} \Delta_f G_{\text{Cd}_{11}\text{Th}}^\circ \\ -4FE_{II} &= \frac{11}{6} \Delta_f G_{\text{Cd}_5\text{Th}}^\circ - \frac{5}{6} \times (-4FE_I + 11RT \ln x_{\text{Cd}}) \\ \Delta_f G_{\text{Cd}_5\text{Th}}^\circ &= \frac{6}{11} \left[ -4FE_{II} - \frac{5}{6} \times 4FE_I + RT \ln x_{\text{Cd}} \right] \\ \Delta_f G_{\text{Cd}_5\text{Th}}^\circ &= -\frac{4F}{11} (6E_{II} + 5E_I) + \frac{6}{11} RT \ln x_{\text{Cd}} \end{aligned} \quad (2.30)$$

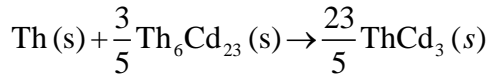
Equilibrium reaction of cell III can be represented as follows:



Standard Gibbs energy of formation of  $\text{Th}_6\text{Cd}_{23}$  alloy ( $\Delta_f G_{\text{Th}_6\text{Cd}_{23}}^\circ$ ) was calculated using Equation 2.31, which was derived as follows.

$$\begin{aligned}
\Delta G_{\text{reaction}} &= \frac{5}{7} \Delta_f G_{\text{Cd}_{23}\text{Th}_6}^\circ - \frac{23}{7} \Delta_f G_{\text{Cd}_3\text{Th}}^\circ \\
-4FE_{III} &= \frac{5}{7} \Delta_f G_{\text{Cd}_{23}\text{Th}_6}^\circ - \frac{23}{7} \times \left( -\frac{4F}{11} (6E_{II} + 5E_I) + \frac{6}{11} RT \ln x_{\text{Cd}} \right) \\
\Delta_f G_{\text{Cd}_{23}\text{Th}_6}^\circ &= \frac{7}{5} \left[ -4FE_{III} - \frac{4F}{77} \times (138E_{II} + 115E_I) + \frac{138}{77} RT \ln x_{\text{Cd}} \right] \\
\Delta_f G_{\text{Cd}_{23}\text{Th}_6}^\circ &= -\frac{4F}{55} (77E_{III} + 138E_{II} + 115E_I) + \frac{138}{55} RT \ln x_{\text{Cd}} \quad (2.31)
\end{aligned}$$

Equilibrium reaction of cell IV is shown below.



Expression of standard Gibbs energy of formation of  $\text{Cd}_3\text{Th}$  ( $\Delta_f G_{\text{Cd}_3\text{Th}}^\circ$ ) alloy is given by Equation 2.32 which is derived as follows.

$$\begin{aligned}
\Delta G_{\text{reaction}} &= \frac{23}{5} \Delta_f G_{\text{Cd}_3\text{Th}}^\circ - \frac{3}{5} \Delta_f G_{\text{Cd}_{23}\text{Th}_6}^\circ \\
-4FE_{IV} &= \frac{23}{5} \Delta_f G_{\text{Cd}_3\text{Th}}^\circ - \frac{3}{5} \times \left( -\frac{4F}{55} (77E_{III} + 138E_{II} + 115E_I) + \frac{138}{55} RT \ln x_{\text{Cd}} \right) \\
\Delta_f G_{\text{Cd}_3\text{Th}}^\circ &= \frac{5}{23} \left[ -4FE_{IV} - \frac{4F}{5} \times \frac{3}{55} (77E_{III} + 138E_{II} + 115E_I) + \frac{414}{275} RT \ln x_{\text{Cd}} \right] \\
\Delta_f G_{\text{Cd}_3\text{Th}}^\circ &= -\frac{4F}{5} \left[ \frac{5}{23} \left( E_{IV} + \frac{21}{5} E_{III} \right) + \frac{3}{23} \left( \frac{138E_{II} + 115E_I}{11} \right) \right] + \frac{18}{55} RT \ln x_{\text{Cd}} \\
\Delta_f G_{\text{Cd}_3\text{Th}}^\circ &= -\frac{4F}{5} \left( \frac{25E_{IV} + 21E_{III}}{23} + \frac{18E_{II} + 15E_I}{11} \right) + \frac{18}{55} RT \ln x_{\text{Cd}} \quad (2.32)
\end{aligned}$$

## CHAPTER 3

### Redox behaviour of $\text{Th}^{4+}$ in LiCl-KCl eutectic melt using transient Techniques

#### Results and discussions

Chapter 3 describes investigations on  $\text{Th}^{4+}|\text{Th}$  redox couple in LiCl-KCl eutectic melt using variety of electrochemical transient techniques to estimate electrochemical and thermodynamic properties of the redox couple. Theoretical equilibrium potential of  $\text{Th}^{4+}|\text{Th}$  couple was estimated and compared with those measured from anodic dissolution of thorium electrode. This is followed by investigations on redox behaviour of  $\text{Th}^{4+}$  at liquid cadmium electrode and influence of  $\text{CdCl}_2$  on cyclic voltammograms of LiCl-KCl- $\text{ThCl}_4$  at inert tungsten electrode. The chapter concludes with simple investigations on disproportionation of  $\text{Th}^{4+}$  in the eutectic melt, comparison with literature and corrosion of alumina crucible while handling dilute solutions of  $\text{ThCl}_4$  in LiCl-KCl eutectic melt during the course of measurements reported in this thesis.

#### 3.1 Cyclic voltammetry (CV) at inert tungsten electrode

Cyclic voltammogram of blank LiCl-KCl eutectic melt at inert tungsten electrode at 698 K in the potential region of -2.46 to 1.27 V is shown in Figure 3.1. Redox couples ( $A|A'$ ) at -2.4 V and ( $C|C'$ ) at 1.26 V were due to  $\text{Li}^+|\text{Li}$  and  $\text{Cl}|\text{Cl}_2$  couples, respectively [7]. Redox couple ( $B|B'$ ) at potential -1.62 V (reduction) and -1.44 V (oxidation) in cyclic voltammogram (Figure 3.1) recorded for  $9.53 \times 10^{-5} \text{ mol cm}^{-3}$  of  $\text{ThCl}_4$  in LiCl-KCl eutectic melt at 698 K on tungsten electrode is due to  $\text{Th}^{4+}|\text{Th}$  couple. Cyclic voltammograms of  $\text{ThCl}_4$  at tungsten electrode was recorded at scan rates 3-500  $\text{mV s}^{-1}$ . Figure 3.2 shows recorded cyclic voltammograms of  $\text{ThCl}_4$  at 723 K for scan rates 3-10  $\text{mV s}^{-1}$ . A consistent cross-over of cathodic and anodic sweep was observed at -1.563 V and -1.524 V pointing to nucleation of

metallic Th at tungsten electrode. However, this phenomenon was not investigated in the thesis.

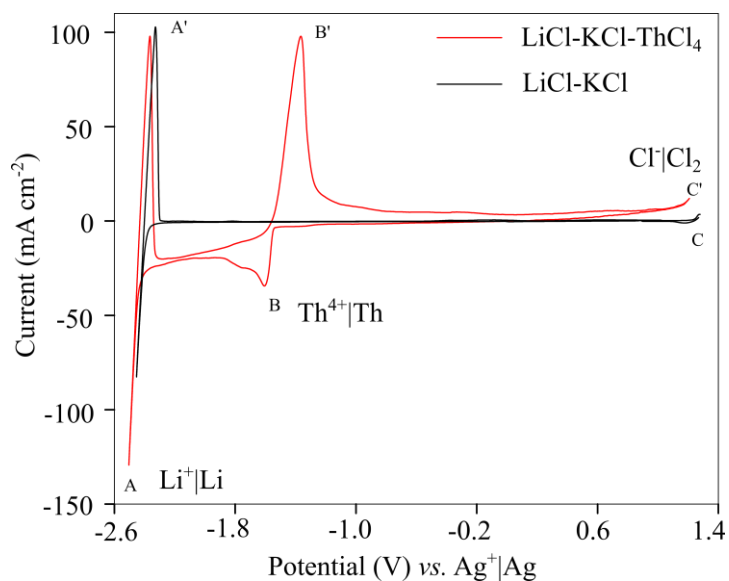


Figure 3.1 Cyclic voltammograms of blank LiCl-KCl eutectic melt and LiCl-KCl-ThCl<sub>4</sub> at inert tungsten electrode,  $T = 723 \text{ K}$ ,  $C_{\text{ThCl}_4} = 9.53 \times 10^{-5} \text{ mol cm}^{-3}$ ,  $A = 0.25 \text{ cm}^2$ .

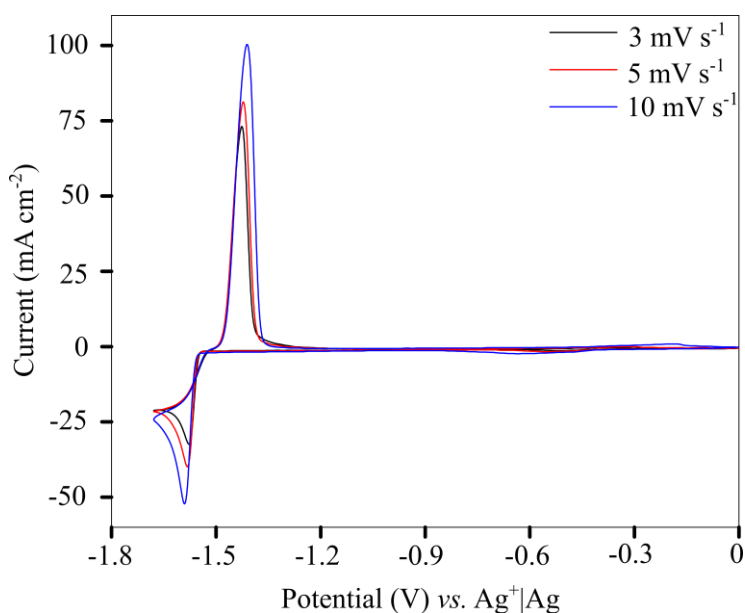


Figure 3.2 Cyclic voltammograms of Th<sup>4+</sup>/Th couple at inert tungsten electrode in LiCl-KCl eutectic melt for scan rates 3-10 mV s<sup>-1</sup>,  $T = 698 \text{ K}$ ,  $C_{\text{ThCl}_4} = 9.53 \times 10^{-5} \text{ mol cm}^{-3}$ ,  $A = 0.25 \text{ cm}^2$ .

Cyclic voltammograms of ThCl<sub>4</sub> in LiCl-KCl eutectic melt of different ThCl<sub>4</sub> concentrations ( $2.04 \times 10^{-5}$ ,  $2.72 \times 10^{-5}$  and  $9.53 \times 10^{-5} \text{ mol cm}^{-3}$ ) were recorded at various scan rates (10-500

mV s<sup>-1</sup>) at inert tungsten electrode in the temperature range of 698-803K. Cyclic voltammograms recorded for  $2.04 \times 10^{-5}$  mol cm<sup>-3</sup> ThCl<sub>4</sub> at 723 K are shown in Figure 3.3. In Figure 3.3 it is found that there is shift of cathodic peak potential by -30 mV from scan rate 10 to 300 mV s<sup>-1</sup>. However, potential shift is quite apparent beyond 200 mV s<sup>-1</sup>.

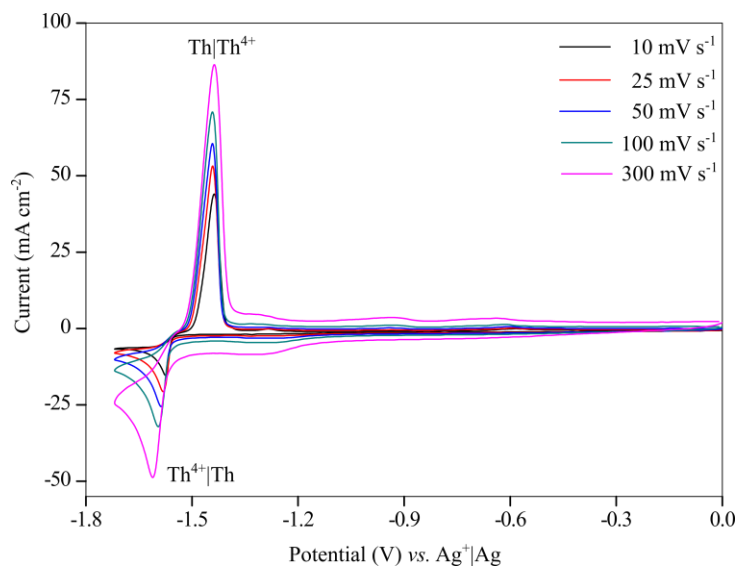


Figure 3.3 Cyclic voltammograms of Th<sup>4+</sup>|Th couple at inert tungsten electrode in LiCl-KCl eutectic melt,  $T = 723$  K,  $C_{ThCl_4} = 2.04 \times 10^{-5}$  mol cm<sup>-3</sup>,  $A = 0.25$  cm<sup>2</sup>.

$E_{pc}$  and  $(E_p - E_{p/2})_c$  values at various scan rates from cyclic voltammogram recorded in temperature range 698-803 K are shown in Table 3.1. For a reversible electrochemical system  $E_{pc}$  and  $(E_p - E_{p/2})_c$  for cathodic process remains constant with scan rates and for irreversible system large cathodic shift is observed. Therefore, small variation of  $E_{pc}$  and  $(E_p - E_{p/2})_c$  values suggests the quasireversible nature of Th<sup>4+</sup>|Th redox couple at scan rates 10 - 200 mV s<sup>-1</sup> [27, 76]. Quasireversible nature of Th<sup>4+</sup>|Th couple was further confirmed by electrochemical impedance spectroscopy study (EIS) and is discussed in Chapter 5.

$n$  value for  $\text{Th}^{4+}|\text{Th}$  redox couple was calculated using Equation 3.1 [77], which is applicable for a reversible system involving soluble-insoluble redox couple and tabulated in Table 3.1, which suggest non-reversibility of the redox couple.

$$E_p - E_{p/2} = -0.7725 \frac{RT}{nF} \quad (3.1)$$

Table 3.1 Cathodic peak analysis of  $\text{Th}^{4+}|\text{Th}$  couple in LiCl-KCl eutectic melt,  $C_{\text{ThCl}_4} = 2.72 \times 10^{-5} \text{ mol cm}^{-3}$ .

$T / \text{K}$	Scan rate ( $\text{mV s}^{-1}$ )	$E_{pc}$ (V)	$(E_p - E_{p/2})_c$ (V)	$n$ value using Equation 3.1	$\alpha n$ value using Equation 3.2
698	10	-1.621	-0.015	3.1	7.4
	25	-1.631	-0.014	3.3	7.9
	50	-1.642	-0.016	2.9	7.1
	75	-1.642	-0.016	2.9	7.1
	100	-1.642	-0.017	2.7	6.5
	125	-1.652	-0.018	2.5	6.1
	150	-1.652	-0.019	2.5	6.0
	175	-1.652	-0.019	2.4	5.7
	200	-1.652	-0.020	2.3	5.6
	723	10	-1.591	-0.015	3.3
25		-1.601	-0.015	3.3	7.8
50		-1.611	-0.016	3.1	7.3
75		-1.621	-0.023	2.1	5.0
100		-1.621	-0.020	2.4	5.7
125		-1.621	-0.019	2.6	6.1
150		-1.621	-0.018	2.7	6.4
175		-1.621	-0.017	2.8	6.7
200		-1.621	-0.017	2.9	6.9
748		10	-1.571	-0.015	3.4
	25	-1.581	-0.013	3.8	9.2
	50	-1.591	-0.018	2.7	6.6
	75	-1.601	-0.023	2.1	5.1
	100	-1.601	-0.022	2.3	5.5
	125	-1.601	-0.019	2.6	6.2
	150	-1.601	-0.018	3.0	6.7
	175	-1.601	-0.017	3.1	7.1
	200	-1.601	-0.016	2.0	7.5
	773	10	-1.551	-0.014	2.3
25		-1.561	-0.017	3.7	7.1

	50	-1.561	-0.014	3.0	8.8
	75	-1.571	-0.021	3.7	5.8
	100	-1.571	-0.019	2.4	6.5
	125	-1.571	-0.017	2.7	7.3
	150	-1.571	-0.015	3.0	8.2
	175	-1.581	-0.024	3.4	5.2
	200	-1.581	-0.023	2.1	5.4
803	10	-1.521	-0.009	5.9	14.3
	25	-1.531	-0.015	3.6	8.6
	50	-1.531	-0.011	4.8	11.7
	75	-1.541	-0.019	2.8	6.7
	100	-1.541	-0.017	3.1	7.5
	125	-1.541	-0.016	3.3	8.0
	150	-1.541	-0.015	3.6	8.6
	175	-1.551	-0.025	2.1	5.1
	200	-1.551	-0.023	2.3	5.6

Equation 3.2 [78], which is applicable for an irreversible system was used to calculate  $\alpha n$  value and tabulated in Table 3.1.

$$E_p - E_{p/2} = -1.857 \frac{RT}{\alpha n F} \quad (3.2)$$

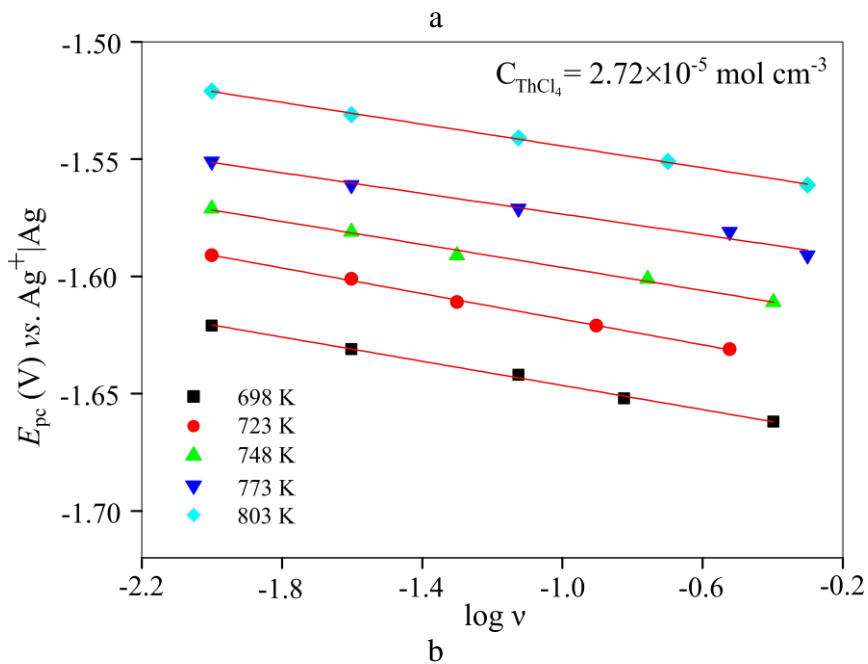
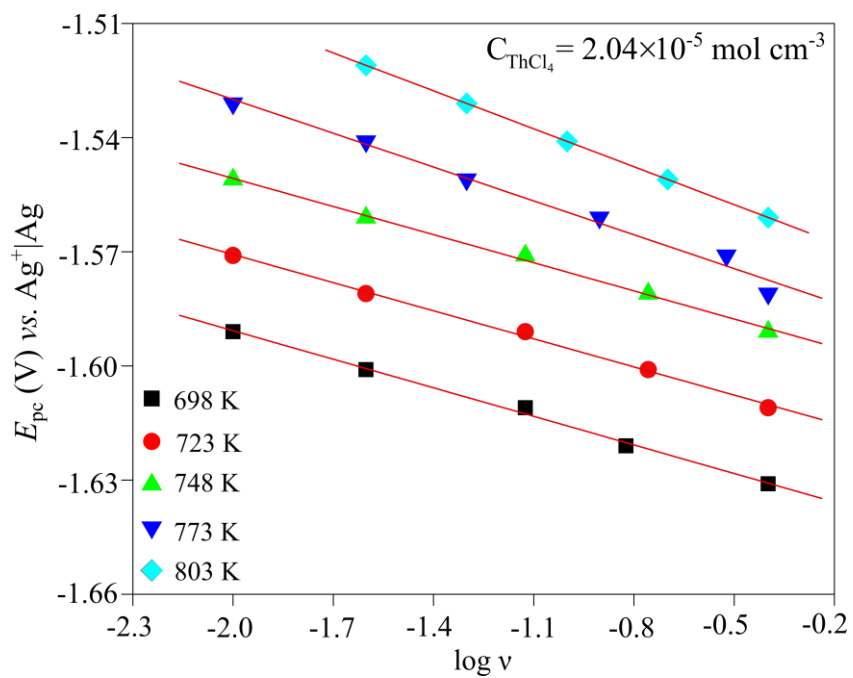
$\alpha n$  value calculated using Equation 3.2, produced  $\alpha > 1$  which is unrealistic as it should be between 0 and 1. The observations suggested that reduction process was not completely irreversible and Equation 3.2 is not applicable for investigating Th<sup>4+</sup>|Th couple.  $\alpha n$  value was also calculated using Equation 3.3 (applicable for both reversible and quasireversible system) [79, 80].

$$\frac{\Delta E_{pc}}{\Delta \log \nu} = 2.303 \frac{RT}{2\alpha n F} \quad (3.3)$$

$\alpha n$  value was calculated from slope of plot of  $E_{pc}$  versus  $\log \nu$  (Figure 3.4) for scan rates 10–400 mV s<sup>-1</sup> in temperature range of 698–803 K for various concentrations of ThCl<sub>4</sub> in molten LiCl-KCl eutectic melt, which are tabulated in Table 3.2. Calculated  $\alpha n$  values using Equation 3.3 were more realistic as compared to that obtained by Equation 3.2.

Table 3.2 Calculated  $\alpha$  value for  $Th^{4+}/Th$  couple by cyclic voltammetry.

$C_{ThCl_4} \times 10^5$ (mol cm <sup>-3</sup> )	$T / K$				
	698	723	748	773	803
2.04	2.8	2.9	3.0	2.6	2.4
2.72	2.7	2.6	2.7	3.3	3.4
9.53	2.8	-	1.9	2.3	3.0



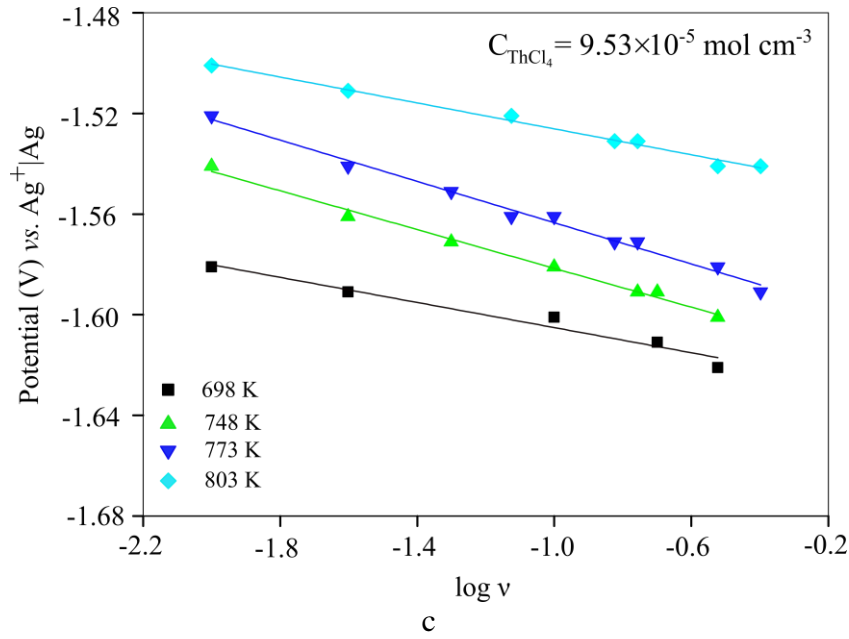
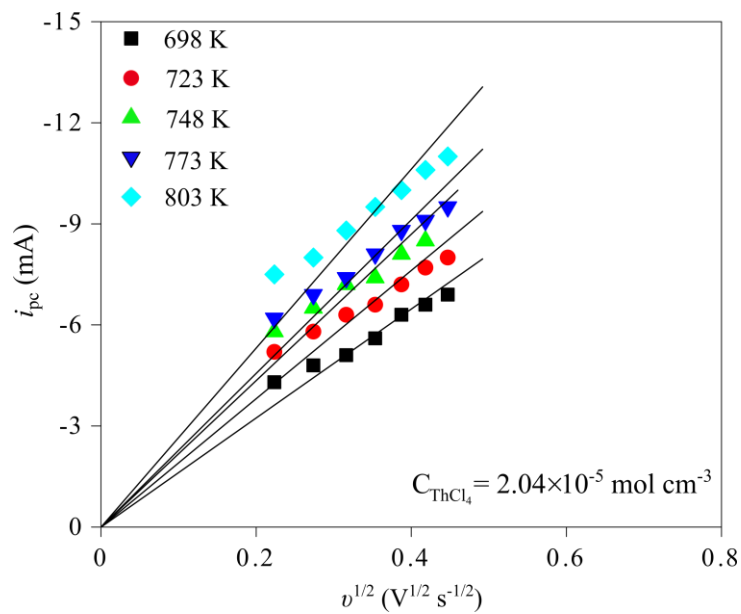
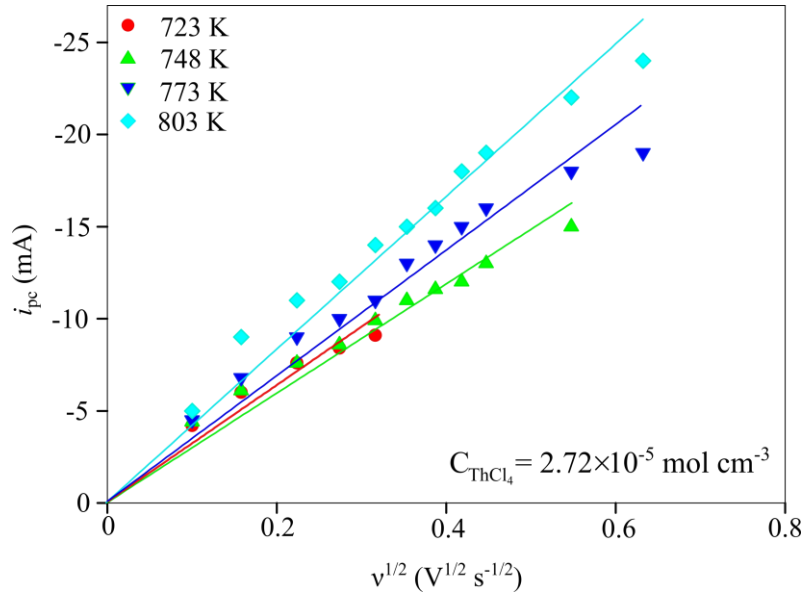


Figure 3.4  $E_{pc}$  vs.  $\log v$  for  $Th^{4+}/Th$  couple at inert tungsten electrode in LiCl-KCl eutectic melt, (a)  $C_{ThCl_4} = 2.04 \times 10^{-5} \text{ mol cm}^{-3}$ , (b)  $C_{ThCl_4} = 2.72 \times 10^{-5} \text{ mol cm}^{-3}$ , (c)  $C_{ThCl_4} = 9.53 \times 10^{-5} \text{ mol cm}^{-3}$   $T = 698\text{--}803 \text{ K}$ ,  $A = 0.25 \text{ cm}^2$ .

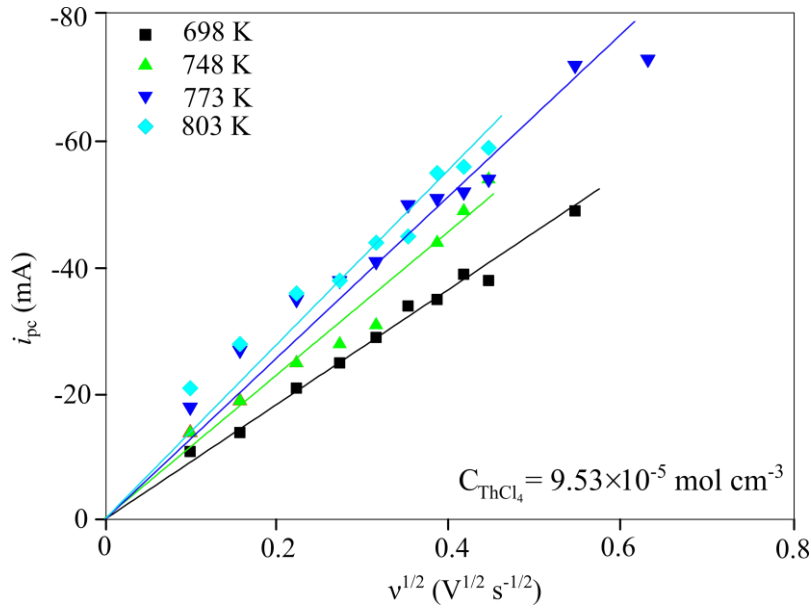
In similar manner  $i_{pc}$  was plotted against  $v^{1/2}$  in scan range of 10–200  $\text{mV s}^{-1}$  and shown in Figure 3.5. A linear variation was observed suggesting that reduction of  $Th^{4+}$  was a diffusion controlled process. Linear least squares fits of  $i_{pc}$  against  $v^{1/2}$  with a fixed intercept of zero are also shown in Figure 3.5.



a



b

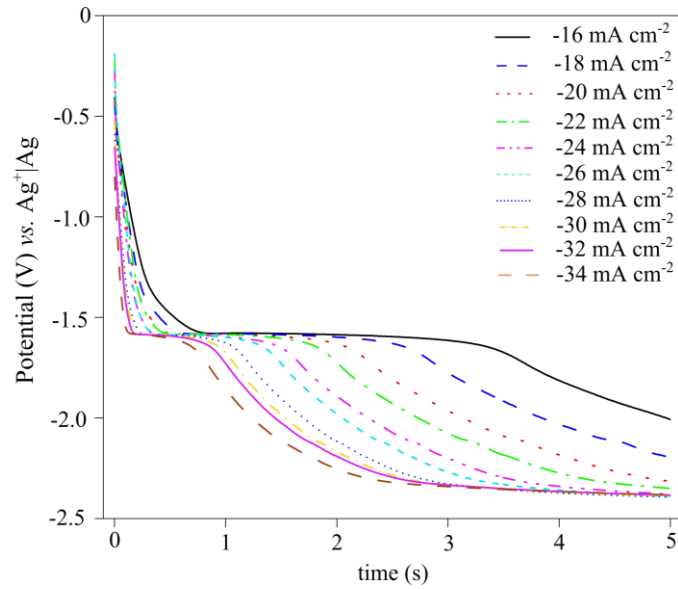


c

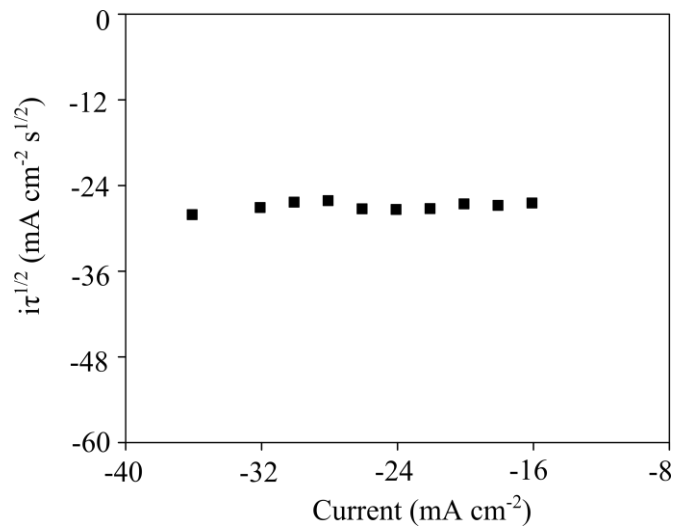
Figure 3.5 Variation of  $i_{pc}$  vs.  $v^{1/2}$  of  $Th^{4+}/Th$  couple at inert tungsten electrode in molten LiCl-KCl eutectic melt, (a)  $C_{ThCl_4} = 2.04 \times 10^{-5} \text{ mol cm}^{-3}$ , (b)  $C_{ThCl_4} = 2.72 \times 10^{-5} \text{ mol cm}^{-3}$ , (c)  $C_{ThCl_4} = 9.53 \times 10^{-5} \text{ mol cm}^{-3}$ ,  $T = 698\text{--}803 \text{ K}$ ,  $A = 0.25 \text{ cm}^2$ .

### 3.2 Chronopotentiometry (CP) at inert tungsten electrode

Chronopotentiograms for  $2.04 \times 10^{-5} \text{ mol cm}^{-3}$   $ThCl_4$  in molten LiCl-KCl eutectic at various current densities on W electrode at 723 K are shown in Figure 3.6a. A single plateau was observed in the chronopotentiograms at -1.57 V corresponding to reduction of  $Th^{4+}$  to Th.



a



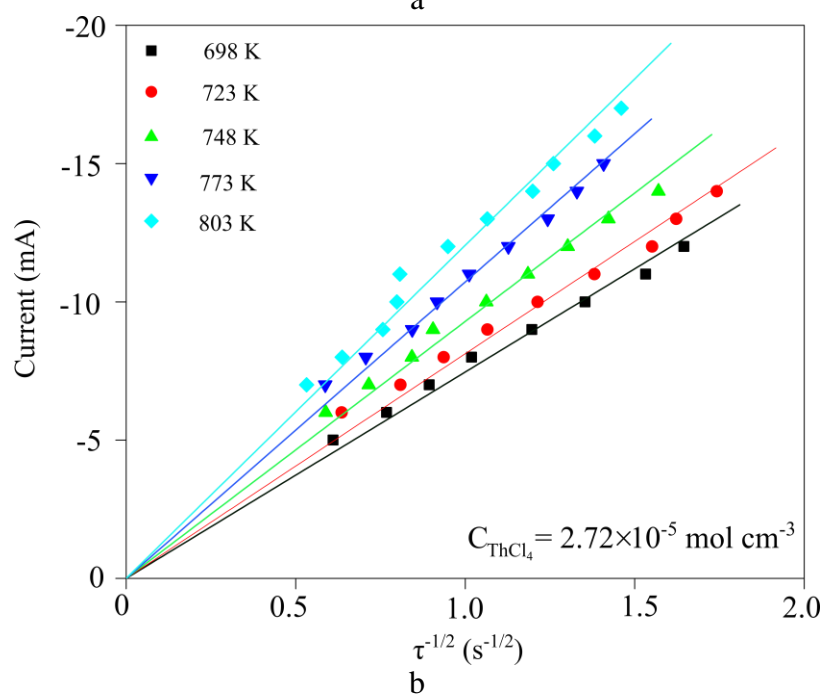
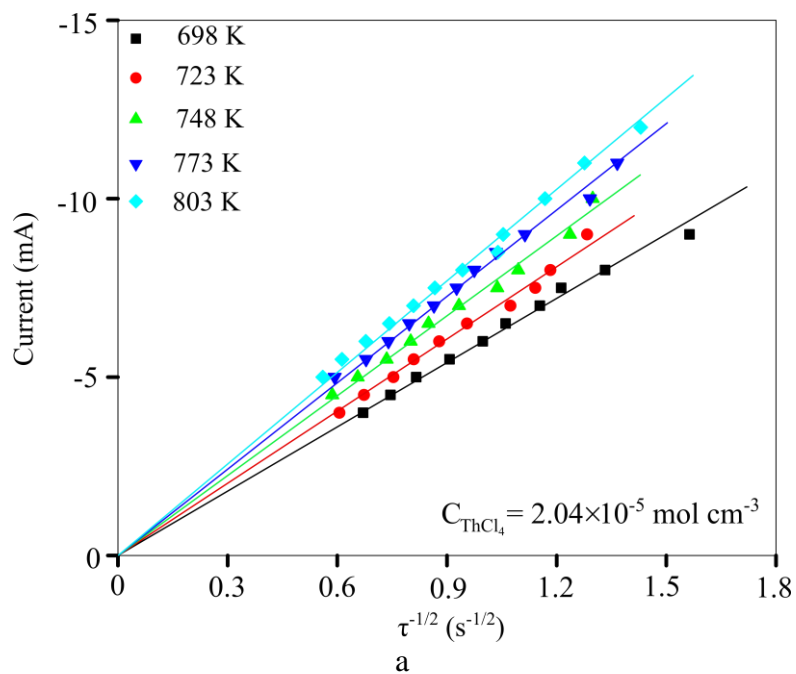
b

Figure 3.6 (a) Chronopotentiograms of  $Th^{4+}/Th$  couple at tungsten electrode in LiCl-KCl eutectic melt, (b) Variation of  $i\tau^{1/2}$  versus current density,  $T=723\text{ K}$ ,  $C_{ThCl_4}=2.04\times 10^{-5}\text{ mol cm}^{-3}$ ,  $A=0.25\text{ cm}^2$ .

Relationship between  $i$  and  $\tau$  is given by Sand's Equation 3.4 [60].

$$i\tau^{1/2} = 0.5nFAC_{Th^{4+}}\pi^{1/2}D_{Th^{4+}}^{1/2} \quad (3.4)$$

$i\tau^{1/2}$  remained almost constant in current range studied as shown in Figure 3.6b suggesting reversibility of the process at all current densities. Plot of  $i$  versus  $\tau^{-1/2}$  is shown in the Figure 3.7 at various temperatures.



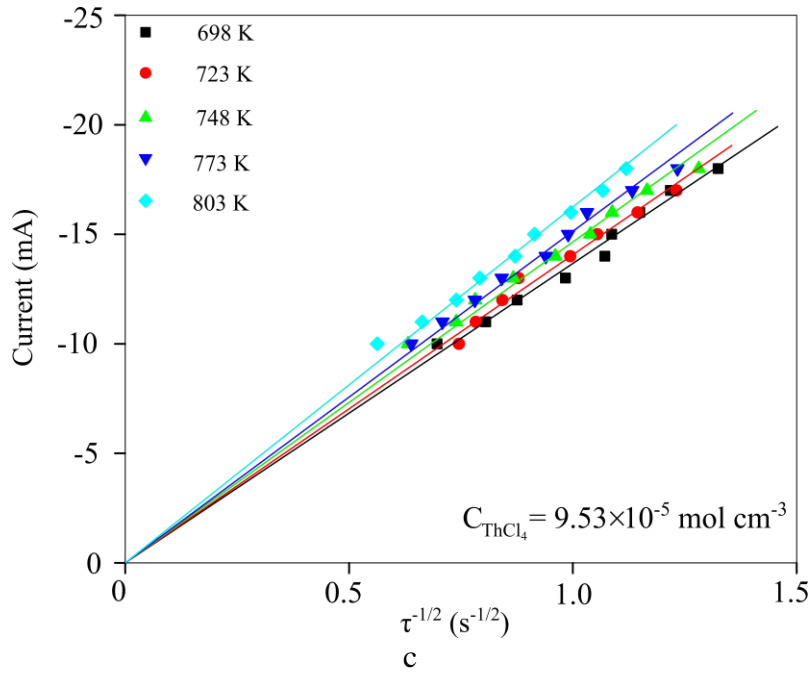


Figure 3.7 Plot of  $i$  versus  $\tau^{-1/2}$ , (a)  $C_{ThCl_4} = 2.04 \times 10^{-5} \text{ mol cm}^{-3}$ , (b)  $C_{ThCl_4} = 2.72 \times 10^{-5} \text{ mol cm}^{-3}$ , (c)  $C_{ThCl_4} = 9.53 \times 10^{-5} \text{ mol cm}^{-3}$ ,  $T = 698\text{--}803 \text{ K}$ ,  $A = 0.25 \text{ cm}^2$ .

### 3.3 Square wave voltammetry (SWV) at inert tungsten electrode

In Figure 3.8a, square wave voltammograms are shown for  $ThCl_4$  ( $C_{ThCl_4} = 2.04 \times 10^{-5} \text{ mol cm}^{-3}$ ) in LiCl-KCl eutectic melt at tungsten electrode at 723 K. Only reduction peak appearing at  $-1.575 \text{ V}$  was attributed to  $Th^{4+}|Th$  couple.  $n$  was calculated using Equation 3.5 which is valid for a perfectly Gaussian peak [81-87] and tabulated in Table 3.3.

$$W_{1/2} = 3.52 \frac{RT}{nF} \quad (3.5)$$

$i$  and  $E_{pc}$  were plotted against  $f^{1/2}$  for a fixed amplitude of 25 mV at 723 K for  $C_{ThCl_4} = 2.04 \times 10^{-5} \text{ mol cm}^{-3}$  and are shown in Figure 3.8b. Linear dependence of  $i$  versus  $f^{1/2}$  and invariance of  $E_{pc}$  versus  $f^{1/2}$  in both profiles suggest that reduction process was quasireversible. It was therefore proved that reduction of  $Th^{4+}$  at tungsten electrode was single step quasireversible process involving four electrons.

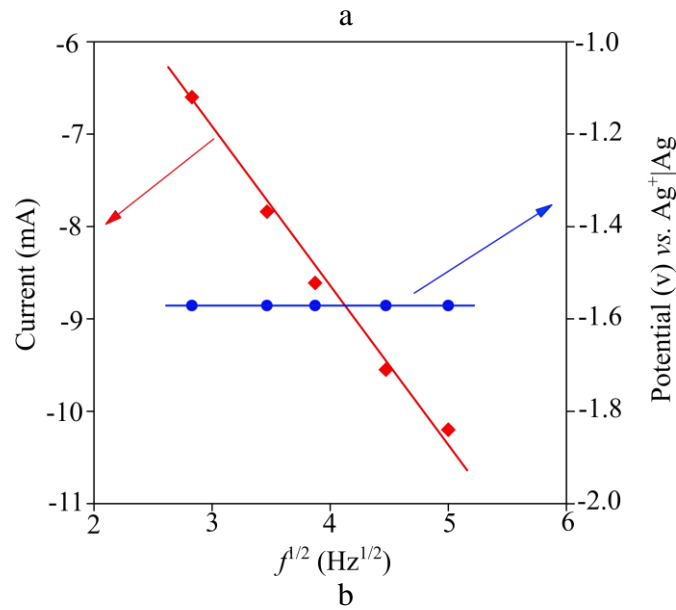
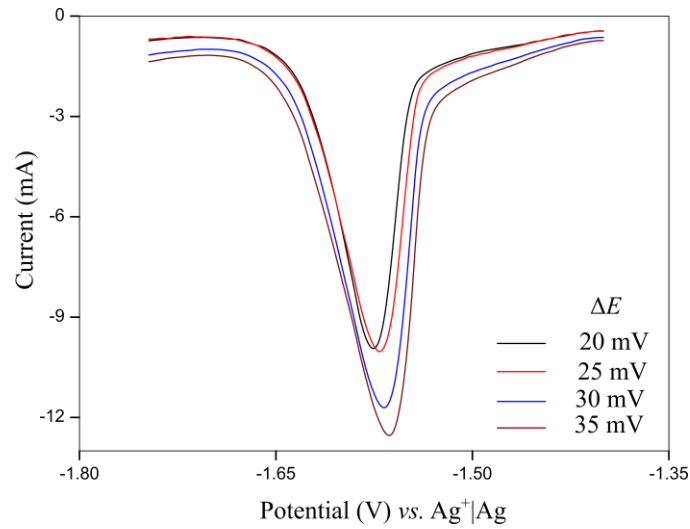


Figure 3.8 (a) Square wave voltammograms of  $Th^{4+}/Th$  couple at inert tungsten electrode in LiCl-KCl eutectic melt,  $T=723\text{ K}$ ,  $C_{ThCl_4}=2.04\times 10^{-5}\text{ mol cm}^{-3}$ ,  $f=25\text{ Hz}$ ,  $\Delta E=20, 25, 30, 35\text{ mV}$ ,  $A=0.25\text{ cm}^2$ . (b) Linear relationship of  $i_{pc}$  (left axis) and  $E_{pc}$  (right axis) versus  $f^{1/2}$ ,  $T=723\text{ K}$ ,  $\Delta E=25\text{ mV}$ .

Table 3.3  $n$  of  $Th^{4+}/Th$  couple calculated by squarewave voltammogram,  $C_{ThCl_4}=2.72\times 10^{-5}\text{ mol cm}^{-3}$ ,  $A=0.25\text{ cm}^2$ .

$f/\text{Hz}$	$\Delta E/\text{mV}$	723 K		748 K		773 K	
		$W_{1/2}$	$n$	$W_{1/2}$	$n$	$W_{1/2}$	$N$
8	30	0.0537	4.1	0.0537	4.2	0.0537	4.4
	35	0.0635	3.5	0.0586	3.9	0.0537	4.4

15	30	0.0586	3.7	0.0537	4.2	0.0586	4.0
	35	0.0635	3.5	0.0537	4.2	0.0586	4.0
20	30	0.0586	3.7	0.0537	4.2	0.0635	3.7
	35	0.0684	3.2	0.0586	3.9	0.0635	3.7
25	30	0.0586	3.7	0.0537	4.2	0.0684	3.4
	35	0.0537	4.1	0.0586	3.9	0.0586	4.0

### 3.4 Semi-integral voltammetry (SIV)

Semi-integral of cyclic voltammetric data gives a convoluted curve similar to steady state voltammetric curves [88, 89]. In Figure 3.9 semi-integral curve for  $\text{ThCl}_4$  ( $C_{\text{ThCl}_4} = 2.04 \times 10^{-5} \text{ mol cm}^{-3}$ ) in LiCl-KCl eutectic melt on W electrode for scan rate of 50  $\text{mV s}^{-1}$  at 773 K is shown.

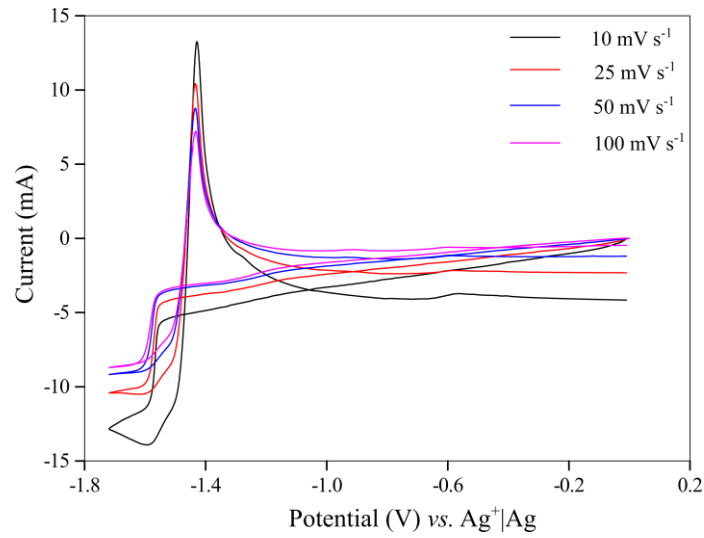


Figure 3.9 Semi-integral curve of voltammogram for  $\text{Th}^{4+}/\text{Th}$  couple at inert tungsten electrode in LiCl-KCl eutectic melt,  $T=723 \text{ K}$ ,  $C_{\text{ThCl}_4} = 2.04 \times 10^{-5} \text{ mol cm}^{-3}$ ,  $A=0.25 \text{ cm}^2$ .

Expression of  $m(t)$  is given by,

$$m(t) = \left( \frac{d^{-1/2} i(t)}{dt^{-1/2}} \right) = \frac{1}{\sqrt{\pi}} \int_0^t \frac{i(\tau)}{\sqrt{t-\tau}} d\tau \quad (3.6)$$

For reversible deposition of an insoluble species, governing equation for relating  $E(t)$ ,  $m(t)$  and  $m_c(\infty)$  is given by Equation 3.7 [90-93].

$$E(t) = E_{\text{Th}^{4+}|\text{Th}}^{\circ*} + \frac{RT}{nF} \ln x_{\text{ThCl}_4} + \frac{RT}{nF} \ln \left( \frac{m_c(\infty) - m}{m_c(\infty)} \right) \quad (3.7)$$

Plot of  $\ln \left( \frac{m_c(\infty) - m(t)}{m_c(\infty)} \right)$  vs.  $E(t)$  should yield a straight line with slope of  $RT/nF$ . Similar equations have been derived by Oldham *et al.* [91] for quasireversible and irreversible processes.

For a quasireversible process a plot of  $\ln \left\{ \frac{m_c(\infty) - m(t) \left[ 1 + \exp \left\{ \frac{nF}{RT} (E - E_{v_2}) \right\} \right]}{i(t)} \right\}$  vs.  $E(t)$  should

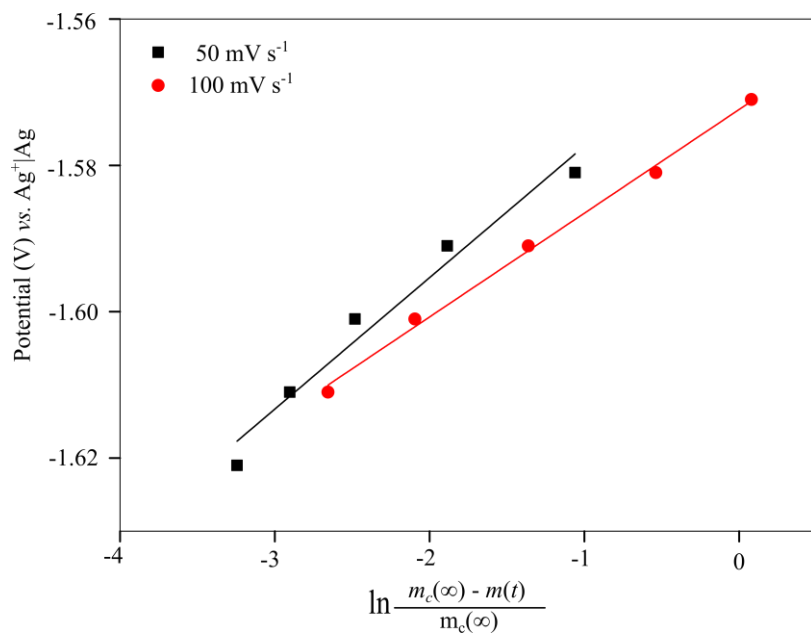
yield a straight line with a slope of  $RT/anF$ . From slope  $an$  value can be calculated.

For an irreversible process a plot of  $\ln \left( \frac{m_c(\infty) - m(t)}{i(t)} \right)$  versus  $E(t)$  should yield a straight line

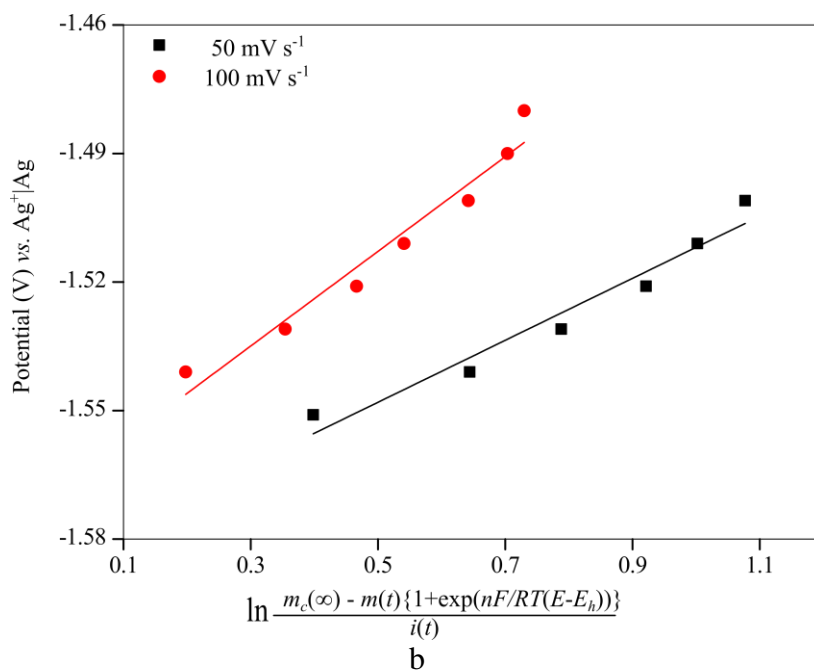
with a slope  $RT/anF$  and  $an$  can be calculated. Figure 3.10a shows the plots of  $E(t)$  versus

$\ln \left( \frac{m_c(\infty) - m(t)}{m_c(\infty)} \right)$  assuming reduction as reversible process. Figure 10b and 10c show the

plots assuming quasireversible and irreversible respectively. Values of  $n$ ,  $an$ ,  $\alpha$  calculated using reversible, quasireversible and irreversible hypothesis for various concentrations of  $\text{ThCl}_4$  in  $\text{LiCl-KCl}$  eutectic in the temperature range 698-803 K for scan rates of 10-500  $\text{mV s}^{-1}$  are shown in Table 3.4. Considering reduction process as reversible, calculated  $n$  value decreased with increasing scan rate as shown in Table 3.4. Considering reduction process as quasireversible it was found that  $an$  and  $\alpha$  values decrease with increasing scan rates. The reduction process was found to be irreversible at higher scan rates as  $an$  and  $\alpha$  value increased with increasing scan rates. So from the results shown in the Table 3.4 it was recognized that the reduction process was quasireversible at lower scan rates (10-100  $\text{mV s}^{-1}$ ) but irreversible at higher scan rates (500  $\text{mV s}^{-1}$ ).



a



b

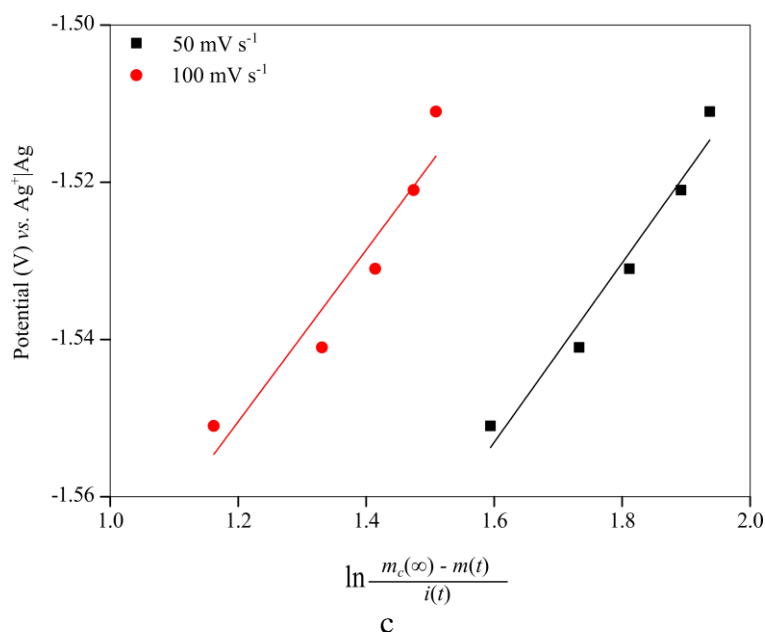


Figure 3.10 Logarithmic analysis of semi-integral curve of  $\text{Th}^{4+}/\text{Th}$  couple as per (a) Reversible, (b) quasireversible and (c) irreversible hypothesis,  $C_{\text{ThCl}_4} = 2.04 \times 10^{-5} \text{ mol cm}^{-3}$ ,  $T = 723 \text{ K}$ ,  $A = 0.25 \text{ cm}^2$ .

Table 3.4  $n$ ,  $\alpha$ ,  $\alpha n$  values for  $\text{Th}^{4+}/\text{Th}$  couple using reversible, quasireversible and irreversible hypothesis in semi-integral voltammetry.

$C_{\text{ThCl}_4} \times 10^5$ ( $\text{mol cm}^{-3}$ )	$T / \text{K}$	Scan rate ( $\text{mV s}^{-1}$ )	Reversible	Quasireversible		Irreversible	
			process	process	Process	Process	
			$n$	$\alpha n$	$\alpha$	$\alpha n$	$\alpha$
2.04	723	10	3.5	1.73	0.43	1.4	0.35
		50	3.5	1.45	0.36	0.86	0.22
		100	3.5	1.23	0.31	0.74	0.19
		500	2.9	0.83	0.21	0.54	0.14
	748	10	3.8	1.86	0.47	1.04	0.26
		50	4.1	1.57	0.39	0.62	0.15
		100	4.1	1.30	0.33	0.69	0.17
		500	3.2	1.06	0.27	0.66	0.16
	773	10	3.7	1.98	0.50	1.06	0.27
		50	4	1.25	0.31	0.9	0.22
		100	4.1	1.52	0.38	0.88	0.22
		500	2.9	0.74	0.19	0.68	0.17
	803	10	3.6	2.05	0.51	1.01	0.25
		50	3.7	2.02	0.51	0.97	0.24
		100	3.9	1.36	0.34	0.99	0.25
		500	2.7	0.89	0.22	0.76	0.19
2.72	723	10	3.5	2.49	0.62	1.27	0.32

		50	3.5	1.66	0.42	1.22	0.31
		100	3.1	1.27	0.32	0.82	0.21
		500	2.1	0.97	0.29	0.57	0.14
	748	10	3.5	3.06	0.77	1.47	0.37
		50	3.5	1.80	0.45	1.31	0.33
		100	3.4	1.35	0.34	0.84	0.21
		500	2.7	1.12	0.28	0.56	0.14
	773	10	3.3	1.94	0.48	1.48	0.37
		50	3.3	1.81	0.45	0.93	0.23
		100	3.4	1.32	0.33	0.79	0.2
		500	3.3	0.97	0.24	0.71	0.18
	803	10	2.7	3.01	0.75	1.25	0.32
		50	3.5	2.07	0.52	1.37	0.34
		100	3.7	1.75	0.44	0.98	0.24
		500	3.5	1.16	0.29	0.8	0.2
9.53	748	10	4.2	1.73	0.43	0.46	0.11
		50	4	1.61	0.40	0.59	0.15
		100	3.7	1.61	0.40	0.54	0.14
		500	2.4	0.62	0.16	0.41	0.1
	773	10	4.1	2.66	0.67	0.74	0.19
		50	3.8	2.64	0.66	0.43	0.11
		100	3.6	1.58	0.39	0.48	0.12
		500	2.2	1.29	0.32	0.43	0.11
	803	10	3.5	2.04	0.51	1.08	0.27
		50	3.7	1.91	0.48	0.49	0.12
		100	3.1	1.69	0.42	0.48	0.12
		500	2.3	1.16	0.29	0.44	0.11

### 3.5 Estimation of diffusion coefficient of Th<sup>4+</sup>

$D_{\text{Th}^{4+}}$  of Th<sup>4+</sup> in LiCl-KCl eutectic melt was calculated from slope of linear fit of  $i_{pc}$  versus  $\nu^{1/2}$  obtained from cyclic voltammetry (discussed in section 3.1). Berzins-Delahay (applicable for quasi-reversible and irreversible couples) [94, 95] and Randle-Sevic [60, 96, 97] (applicable for reversible and quasireversible systems) equations represented by Equations 3.8 and 3.9 respectively, were used to calculate  $D_{\text{Th}^{4+}}$ . Estimated  $D_{\text{Th}^{4+}}$  values at various temperatures and three different ThCl<sub>4</sub> concentrations are given in Table 3.5.

$$i_{pc} = 0.496nFAC_{\text{ThCl}_4} \left( \frac{\alpha nF}{RT} \right)^{1/2} (D_{\text{Th}^{4+}} \nu)^{1/2} \quad (3.8)$$

$$i_{pc} = 0.61nFAC_{\text{ThCl}_4} \left( \frac{nF}{RT} \right)^{1/2} (D_{\text{Th}^{4+}} \nu)^{1/2} \quad (3.9)$$

$D_{\text{Th}^{4+}}$  was also estimated from chronopotentiograms using Sand's Equation (3.4) [60] (discussed in Section 3.2).

In square wave voltammetry  $i_{pc}$  varies linearly with  $C_{\text{ThCl}_4}$  and with  $f^{1/2}$  according to Equation 3.10 [82]. This method may be extended to any electrochemical system. Diffusion coefficient of  $\text{Th}^{4+}$  was estimated by squarewave voltammetry using Equation 3.10 and tabulated in Table 3.5.

$$i_p = nFAC_{\text{ThCl}_4} \frac{1-\Gamma}{1+\Gamma} \sqrt{\frac{D_{\text{Th}^{4+}} f}{\pi}} \quad (3.10)$$

$$\text{Here, } \Gamma = \exp\left(\frac{nF}{RT} \frac{\Delta E}{2}\right) \quad (3.11)$$

Semi-integral voltammetry was used to estimate  $D_{\text{Th}^{4+}}$  using Equation 3.12 [98].

$$m_c(\infty) = -nFAC_{\text{ThCl}_4} D_{\text{Th}^{4+}}^{1/2} \quad (3.12)$$

Estimated  $D_{\text{Th}^{4+}}$  values estimated by different techniques were in good agreement, given in Table 3.5.  $D_{\text{Th}^{4+}}$  value was found in the range of  $0.26 \times 10^{-5}$  to  $6.56 \times 10^{-5} \text{ cm}^2 \text{ s}^{-1}$  in the temperature range of 698-803 K for entire concentration range of  $\text{ThCl}_4$  used in the present study, is in good agreement with the reported value of  $0.27 \times 10^{-5} \text{ cm}^2 \text{ s}^{-1}$  at 673 K by Martinot [5],  $2.23 \pm 0.16 \times 10^{-5} \text{ cm}^2 \text{ s}^{-1}$  at 723 K by Liu *et al.* [6] and  $3.15 \pm 0.2 \times 10^{-5} \text{ cm}^2 \text{ s}^{-1}$  at 723 K by Cassayre *et al.* [7] by cyclic voltammetric method.

Combined  $\ln D_{\text{Th}^{4+}}$  obtained from CV, CP, SIV and SWV were plotted against temperature and linear least square fit is shown in Figure 3.11.  $E_a$  for diffusion of  $\text{Th}^{4+}$  ion in LiCl-KCl

eutectic melt was calculated from slope of the plot of  $\ln D_{\text{Th}^{4+}}$  vs.  $1/T$ . The relationship among  $D_{\text{Th}^{4+}}$ ,  $T$  and  $E_a$  is given in Arrhenius equation 3.13.

Table 3.5  $D_{\text{Th}^{4+}}$  of  $\text{Th}^{4+}$  in LiCl-KCl eutectic melt obtained from CV, CP, SIV, SWV.

$C_{\text{ThCl}_4} \times 10^5$ (mol cm <sup>-3</sup> )	$T/K$	$D_{\text{Th}^{4+}} \times 10^5 / \text{cm}^2 \text{ s}^{-1}$				
		CV		CP	SIV	SWV
		Using Eq. (3.8)	Using Eq. (3.9)			
9.53	698	$0.83 \pm 0.02$	$0.38 \pm 0.01$	$2.06 \pm 0.18$	$1.61 \pm 0.18$	-
	748	$2.05 \pm 0.01$	$0.64 \pm 0.03$	$3.61 \pm 0.23$	$3.35 \pm 0.37$	-
	773	$2.19 \pm 0.01$	$0.85 \pm 0.05$	$5.60 \pm 0.19$	-	-
	803	$2.33 \pm 0.01$	$1.02 \pm 0.07$	$6.56 \pm 0.23$	$6.16 \pm 0.50$	-
2.72	698	-	-	$1.01 \pm 0.03$	$3.03 \pm 0.34$	-
	723	$1.38 \pm 0.15$	$0.59 \pm 0.06$	$1.19 \pm 0.03$	$3.86 \pm 0.55$	$2.12 \pm 0.10$
	748	$1.49 \pm 0.11$	$0.64 \pm 0.05$	$1.56 \pm 0.04$	$4.31 \pm 0.26$	$3.04 \pm 0.15$
	773	$1.59 \pm 0.06$	$0.84 \pm 0.03$	$2.07 \pm 0.04$	$5.05 \pm 0.96$	$4.46 \pm 0.14$
	803	$1.89 \pm 0.09$	$1.13 \pm 0.06$	$2.62 \pm 0.08$	$5.97 \pm 0.52$	-
2.04	698	$0.56 \pm 0.03$	$0.26 \pm 0.01$	$1.17 \pm 0.02$	$2.02 \pm 0.73$	-
	723	$0.85 \pm 0.04$	$0.41 \pm 0.02$	$1.47 \pm 0.02$	$2.24 \pm 0.40$	$2.43 \pm 0.10$
	748	$1.02 \pm 0.07$	$0.51 \pm 0.03$	$1.81 \pm 0.03$	$2.63 \pm 0.21$	$3.17 \pm 0.10$
	773	$1.33 \pm 0.08$	$0.58 \pm 0.03$	$2.12 \pm 0.03$	$2.97 \pm 0.67$	$4.15 \pm 0.13$
	803	$2.04 \pm 0.14$	$0.82 \pm 0.05$	$2.38 \pm 0.03$	$4.42 \pm 0.52$	-
Martinot [5]	673	0.27	673			
Liu <i>et al.</i> [6]	773			$2.23 \pm 0.16$		
Cassayre <i>et al.</i> [7]	723			$3.15 \pm 0.15$		

$$D_{\text{Th}^{4+}} = D_{\text{Th}^{4+}}^{\circ} \exp\left(\frac{E_a}{RT}\right) \quad (3.13)$$

Fitted equation of  $\ln D_{\text{Th}^{4+}}$  vs.  $1/T$  is given by,

$$\ln D_{\text{Th}^{4+}} = -(4.64 \pm 1.93) - \frac{4755 \pm 1451}{T(\text{K})} \quad (3.14)$$

From Equations 3.13 and 3.14, activation energy for  $\text{Th}^{4+}|\text{Th}$  couple in LiCl-KCl eutectic melt was calculated to be  $39.53 \pm 12.06 \text{ kJ mol}^{-1}$ . Reported  $E_a$  for diffusion of  $\text{Th}^{4+}$  in LiF-

CaF<sub>2</sub> using cyclic voltammetry was 55.5 kJ mol<sup>-1</sup> by Chamelot *et al.*[27]. Difference may be due to different molten salt media used by Chamelot *et al.* than in present work. Concentration dependence of  $D_{Th^{4+}}$  was found to be very weak in for dilute concentrations of ThCl<sub>4</sub> employed in present study. Figure 3.12 shows variation of diffusion coefficient with concentration and temperature.

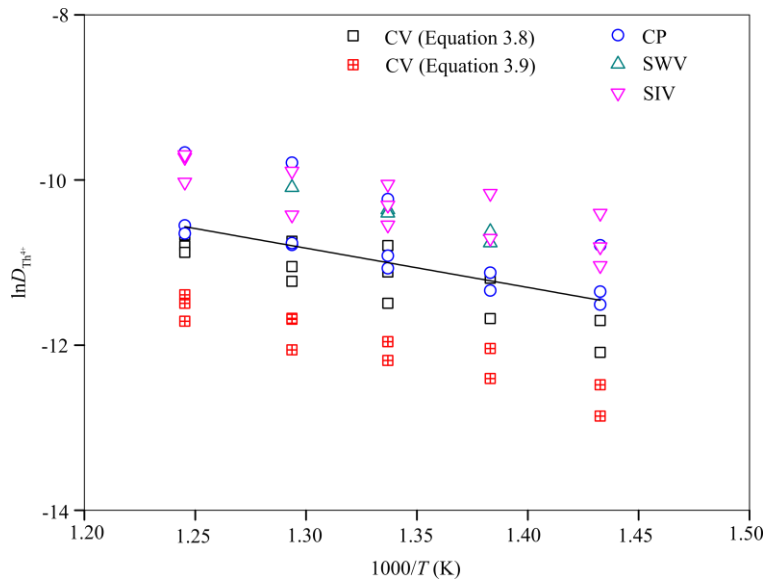


Figure 3.11 Variation of  $\ln D_{Th^{4+}}$  versus  $1/T$  for ThCl<sub>4</sub> in LiCl-KCl eutectic melt.

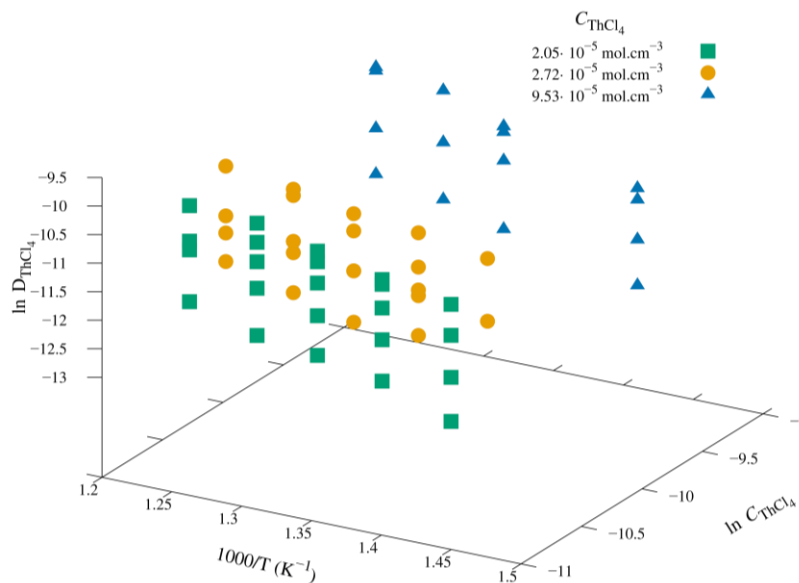


Figure 3.12 Concentration and temperature dependence of  $D_{Th^{4+}}$  of Th<sup>4+</sup> in LiCl-KCl eutectic melt.

### 3.6 Estimation of $E_{\text{Th}^{4+}|\text{Th}}^{\circ*}$ from CP and SIV

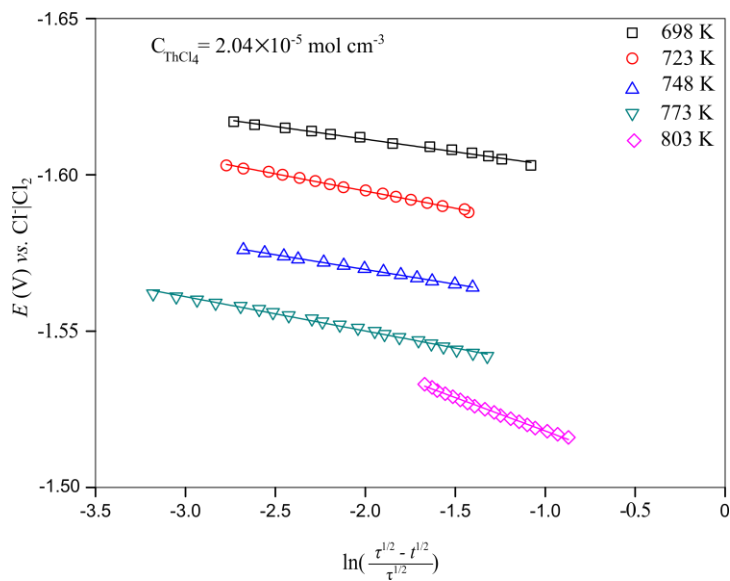
$E_{\text{Th}^{4+}|\text{Th}}^{\circ*}$  was calculated from chronopotentiograms as discussed below. Potential-time relationship for a reversible system with the formation of an insoluble metallic species is expressed by Equation 3.15 [60].

$$E(t) = E_{\text{Th}^{4+}|\text{Th}}^{\circ*} + \frac{RT}{nF} \ln x_{\text{ThCl}_4} + \frac{RT}{nF} \ln \left( \frac{\tau^{1/2} - t^{1/2}}{\tau^{1/2}} \right) \quad (3.15)$$

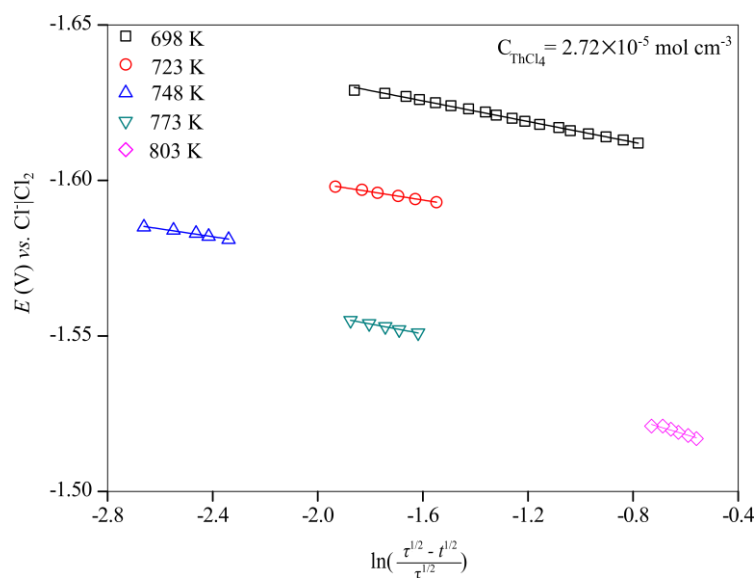
Plot of  $\ln \left( \frac{\tau^{1/2} - t^{1/2}}{\tau^{1/2}} \right)$  vs.  $E(t)$  shown in Figure 3.13 was found to be linear. From intercept of

the plot  $E_{\text{Th}^{4+}|\text{Th}}^{\circ*}$  was evaluated for different temperatures on tungsten electrode for three different concentrations of  $\text{ThCl}_4$  in LiCl-KCl eutectic melt. Calculated values of  $E_{\text{Th}^{4+}|\text{Th}}^{\circ*}$  are given in the Table 3.6.

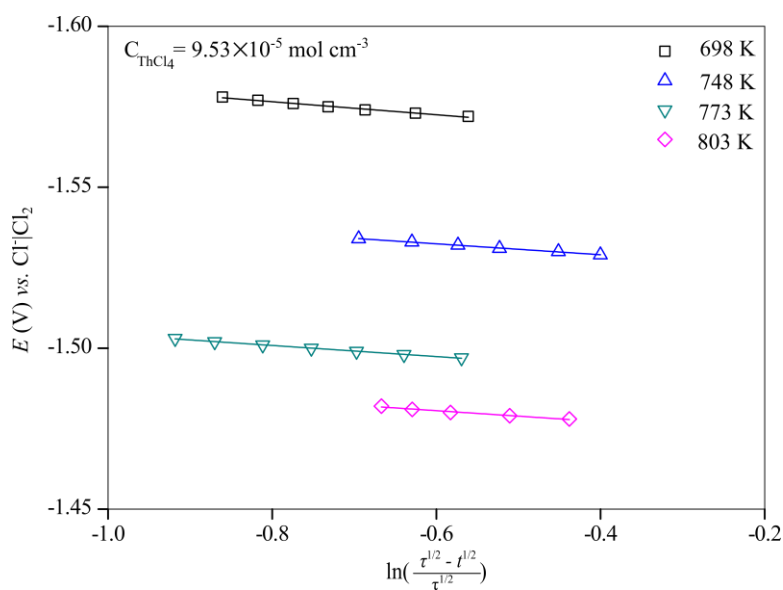
Potential data have been calculated against  $\text{Cl}_2|\text{Cl}^-$  reference using Equations 2.20 and 2.21 (discussed in Chapter 2).



a



b



c

Figure 3.13 Logarithmic analysis of chronopotentiogram of  $\text{Th}^{4+}/\text{Th}$  couple for tungsten electrode in  $\text{LiCl-KCl}$  eutectic melt, (a)  $C_{\text{ThCl}_4} = 2.04 \times 10^{-5} \text{ mol cm}^{-3}$ , (b)  $C_{\text{ThCl}_4} = 2.72 \times 10^{-5} \text{ mol cm}^{-3}$ , (c)  $C_{\text{ThCl}_4} = 9.53 \times 10^{-5} \text{ mol cm}^{-3}$ ,  $T = 698\text{--}803 \text{ K}$ ,  $A = 0.25 \text{ cm}^2$ .

Table 3.6 Estimated  $E_{\text{Th}^{4+}/\text{Th}}^{\circ\circ}$  of  $\text{Th}^{4+}/\text{Th}$  couple from CP and comparison with literature data.

$C_{\text{ThCl}_4} \times 10^5$ ( $\text{mol cm}^{-3}$ )	$T / \text{K}$	698	723	748	773	803
2.04	$E_{\text{Th}^{4+}/\text{Th}}^{\circ\circ} / \text{V vs. Ag}^+ \text{Ag}$	-1.477	-1.452	-1.426	-1.401	-1.376
	$E_{\text{Th}^{4+}/\text{Th}}^{\circ\circ} / \text{V vs. Cl}^- \text{Cl}_2$	-2.687	-2.667	-2.645	-2.624	-2.604
2.72	$E_{\text{Th}^{4+}/\text{Th}}^{\circ\circ} / \text{V vs. Ag}^+ \text{Ag}$	-1.495	-1.461	-1.438	-1.410	-1.386

	$E_{\text{Th}^{4+} \text{Th}}^{\circ*} / \text{V vs. Cl}^- \text{Cl}_2$	-2.709	-2.676	-2.657	-2.633	-2.614
9.53	$E_{\text{Th}^{4+} \text{Th}}^{\circ*} / \text{V vs. Ag}^+ \text{Ag}$	-1.477	-	-1.430	-1.392	-1.371
	$E_{\text{Th}^{4+} \text{Th}}^{\circ*} / \text{V vs. Cl}^- \text{Cl}_2$	-2.687	-	-2.649	-2.615	-2.599
Present work	$E_{\text{Th}^{4+} \text{Th}}^{\circ*} / \text{V vs. Ag}^+ \text{Ag}$	$-(2.197 \pm 0.041) + (1.02 \pm 0.05) \times 10^{-3} T(\text{K})$				
	$E_{\text{Th}^{4+} \text{Th}}^{\circ*} / \text{V vs. Cl}^- \text{Cl}_2$	$-(3.289 \pm 0.042) + (1.20 \pm 0.05) \times 10^{-3} T(\text{K})$				
Cassayre <i>et al.</i> [7]	$E_{\text{Th}^{4+} \text{Th}}^{\circ*} / \text{V vs. Cl}^- \text{Cl}_2$	$-2.983 + 5.540 \times 10^{-4} T(\text{K})$ in LiCl-KCl eutectic melt (693-823 K)				
Kudyakov <i>et al.</i> [18]	$E_{\text{Th}^{4+} \text{Th}}^{\circ*} / \text{V vs. Cl}^- \text{Cl}_2$	$-3.17 + 6.70 \times 10^{-4} T(\text{K})$ in molten KCl (800-962 K)				
Srinivasan <i>et al.</i> [24]	$E_{\text{Th}^{4+} \text{Th}}^{\circ*} / \text{V vs. Cl}^- \text{Cl}_2$	$-3.109 + 6.38 \times 10^{-4} T(\text{K})$ in molten NaCl-KCl (943-1123 K)				

$E_{\text{Th}^{4+}|\text{Th}}^{\circ*}$  of  $\text{Th}^{4+}|\text{Th}$  couple was estimated by semi-integral curves using Equation 3.7, applicable for reversible soluble-insoluble system [90]. Estimated  $E_{\text{Th}^{4+}|\text{Th}}^{\circ*}$  data are given in Table 3.7.  $E_{\text{Th}^{4+}|\text{Th}}^{\circ*}$  values were found to be in good agreement with the values calculated by chronopotentiometry method.  $E_{\text{Th}^{4+}|\text{Th}}^{\circ*}$  value was found to be in good agreement with the value obtained by Cassayre *et al.* [7] in LiCl-KCl eutectic melt from OCP measurements, Kudyakov *et al.* [18] in KCl melt and Srinivasan *et al.* [24] in KCl-NaCl melts.

Table 3.7 Estimated  $E_{\text{Th}^{4+}|\text{Th}}^{\circ*}$  values at different  $C_{\text{ThCl}_4}$  from SIV.

$C_{\text{ThCl}_4} \times 10^5$ (mol cm <sup>-3</sup> )	$T / \text{K}$	698	723	748	773	803
2.04	$E_{\text{Th}^{4+} \text{Th}}^{\circ*} / \text{V vs. Ag}^+ \text{Ag}$	-1.465	-1.418	-1.389	-1.381	-1.365
	$E_{\text{Th}^{4+} \text{Th}}^{\circ*} / \text{V vs. Cl}^- \text{Cl}_2$	-2.682	-2.657	-2.643	-2.601	-2.585
2.72	$E_{\text{Th}^{4+} \text{Th}}^{\circ*} / \text{V vs. Ag}^+ \text{Ag}$		-1.467	-1.436	-1.381	-1.371
	$E_{\text{Th}^{4+} \text{Th}}^{\circ*} / \text{V vs. Cl}^- \text{Cl}_2$		-2.687	-2.656	-2.602	-2.591
9.53	$E_{\text{Th}^{4+} \text{Th}}^{\circ*} / \text{V vs. Ag}^+ \text{Ag}$	-1.477		-1.449	-1.413	-1.371
	$E_{\text{Th}^{4+} \text{Th}}^{\circ*} / \text{V vs. Cl}^- \text{Cl}_2$	-2.697		-2.668	-2.633	-2.591
Present	$E_{\text{Th}^{4+} \text{Th}}^{\circ*} / \text{V vs. Ag}^+ \text{Ag}$	$-(2.154 \pm 0.113) + (9.805 \pm 1.501) \times 10^{-3} T(\text{K})$				

work	$E_{\text{Th}^{4+} \text{Th}}^{\circ*} / \text{V vs. Cl}^- \text{Cl}_2$	$-(3.374 \pm 0.113) + (9.805 \pm 1.501) \times 10^{-3} T(\text{K})$
------	---	---

Temperature dependence of  $E_{\text{Th}^{4+}|\text{Th}}^{\circ*}$  estimated by both CP and SIV is shown in Figure 3.14 and linear fit of combined data in Table 3.6 and 3.7 is given by Equation 3.16

$$E_{\text{Th}^{4+}|\text{Th}}^{\circ*} / \text{V vs. Cl}_2|\text{Cl}^- = -(3.377 \pm 0.060) + (9.786 \pm 0.798) \times 10^{-4} T(\text{K}) \quad (3.16)$$

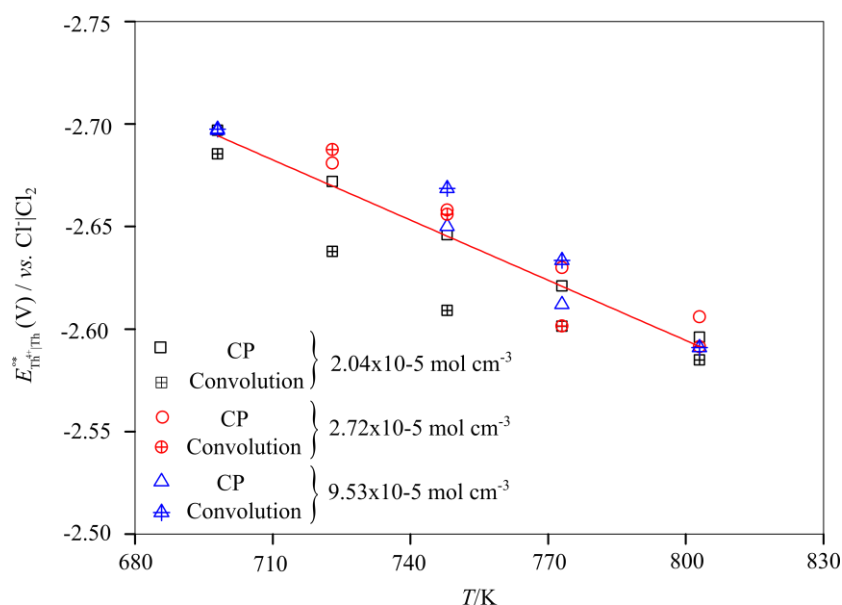


Figure 3.14 Plot of  $E_{\text{Th}^{4+}|\text{Th}}^{\circ*}$  versus  $T$  (K).

### 3.7 Anodic dissolution of Th electrode: Estimation of theoretical equilibrium potential of $\text{Th}^{4+}|\text{Th}$ couple

Cyclic voltammogram of thorium electrode in the potential region -1.65 to -0.80 V at a scan rate of  $25 \text{ mV s}^{-1}$  at 773 K is shown in Figure 3.15. From start potential of -1.65 V onwards, voltammetric current decreases to zero and cuts potential axis at -1.437 V. The point of inflection i.e. potential where voltammetric current changes its sign is called “threshold potential”, also known as “apparent equilibrium potential” denoted by  $E_{\text{Th}^{4+}|\text{Th}}^{\text{app}} = -1.437 \text{ V}$  and represents onset of thorium dissolution corresponding to following reaction:



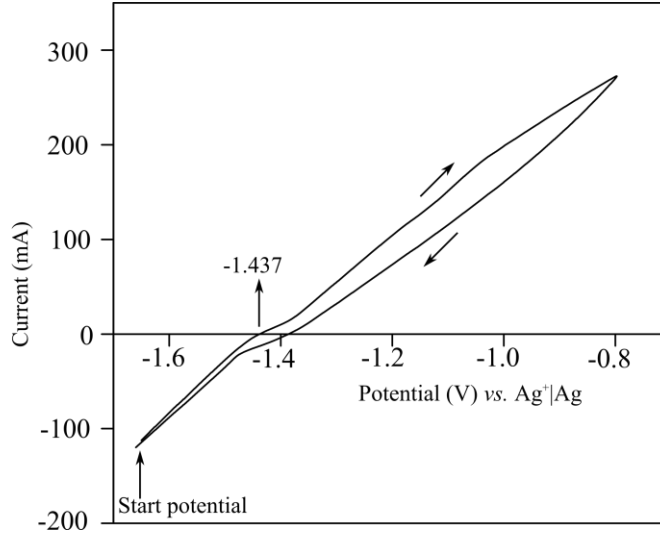


Figure 3.15 Cyclic voltammogram of Th electrode in LiCl-KCl eutectic melt,  $C_{\text{ThCl}_4} = 1.02 \times 10^{-4} \text{ mol cm}^{-3}$ ,  $T=773 \text{ K}$ , Scan rate:  $25 \text{ mV s}^{-1}$ .  $A= 1.50 \text{ cm}^2$ .

A small hump appears in potential region -1.437 to -1.360 V beyond which the voltammogram shows unlimited anodic current. General features of voltammogram are similar to that of uranium and zirconium reported earlier [99-101]. Apparent equilibrium potential was measured from cyclic voltammograms at  $50 \text{ mV s}^{-1}$  and  $100 \text{ mV s}^{-1}$  carried out in temperature range 698-798 K. They are given in Table 3.8, which also shows average “apparent equilibrium potential” versus  $\text{Ag}^+|\text{Ag}$  and  $\text{Cl}^-|\text{Cl}_2$  as reference. Potentials measured against  $\text{Ag}^+|\text{Ag}$  were converted to  $\text{Cl}^-|\text{Cl}_2$  using Equations 2.20 and 2.21 (discussed in Chapter 2). Temperature dependence of  $E_{\text{Th}^{4+}|\text{Th}}^{\text{app}}$  (versus  $\text{Ag}^+|\text{Ag}$  and  $\text{Cl}^-|\text{Cl}_2$ ) is given by Equations 3.17 and 3.18.

$$E_{\text{Th}^{4+}|\text{Th}}^{\text{app}} (\text{vs. Ag}^+|\text{Ag}) (\text{V}) = -(1.983 \pm 0.054) + (7.080 \pm 0.722) \times 10^{-4} T (\text{K}) \quad (3.17)$$

$$E_{\text{Th}^{4+}|\text{Th}}^{\text{app}} (\text{vs. Cl}^-|\text{Cl}_2) (\text{V}) = -(3.075 \pm 0.054) + (5.030 \pm 0.720) \times 10^{-4} T (\text{K}) \quad (3.18)$$

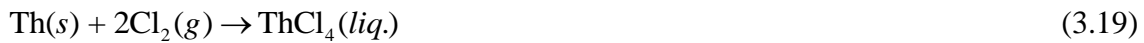
$E_{\text{Th}^{4+}|\text{Th}}^{\text{eq}}$  can be theoretically estimated for  $x_{\text{ThCl}_4} = 3.86 \times 10^{-3}$ , which is the composition of  $\text{ThCl}_4$  used for recording cyclic voltammogram of thorium electrode shown in Figure 3.15. Estimation of equilibrium potential for anodic dissolution of UN, PuN, NpN and (U,Pu)N in

LiCl-KCl eutectic from thermodynamic data has been carried out earlier by Kobayashi *et al.* [102] and Shirai *et al.* [103-105] and a similar procedure is adopted

Table 3.8  $E_{\text{Th}^{4+}|\text{Th}}^{\text{eq}}$  of Th dissolution in LiCl-KCl-ThCl<sub>4</sub> ( $x_{\text{ThCl}_4}=3.86\times 10^{-3}$ ) electrolyte measured using cyclic voltammetry at 50 mV s<sup>-1</sup> and 100 mV s<sup>-1</sup>.

Scan rate (mV s <sup>-1</sup> )	$E_{\text{Th}^{4+} \text{Th}}^{\text{eq}} / \text{V}$				
	698 K	723 K	748 K	773 K	798 K
50	-1.477	-1.468	-1.460	-1.434	-1.411
100	-1.491	-1.479	-1.469	-1.435	-1.418
Avg. (versus Ag <sup>+</sup>  Ag)	-1.484	-1.474	-1.461	-1.435	-1.415
Avg. (versus Cl <sup>-</sup>  Cl <sub>2</sub> )	-2.718	-2.713	-2.705	-2.684	-2.699

Table 3.9 shows a comparison of theoretical equilibrium potential  $E_{\text{Th}^{4+}|\text{Th}}^{\text{eq}}$  estimated from various literature sources using different thermochemical databases. Thermochemical data for  $\Delta_f G_{\text{ThCl}_4, \text{liq.}}^\circ$  have been taken from Glassner [106], Martinot *et al.* [107] and Fuger *et al.* [108] for estimating  $\gamma_{\text{ThCl}_4}$ .  $\Delta_f G_{\text{ThCl}_4, \text{liq.}}^\circ$  was also calculated using FactSage 6.4 software [109] using the Equation 3.19 and data for ThCl<sub>4</sub> (liq.) was taken from FACTPS database compiled from Barin and Kubaschewski [110].



Yang *et al.* had carried out galvanic cell measurements on uranium, thorium, zirconium and niobium in LiCl-KCl eutectic melt [15]. They had used  $\Delta_f G_{\text{ThCl}_4, \text{liq.}}^\circ$  values from Glassner's compilation [106].

Even though Yang and Hudson measured emf at 772 K and 774 K, it is useful to compare calculated equilibrium potential with that measured in present work at 773 K. At 772 K and 774 K, they reported  $\gamma_{\text{ThCl}_4} = 1.16 \times 10^{-3}$ ,  $\Delta_f G_{\text{ThCl}_4, \text{liq.}}^\circ = -957.86 \text{ kJ mol}^{-1}$  and

$\gamma_{\text{ThCl}_4} = 1.21 \times 10^{-3}$ ,  $\Delta_f G_{\text{ThCl}_4, \text{liq.}}^\circ = -957.52 \text{ kJ mol}^{-1}$ , respectively.  $E_{\text{Th}^{4+}|\text{Th}}^{\text{eq}}$  was estimated at -1.655 V and -1.654 V at 772 K and 774 K, respectively. When reference state data was taken from Barin and Kubaschewski [110],  $\gamma_{\text{ThCl}_4}$  was found to be in  $10^{-7}$  range that led to significantly more negative values of  $E_{\text{Th}^{4+}|\text{Th}}^{\text{eq}}$ .

Martinot *et al.* carried out electromotive force measurements of  $\text{ThCl}_4$  in LiCl-KCl and NaCl-KCl systems [107]. For LiCl-KCl eutectic, they reported following expressions for Gibbs energy of formation of  $\text{ThCl}_4$  in melt and super cooled liquid as reference state:

$$\Delta_f G_{\text{ThCl}_4, \text{LiCl-KCl}}^\circ (\text{J mol}^{-1}) = -1114000 + 207T(\text{K}) \quad (3.20)$$

$$\Delta_f G_{\text{ThCl}_4, \text{liq.}}^\circ (\text{J mol}^{-1}) = -1092000 + 201T(\text{K}) \quad (3.21)$$

$E_{\text{Th}^{4+}|\text{Th}}^{\text{eq}}$  was estimated at -1.385 V. Electromotive force data of Martinot *et al.* was further analysed by fitting method by Roy *et al.* that was used for estimating Gibbs energy of formation of  $\text{UCl}_3$ ,  $\text{PuCl}_3$  and  $\text{NpCl}_3$  in LiCl-KCl eutectic melt [70]. The method involved linear fitting of logarithm of mole-fraction of actinide chloride *versus*  $E + E_{\text{AgCl}}^\circ + \frac{RT}{F} \ln x_{\text{AgCl}}$  at a given temperature  $T$ . Gibbs energy of formation of actinide chloride at temperature  $T$  was given by product of intercept of linear fit (equal to standard electrode potential of actinide chloride in LiCl-KCl eutectic) and  $nF$ . From Martinot *et al.* report,  $x_{\text{AgCl}} = 4.6 \times 10^{-3}$  and  $\Delta_f G_{\text{ThCl}_4, \text{LiCl-KCl}}^\circ$  was found to be  $-977.78 \text{ kJ mol}^{-1}$  at 773 K as against  $-953.99 \text{ kJ mol}^{-1}$  reported by the authors.  $\gamma_{\text{ThCl}_4}$  was found to be  $1.65 \times 10^{-3}$  and  $E_{\text{Th}^{4+}|\text{Th}}^{\text{eq}}$  was estimated at -1.508 V at 773 K.  $E_{\text{Th}^{4+}|\text{Th}}^{\text{eq}}$  was also estimated from Martinot's work using thermochemical data for  $\text{ThCl}_4$  (liq.) from Fuger *et al.* [108] and Barin and Kubaschewski [109, 110] using  $\Delta_f G_{\text{ThCl}_4, \text{LiCl-KCl}}^\circ$

reported by Martinot and  $-977.78 \text{ kJ mol}^{-1}$  that was obtained using method of Roy *et al.* [70].

$E_{\text{Th}^{4+}|\text{Th}}^{\text{eq}}$  was found to be in the range  $-1.354$  to  $-1.503 \text{ V}$ .

From Cassayre *et al.* work [7],  $E_{\text{Th}^{4+}|\text{Th}}^{\text{eq}}$  was estimated at  $-1.536 \text{ V}$  and  $-1.528 \text{ V}$  using reference state data from Fuger *et al.* [108] and Barin and Kubaschewski [109, 110], respectively.

From Table 3.9, it is clear that

- a. Yang *et al.* [15] estimated more negative value of  $\Delta_f G_{\text{ThCl}_4, \text{LiCl-KCl}}^\circ$  at  $772 \text{ K}$  and  $774 \text{ K}$  than those reported by Refs. [7, 107], which leads to large negative values of  $E_{\text{Th}^{4+}|\text{Th}}^{\text{eq}}$ .  $E_{\text{Th}^{4+}|\text{Th}}^{\text{eq}}$  value estimated using reference state data of Barin *et al.* [110] was observed to be more negative than that estimated from the works of Cassayre *et al.* [7] and Martinot *et al.* [107].
- b. Martinot *et al.* [107] have reported  $\Delta_f G_{\text{ThCl}_4, \text{LiCl-KCl}}^\circ = -953.99 \text{ kJ mol}^{-1}$  whereas it is calculated to be  $-977.78 \text{ kJ mol}^{-1}$  from linear fitting of emf data using the procedure by Roy *et al.* [70]. Using  $\Delta_f G_{\text{ThCl}_4, \text{LiCl}}^\circ$  reference state data from Refs. [107, 108, 110]  $E_{\text{Th}^{4+}|\text{Th}}^{\text{eq}}$  is calculated in the range  $-1.354$  to  $-1.508 \text{ V}$  and his variation may be considered marginal.
- c.  $E_{\text{Th}^{4+}|\text{Th}}^{\text{eq}}$  is estimated in the range of  $-1.528$  to  $-1.559 \text{ V}$  from the work of Cassayre *et al.* using reference state data from Refs. [107, 108, 110].
- d. Variation in  $E_{\text{Th}^{4+}|\text{Th}}^{\text{eq}}$  is found to be marginal among the works of Martinot *et al.* [107] and Cassayre *et al.* [7] estimated using reference state data from Martinot *et al.* [107], Fuger *et al.* [108] and Barin *et al.* [110] whereas variation is quite large from reference state data of Yang *et al.* [15]. The reason for this deviation is presently not known.

e. Therefore, average theoretical equilibrium potential is estimated only from reports of Martinot *et al.* [107], Cassayre *et al.* [7] and it is found to be  $-1.469 \pm 0.076$  V for  $x_{\text{ThCl}_4} = 3.86 \times 10^{-3}$  which is in good agreement with that measured by cyclic voltammetry (Table 3.9) considering variations due to experimental conditions employed in different works, method of fitting emf data for obtaining  $\Delta_f G_{\text{ThCl}_4, \text{LiCl-KCl}}^\circ$  and source of thermochemical data  $\Delta_f G_{\text{ThCl}_4, \text{liq.}}^\circ$ .

Based on above analysis, it can be said that values of  $\Delta_f G_{\text{ThCl}_4, \text{liq.}}^\circ$  from various thermochemical data resources is the most important factor behind large deviation of  $E_{\text{Th}^{4+}|\text{Th}}^{\text{eq}}$  from experimental values and influences the estimation of  $\gamma_{\text{ThCl}_4}$  (Equation 2.22, discussed in Chapter 2).

*Table 3.9 Summary of calculated equilibrium potential of thorium dissolution in LiCl-KCl eutectic melt at  $T=773$  K from various literature sources. Data of Yang *et al.* [15] are at 772 K and 774 K.  $x_{\text{ThCl}_4} = 3.86 \times 10^{-3}$  is assumed for all calculations.*

References	$\Delta_f G_{\text{ThCl}_4, \text{LiCl-KCl}}^\circ$ (kJ mol <sup>-1</sup> )	$\Delta_f G_{\text{ThCl}_4, \text{liq.}}^\circ$ (kJ mol <sup>-1</sup> )	$\gamma_{\text{ThCl}_4}$	$E$ / V
Yang <i>et al.</i> [15]	-1036.90 <sup>a</sup>	-957.86 <sup>c</sup>	$1.16 \times 10^{-3}$	-1.655
		-944.33 <sup>d</sup>	$5.45 \times 10^{-7}$	-1.783
	-1036.58 <sup>b</sup>	-957.52 <sup>c</sup>	$1.21 \times 10^{-3}$	-1.654
		-943.34 <sup>d</sup>	$5.51 \times 10^{-7}$	-1.782
Martinot <i>et al.</i> [107]	-953.99	-936.63 [107]	$6.71 \times 10^{-2}$	-1.385
		-944.09 <sup>d</sup>	0.214	-1.354
	-977.78 <sup>f</sup>	-938.99 <sup>e</sup>	$9.69 \times 10^{-2}$	-1.379
		-936.63 [107]	$1.65 \times 10^{-3}$	-1.508
		-944.09 <sup>d</sup>	$5.29 \times 10^{-3}$	-1.477
		-938.99 <sup>e</sup>	$2.39 \times 10^{-3}$	-1.503
Cassayre <i>et al.</i> [7]	-987.62	-938.99 <sup>e</sup>	$6.80 \times 10^{-4}$	-1.536
		-944.09 <sup>d</sup>	$1.14 \times 10^{-3}$	-1.528
		-936.63 [107]	$3.58 \times 10^{-3}$	-1.559
Present study	-972.01	-938.99 <sup>e</sup>	$5.56 \times 10^{-3}$	-1.462
		-944.09 <sup>d</sup>	$1.23 \times 10^{-2}$	-1.448
		-936.63 [107]	$4.06 \times 10^{-3}$	-1.479

<sup>a</sup> At T = 772 K

<sup>b</sup> At T = 774 K

<sup>c</sup> From Glassner [106]

<sup>d</sup> From Barin and Kubaschewski [109, 110]

<sup>e</sup> From Fuger *et al.*[108]

<sup>f</sup> Method of Roy *et al.* [70]

### 3.8 Cyclic voltammetry of Th<sup>4+</sup> at liquid cadmium electrode: Underpotential deposition of Th

Cyclic voltammogram of ThCl<sub>4</sub> at liquid cadmium electrode recorded for 3.55×10<sup>-5</sup> mol cm<sup>-3</sup> ThCl<sub>4</sub> in LiCl-KCl eutectic melt at 773 K is shown in Figure 3.16. Onset potential for reduction of thorium in cadmium appears at -1.21 V, which signifies underpotential deposition of thorium and formation of Cd-Th alloy. Cyclic voltammogram is associated with appearance of two cathodic peaks at -1.31 V and -1.38 V which correspond to the formations of two Cd-Th alloys, Cd<sub>11</sub>Th and Cd<sub>5</sub>Th respectively. At -1.31 V Cd<sub>11</sub>Th is in equilibrium with Cd and at -1.38 V Cd<sub>5</sub>Th is in equilibrium with Cd<sub>11</sub>Th forming two phase alloys. Electrochemical reactions for formation of Cd<sub>11</sub>Th and Cd<sub>5</sub>Th alloys are given by Equations 3.22 and 3.23 respectively.



Cyclic voltammograms of ThCl<sub>4</sub> at liquid cadmium cathode for different scan rates are shown in Figure 3.17. It was observed that though two cathodic peaks were appeared at lower scan rates but at higher scan rates only one cathodic peak appeared.

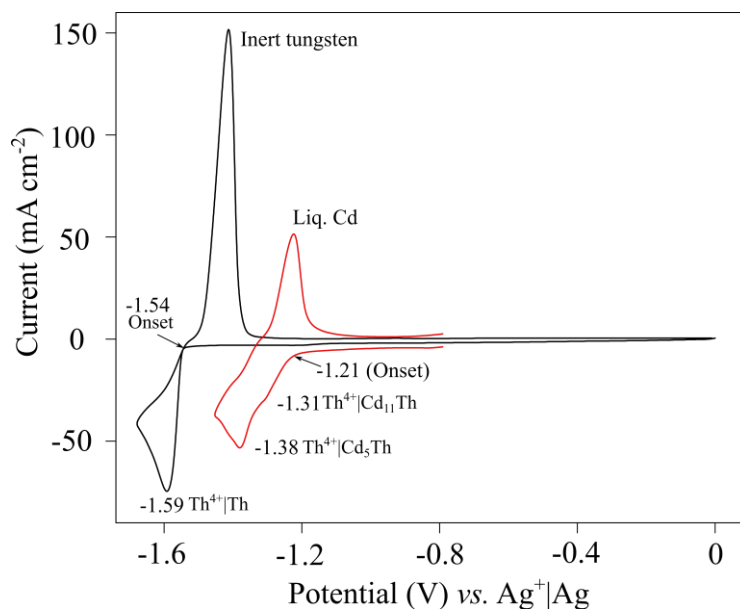


Figure 3.16 Cyclic voltammograms of  $\text{LiCl-KCl-ThCl}_4$  at inert tungsten and liquid cadmium electrode,  $C_{\text{ThCl}_4} = 3.55 \times 10^{-5} \text{ mol cm}^{-3}$ ,  $A = 0.25 \text{ cm}^2$  at inert tungsten electrode;  $C_{\text{ThCl}_4} = 1.08 \times 10^{-4} \text{ mol cm}^{-3}$ ,  $A = 1.48 \text{ cm}^2$  at liquid cadmium electrode, scan rate for both the voltammograms is  $25 \text{ mV s}^{-1}$ ,  $T = 773\text{K}$ .

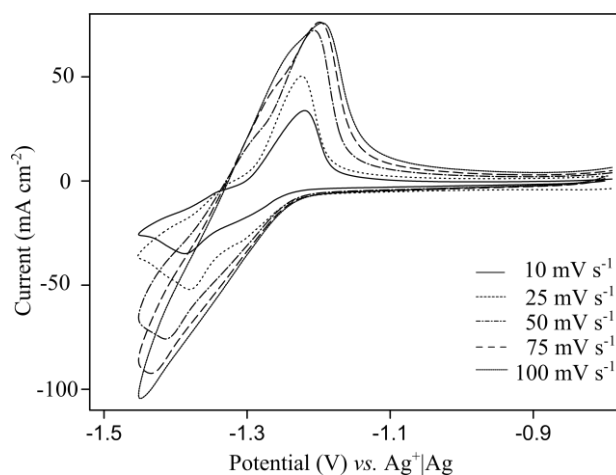
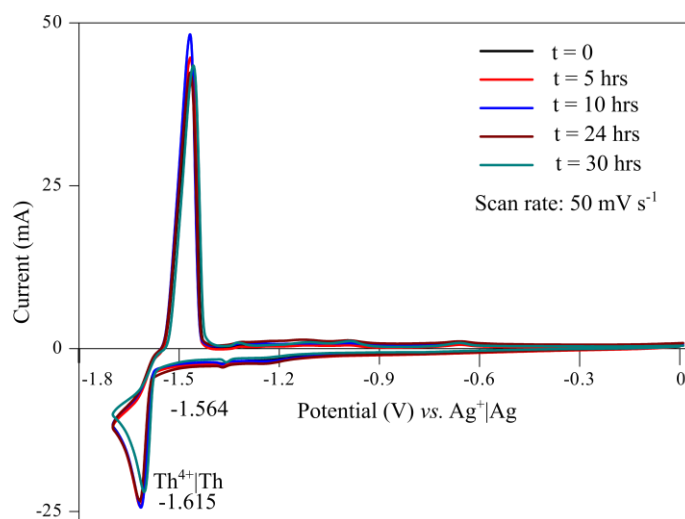


Figure 3.17 Cyclic voltammograms of  $\text{LiCl-KCl-ThCl}_4$  at liquid cadmium electrode at various scan rates.  $T = 698$ ,  $C_{\text{ThCl}_4} = 1.08 \times 10^{-4} \text{ mol cm}^{-3}$ .

### 3.9 Influence of $\text{CdCl}_2$ on redox behaviour of $\text{Th}^{4+}$ and investigation of disproportionation of $\text{Th}^{4+}$

Qualitative analysis of cadmium in  $\text{LiCl-KCl-ThCl}_4$  was done by cyclic voltammetry at inert tungsten electrode. Cyclic voltammogram of  $\text{LiCl-KCl-ThCl}_4$  salt (prepared by equilibration method discussed in Chapter 2) recorded at inert tungsten electrode over a period of 30 h are

shown in Figure 3.18. The voltammograms were found to be reproducible and similar to what is already described in Figure 3.3. No additional peak is appeared for  $\text{Cd}^{2+}|\text{Cd}$  couple. Figure 3.18 confirms that there is no contamination of cadmium in the melt, which could lead to underpotential deposition of thorium.



*Figure 3.18 Cyclic voltammograms of  $\text{LiCl-KCl-ThCl}_4$  at inert tungsten electrode over period of 30 h,  $T=773$  K.*

In order to show underpotential deposition of thorium cyclic voltammogram of  $\text{LiCl-KCl-ThCl}_4\text{-CdCl}_2$  electrolyte was recorded at inert tungsten working electrode, which is shown in Figure 3.19. Cathodic peak at  $-0.616$  V with an onset at  $-0.543$  V corresponds to  $\text{Cd}^{2+}|\text{Cd}$  couple. Onset at  $-1.303$  V with a cathodic peak at  $-1.407$  V and corresponding anodic peak at  $-1.305$  V pertains to underpotential deposition of thorium in cadmium due to formation of  $\text{Cd}_{11}\text{Th}$ . Cathodic peak at  $-1.612$  V with an onset at  $-1.557$  V and a corresponding anodic peak at  $-1.422$  V is attributed to  $\text{Th}^{4+}|\text{Th}$  couple.

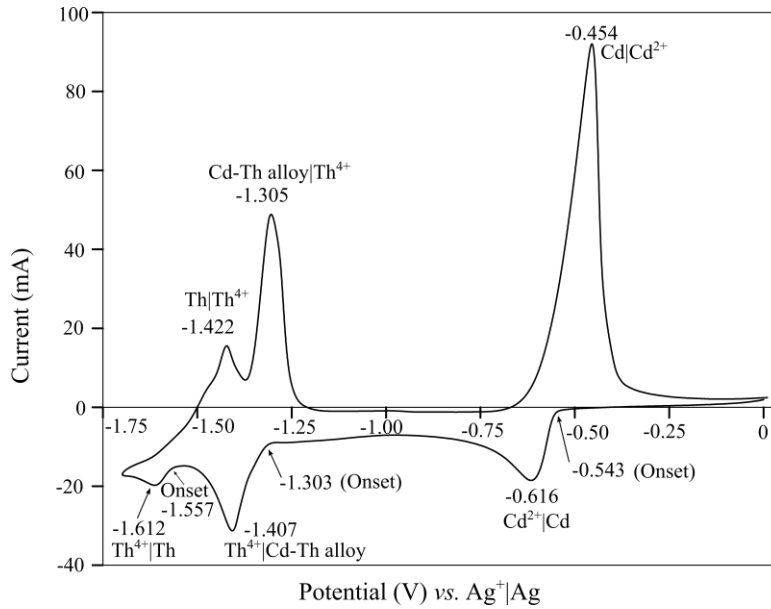
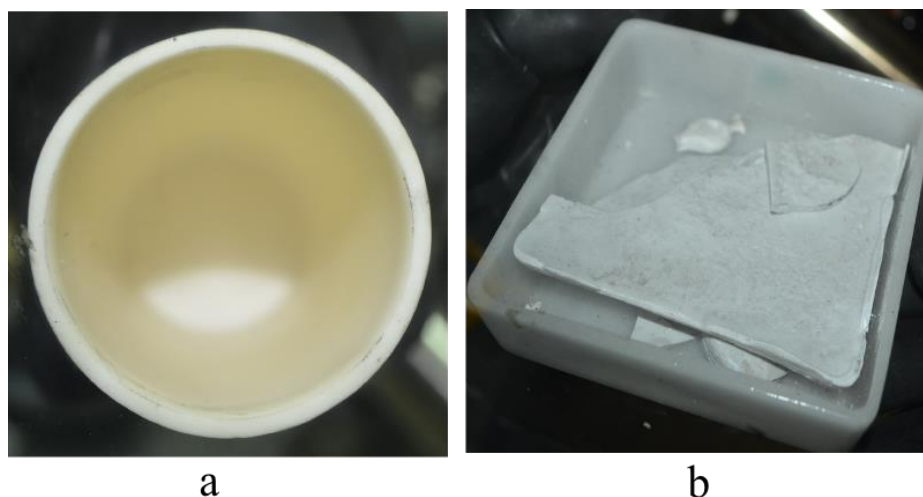


Figure 3.19 Cyclic voltammogram of LiCl-KCl eutectic containing  $\text{ThCl}_4$  and  $\text{CdCl}_2$  at inert tungsten electrode,  $T = 773 \text{ K}$ .  $C_{\text{ThCl}_4} = 1.08 \times 10^{-4} \text{ mol cm}^{-3}$ ,  $C_{\text{CdCl}_2} = 5.20 \times 10^{-5} \text{ mol cm}^{-3}$ .

### 3.10 Corrosion study of alumina crucible during electrochemical measurement

It is seen from the works of [7, 111] that recrystallized alumina was used as container material for LiCl-KCl- $\text{ThCl}_4$  electrolyte during electrochemical measurements. Similar such recrystallized alumina crucible shown in Figure 3.20a was used for present measurements as well, which was initially cleaned with nitric acid and washed with distilled water and acetone and further vacuum dried at 773 K for 6 h before it was used for electrochemical measurements. LiCl-KCl- $\text{ThCl}_4$  electrolyte used for the present measurements is shown in Figure 3.20b. Salt was loaded in recrystallized alumina crucible and heated to 773 K under argon atmosphere for a period of 30 h. Two experiments were carried out; one in which thorium electrode was immersed into the melt and the other in which, it wasn't. After 30 h, the system was cooled and crucible was taken inside the glove box. Th electrode prepared for experiment is shown in Figure 3.21, first one is before experiment and later figure after immersion in the melt. It was then re-melted and poured out of the crucible on fused silica dish.



*Figure 3.20 (a) Recrystallized alumina crucible before experiments, (b) LiCl-KCl-ThCl<sub>4</sub> electrolyte used for the present measurements before experiment.*

The inner surface of alumina crucible that was in contact with LiCl-KCl-ThCl<sub>4</sub> is shown in Figure 3.22a and 3.22b, the latter figure corresponding to the experiment carried out when thorium electrode was immersed into the melt. LiCl-KCl-ThCl<sub>4</sub> electrolyte poured out from the crucible after completion of measurements is shown in Figure 3.23a and 3.23b, the latter figure corresponding to salt in which measurements were carried out with thorium electrode immersed into it. As can be seen from the figures, there was no signature of corrosion of alumina crucible due to ThCl<sub>4</sub> or metallic thorium in contact with the salt. Alumina crucible, after cleaning with distilled water and nitric acid followed by washing it with acetone and distilled water, could be re-used for further experiments. Corrosion of alumina crucible in presence of LiCl-KCl-ThCl<sub>4</sub> electrolyte was checked by carrying out cyclic voltammetry experiments of the electrolyte in presence of thorium metal and in absence of thorium metal in the melt to show that there is no formation of Th<sup>2+</sup> ion and no formation of any oxychlorides of thorium due to corrosion of alumina crucible. Both experiments were carried out over a period of 30 h at 773 K in order to get reproducible data.



*Figure 3.21 Th electrode prepared for experiment (a) before immersion in the melt and (b) after immersion in the melt.*

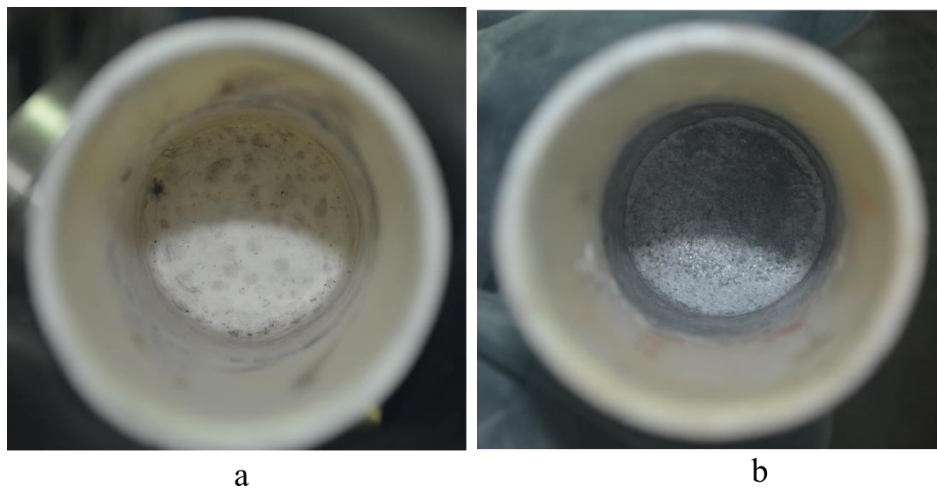


*Figure 3.22 Alumina crucible after experiment (a) when Th electrode was not immersed and (b) when Th electrode was immersed in the melt.*

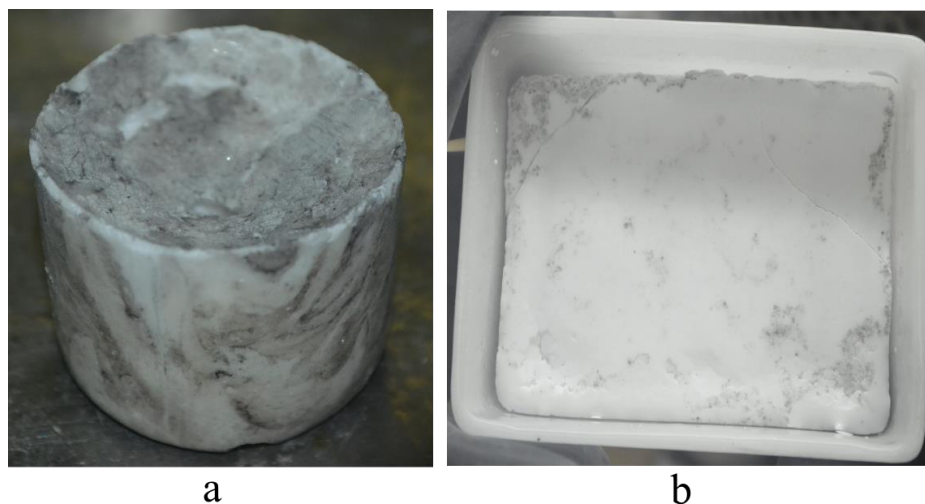


*Figure 3.23 LiCl-KCl-ThCl<sub>4</sub> electrolyte after experiment (a) when Th electrode was not immersed and (b) when Th electrode was immersed in the melt.*

Cyclic voltammograms of LiCl-KCl-ThCl<sub>4</sub> electrolyte for inert tungsten electrode recorded at various time intervals when thorium electrode was not immersed into the melt are shown in Figure 3.18. It can be seen from all the voltammograms that they are quite reproducible even after  $t = 30$  h. This along with the fact that there was no corrosion of alumina crucible as described above was suggestive of the fact that there was neither any formation of oxychlorides of thorium nor was there any reaction of ThCl<sub>4</sub> with oxide species. This experiment confirmed that the only stable oxidation state of thorium in LiCl-KCl eutectic was +4 and the salt electrolyte did not react with alumina crucible.

A similar behaviour was observed when cyclic voltammograms were recorded at inert tungsten electrode with metallic thorium electrode was immersed into the melt. Cyclic voltammograms recorded at various time intervals are shown in Figure 3.24, which have similar features as in those shown in Figure 3.18 that confirmed there was no reduction of Th<sup>4+</sup> to Th<sup>2+</sup> in presence of metallic thorium.

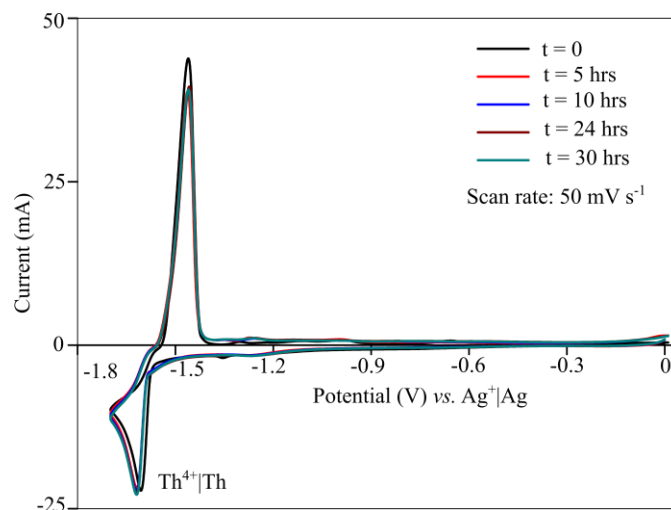


Figure 3.24 Cyclic voltammograms of  $\text{LiCl-KCl-ThCl}_4$  at inert tungsten electrode over period of 30 h,  $T=773$  K, thorium electrode was kept immersed into the melt during cyclic voltammetric measurements.

### 3.11 Conclusions

Electrochemical investigations on  $\text{Th}^{4+}|\text{Th}$  couple were carried out by different transient techniques like cyclic voltammetry, chronopotentiometry, squarewave voltammetry and compared with literature data. Following conclusions are drawn on redox behaviour of  $\text{Th}^{4+}|\text{Th}$  couple:

1. Based on the values of  $n$ ,  $an$  (Table 3.1 and 3.4) and other salient features observed in transient measurements,  $\text{Th}^{4+}|\text{Th}$  redox couple was established to be quasi-reversible in nature at the composition and temperature range studied in the present work.
2.  $D_{\text{Th}^{4+}}$  estimated using different transient techniques at different temperatures and concentrations were fitted to single expression of temperature dependence (Eq. 3.14). Concentration dependence of  $D_{\text{Th}^{4+}}$  although not as prominent as its temperature dependence, was difficult to quantify as the concentration range of  $\text{ThCl}_4$  in the present work was limited. Further experiments are needed to make substantiable conclusions.

3.  $E_{\text{Th}^{4+}|\text{Th}}^{\circ*}$  estimated using semi-integral voltammetry and chronopotentiometry was fitted to single temperature dependence expression and compared with literature data. Eq. 3.16 is the recommended expression for  $E_{\text{Th}^{4+}|\text{Th}}^{\circ*}$  in this work. This work is further discussed in Chapter 6.

## CHAPTER 4

### Exchange current density of Th<sup>4+</sup>|Th couple in LiCl-KCl eutectic melt

#### Results and Discussions

This chapter describes estimation of  $i_0$  of Th<sup>4+</sup>|Th couple at inert tungsten, liquid cadmium and thorium electrodes in LiCl-KCl eutectic melt using DC amperometry. Anodic and cathodic polarization data were subsequently analysed by Tafel and Allen-Hickling methods for estimation of  $i_0$ .  $i_0$  estimated at inert tungsten electrode using DC amperometry was compared with that calculated from cyclic voltammograms of LiCl-KCl-ThCl<sub>4</sub>. The chapter concludes with discussion on temperature and composition dependence of  $i_0$ .

#### 4.1 Estimation of $i_0$ at inert tungsten electrode

##### 4.1.1 Estimation of $i_0$ from polarization curves

Exchange current density of Th<sup>4+</sup>|Th couple at inert tungsten electrode was estimated by both polarization and cyclic voltammetry techniques. In polarization technique inert tungsten electrode was cathodically polarized at different cathodic overpotential values. Cathodic polarization runs were carried out at inert tungsten electrode in the temperature range 698-798 K.  $i$  vs.  $t$  profile recorded at various cathodic potentials at 773 K is shown in Figure 4.1. Current was sampled at  $t=30$ s for all applied potentials and was plotted against  $E$  and  $i$  vs.  $E$  profiles for cathodic and anodic polarization of thorium at inert tungsten, liq. Cd and Th electrodes are shown in Figure 4.2.

$i_0$  of thorium at inert tungsten electrode in LiCl-KCl eutectic melt was estimated by analyzing the polarization curve by Tafel and Allen-Hickling methods. In Tafel method,  $\ln i$  was plotted against overpotential ( $\eta$ ), which is shown in Figure 4.3. The governing equation for Tafel analysis can be rearranged as Equation 4.1.

$$\ln i = \ln i_o - \frac{n\alpha F}{RT} \eta \quad (4.1)$$

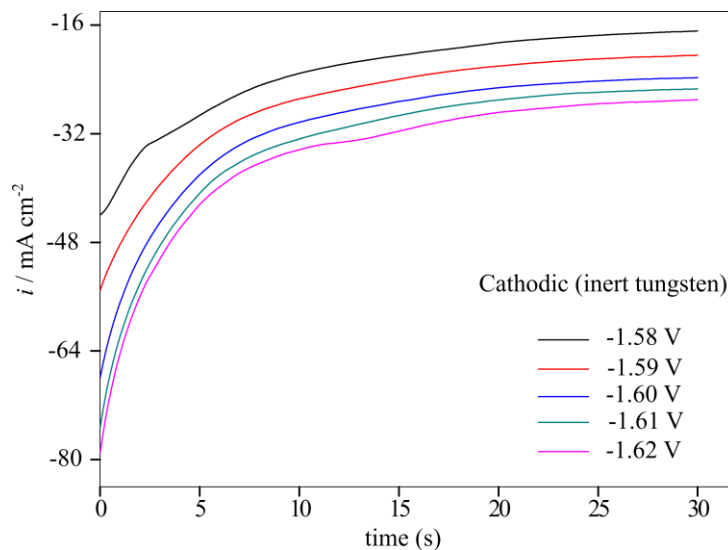


Figure 4.1  $i$  vs.  $t$  profile for cathodic polarization of thorium at inert tungsten electrode at various potentials,  $T = 773$  K.

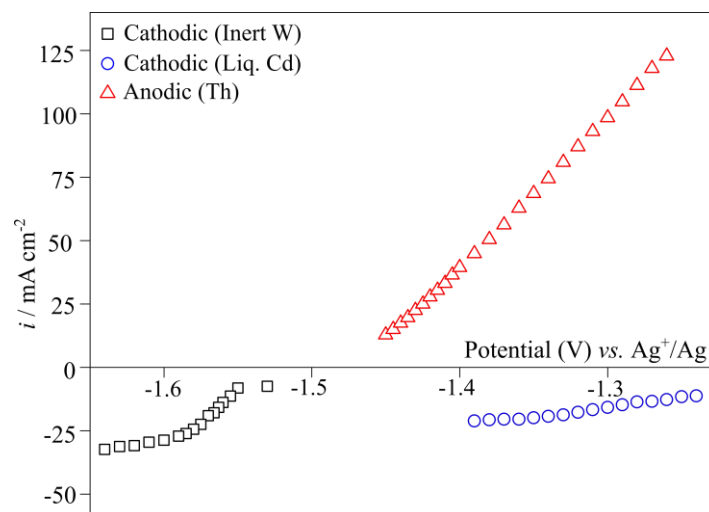


Figure 4.2  $i$  vs.  $E$  profile for cathodic and anodic polarization of thorium at inert tungsten, liq. Cd and Th electrodes at various potentials,  $T = 773$  K.

In Allen-Hickling method,  $\ln \left( \frac{i}{1 - e^{-\frac{nF}{RT} \eta}} \right)$  was plotted against  $\eta$ , which is shown in Figure 4.4.

Tafel and Allen-Hickling constants were estimated as discussed in Chapter 2.  $i_o$ ,  $a_{\text{Tafel}}$ ,  $b_{\text{Tafel}}$  and  $b_{\text{Allen-Hickling}}$  for cathodic polarization at inert tungsten electrode in the temperature range of 698-798 K are tabulated in Table 4.1.

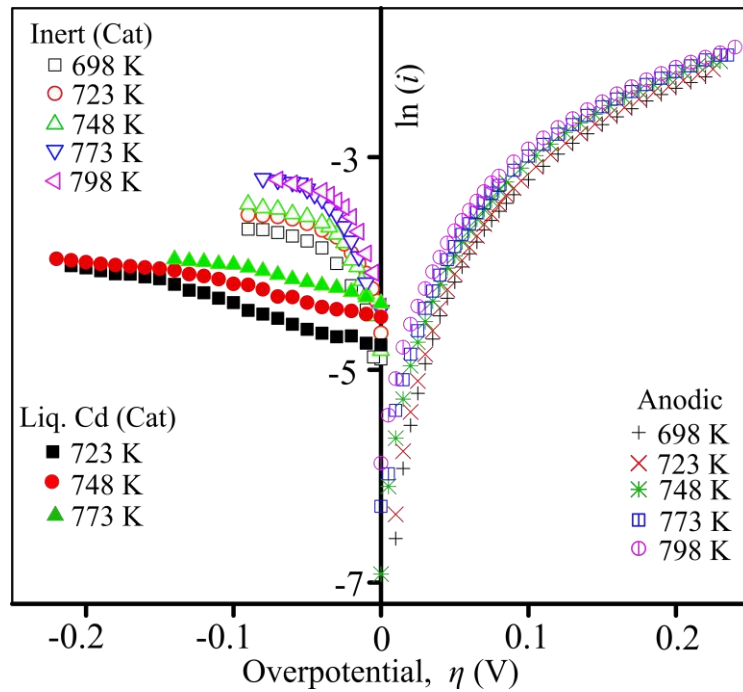


Figure 4.3 Tafel plots for anodic and cathodic polarization of thorium at inert tungsten and liquid cadmium cathodes in LiCl-KCl eutectic melt.  $C_{\text{ThCl}_4} = 1.08 \times 10^{-4} \text{ mol cm}^{-3}$  for inert (cathodic) and anodic;  $C_{\text{ThCl}_4} = 6.91 \times 10^{-5} \text{ mol cm}^{-3}$  for liq. Cd (cathodic).

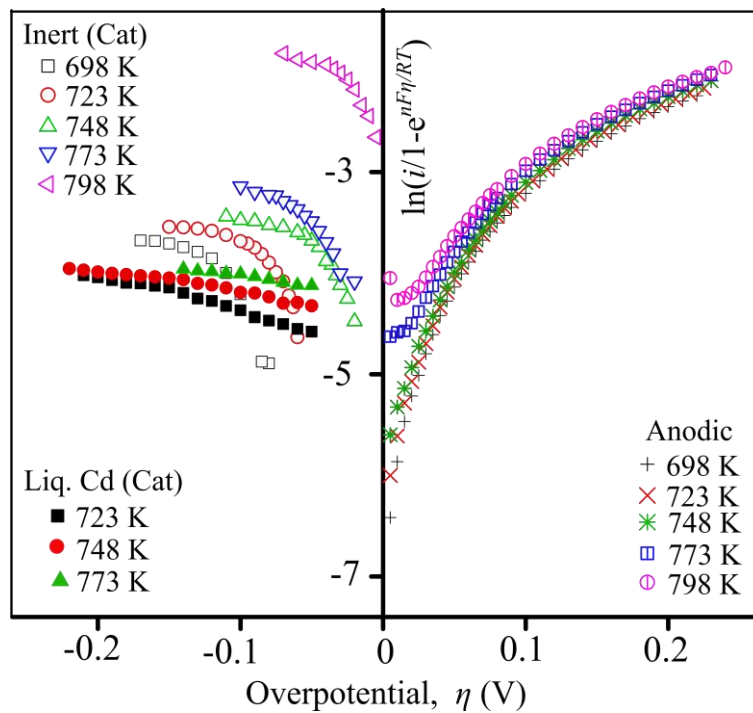


Figure 4.4 Allen-Hickling plots of anodic and cathodic polarization of thorium at inert tungsten and liquid cadmium cathode in LiCl-KCl eutectic

*melt.*  $C_{\text{ThCl}_4} = 1.08 \times 10^{-4} \text{ mol cm}^{-3}$  for inert (cathodic) and anodic;  
 $C_{\text{ThCl}_4} = 6.91 \times 10^{-5} \text{ mol cm}^{-3}$  for liq. Cd (cathodic).

Table 4.1  $i_o$ ,  $a_{\text{Tafel}}$ ,  $b_{\text{Tafel}}$  and  $b_{\text{Allen-Hickling}}$  of thorium at inert tungsten electrode in LiCl-KCl eutectic melt.

$C_{\text{ThCl}_4} \times 10^5$ (mol cm <sup>-3</sup> )	T/K	Tafel method			Allen-Hickling method	
		$a_{\text{Tafel}}$ (mV)	$b_{\text{Tafel}}$ (mV)	$i_o$ (mA cm <sup>-2</sup> )	$b_{\text{Allen-Hickling}}$ (V <sup>-1</sup> )	$i_o$ (mA cm <sup>-2</sup> )
10.8	698	1040 ± 140	-260 ± 30	19.83 ± 0.97	2.86 ± 0.44	15.97 ± 0.93
	723	1200 ± 220	-320 ± 60	21.78 ± 0.97	2.71 ± 0.52	19.91 ± 0.93
	748	1080 ± 90	-280 ± 20	23.78 ± 0.98	2.93 ± 0.24	23.57 ± 0.98
	773	730 ± 170	-210 ± 80	28.25 ± 0.96	4.24 ± 0.62	28.53 ± 0.95
	798	720 ± 80	-210 ± 20	30.72 ± 0.98	3.91 ± 0.44	31.09 ± 0.98
3.55	698	1243 ± 307	-406 ± 96	18.98 ± 0.47	-	-
	723	996 ± 59	-322 ± 18	21.98 ± 0.83	3.14 ± 0.02	16.57 ± 0.99
	748	858 ± 54	-267 ± 15	24.78 ± 0.82	3.38 ± 0.18	21.49 ± 0.98
	773	2969 ± 908	-819 ± 245	37.54 ± 0.33	0.02 ± 0.12	40.93 ± 0.99
	798	2504 ± 339	-657 ± 87	45.49 ± 0.59	0.79 ± 0.13	51.25 ± 0.98
2.72	698	2508 ± 90	-827 ± 29	20.69 ± 0.89	0.83 ± 0.08	21.24 ± 0.99
	723	747 ± 69	-233 ± 20	24.78 ± 0.74	3.69 ± 0.32	24.09 ± 0.97
	748	873 ± 75	-247 ± 19	33.78 ± 0.74	3.42 ± 0.26	35.68 ± 0.98
	773	2571 ± 330	-666 ± 83	46.99 ± 0.61	0.66 ± 0.10	50.44 ± 0.99
	798	4674 ± 346	-1192 ± 869	50.79 ± 0.75	0.56 ± 0.05	51.30 ± 0.94
2.04	698	7568 ± 170	-2523 ± 562	19.49 ± 0.93	-	-
	723	2939 ± 608	-982 ± 197	20.28 ± 0.54	1.00 ± 0.12	19.10 ± 0.98
	748	2296 ± 393	-739 ± 122	22.35 ± 0.59	0.98 ± 0.17	22.96 ± 0.98
	773	5206 ± 557	-1549 ± 163	28.79 ± 0.69	0.73 ± 0.14	28.04 ± 0.98
	798	1698 ± 285	-498 ± 81	30.26 ± 0.56	1.00 ± 0.09	31.74 ± 0.99

#### 4.1.2 Estimation of $i_o$ at inert tungsten electrode by cyclic voltammetry

$i_o$  of Th<sup>4+</sup>|Th couple was estimated by cyclic voltammetry using method described by Cumberland and Yim [112, 113]. They adopted a linear approximation method (Equation

4.2) applicable for cyclic voltammograms recorded at higher scan rates.  $i_o$  was estimated using scan rates of 100 and 200  $\text{mV s}^{-1}$  (Cyclic voltammetric data taken from Chapter 3) and results are tabulated in Table 4.2.

$$i_o = \frac{RT\Delta i}{nF\Delta\eta} \quad (4.2)$$

Table 4.2  $i_o$  of  $\text{Th}^{4+}/\text{Th}$  couple at inert tungsten electrode from cyclic voltammetric data (Chapter 3).

$C_{\text{ThCl}_4} \times 10^5$ ( $\text{mol cm}^{-3}$ )	$T / \text{K}$	Scan rate ( $\text{mV s}^{-1}$ )	$\Delta i / \Delta\eta$ ( $\Omega^{-1}$ )	$i_o$ ( $\text{mA cm}^{-2}$ )	
2.04	698	100	$0.25 \pm 0.03$	$14.82 \pm 0.42$	
		200	$0.26 \pm 0.03$	$15.41 \pm 0.42$	
	723	100	$0.29 \pm 0.03$	$17.68 \pm 0.45$	
		200	$0.28 \pm 0.02$	$17.31 \pm 0.39$	
	748	100	$0.31 \pm 0.03$	$19.60 \pm 0.49$	
		200	$0.30 \pm 0.03$	$18.97 \pm 0.42$	
	773	100	$0.22 \pm 0.02$	$19.34 \pm 0.30$	
		200	$0.31 \pm 0.03$	$20.46 \pm 0.47$	
	2.72	698	100	$0.31 \pm 0.04$	$18.37 \pm 0.57$
			200	$0.39 \pm 0.05$	$23.12 \pm 0.79$
		723	100	$0.34 \pm 0.03$	$21.10 \pm 0.41$
			200	$0.36 \pm 0.03$	$22.34 \pm 0.50$
748		100	$0.44 \pm 0.04$	$27.83 \pm 0.70$	
		200	$0.44 \pm 0.03$	$27.83 \pm 0.45$	
773		100	$0.46 \pm 0.02$	$29.98 \pm 0.37$	
		200	$0.47 \pm 0.04$	$30.92 \pm 0.25$	
3.55		698	100	$0.44 \pm 0.08$	$26.14 \pm 1.17$
			200	$0.47 \pm 0.06$	$27.92 \pm 0.96$
		723	100	$0.59 \pm 0.06$	$36.42 \pm 0.97$
			200	$0.52 \pm 0.06$	$32.21 \pm 0.91$
	748	100	$0.58 \pm 0.06$	$36.74 \pm 0.94$	
		200	$0.57 \pm 0.06$	$35.73 \pm 0.99$	

773	100	$0.61 \pm 0.06$	$40.41 \pm 0.96$
	200	$0.65 \pm 0.03$	$42.84 \pm 0.48$

#### 4.1.3 Dependence of $i_o$ on $C_{\text{ThCl}_4}$ at inert tungsten electrode

Concentration dependence of  $i_o$  is shown in Figure 4.5, where  $i_o$  is plotted against  $\ln C_{\text{ThCl}_4}$ .  $C_{\text{ThCl}_4}$  chosen for the polarization and cyclic voltammetric measurements were not exactly same, so it might be expected that  $i_o$  may have a small compositional dependence. Before we investigate this further, it was important to compare the results of  $i_o$  obtained from polarization (Table 4.1) and cyclic voltammetry data at inert electrode (Table 4.2). Maximum variation of  $i_o$  was observed to be  $10 \text{ mA cm}^{-2}$  at 773 K for each successive variation of composition from  $2.04 \times 10^{-5}$  to  $3.55 \times 10^{-5} \text{ mol cm}^{-3}$  in voltammetric method, whereas,  $i_o$  estimated by polarization method varies in the range 28-47  $\text{mA cm}^{-2}$  at 773 K in the same compositional domain.  $i_o$  value estimated by polarization technique are in good agreement with values obtained from cyclic voltammetry.

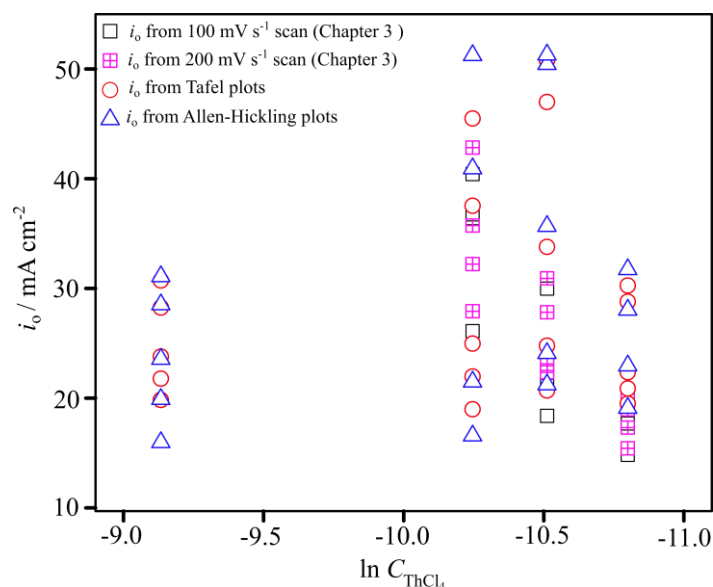


Figure 4.5  $i_o$  versus  $\ln C_{\text{ThCl}_4}$  ( $\text{mol cm}^{-3}$ ) profile for cathodic polarization data at tungsten electrode in temperature range 698-798 K,  $i_o$  estimated from both polarization and cyclic voltammetric data are shown.

The variation in  $i_0$  estimated from polarization data is in the range of 15-30 mA cm<sup>-2</sup>. On the other hand, the variation in  $i_0$  estimated from voltammetric data is not same at all concentrations. Considering data from voltammetry alone, it can be said that  $i_0$  increases with  $C_{\text{ThCl}_4}$ . Due to lack of data at higher concentrations of thorium, it is difficult to predict the behaviour of the concentration dependence of  $i_0$ . In the limited concentration range, however,  $i_0$  linearly increases with  $\ln C_{\text{Th}^{4+}}$ . At higher concentrations, it is expected that  $i_0$  will either continue to linearly increase or have weak composition dependence. From Figure 4.5 it can be seen that variation in  $i_0$  at  $10.8 \times 10^{-5}$  mol cm<sup>-3</sup> is slightly lower than that seen at  $3.55 \times 10^{-5}$  mol cm<sup>-3</sup>. Variation in  $i_0$  at  $2.04 \times 10^{-5}$ ,  $2.72 \times 10^{-5}$  and  $3.55 \times 10^{-5}$  mol cm<sup>-3</sup> is similar. Therefore, concentration dependence of  $i_0$  is considered to be practically insignificant in range of concentrations chosen in present work. By and large,  $i_0$  varies from 20-50 mA cm<sup>-2</sup> in temperature range 698-798 K at all concentrations.

#### 4.2 Estimation of $i_0$ at liquid cadmium cathode

$i_0$  of Th<sup>4+</sup>|Th couple was estimated at liquid cadmium cathode in the temperature range of 723-773 K. Liq. Cd cathode was cathodically polarized from equilibrium potential of -1.25 V against Ag<sup>+</sup>|Ag reference.  $i$  vs.  $t$  profile recorded for cathodic polarization of thorium at liq. Cd cathode at 773 K is shown in Figure 4.6. Polarization data were analyzed by Tafel and Allen-Hickling methods. Tafel and Allen-Hickling plots of Th<sup>4+</sup>|Th couple at liq. Cd cathode are shown in Figure 4.3 and 4.4 respectively.  $i_0$  estimated using Tafel and Allen-Hickling methods were found to be in good agreement with each other, as shown in Table 4.3. Tafel and Allen-Hickling constants are also given in Table 4.3.  $i_0$  was estimated in the range of 12-16 mA cm<sup>-2</sup>, which is slightly lower than those at the inert electrode. This observation is

similar to what is observed in case of cathodic polarization of uranium, gadolinium and zirconium at liquid cadmium electrode [99].

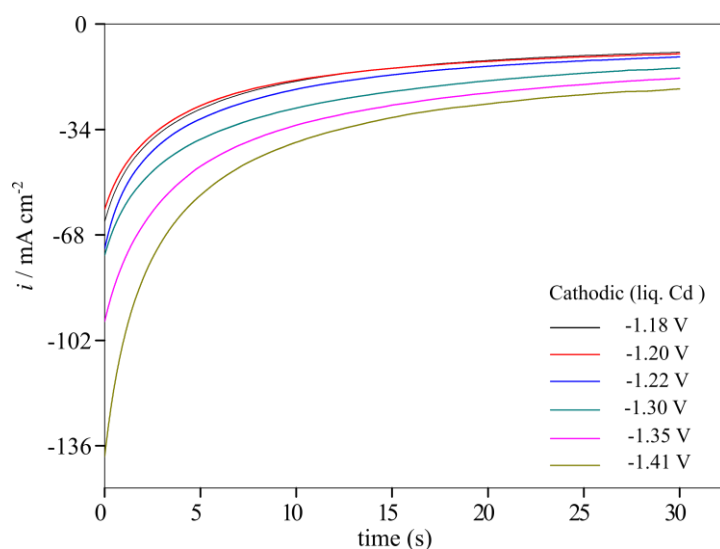


Figure 4.6  $i$  vs.  $t$  profile for cathodic polarization of thorium at liq. Cd electrode at various potentials,  $T = 773$  K.

Table 4.3  $i_0$  of  $\text{Th}^{4+}/\text{Th}$  couple at liquid cadmium electrode at various temperatures,  $C_{\text{ThCl}_4} = 6.91 \times 10^{-5} \text{ mol cm}^{-3}$ .

$T/\text{K}$	Tafel method			Allen-Hickling method	
	$a_{\text{Tafel}}$ (mV)	$b_{\text{Tafel}}$ (mV)	$i_0$ ( $\text{mA cm}^{-2}$ )	$b_{\text{Allen-Hickling}}$ ( $\text{V}^{-1}$ )	$i_0$ ( $\text{mA cm}^{-2}$ )
723	$2170 \pm 120$	$-480 \pm 30$	$12.23 \pm 0.98$	$2.02 \pm 0.12$	$11.69 \pm 0.98$
748	$3.19 \pm 0.08$	$-750 \pm 20$	$14.26 \pm 0.99$	$1.32 \pm 0.05$	$14.26 \pm 0.99$
773	$2790 \pm 220$	$-670 \pm 50$	$15.91 \pm 0.99$	$1.37 \pm 0.11$	$15.74 \pm 0.99$

### 4.3 Estimation of $i_0$ for anodic polarization of Th electrode

$i_0$  of  $\text{Th}^{4+}/\text{Th}$  couple was estimated for anodic polarization of thorium in the temperature range of 698-798 K. Thorium electrode was anodically polarized from equilibrium potential of -1.50 V against  $\text{Ag}^+/\text{Ag}$  reference.  $i$  vs.  $t$  profile recorded for anodic polarization of thorium electrode at 773 K is shown in Figure 4.7. Exchange current density of  $\text{Th}^{4+}/\text{Th}$  couple was estimated at thorium electrode by Tafel and Allen-Hickling methods in the temperature range

of 698-798 K, which are given in Table 4.4. Tafel and Allen-Hickling plots for anodic polarization are shown in Figure 4.3 and 4.4, respectively.  $i_o$  was estimated in the range of 22-34 mA cm<sup>-2</sup> by both methods.

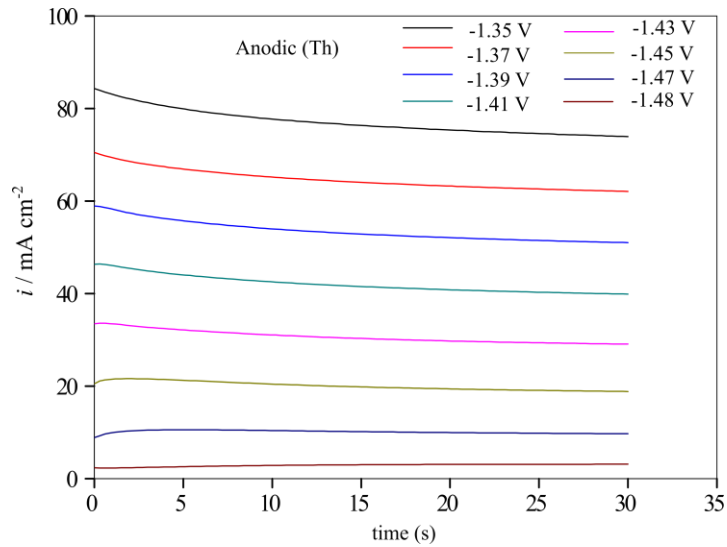


Figure 4.7  $i$  vs.  $t$  profile for anodic polarization of thorium electrode at various potentials,  $T = 773$  K.

Table 4.4  $i_o$  of thorium in LiCl-KCl eutectic melt in temperature range 698-798 K,  $C_{\text{ThCl}_4} = 1.08 \times 10^{-4}$  mol cm<sup>-3</sup>.

$T/K$	Tafel method			Allen-Hickling method	
	$a_{\text{Tafel}}$ (mV)	$b_{\text{Tafel}}$ (mV)	$i_o$ (mA cm <sup>-2</sup> )	$b_{\text{Allen-Hickling}}$ (V <sup>-1</sup> )	$i_o$ (mA cm <sup>-2</sup> )
698	-523 ± 12	137 ± 4	22.59 ± 0.96	6.67 ± 0.20	23.78 ± 0.96
723	-529 ± 12	143 ± 5	24.97 ± 0.96	6.68 ± 0.23	26.04 ± 0.96
748	-530 ± 11	148 ± 4	28.15 ± 0.96	6.69 ± 0.21	27.27 ± 0.96
773	-537 ± 10	153 ± 4	29.89 ± 0.97	6.29 ± 0.16	31.27 ± 0.96
798	-547 ± 13	159 ± 5	33.37 ± 0.96	6.02 ± 0.19	33.98 ± 0.97

#### 4.4 Temperature dependence of $i_o$

Temperature dependence of  $i_o$  was studied by plotting  $\ln i_o$  against reciprocal of temperature and fitted to the following equation which represents Arrhenius equation for reaction kinetics:

$$\ln i_o = \ln A - \frac{B}{T} \quad (4.3)$$

Where,  $B = E_a / R$ . Data from both Tafel and Allen-Hickling plots for each case were fitted to the same equation. Temperature dependence of  $i_0$  in case of inert tungsten cathode was fitted to data from both polarization (Table 4.1) and voltammetric measurements (Table 4.2), which is shown in Figure 4.8 in order to compare fit of only polarization data. Linear fits for anodic and cathodic (liq. Cd cathode) cases are shown in Figure 4.9. The fit parameters  $A$ ,  $B$  and  $E_a$  are summarised in Table 4.5. Increase in  $i_0$  with temperature is attributed to higher symmetry of activation barrier, as discussed by Rose *et al.* [114]. A similar trend is observed in present work as well.  $E_a$  at tungsten electrode was estimated in the range 32-36 kJ mol<sup>-1</sup> from polarization and polarization+voltammetry data, which is considered to be in close agreement while that at liquid cadmium electrode is 26.1±1.9 kJ mol<sup>-1</sup>. This is quite close to the activation energy of U<sup>3+</sup>|U couple in LiCl-KCl eutectic reported at 34.4 kJ mol<sup>-1</sup> by Rose *et al* [114] by polarization method. On the other hand,  $E_a$  for anodic dissolution of thorium is 17.2 ± 0.8 kJ mol<sup>-1</sup>, which is about 18 kJ mol<sup>-1</sup> less than calculated for tungsten electrode. The difference of 8 kJ mol<sup>-1</sup> can be considered marginal.

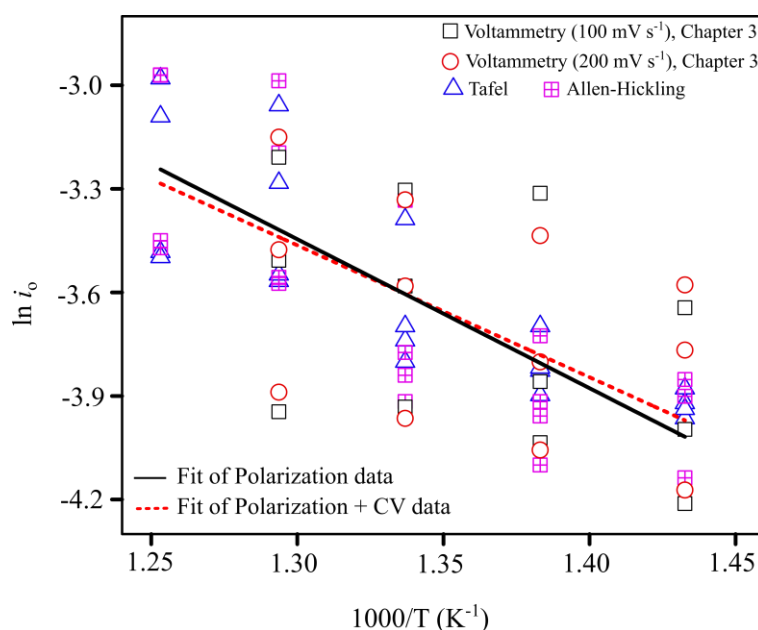


Figure 4.8 Temperature dependence of  $\ln i_0$  at tungsten electrode (cathodic polarization), fits of only polarization data and polarization+voltammetry data (Chapter 3) are shown.

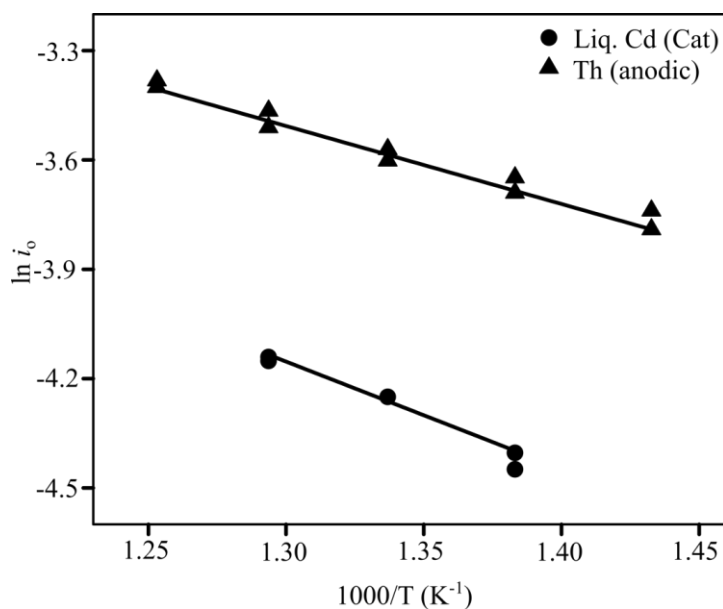


Figure 4.9 Temperature dependence of  $\ln i_0$  at liquid cadmium (cathodic polarization) and for anodic dissolution of thorium in LiCl-KCl eutectic melt.

Table 4.5 Fit parameters of  $\ln i_0$  versus  $1/T$  plot for cathodic and anodic polarization data.

Electrode/Type of polarization	A	B	$E_a$ (kJ mol <sup>-1</sup> )
Inert (cathodic) <sup>a</sup>	$8.7 \pm 2.1$	$4315 \pm 522$	$35.9 \pm 4.3$
Inert (cathodic) <sup>b</sup>	$4.50 \pm 1.9$	$3821 \pm 502$	$31.8 \pm 4.2$
Liq. Cadmium (Cathodic) <sup>a</sup>	0.97	$3140 \pm 273$	$26.1 \pm 1.9$
Thorium (Anodic) <sup>a</sup>	0.44	$2066 \pm 118$	$17.2 \pm 0.8$

<sup>a</sup>Fit using both Tafel and Allen-Hickling data

<sup>b</sup>Fit using both polarization and cyclic voltammetry data

## 4.5 Conclusions

Electrochemical behaviour of thorium in LiCl-KCl eutectic was investigated in the present work with special emphasis on the determination of  $i_0$  for both cathodic and anodic polarization. Following conclusions are made based on investigations carried out in this chapter:

1.  $i_0$  estimated by both Tafel and Allen-Hickling methods was found to be in excellent agreement.

2. Observed insignificant variation of  $i_0$  with concentration of  $\text{ThCl}_4$  in the concentration range chosen for the thesis.  $i_0$  varies in the range of  $20\text{-}50 \text{ mA cm}^{-2}$  in the temperature range  $698\text{-}798 \text{ K}$ .
3.  $i_0$  estimated by method of Cumberland and Yim was found to be in good agreement with those estimated by polarization methods. Agreement is expected to be better the data is normalized with respect to concentration of thorium employed in measurements.
4. Temperature dependence of  $i_0$  was found to follow Arrhenius equation, from which the activation energy associated with redox couple was determined.

## CHAPTER 5

### Anodic dissolution of Th and cathodic deposition of Th<sup>4+</sup> at inert tungsten and cadmium electrodes by electrochemical impedance spectroscopy

#### Results and discussions

This chapter describes investigations on electrochemical behaviour of Th<sup>4+</sup>|Th couple at inert tungsten, liquid cadmium and thorium electrodes in LiCl-KCl eutectic melt by electrochemical impedance spectroscopy. Complex impedance data recorded at different electrodes were validated by Kramers-Kronig transforms and analysed by equivalent circuit models. Mechanism of anodic dissolution was proposed based on analysis of complex impedance data by equivalent circuit fitting. The chapter concludes with estimation of heterogeneous rate constant from charge transfer resistance of Th<sup>4+</sup>|Th couple estimated from equivalent circuit fitting and reversibility of Th<sup>4+</sup>|Th couple in LiCl-KCl eutectic melt is finally discussed. Equivalent circuit shown in Figure 5.1 (reproduced from Figure 2.13, Chapter 2) was used for fitting of complex impedance spectra.

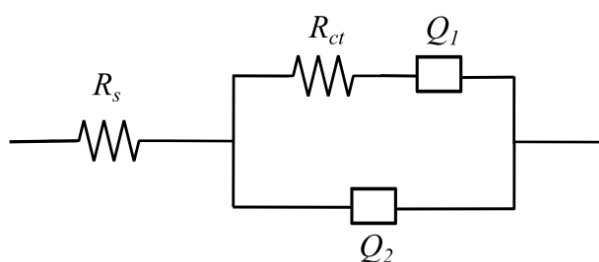


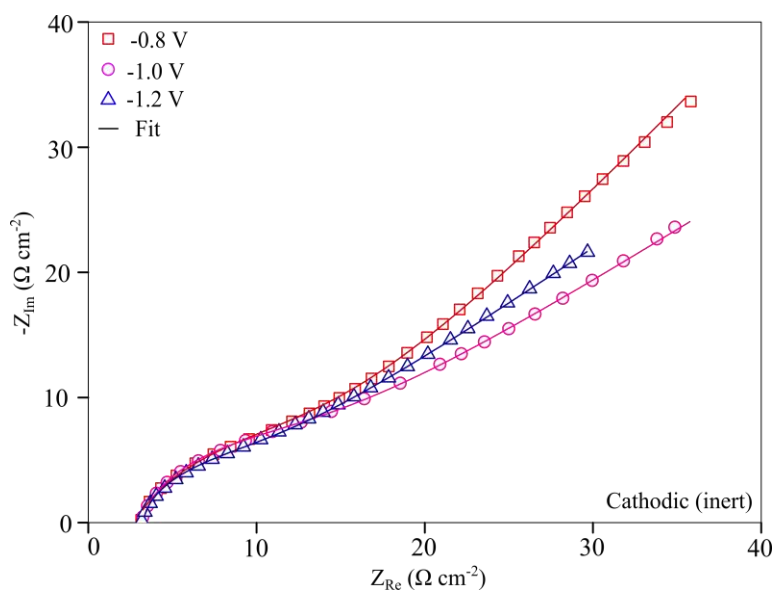
*Figure 5.1 Equivalent circuit used for fitting complex impedance data for cathodic polarization of thorium at inert tungsten and cadmium electrodes and anodic polarization of metallic thorium electrode.*

#### 5.1 Cathodic: at inert tungsten electrode

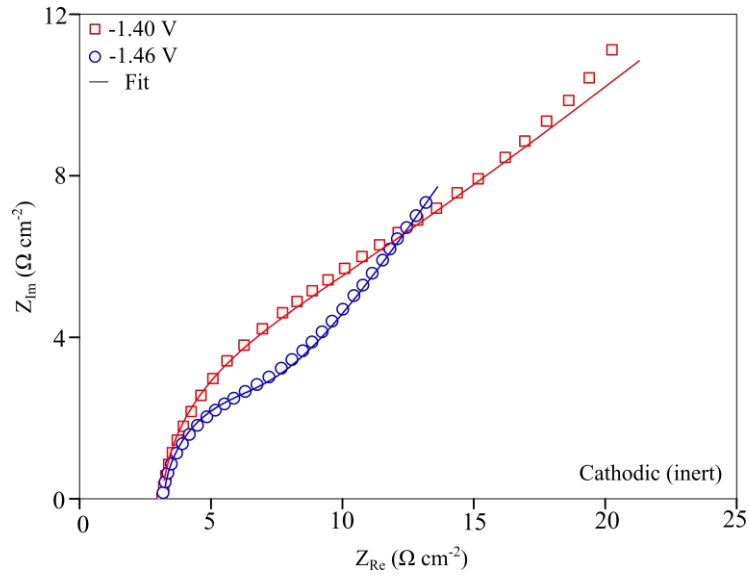
Complex impedance spectra were recorded for cathodic polarization of Th<sup>4+</sup> at inert tungsten electrode in LiCl-KCl eutectic melt at applied potentials in the range of -0.80 V to -1.57 V,

which covered the complete potential domain in the cathodic sweep and are shown in Figure 5.2.

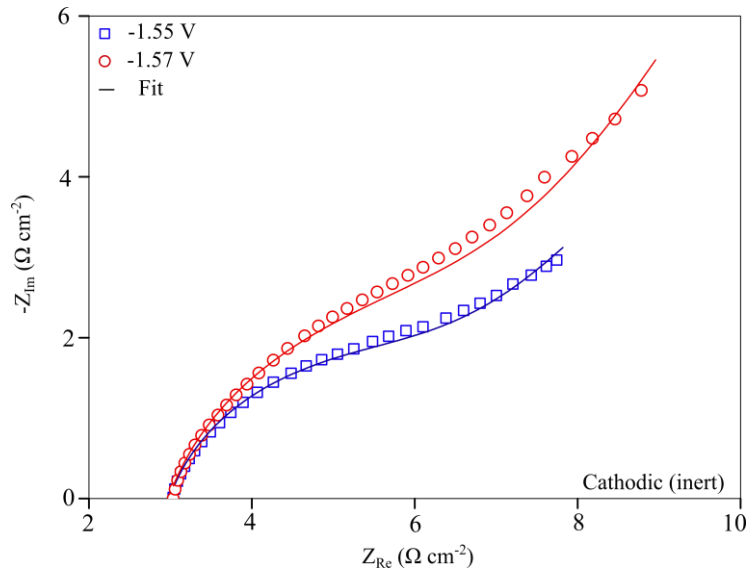
The impedance plots are characterized by a flattened semicircle at higher frequencies and a linear region at lower frequencies. The flattened semicircle suggests a very fast charge transfer process whereas the linear part is related to the mass transfer of  $\text{Th}^{4+}$  ions. In the potential region  $-0.80\text{ V}$   $-1.20\text{ V}$ , the kinetically controlled region is not well defined and therefore, the process is always diffusion controlled. The linear parts of the plots extend in a similar manner at all applied potentials and their slope is 1.20 at  $-0.80\text{ V}$ , 0.81 at  $-1.00\text{ V}$  and 0.85 at  $-1.20\text{ V}$ .



a



b



c

Figure 5.2 Nyquist plots of  $\text{ThCl}_4$  at inert tungsten electrode in  $\text{LiCl-KCl}$  eutectic melt,  $C_{\text{ThCl}_4} = 1.02 \times 10^{-4} \text{ mol cm}^{-3}$ ,  $T = 773 \text{ K}$ ,  $A = 0.25 \text{ cm}^2$ , Frequency range of measurement: 10 Hz to 10 kHz.

The semicircle in high frequency range becomes more prominent at higher cathodic applied potentials whereas the linear region spreads over a limited frequency range as evident from the impedance plots at -1.40 V and -1.46 V in Figure 5.2b. This is suggestive of the reduction of thorium under mixed control due to semi-infinite Warburg diffusion (mass transfer control) and charge transfer (kinetic control). At -1.46 V, predominating feature is charge transfer and the process is pure kinetic controlled with a linear region having slope of 0.81.

Impedance plots recorded at -1.55 V and -1.57 V shown in Figure 5.2c are similar to each other except that in the latter; semicircle appears less prominent than it is in the former. The linear region at -1.57 V (slope of 0.81) is also spread in a larger frequency range than it is at -1.55 V (slope of 0.51). This suggests that the process is diffusion controlled at -1.57 V and is under mixed control at -1.55 V. Complex impedance spectra recorded at equilibrium potential of  $\text{Th}^{4+}|\text{Th}$  couple at various temperatures are shown in Figure 5.3.

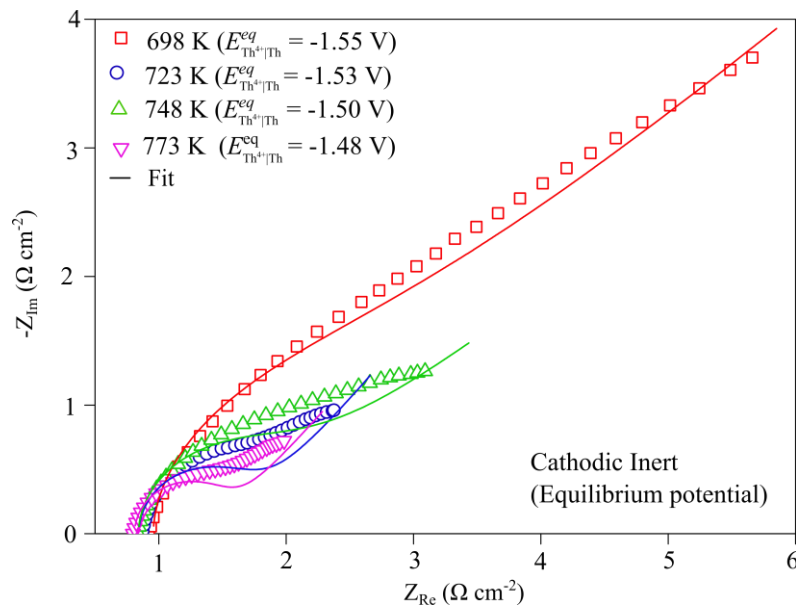


Figure 5.3 Nyquist plots of  $\text{ThCl}_4$  at inert tungsten electrode in  $\text{LiCl-KCl}$  eutectic at  $E_{\text{Th}^{4+}|\text{Th}}^{\text{eq}}$  versus  $\text{Ag}^+|\text{Ag}$  reference,  $C_{\text{ThCl}_4} = 1.02 \times 10^{-4} \text{ mol cm}^{-3}$ ,  $T = 698\text{-}773 \text{ K}$ ,  $A = 0.25 \text{ cm}^2$ , Frequency range of measurement: 10 Hz to 10 kHz.

The equivalent circuit fitting of impedance plots are also shown in Figure 5.2 and the values of  $R_s$ ,  $R_{ct}$ ,  $Q_1$  and  $Q_2$  obtained are provided in Table 5.1. The following observations are made from the equivalent circuit fits:

- $R_s$  varies by 127 m $\Omega$  in the potential range -0.8 to -1.57 V and can be considered as constant.
- $R_{ct}$  gradually decreases with increase in cathodic applied potential, goes through a minimum and increases again. The potential at which it is minimum corresponds to the

equilibrium potential of thorium. For example,  $R_{ct}$  is 991 m $\Omega$  at -1.46 V and increases gradually to 1701 m $\Omega$  at -1.57 V.

- c. Constant phase element  $Q_1$  is characterized to be Warburg impedance (diffusion related impedance) by  $m$  value about 0.5. Beyond the equilibrium potential of -1.46 V,  $m$  increases to 0.56 at -1.47 V and 0.65 at -1.55 V.
- d. Constant phase element  $Q_2$  is characterized to be double layer capacitance by  $m$  value around 1.0, although it decreases to 0.80 at -1.5 V and 0.75 at -0.57 V.

Variation of  $R_{ct}$  was also studied as a function of applied potential at 773 K and is shown in Figure 5.4. The plot can be divided into three linear regions; first region spans -0.80 V to -1.40 V, second region spans -1.40 V to -1.50 V and the third region is from -1.50 V to -1.57 V. Each region can be approximated by a straight line spanning the applied potential range.

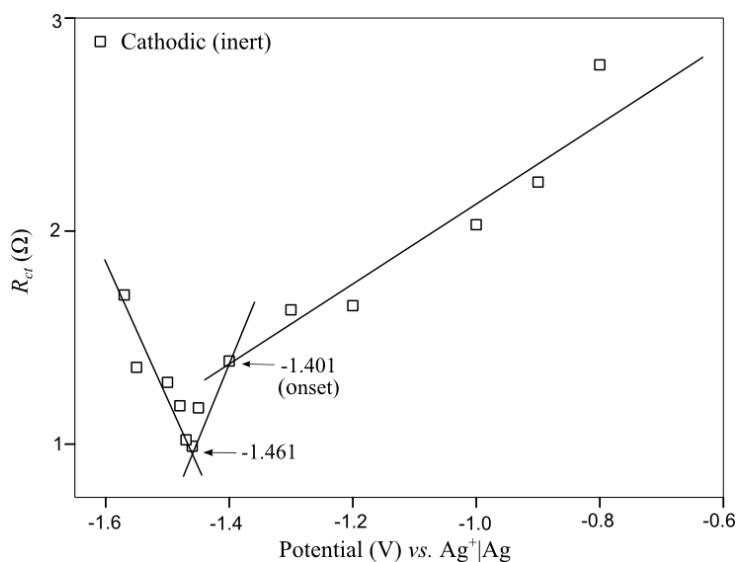


Figure 5.4 Variation of  $R_{ct}$  versus applied potential at tungsten electrode (cathodic),  $C_{ThCl_4} = 1.02 \times 10^{-4} \text{ mol cm}^{-3}$ ,  $A = 0.25 \text{ cm}^2$ ,  $T = 773 \text{ K}$ .

The points of intersection are found at -1.401 V and -1.461 V that can be considered as onset of thorium deposition and equilibrium potential of thorium at tungsten electrode. This is in general agreement with that measured from cyclic voltammograms, which is discussed in

Chapter 3. This analysis is similar to that carried out by Bachtler *et al.* [115] for elucidating the mechanism of tantalum in molten alkali chlorides.

Table 5.1 EIS data of cathodic polarization of thorium in LiCl-KCl-ThCl<sub>4</sub> electrolyte at tungsten electrode,  $C_{\text{ThCl}_4} = 1.02 \times 10^{-4} \text{ mol cm}^{-3}$ ,  $A = 0.25 \text{ cm}^2$ .

T / K	E / V	$R_s$ (mΩ)	$R_{ct}$ (mΩ)	$Q_1$		$Q_2$	
				$Y_0 \times 10^2$	$m$	$Y_0 \times 10^3$	$m$
698	-0.7	946	4364	0.33	0.70	0.29	0.89
	-0.8	942	4254	0.29	0.72	0.32	0.86
	-0.9	948	3661	0.32	0.71	0.27	0.87
	-1.0	966	3682	0.294	0.76	0.27	0.88
	-1.1	956	3611	0.35	0.75	0.27	0.89
	-1.2	948	3534	0.43	0.72	0.33	0.92
	-1.3	940	2853	0.61	0.66	0.54	0.95
	-1.4	944	2791	0.64	0.68	0.38	0.93
	-1.5	949	2322	0.75	0.67	0.37	0.93
	-1.55	952	1922	2.77	0.43	0.23	1.00
	-1.6	903	1853	7.69	0.44	1.27	0.82
	-1.65	912	2234	1.74	0.57	0.88	0.87
	723	-0.9	902	3883	0.37	0.70	0.27
-1.0		905	3801	0.42	0.69	0.25	0.89
-1.1		888	3661	0.48	0.68	0.31	0.88
-1.2		896	3262	0.56	0.66	0.26	0.92
-1.3		891	2223	0.93	0.60	0.31	1.00
-1.4		899	1752	0.87	0.60	0.21	0.98
-1.5		898	1884	1.19	0.55	0.23	0.99
-1.52		874	1781	1.81	0.51	0.27	0.95
-1.53		796	1593	2.29	0.57	2.34	0.75
-1.55		832	2041	5.33	0.46	2.52	1.00
-1.6		800	2131	2.32	0.56	14.99	1.00
748	-1.0	900	2691	0.84	0.55	0.09	0.97
	-1.10	882	2213	0.97	0.56	0.14	0.97
	-1.40	864	1384	1.79	0.47	0.16	1.00
	-1.50	831	3312	0.60	0.64	9.78	1.00
	-1.55	788	815	11.65	0.47	40.93	1.00
773	-0.8	717	2781	0.74	0.59	0.06	0.79
	-0.9	844	2234	1.10	0.52	0.08	1.00
	-1.0	844	2034	1.71	0.45	0.08	1.00
	-1.20	836	1651	1.80	0.47	0.11	1.00
	-1.30	831	1632	2.92	0.42	0.28	0.93
	-1.40	806	1393	4.34	0.39	0.29	0.94
	-1.45	827	1172	4.18	0.46	0.33	0.91
	-1.46	819	991	4.68	0.50	0.54	0.91
	-1.47	820	1021	5.33	0.56	2.02	0.99
	-1.48	682	1183	0.99	0.57	14.06	1.00
	-1.50	744	1291	9.93	0.58	5.15	0.80

	-1.55	762	1316	3.98	0.65	3.38	0.84
	-1.57	743	1701	2.91	0.62	6.45	0.75
798	-0.9	749	4501	0.14	0.59	0.16	1.00
	-1.0	760	3241	0.15	0.63	0.14	1.00
	-1.10	758	2282	0.27	0.61	0.18	1.00
	-1.11	748	1513	0.48	0.62	0.26	1.00
	-1.20	749	1492	0.49	0.62	0.25	1.00
	-1.30	754	911	0.57	0.57	0.30	1.00
	-1.40	745	892	0.55	0.48	0.52	0.95
	-1.50	730	673	0.56	0.53	0.46	0.99

## 5.2 Cathodic: at liquid cadmium electrode

Complex impedance plots of cathodic polarization of  $\text{Th}^{4+}$  at liquid cadmium electrode in LiCl-KCl eutectic in the potential range of -0.90 V to -1.47 V are shown in Figure 5.5a and b. Complex impedance plots at -0.90 V and -1.00 V in Figure 5.5a are similar to that recorded at inert tungsten electrode (Figure 5.2a) consisting of a flattened semicircle at higher frequencies, which is characteristic of a very fast charge transfer process at salt|cadmium interface, and a linear region at lower frequencies, which is associated with semi-infinite Warburg diffusion. Spread of linear region is more at applied potentials of -0.90 V and -1.00 V than it is at -1.10 V. Therefore, the process is controlled by mass transfer at these applied potentials. The slope of linear region is 0.69 and 0.65 at -0.90 V and -1.00 V, respectively. Impedance plots at potential -1.10 V in Figure 5.5a and -1.20 V in Figure 5.5b are very similar with a limited linear region at lower frequencies and a more prominent semicircle at higher frequencies and slope of linear region is 0.62 and 0.51 at -1.10 V and -1.20 V, respectively. The process is kinetically controlled at these applied potentials. At -1.30 V, -1.40 V and -1.47 V, complex impedance plots show a fairly small kinetically controlled region at higher frequencies and a prominent linear region at lower frequencies. Although some scattering in linear region is observed in the plots recorded at -1.30V and -1.40 V, it is spread over large frequency range with slope 0.76 and 0.92, respectively. The scattering observed at lower frequencies has been attributed to the movements of the liquid electrode

under polarization conditions [116]. At very large cathodic applied potentials, continuous deposition of thorium may create movements on the surface of liquid cadmium leading to scattering of data. Impedance plot at -1.47 V is similar to that at -1.40 V with slope of linear region of 0.83.

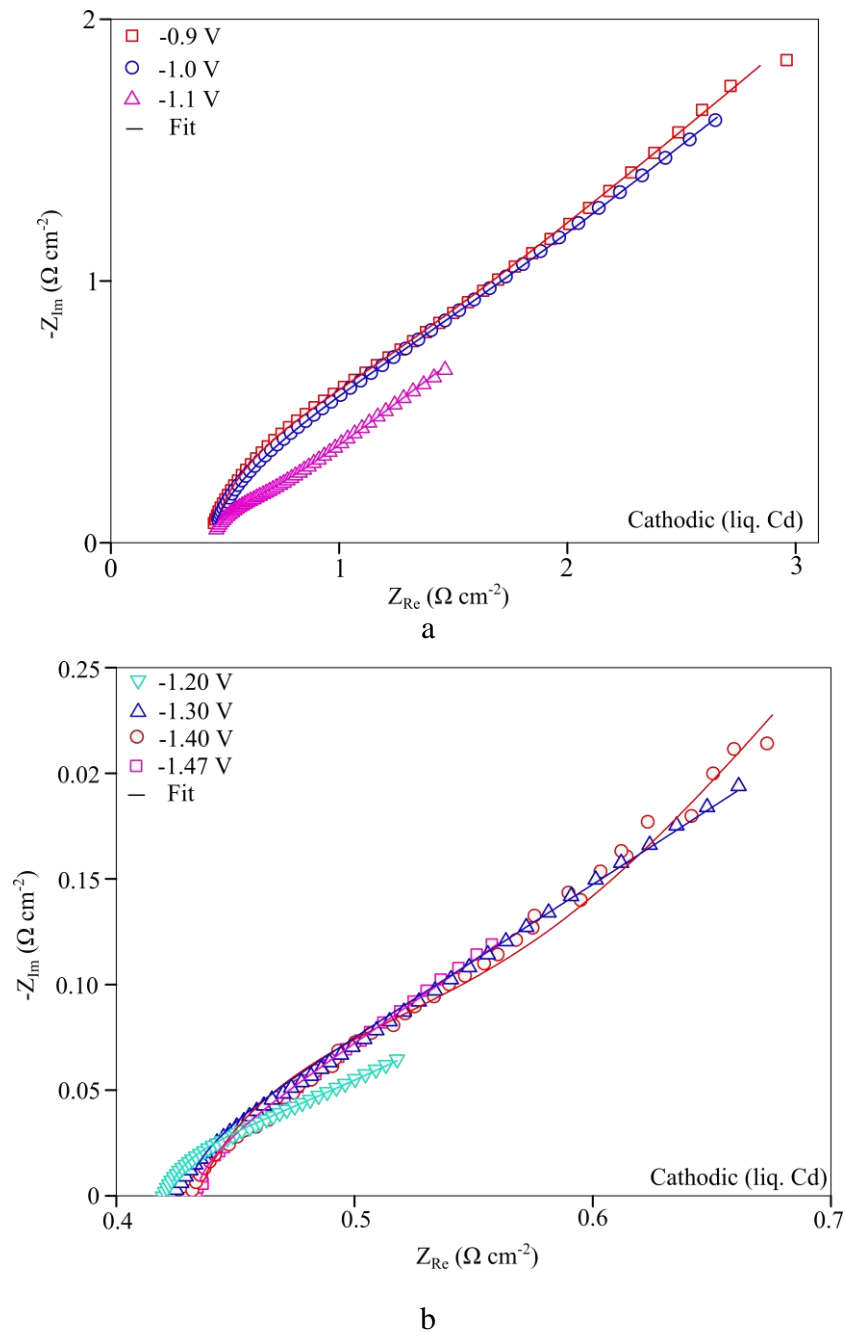


Figure 5.5 Nyquist plots of  $ThCl_4$  at liquid cadmium electrode in  $LiCl-KCl$  eutectic melt,  $C_{ThCl_4} = 1.02 \times 10^{-4} \text{ mol cm}^{-3}$ ,  $T = 773 \text{ K}$ ,  $A = 1.48 \text{ cm}^2$ , Frequency range of measurement: 10 Hz-10 kHz.

Complex impedance plots were fitted to an equivalent circuit shown in Figure 5.1 and they are shown along with measured data in Figure 5.5. The values of  $R_s$ ,  $R_{ct}$ ,  $Q_1$  and  $Q_2$  obtained from the fits are shown in Table 5.2 from which the following observations are made (at 773 K):

1.  $R_s$  varies within 50 m $\Omega$  in the potential range of -0.9 to -1.50 V and can be considered as constant.
2. Variation of  $R_{ct}$  with applied cathodic potential is observed with gradual decrease in  $R_{ct}$  with increase in cathodic applied potential, goes through two minimum and increases again. For example, at 773 K, onset of thorium deposition in cadmium is at -1.157 V and formation of Cd<sub>11</sub>Th appears at -1.225 V. Onset of formation of Cd<sub>5</sub>Th appears at -1.434 V whereas the peak potential is estimated at -1.447 V. These points were arrived in a similar manner as explained above by joining points in a specified potential range by a straight line and finding the potentials for onset of deposition, formation of Cd<sub>11</sub>Th and Cd<sub>5</sub>Th from the points of intersection in the plot of  $R_{ct}$  versus applied potential as shown in Figure 5.6. From equivalent circuit fitting, minimum in  $R_{ct}$  is obtained at -1.17 V (14 m $\Omega$ ) and -1.42 V (21 m $\Omega$ ).
3.  $Q_1$  is characterized to be Warburg impedance element by  $m$  value around 0.38 - 0.54 in the potential range -0.90 V to -1.42 V.
4.  $Q_2$  is characterized to be double layer capacitance by  $m$  value of 1.00 in the potential range -0.90 V to -1.50 V except at -1.37 V and -1.40 V, where it is 0.75 and 0.81, respectively.

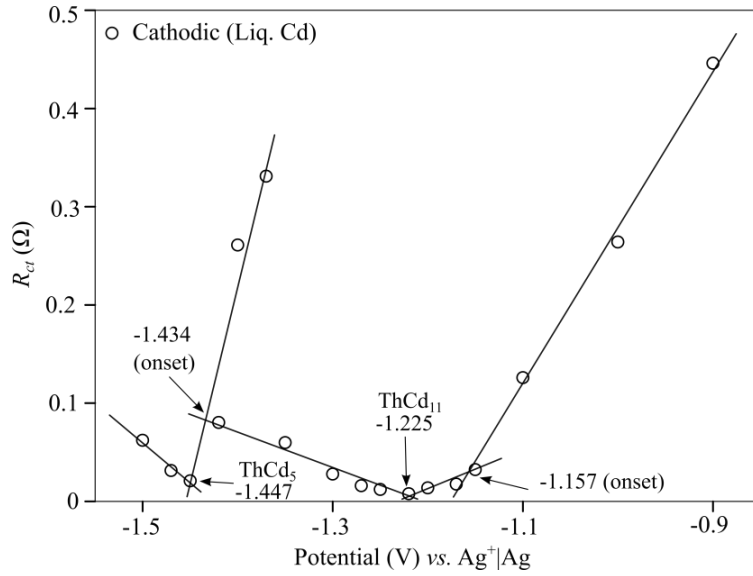


Figure 5.6 Variation of  $R_{ct}$  versus applied potential at liquid cadmium electrode (cathodic),

$$C_{ThCl_4} = 1.02 \times 10^{-4} \text{ mol cm}^{-3}, T = 773 \text{ K}, A = 1.48 \text{ cm}^2.$$

Table 5.2 EIS data of cathodic polarization of thorium in liquid cadmium,

$$C_{ThCl_4} = 1.02 \times 10^{-4} \text{ mol cm}^{-3}, A = 1.48 \text{ cm}^2.$$

$T / K$	$E / V$	$R_s$ (m $\Omega$ )	$R_{ct}$ (m $\Omega$ )	$Q_1$		$Q_2$	
				$Y_0 \times 10^2$	$m$	$Y_0 \times 10^3$	$m$
698	-0.90	694	796	6.24	0.40	0.63	0.89
	-1.00	710	403	7.48	0.43	0.46	0.94
	-1.15	718	195	7.61	0.45	0.73	0.91
	-1.17	728	175	12.54	0.44	0.37	1.00
	-1.20	721	70	35.49	0.44	1.47	1.00
	-1.22	703	38	74.15	0.42	3.22	1.00
	-1.25	683	30	109.5	0.37	2.35	1.00
	-1.27	683	21	40.04	0.41	2.79	1.00
	-1.30	684	23	52.21	0.43	1.95	1.00
	-1.32	689	28	44.26	0.44	1.37	1.00
	-1.35	696	39	45.90	0.46	0.69	1.00
	-1.37	707	57	10.95	0.47	0.91	1.00
	-1.39	707	130	10.16	0.51	1.19	1.00
	-1.40	703	115	11.20	0.51	1.46	1.00
	-1.42	698	107	13.57	0.52	1.92	1.00
	-1.45	693	84	17.59	0.52	2.65	1.00
-1.47	691	67	22.18	0.51	3.33	1.00	
-1.50	688	45	32.90	0.48	3.59	1.00	
-1.55	685	59	63.73	0.46	6.59	0.98	
-1.60	665	33	147.5	0.31	2.58	1.00	
723	-0.90	628	278	3.08	0.38	0.24	0.94
	-1.00	615	176	2.59	0.44	0.08	1.00
	-1.10	631	101	3.23	0.39	0.17	0.95
	-1.2	693	28	43.64	0.36	0.81	1.00

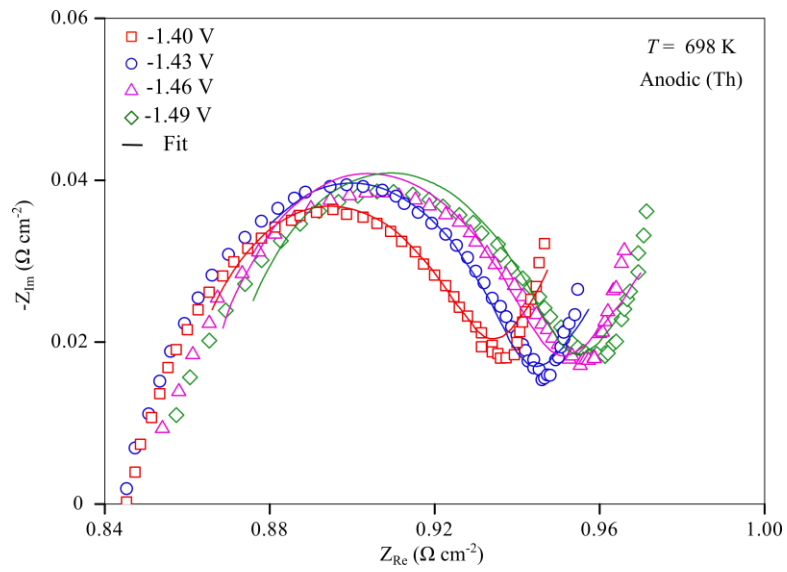
	-1.25	660	13	122.4	0.35	4.19	1.00
	-1.27	655	14	96.31	0.37	4.07	1.00
	-1.29	656	16	55.84	0.41	2.93	1.00
	-1.32	667	29	22.00	0.45	0.90	1.00
	-1.34	693	86	13.98	0.47	1.33	1.00
	-1.35	694	99	12.50	0.47	1.20	1.00
	-1.37	690	83	11.40	0.47	1.03	1.00
	-1.39	683	110	11.35	0.49	1.16	1.00
	-1.40	679	117	11.77	0.51	1.33	1.00
	-1.44	658	240	11.54	0.58	27.56	0.72
	-1.45	661	210	16.16	0.55	12.85	0.83
	-1.47	660	76	23.30	0.52	3.53	1.00
	-1.49	638	19	35.83	0.45	1.98	1.00
	-1.50	643	21	38.92	0.46	1.92	1.00
748	-0.90	613	566	2.84	0.38	0.36	0.94
	-1.00	604	479	2.92	0.38	0.61	0.87
	-1.10	679	333	6.25	0.43	0.26	1.00
	-1.12	686	228	9.03	0.44	0.30	1.00
	-1.14	692	106	15.35	0.43	0.47	1.00
	-1.16	685	63	27.82	0.41	1.25	1.00
	-1.18	667	37	53.44	0.40	3.05	1.00
	-1.20	640	15	101.3	0.35	3.36	1.00
	-1.22	630	14	150.5	0.35	4.68	1.00
	-1.24	633	30	133.5	0.45	12.83	1.00
	-1.26	633	35	98.27	0.47	11.69	1.00
	-1.28	640	43	57.21	0.50	8.07	1.00
	-1.30	636	53	41.18	0.46	0.71	1.00
	-1.32	649	25	26.04	0.45	1.16	1.00
	-1.34	672	31	18.44	0.43	0.98	1.00
	-1.35	694	34	17.61	0.42	1.15	1.00
	-1.36	653	46	17.63	0.44	0.63	1.00
	-1.38	642	91	37.73	0.68	25.85	0.89
	-1.40	639	95	29.55	0.64	11.97	0.95
	-1.42	644	63	40.68	0.55	5.50	1.00
	-1.45	633	19	46.68	0.48	2.76	1.00
	-1.50	638	17	54.67	0.45	2.86	1.00
773	-0.90	669	446	4.14	0.42	0.22	1.00
	-1.00	663	264	4.95	0.39	0.20	1.00
	-1.10	666	32	12.01	0.38	0.24	1.00
	-1.15	667	18	40.13	0.37	1.40	1.00
	-1.17	636	14	71.36	0.34	2.06	1.00
	-1.20	617	30	140.6	0.33	4.84	1.00
	-1.22	618	12	156.7	0.41	13.08	1.00
	-1.25	609	16	141.4	0.36	6.09	1.00
	-1.27	613	28	84.84	0.39	3.81	1.00
	-1.30	624	60	39.55	0.40	1.43	1.00
	-1.35	642	331	26.07	0.42	1.64	1.00
	-1.37	628	261	16.97	0.58	20.07	0.75
	-1.40	642	80	18.37	0.61	17.01	0.81
	-1.42	652	21	30.88	0.54	7.17	1.00

	-1.45	634	31	48.77	0.45	2.85	1.00
	-1.47	634	62	61.18	0.43	4.94	1.00
	-1.50	633	446	25.65	0.46	6.87	1.00
798	-0.80	531	316	6.74	0.37	0.097	1.00
	-0.90	556	180	6.47	0.37	0.079	1.00
	-1.00	645	93	7.84	0.38	0.22	1.00
	-1.10	655	53	21.09	0.38	0.40	1.00
	-1.15	619	22	72.65	0.33	1.44	1.00
	-1.17	619	33	106.8	0.38	5.49	1.00
	-1.20	606	23	189.5	0.36	10.45	1.00
	-1.22	604	29	183.0	0.40	13.74	1.00
	-1.25	604	24	128.0	0.40	10.68	1.00
	-1.27	611	36	76.49	0.43	7.05	1.00
	-1.30	621	46	45.27	0.42	3.38	1.00
	-1.32	626	48	40.06	0.40	2.44	1.00
	-1.35	624	61	34.33	0.42	2.38	1.00
	-1.37	619	73	31.21	0.46	2.83	1.00
	-1.40	598	30	39.99	0.43	1.32	1.00
	-1.42	594	24	48.50	0.44	1.78	1.00
	-1.45	592	21	64.64	0.43	2.56	1.00
	-1.47	591	16	77.94	0.44	3.310	1.00
	-1.50	595	34	86.09	0.53	18.10	1.00
	-1.55	591	28	122.7	0.57	31.33	1.00

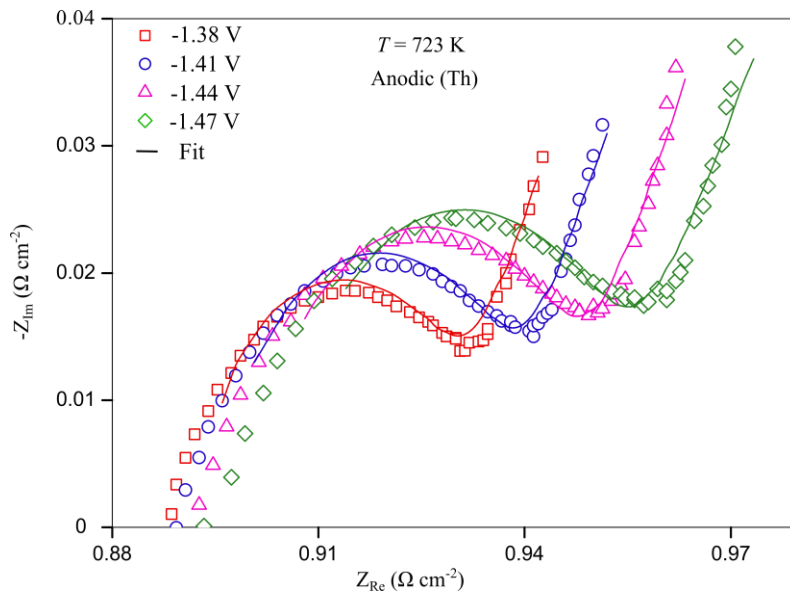
### 5.3 Anodic dissolution of Th electrode

Complex impedance spectra of anodic dissolution of thorium in LiCl-KCl eutectic melt in the potential range of -1.43 V to -1.34 V are shown in Figure 5.7. Impedance spectra are characterized by a very prominent semicircle at higher frequencies and a comparatively smaller linear region at lower frequencies. As the applied potential is anodically increased the frequency of onset for linear region gradually decreases, which is evident from Figure 5.7. For example, impedance spectra recorded at -1.43 V at 773 K (Figure 5.7d) has the onset of linear region at 1052 Hz whereas at -1.34 V, it appears at 370 Hz leading to lowering of  $R_{ct}$  with increase in the anodic applied potential. The charge transfer process at higher frequencies is associated with a large capacitive contribution due to continuous accumulation of  $\text{Th}^{4+}$  ions near the Th|melt interface as a result of anodic polarization of thorium. Another feature in the impedance plots that is distinctly different from that in Figure 5.2 and 5.5 is the

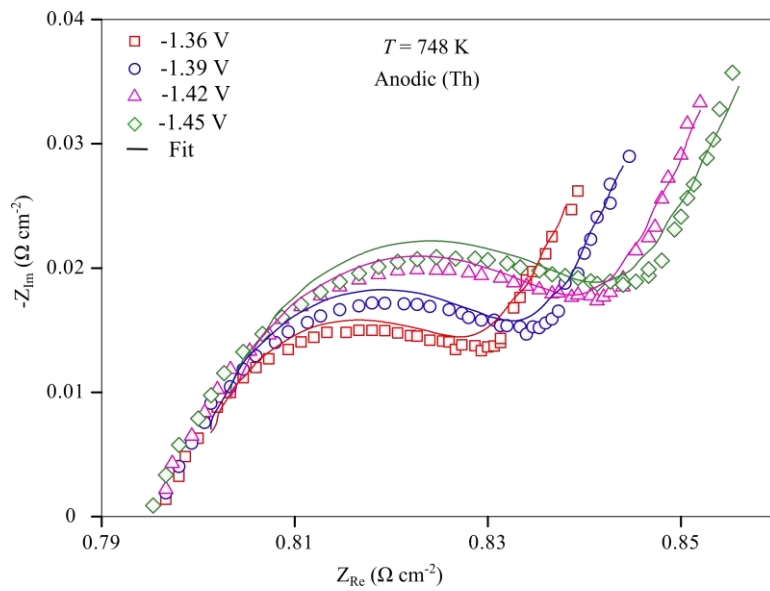
slope of the linear region at lower frequencies, which varies from 1.33 to 1.59 in the applied potential range of -1.34 V to -1.43 V.



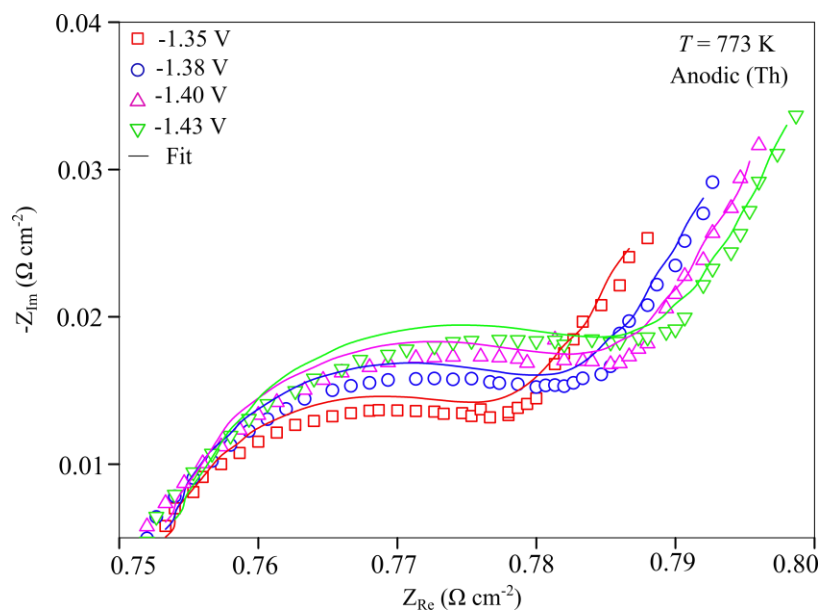
a



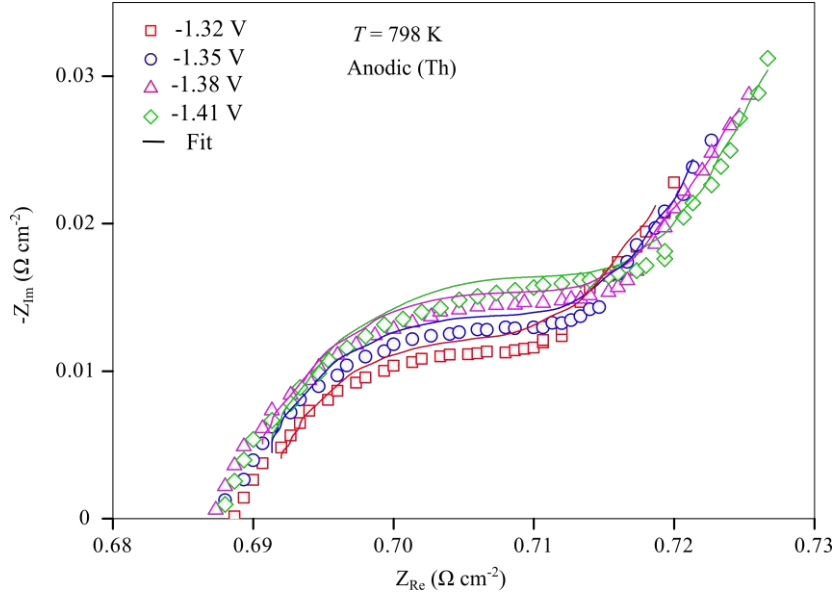
b



c



d



e

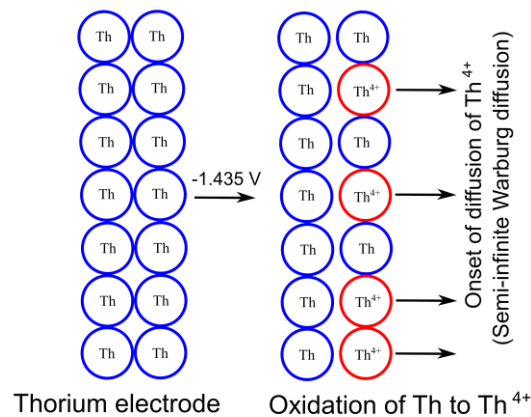
Figure 5.7 Nyquist plots of thorium electrode (anodic) in  $\text{LiCl-KCl-ThCl}_4$ ,  $C_{\text{ThCl}_4} = 1.02 \times 10^{-4} \text{ mol cm}^{-3}$ ,  $T = 698\text{-}798 \text{ K}$ ,  $A = 1.5 \text{ cm}^2$ , Frequency range of measurement:  $10\text{Hz-}10 \text{ kHz}$ .

A diagrammatic representation of the anodic dissolution of thorium is shown in Figure 5.8 that comprises of following three steps:

1. Step 1 (Oxidation of Th to  $\text{Th}^{4+}$  and semi-infinite Warburg diffusion of  $\text{Th}^{4+}$ ): At an applied potential of  $-1.430 \text{ V}$ , which is  $50 \text{ mV}$  more anodic than the equilibrium potential, Th anodically dissolves to form  $\text{Th}^{4+}$  in the melt and this process is kinetically controlled at higher frequencies ( $5 \text{ kHz} - 1 \text{ kHz}$ ). At lower frequencies ( $< 1 \text{ kHz}$ ), semi-infinite Warburg diffusion prevails and there is no restricted diffusion of  $\text{Th}^{4+}$  as the coverage or accumulation of  $\text{Th}^{4+}$  at the Th|melt interface is not uniform (Figure 5.8a).
2. Step 2 (Double layer charging at Th|melt interface): As the applied potential is anodically increased, accumulation of  $\text{Th}^{4+}$  at Th|melt also increases due to contribution of double layer charging effects. This is reflected in the impedance plots by a large semicircle at higher frequencies due to high capacitive contribution. The subsequent diffusion of  $\text{Th}^{4+}$  is largely semi-infinite in nature (Figure 5.8b).

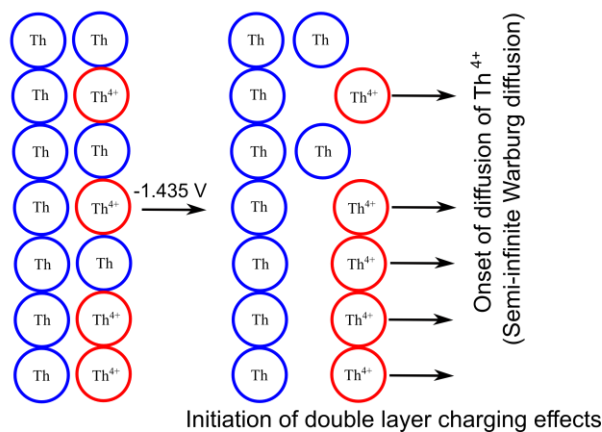
3. Step 3 (Increased capacitive contribution due to partial accumulation of  $\text{Th}^{4+}$ ): With increased anodic polarization of thorium, there is an increase of  $\text{Th}^{4+}$  ions at Th|melt interface leading to partial blocking of ions diffusing in bulk, although the diffusion remains semi-infinite Warburg type (Figure 5.8c). Due to this phenomenon, which is largely transient in nature, the slope of the complex impedance plot is greater than 0.5. For example, slope of linear region of impedance plots recorded at -1.35V, -1.38 V, -1.40 V and -1.43 V are 1.33, 1.54, 1.70 and 1.59, respectively. The accumulation of  $\text{Th}^{4+}$  leads to large capacitive contribution, which is reflected in impedance plots shown in Figure 5.7.

Step 1: Formation of  $\text{Th}^{4+}$  ions during anodic dissolution  
T=773 K

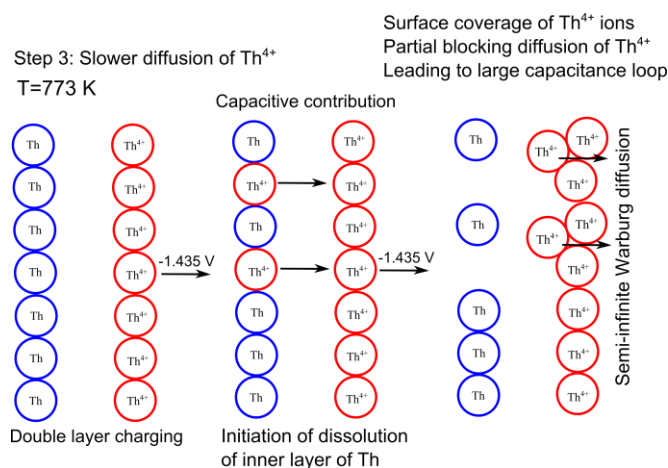


(a) Step 1: Oxidation of Th to  $\text{Th}^{4+}$  and semi-infinite Warburg diffusion of  $\text{Th}^{4+}$

Step 2: Double layer charging at Th|melt interface  
T=773 K



(b) Step 2: Double layer charging at Th|melt interface and semi-infinite Warburg diffusion of  $\text{Th}^{4+}$ . Capacitive contribution to charge transfer process also increases.



(c) Step 3: *Partial accumulation of  $\text{Th}^{4+}$  leading to large capacitive response. Diffusion of  $\text{Th}^{4+}$  remains semi-infinite.*

*Figure 5.8 Diagrammatic representation of anodic dissolution of thorium in LiCl-KCl eutectic melt; distinct features of complex impedance plots include large capacitive response at higher frequencies and slope of linear region at lower frequencies greater than 1.0; -1.435 V is the equilibrium potential for thorium dissolution.*

The complex impedance spectra were fitted to an equivalent circuit shown in Figure 5.1 and fitted values of  $R_s$ ,  $R_{ct}$ ,  $Q_1$  and  $Q_2$  thus obtained are shown in Table 5.3 from which the following observations are made (at 773 K):

1.  $R_s$  varies within 2 m $\Omega$  in the potential range -1.34 to -1.43 V and can be considered as constant. It is observed that  $R_s$  value is 450 m $\Omega$  higher than that obtained in fits for inert tungsten and liquid cadmium electrodes.
2.  $R_{ct}$  gradually decreases with increasing anodic potential and the variation is not more than 10 m $\Omega$  in potential range -1.34 to -1.43 V.
3.  $Q_1$  is characterized to be Warburg impedance element by fitted  $m$  value around 0.70.
4.  $Q_2$  is characterized to be double layer capacitance by  $m$  value of 1.00 at all applied potentials.

The variation of  $R_{ct}$  with applied potential is shown in Figure 5.9, which shows that there is a gradual decrease in  $R_{ct}$  when potential varied anodically from -1.43 V to -1.40 V after which

it decreases more rapidly in the potential range of -1.39 V to -1.34 V even though the overall change in  $R_{ct}$  is small. The onset of thorium dissolution is estimated at -1.401 V from Figure 5.9.

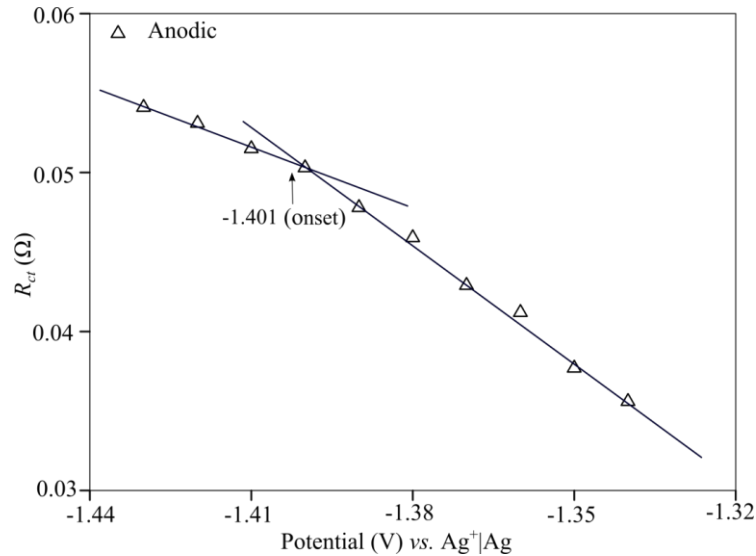


Figure 5.9 Variation of  $R_{ct}$  versus applied potential for Th electrode (anodic),  $C_{ThCl_4} = 1.02 \times 10^{-4} \text{ mol cm}^{-3}$ ,  $T = 773 \text{ K}$ .

Table 5.3 EIS data of anodic polarization of thorium electrode in LiCl-KCl-ThCl<sub>4</sub> electrolyte,  $C_{ThCl_4} = 1.02 \times 10^{-4} \text{ mol cm}^{-3}$ ,  $A = 1.5 \text{ cm}^2$ .

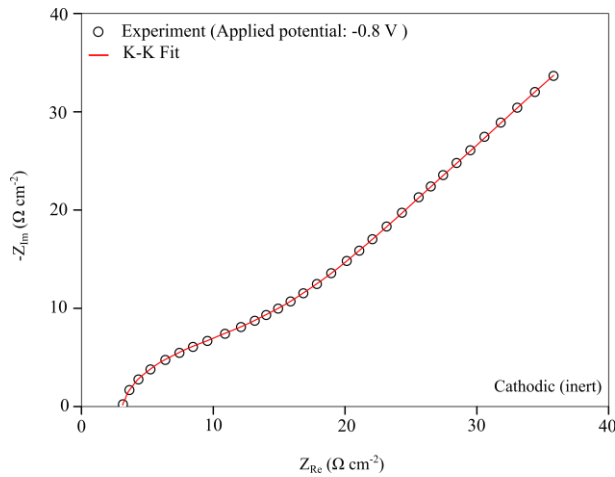
$T / \text{K}$	$E / \text{V}$	$R_s$ (mΩ)	$R_{ct}$ (mΩ)	$Q_1$		$Q_2$	
				$Y_0 \times 10^2$	$m$	$Y_0 \times 10^3$	$m$
698	-1.40	1277	109.9	2.26	0.51	3.24	0.99
	-1.41	1277	118.7	2.25	0.55	3.09	0.98
	-1.42	1277	122.2	2.56	0.51	2.61	0.98
	-1.43	1279	125.0	2.74	0.49	2.24	0.97
	-1.44	1282	127.3	2.36	0.51	2.26	0.96
	-1.45	1285	127.5	2.27	0.51	2.11	0.96
	-1.46	1289	128.1	2.03	0.52	1.97	0.96
	-1.47	1291	128.7	1.83	0.54	1.99	0.95
	-1.48	1294	129.3	1.68	0.55	1.67	0.96
-1.49	1294	129.7	1.67	0.55	1.67	0.96	
723	-1.38	1337	57.9	1.36	0.68	8.16	1.00
	-1.39	1340	59.4	1.35	0.67	8.30	1.00
	-1.40	1341	61.4	1.29	0.67	7.33	1.00
	-1.41	1343	63.5	1.22	0.67	6.60	1.00
	-1.42	1344	66.3	1.19	0.66	5.74	1.00
	-1.43	1345	69.1	1.15	0.66	5.14	1.00

	-1.44	1347	71.9	1.12	0.66	4.72	1.00
	-1.45	1349	74.4	1.10	0.65	4.28	1.00
	-1.46	1351	75.2	1.10	0.65	4.09	1.00
	-1.47	1354	76.7	1.12	0.64	4.03	1.00
748	-1.36	1199	43.1	1.79	0.64	16.83	1.00
	-1.37	1198	45.5	1.64	0.65	15.33	1.00
	-1.38	1199	47.8	1.52	0.66	14.16	1.00
	-1.39	1199	50.6	1.38	0.67	13.10	1.00
	-1.40	1199	53.8	1.31	0.67	12.17	1.00
	-1.41	1200	56.8	1.17	0.68	11.28	1.00
	-1.42	1200	60.0	1.11	0.69	10.62	1.00
	-1.43	1201	62.0	1.01	0.70	10.15	1.00
	-1.44	1199	62.0	1.00	0.70	9.81	1.00
	-1.45	1200	64.6	1.01	0.70	9.72	1.00
773	-1.34	1128	38.4	1.48	0.70	26.06	1.00
	-1.35	1129	40.3	1.35	0.71	24.18	1.00
	-1.36	1129	42.6	1.27	0.72	22.37	1.00
	-1.37	1129	43.7	1.22	0.72	21.62	1.00
	-1.38	1129	47.1	1.16	0.72	19.57	1.00
	-1.39	1129	49.1	1.11	0.72	18.64	1.00
	-1.40	1129	51.1	1.07	0.72	17.98	1.00
	-1.41	1129	51.9	1.06	0.71	16.99	1.00
	-1.42	1129	53.6	0.98	0.72	17.37	1.00
	-1.43	1130	54.4	0.94	0.73	17.48	1.00
798	-1.32	1036	27.92	2.45	0.59	35.01	1.00
	-1.33	1035	31.01	2.26	0.61	33.04	1.00
	-1.34	1035	32.2	2.02	0.62	30.74	1.00
	-1.35	1035	35.0	1.61	0.67	29.39	1.00
	-1.36	1034	36.0	1.67	0.65	27.52	1.00
	-1.37	1306	37.8	1.45	0.67	26.63	1.00
	-1.38	1033	40.2	1.38	0.68	25.79	1.00
	-1.39	1033	41.5	1.29	0.68	25.14	1.00
	-1.40	1034	41.8	1.19	0.69	25.06	1.00
	-1.41	1035	42.7	1.15	0.70	25.19	1.00

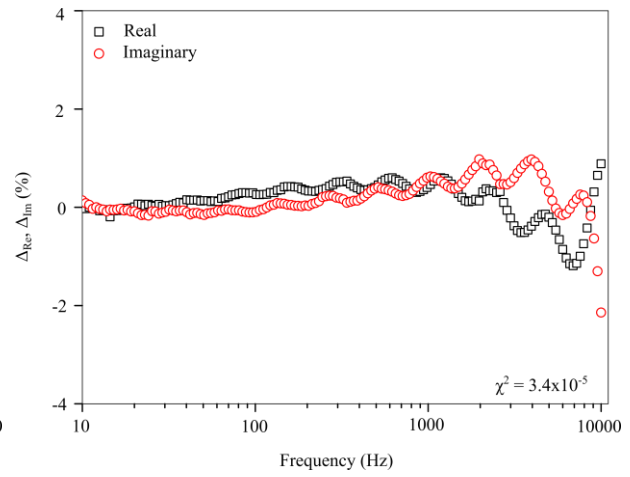
#### 5.4 Validation of complex impedance data by Kramers-Kronig transforms

Validation of complex impedance data recorded at inert tungsten, liquid Cd and thorium electrodes were carried out using Kramers-Kronig transforms. Figure 5.10 shows the Kramers-Kronig validation of impedance data recorded at -0.8 to -1.57 V at inert tungsten electrode and the residual relative errors  $\Delta_{\text{Re},i}$  and  $\Delta_{\text{Im},i}$  between the K-K transforms and real

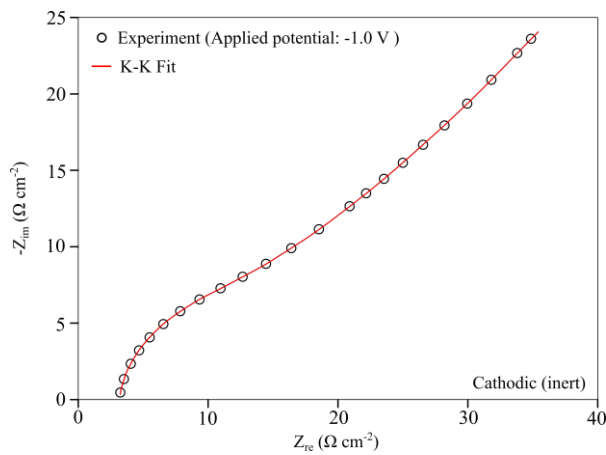
and imaginary part of the complex impedance data calculated using Equations 2.8 and 2.9 (discussed in Chapter 2) are shown in Figure 5.10. The relative residual error varies by less than 2% and is more pronounced at higher  $\log \omega$ . The compliance of K-K transforms calculated frequency dispersion and measured data can be considered good with  $\chi^2$  value of  $1.71 \times 10^{-4}$  to  $2.7 \times 10^{-6}$  in that potential range.



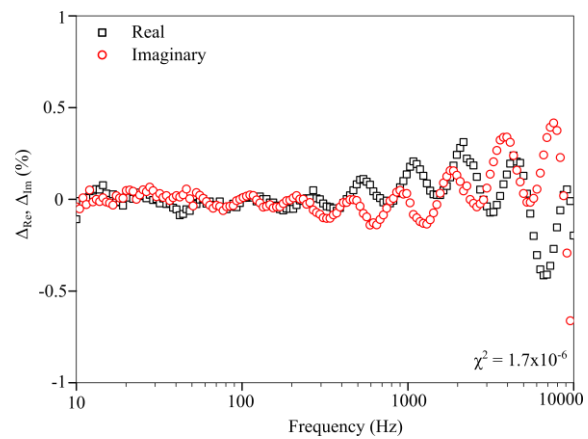
(a) K-K compliance fit



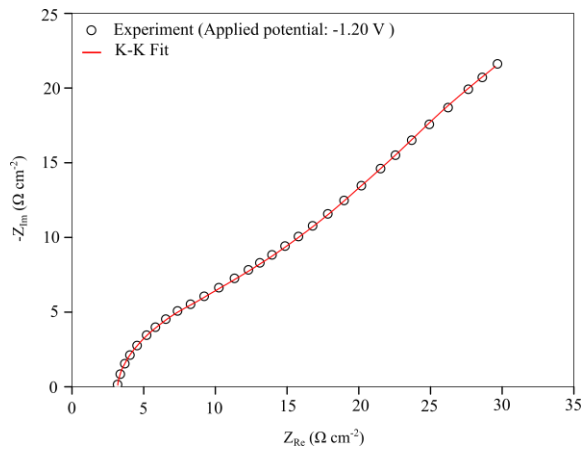
(b) Fit residuals  $\Delta_{Re,i}$  and  $\Delta_{Im,i}$



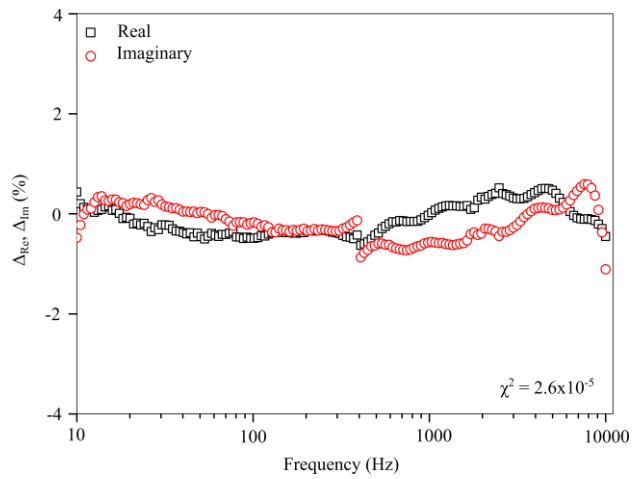
(c) K-K compliance fit



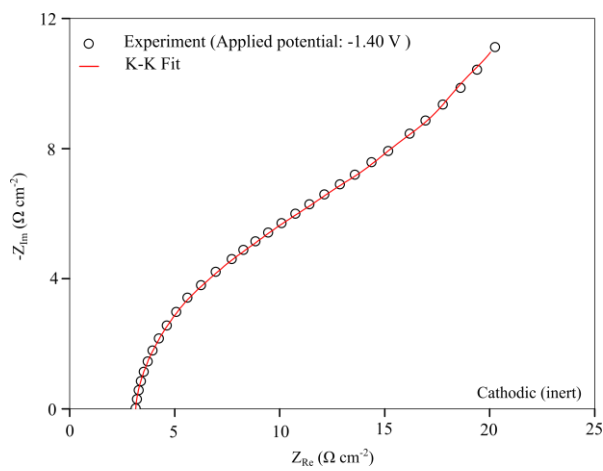
(d) Fit residuals  $\Delta_{Re,i}$  and  $\Delta_{Im,i}$



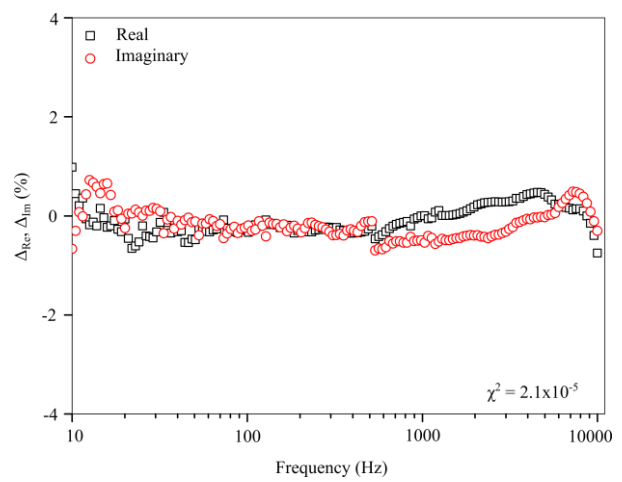
(e) K-K compliance fit



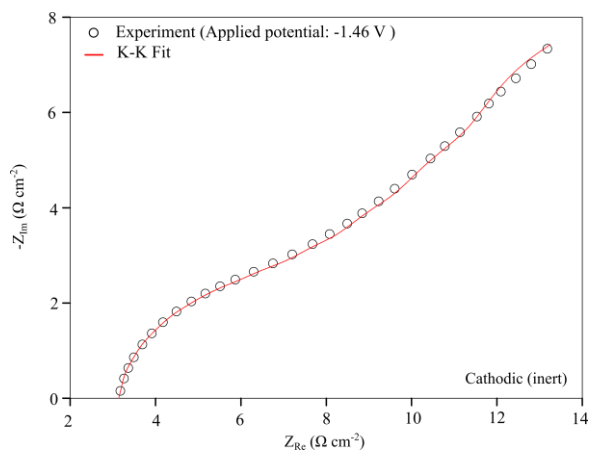
(f) Fit residuals  $\Delta_{Re,i}$  and  $\Delta_{Im,i}$



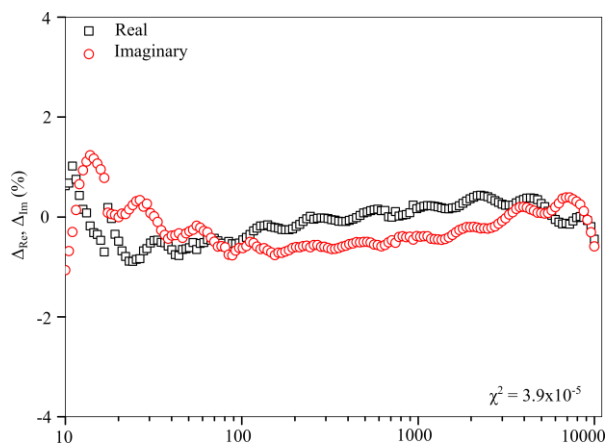
(g) K-K compliance fit



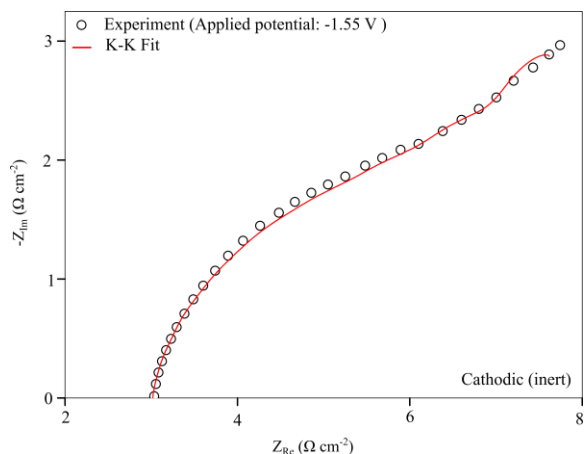
(h) Fit residuals  $\Delta_{Re,i}$  and  $\Delta_{Im,i}$



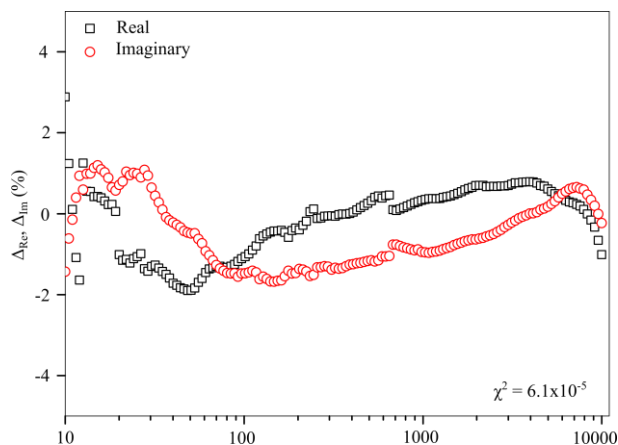
(i) K-K compliance fit



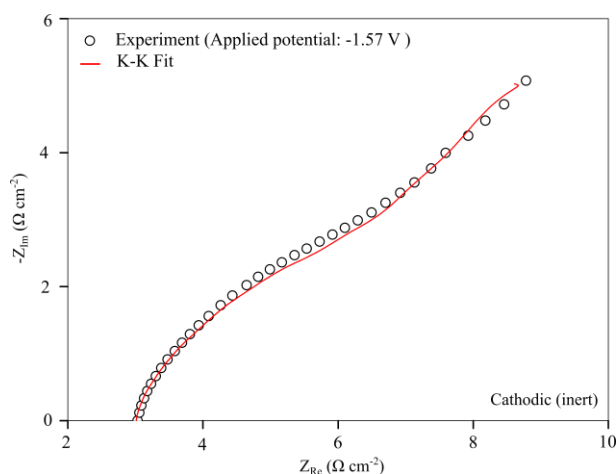
(j) Fit residuals  $\Delta_{Re,i}$  and  $\Delta_{Im,i}$



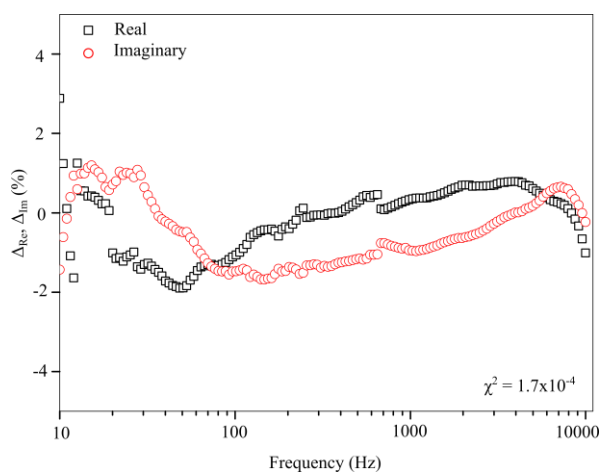
(k) K-K compliance fit



(l) Fit residuals  $\Delta_{Re,i}$  and  $\Delta_{Im,i}$



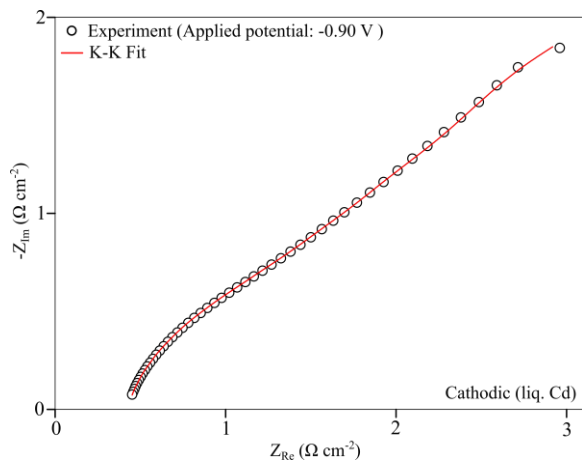
(m) K-K compliance fit



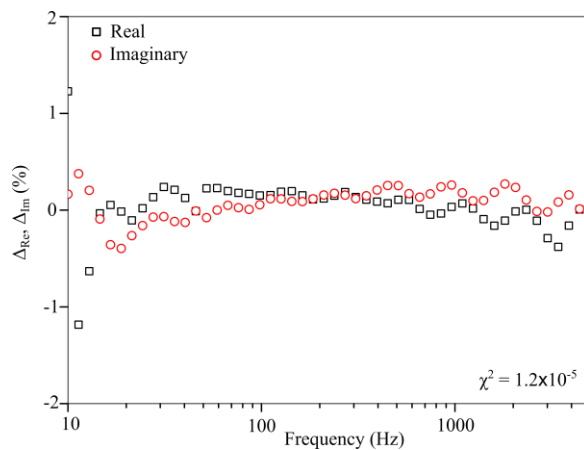
(n) Fit residuals  $\Delta_{Re,i}$  and  $\Delta_{Im,i}$

Figure 5.10 Validation of complex impedance data recorded at inert tungsten electrode using Kramers-Kronig transforms. K-K compliance fit, fit residuals  $\Delta_{Re,i}$  and  $\Delta_{Im,i}$  are shown for cathodic potentials of  $-0.8$  to  $-1.57$  V,  $T = 773$  K,  $A = 0.25$  cm<sup>2</sup>.

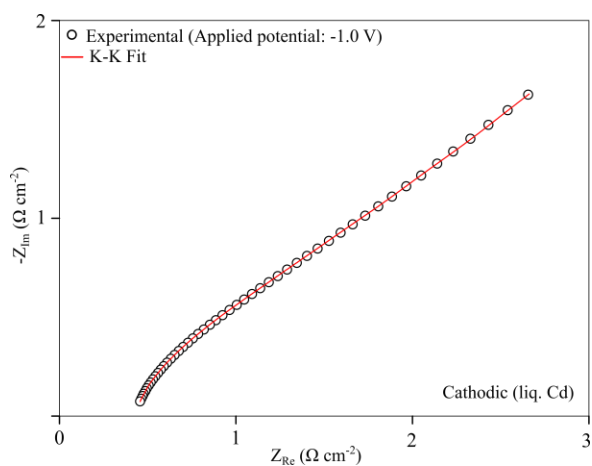
Validation of complex impedance data recorded at liquid cadmium electrode was carried out in a similar manner as described above. K-K compliance fit of impedance data recorded at  $-0.90$  to  $-1.47$  V and the variation of  $\Delta_{Re,i}$  and  $\Delta_{Im,i}$  with  $\log \omega$  are shown in Figure 5.11. A good K-K compliance fit is obtained for the measured data and the relative residual errors vary within 2% with  $\chi^2$  value of  $4.8 \times 10^{-5}$  to  $8.9 \times 10^{-6}$  in that potential range, but with small oscillations at lower and higher frequencies.



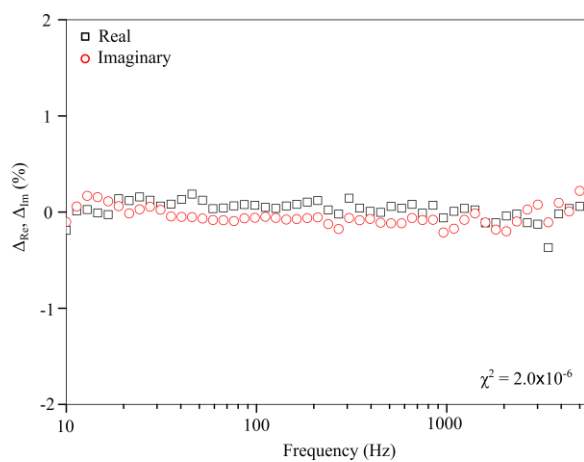
(a) K-K compliance fit



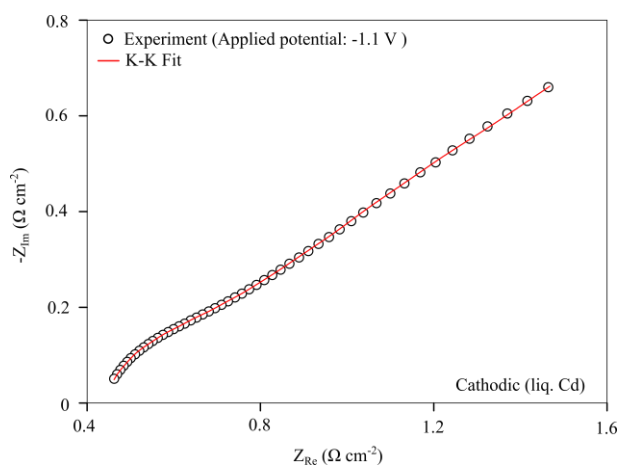
(b) Fit residuals  $\Delta_{Re,i}$  and  $\Delta_{Im,i}$



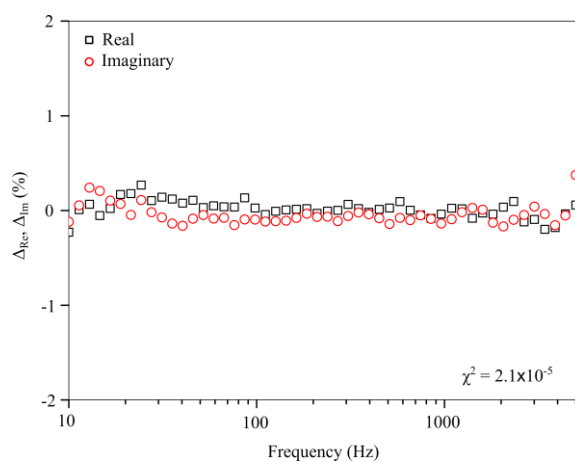
(c) K-K compliance fit



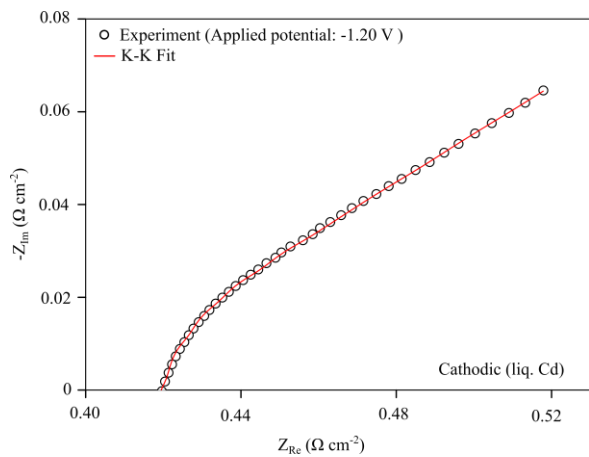
(d) Fit residuals  $\Delta_{Re,i}$  and  $\Delta_{Im,i}$



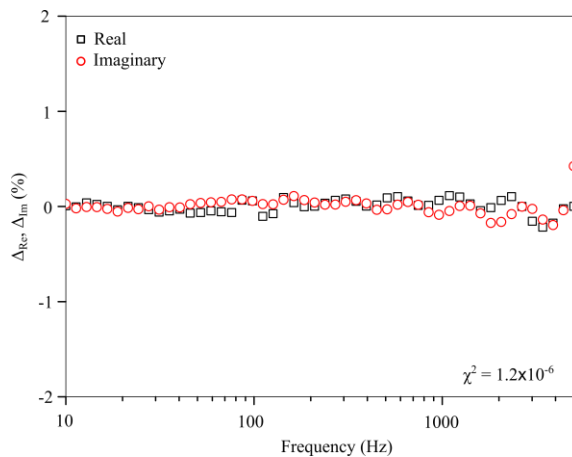
(e) K-K compliance fit



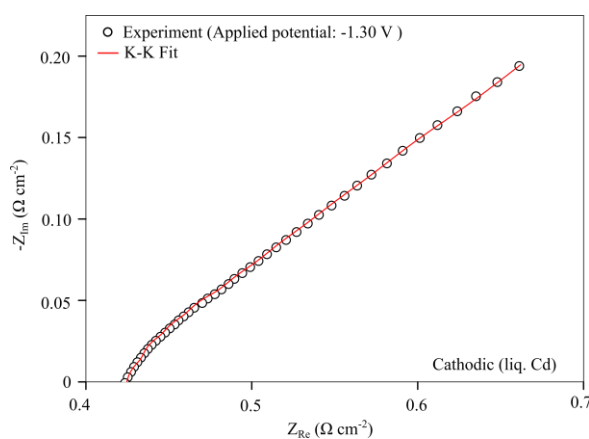
(f) Fit residuals  $\Delta_{Re,i}$  and  $\Delta_{Im,i}$



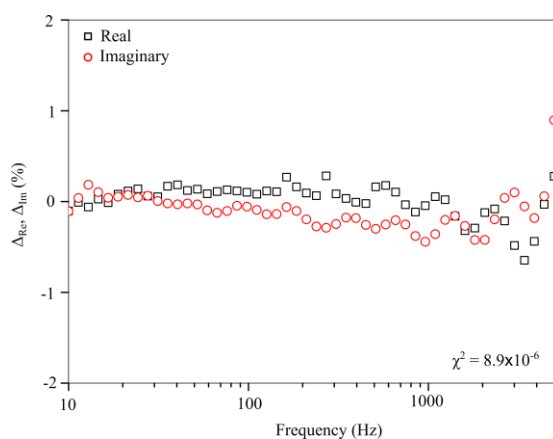
(g) K-K compliance fit



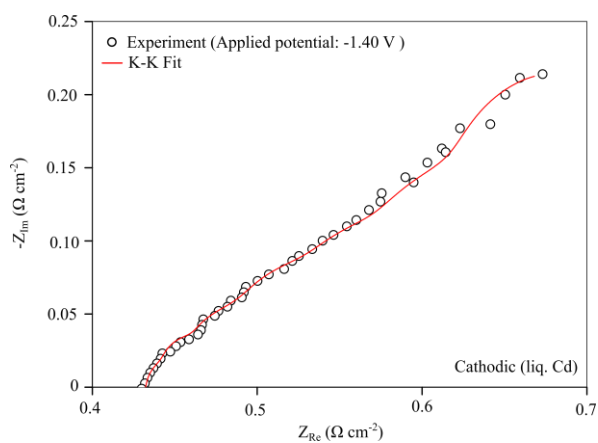
(h) Fit residuals  $\Delta_{Re,i}$  and  $\Delta_{Im,i}$



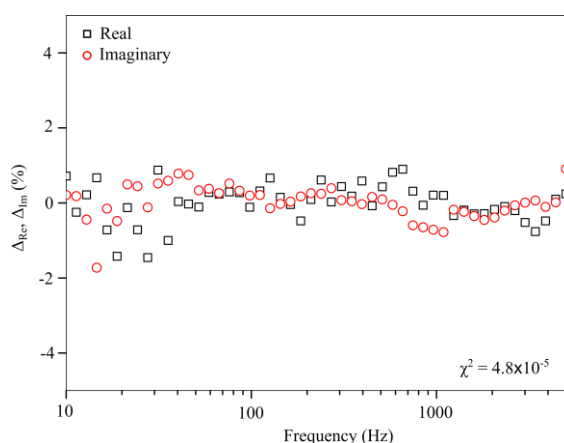
(i) K-K compliance fit



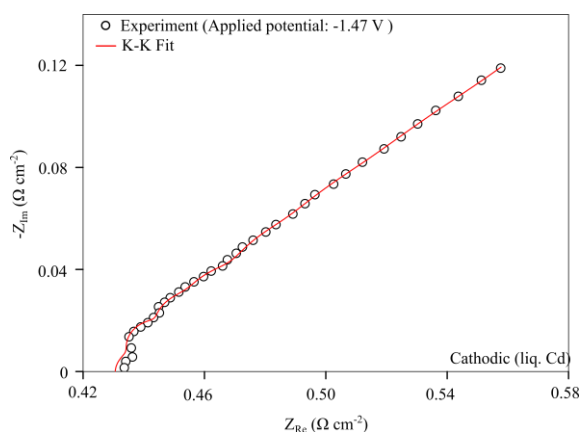
(j) Fit residuals  $\Delta_{Re,i}$  and  $\Delta_{Im,i}$



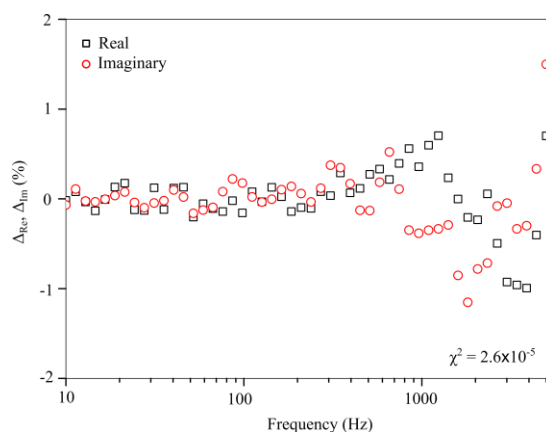
(k) K-K compliance fit



(l) Fit residuals  $\Delta_{Re,i}$  and  $\Delta_{Im,i}$



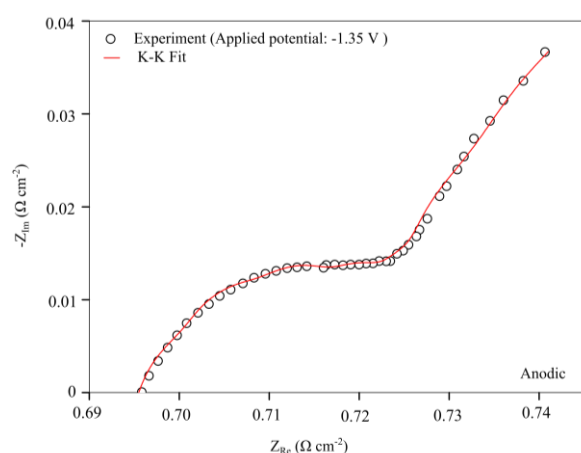
(m) K-K compliance fit



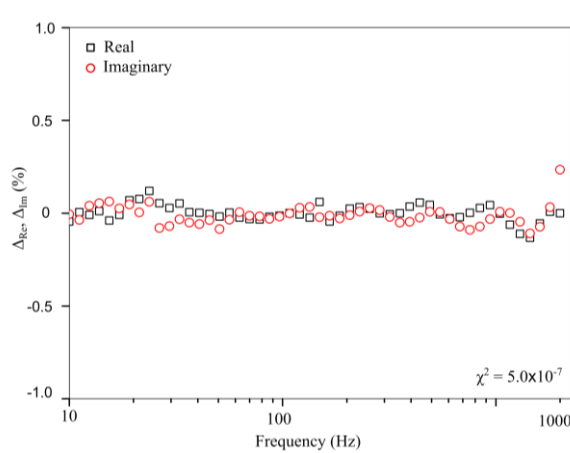
(n) Fit residuals  $\Delta_{Re,i}$  and  $\Delta_{Im,i}$

Figure 5.11 Validation of complex impedance data recorded at liquid cadmium electrode using Kramers-Kronig transforms. K-K compliance fit and fit residuals  $\Delta_{Re,i}$  and  $\Delta_{Im,i}$  are shown for cathodic potential of -0.90 to -1.47 V,  $T = 773$  K,  $A = 1.48$  cm<sup>2</sup>.

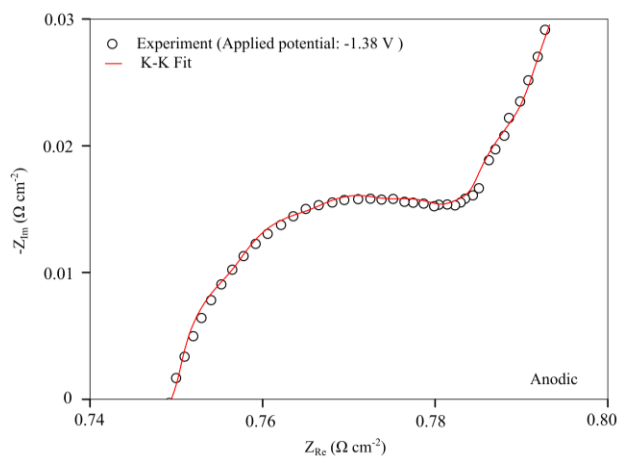
Complex impedance data of metallic thorium electrode recorded in the potential range -1.35 to -1.43 V were validated by K-K transforms. K-K compliance fit and plot of relative residual errors at these potentials are shown in Figure 5.12. A good compliance between measured data and K-K transforms is seen and  $\Delta_{Re,i}$  and  $\Delta_{Im,i}$  vary within 0.5% with  $\chi^2$  value of  $6.5 \times 10^{-7}$  to  $8.2 \times 10^{-7}$  in that potential range.



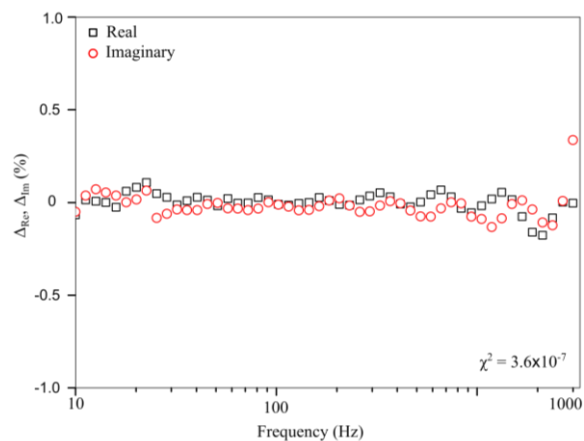
(a) K-K compliance fit



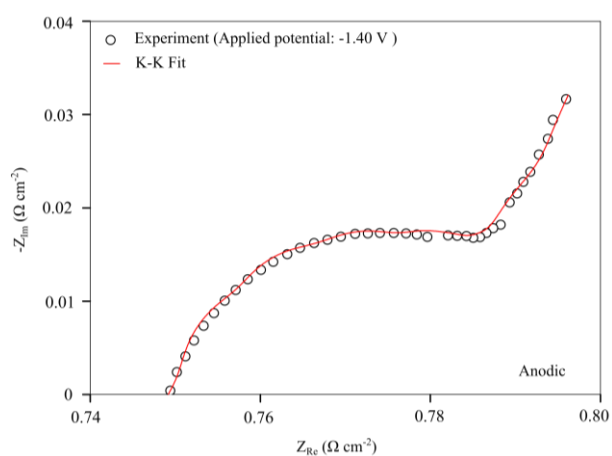
(b) Fit residuals  $\Delta_{Re,i}$  and  $\Delta_{Im,i}$



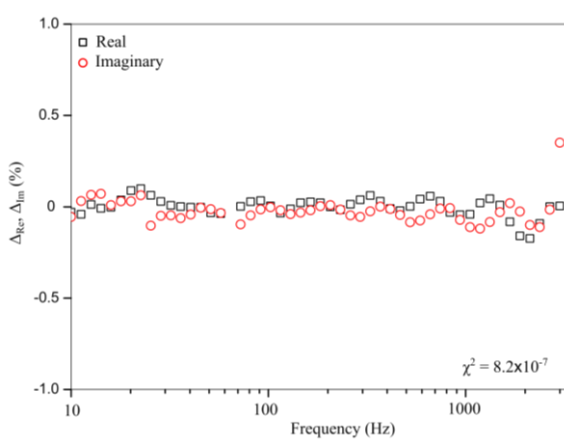
(c) K-K compliance fit



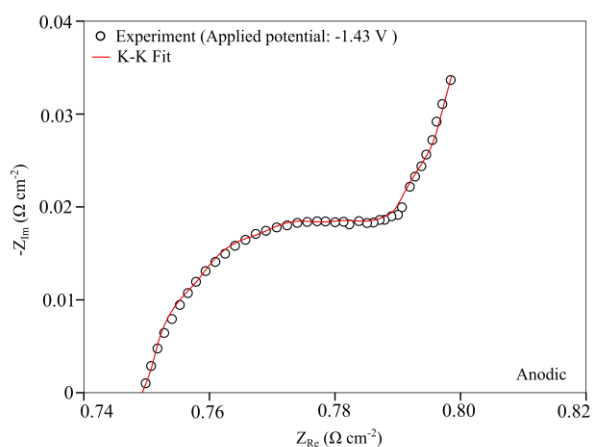
(d) Fit residuals  $\Delta_{Re,i}$  and  $\Delta_{Im,i}$



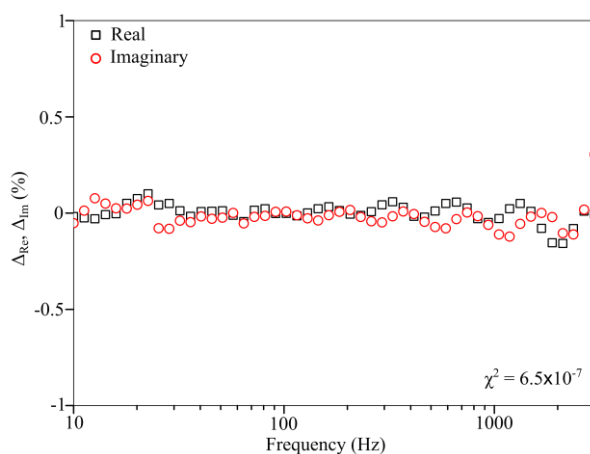
(e) K-K compliance fit



(f) Fit residuals  $\Delta_{Re,i}$  and  $\Delta_{Im,i}$



(g) K-K compliance fit



(h) Fit residuals  $\Delta_{Re,i}$  and  $\Delta_{Im,i}$

Figure 5.12 Validation of complex impedance data recorded at metallic thorium electrode using Kramers-Kronig transforms. K-K compliance fit and fit residuals  $\Delta_{Re,i}$  and  $\Delta_{Im,i}$  are shown for anodic potentials of -1.35 to -1.43 V,  $T = 773 \text{ K}$ ,  $A = 1.5 \text{ cm}^2$ .

## 5.5 Reversibility of Th<sup>4+</sup>|Th couple

Reversibility of Th<sup>4+</sup>|Th couple was studied by estimating heterogeneous rate constant ( $k_s$ ) which is a measure of electrode kinetics.  $R_{ct}$  estimated for applied potentials near equilibrium potential of thorium at inert tungsten (cathodic) and metallic thorium (anodic) electrodes by equivalent circuit fitting was used to calculate heterogeneous rate constant  $k_s$  using the following expression [65, 117, 118]:

$$k_s = \frac{RT}{n^2 \alpha^2 F^2 A R_{ct} C_{Th^{4+}}} \quad (5.1)$$

where,  $C_{Th^{4+}} = 1.02 \times 10^{-4} \text{ mol cm}^{-3}$ . Values of  $R_{ct}$  and  $k_s$  are tabulated in Table 5.4. Variation of  $\ln k_s$  vs.  $1/T$  for cathodic and anodic polarization cases is shown in Figure 5.13 and expressed as

$$\text{Cathodic: } \ln k_s = (2.491 \pm 1.181) - \frac{(6.27 \pm 0.88) \times 10^3}{T(\text{K})} \quad (5.2)$$

$$\text{Anodic: } \ln k_s = (3.939 \pm 0.992) - \frac{(6.53 \pm 0.74) \times 10^3}{T(\text{K})} \quad (5.3)$$

Table 5.4  $k_s$  estimated for cathodic and anodic polarization of thorium in LiCl-KCl eutectic.

System		698 K	723 K	748 K	773 K	798 K
Cathodic (inert)	$R_{ct}$ (mΩ)	1853	1593	1384	991	911
	$K_s \times 10^3$ (cm s <sup>-1</sup> )	1.66 ± 0.01	2.01 ± 0.03	2.39 ± 0.04	3.44 ± 0.11	5.25 ± 0.22
Anodic	$R_{ct}$ (mΩ)	129.7	76.7	64.6	54.4	42.7
	$K_s \times 10^3$ (cm s <sup>-1</sup> )	4.03 ± 0.05	7.08 ± 0.10	8.62 ± 0.22	10.58 ± 0.39	14.15 ± 0.70

The activation energy for charge transfer process was estimated at 52.1 ± 7.3 kJ mol<sup>-1</sup> (cathodic, inert tungsten) and 54.3 ± 6.2 kJ mol<sup>-1</sup> (anodic, thorium electrode). The reversibility of Th<sup>4+</sup>|Th couple was studied by Matsuda-Ayabe criteria given by the following expressions:

$$\text{Reversible (Nernstian): } \frac{k_s}{\left(\frac{D\nu F}{RT}\right)^{\frac{1}{2}}} \geq 15 \quad (5.4)$$

$$\text{Quasireversible: } 10^{-2(1+\alpha)} < \frac{k_s}{\left(\frac{D\nu F}{RT}\right)^{\frac{1}{2}}} < 15 \quad (5.5)$$

$$\text{Irreversible: } \frac{k_s}{\left(\frac{D\nu F}{RT}\right)^{\frac{1}{2}}} < 10^{-2(1+\alpha)} \quad (5.6)$$

$\alpha = 0.70$ ,  $10^{-2(1+\alpha)} = 3.98 \times 10^{-4}$  and  $D_{\text{Th}^{4+}}$  of  $\text{Th}^{4+}$  was taken from Table 3.3 (discussed in Chapter 3). Results are shown in Table 5.5 where,  $\frac{k_s}{\left(\frac{D\nu F}{RT}\right)^{\frac{1}{2}}}$  was estimated at 25 mV s<sup>-1</sup> and

100 mV s<sup>-1</sup> in the temperature range of 698-798 K. Calculations were also carried out at 10 mV s<sup>-1</sup>, 50 mV s<sup>-1</sup> and the results shown that they comply with inequality [70], and hence  $\text{Th}^{4+}|\text{Th}$  couple is quasireversible in nature in the scan rate range 25-100 mV s<sup>-1</sup> and temperature range 698-798 K.

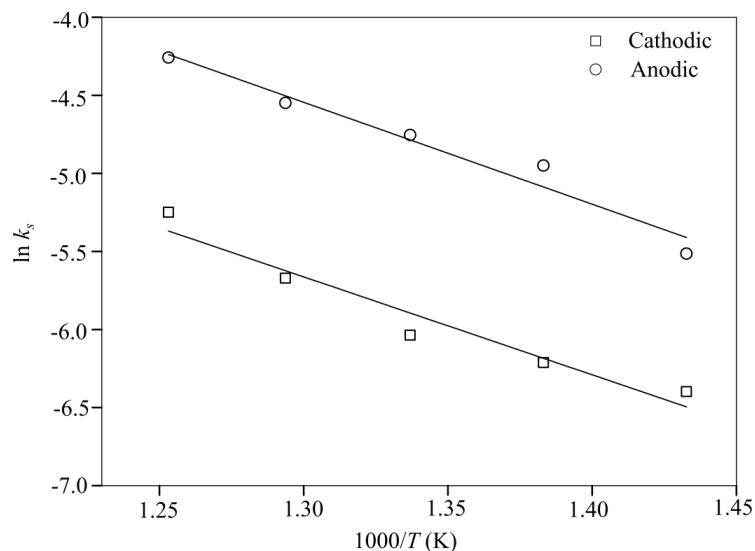


Figure 5.13 Temperature dependence of  $\ln k_s$  for cathodic (inert tungsten) and anodic (thorium) polarization cases.

Table 5.5 Matsuda-Ayabe criteria applied to  $\text{Th}^{4+}/\text{Th}$  couple for cathodic and anodic polarization cases in LiCl-KCl eutectic melt,  $10^{-2(1+\alpha)} = 3.98 \times 10^{-4}$  for all cases.

System	Scan rate ( $\text{mV s}^{-1}$ )	$\frac{k_s}{\left(\frac{DnFv}{RT}\right)^{1/2}}$				
		698 K	723 K	748 K	773 K	798 K
Cathodic (Inert)	25	0.405	0.459	0.486	0.617	0.851
	100	0.203	0.229	0.243	0.308	0.425
Anodic (Thorium)	25	0.983	1.619	1.752	1.898	2.292
	100	0.492	0.809	0.876	0.949	1.146

## 5.6 Conclusions

The present study involved investigation on  $\text{Th}^{4+}/\text{Th}$  couple using electrochemical impedance spectroscopy that was used to elucidate the contribution of kinetic and mass transfer process during cathodic and anodic polarization of thorium in LiCl-KCl eutectic melt. Based on experimental observations and analysis of EIS data following conclusions were drawn:

1. Reduction of  $\text{Th}^{4+}$  at inert tungsten and liquid cadmium electrodes was mainly charge transfer controlled process near equilibrium potential and diffusion controlled process at low and very high cathodic potentials.
2. Scattering of impedance data at low frequency observed at large applied cathodic potential liquid cadmium electrode could be ascribed to movements of liquid cadmium surface due to continuous deposition of thorium.
3. Variation of  $R_{ct}$  versus applied potential showed one minimum for inert tungsten electrode corresponding to equilibrium potential of thorium and two minimum at liquid cadmium electrode corresponding to formation of  $\text{Cd}_{11}\text{Th}$  and  $\text{Cd}_5\text{Th}$ . Although this aspect was not investigated in greater detail.

4. EIS study was used to address the reversibility of  $\text{Th}^{4+}|\text{Th}$  couple, which was found to be quasireversible in the temperature range of 698-798 K using Matsuda-Ayabe criteria.

## CHAPTER 6

### Thermochemical evaluation of $E_{\text{Th}^{4+}|\text{Th}}^{\circ}$ and $\Delta_f G_{\text{ThCl}_4}^{\circ}$ in LiCl-KCl eutectic melt

#### Results and discussions

In this chapter, thermodynamic evaluation of  $E_{\text{Th}^{4+}|\text{Th}}^{\circ}$  and  $\Delta_f G_{\text{ThCl}_4}^{\circ}$  is performed based on apparent standard electrode potential calculated in Chapter 3 and literature data. Electromotive force measurements were carried out at various compositions of  $\text{ThCl}_4$  in LiCl-KCl eutectic melt to estimate  $E_{\text{Th}^{4+}|\text{Th}}^{\circ}$  and  $\Delta_f G_{\text{ThCl}_4}^{\circ}$  from the variation of equilibrium potential against  $\ln x_{\text{ThCl}_4}$  and  $x_{\text{ThCl}_4}$ . The chapter concludes with recommendations on  $E_{\text{Th}^{4+}|\text{Th}}^{\circ}$  and  $RT \ln \gamma_{\text{ThCl}_4}$  obtained from statistical data analysis. A summary of electrochemical studies carried out in LiCl-KCl eutectic melt containing  $\text{ThCl}_4$  across various research groups is presented in Table 6.1.

Table 6.1 Literature survey on thermodynamic behaviour of ThCl<sub>4</sub> in LiCl-KCl eutectic melt.

Reference(s)	$x_{\text{AgCl}}$	$x_{\text{ThCl}_4}$	Technique	$T / \text{K}$	Brief summary of work
Cassayre <i>et al.</i> [7]	$3.9 \times 10^{-3}$	$3.51 \times 10^{-3}$ to $4.79 \times 10^{-3}$	OCP	693-823	Investigated electrochemical behaviour of Th <sup>4+</sup> in LiCl-KCl eutectic melt and reported $E_{\text{Th}^{4+} \text{Th}}^\circ$ and $\gamma_{\text{ThCl}_4}$ values at various temperatures.
Chiotti <i>et al.</i> [9, 10]	$1.31 \times 10^{-2}$	$1.74 \times 10^{-4}$ to $6.65 \times 10^{-5}$	emf	723-923	Carried out electromotive force measurements at various compositions of ThCl <sub>4</sub> in LiCl-KCl eutectic melt and reported $E_{\text{Th}^{4+} \text{Th}}^\circ$ and $\gamma_{\text{ThCl}_4}$ values at various temperatures.
Inman <i>et al.</i> [14]	$2.20 \times 10^{-3}$	$4.12 \times 10^{-4}$ , $1.40 \times 10^{-3}$	emf	673-773	Estimated thermodynamic properties such as $\Delta_f G_{\text{ThCl}_4}^\circ$ and $\gamma_{\text{ThCl}_4}$ in LiCl-KCl eutectic melt
Yang <i>et al.</i> [15]	$8.00 \times 10^{-2}$ , $8.05 \times 10^{-2}$ , $7.62 \times 10^{-2}$	$4.8 \times 10^{-4}$ to $3.77 \times 10^{-3}$	emf	763-828	Carried out electromotive force measurements at various compositions of ThCl <sub>4</sub> in LiCl-KCl eutectic melt and reported $E_{\text{Th}^{4+} \text{Th}}^\circ$ and $\gamma_{\text{ThCl}_4}$ values at various temperatures
Martinot <i>et al.</i> [107]	$2.0 \times 10^{-3}$	$2.8 \times 10^{-3}$ to $12.9 \times 10^{-3}$	emf	673-773	Carried out electromotive force measurements at various compositions of ThCl <sub>4</sub> in LiCl-KCl eutectic melt and reported $E_{\text{Th}^{4+} \text{Th}}^\circ$ and $\gamma_{\text{ThCl}_4}$ values at various temperatures

## 6.1 Analysis of electromotive force data

$E_{\text{Th}^{4+}|\text{Th}}^{eq}$  versus  $\text{Ag}^+|\text{Ag}$  reference electrode at various  $x_{\text{ThCl}_4}$  ( $3.26 \times 10^{-3}$  to  $8.05 \times 10^{-4}$ ) in LiCl-KCl eutectic melt was measured in the temperature range of 677-798 K for both heating and cooling cycles. Average of equilibrium potential recorded in heating and cooling cycles is graphically shown in Figure 6.1 and tabulated in Table 6.2.

The variation of  $E_{\text{Th}^{4+}|\text{Th}}^{eq} + E_{\text{AgCl}}^\circ + \frac{RT}{F} \ln x_{\text{AgCl}}$  (vs.  $\text{Cl}^-|\text{Cl}_2$ ) vs.  $\ln x_{\text{ThCl}_4}$  (Method of Roy *et al.*

[70, 71]) and  $E_{\text{Th}^{4+}|\text{Th}}^{eq} + E_{\text{AgCl}}^\circ + \frac{RT}{F} \ln x_{\text{AgCl}} - \frac{RT}{4F} \ln x_{\text{ThCl}_4}$  (vs.  $\text{Cl}^-|\text{Cl}_2$ ) vs.  $x_{\text{ThCl}_4}$  (Method of

Lantelme *et al.* [72-74]) at various temperatures with corresponding linear fits are shown in

Figure 6.2 and 6.3, respectively. In the method of Roy *et al.*,  $E_{\text{Th}^{4+}|\text{Th}}^\circ$  at any given temperature

$T$  is obtained by extrapolating the linear fit to  $\ln x_{\text{ThCl}_4} \rightarrow 0$  or,  $x_{\text{ThCl}_4} \rightarrow 1$ . Thus

$E_{\text{Th}^{4+}|\text{Th}}^\circ$  obtained by this method can be said to be for  $\text{ThCl}_4$  at unit thermodynamic activity.

On the other hand, in the method of Lantelme *et al.*,  $E_{\text{Th}^{4+}|\text{Th}}^\circ$  at any given temperature  $T$  is

obtained by extrapolating the linear fit to  $x_{\text{ThCl}_4} \rightarrow 0$ .  $E_{\text{Th}^{4+}|\text{Th}}^\circ$  can thus be said to be for  $\text{ThCl}_4$

at infinite dilution in LiCl-KCl eutectic melt.

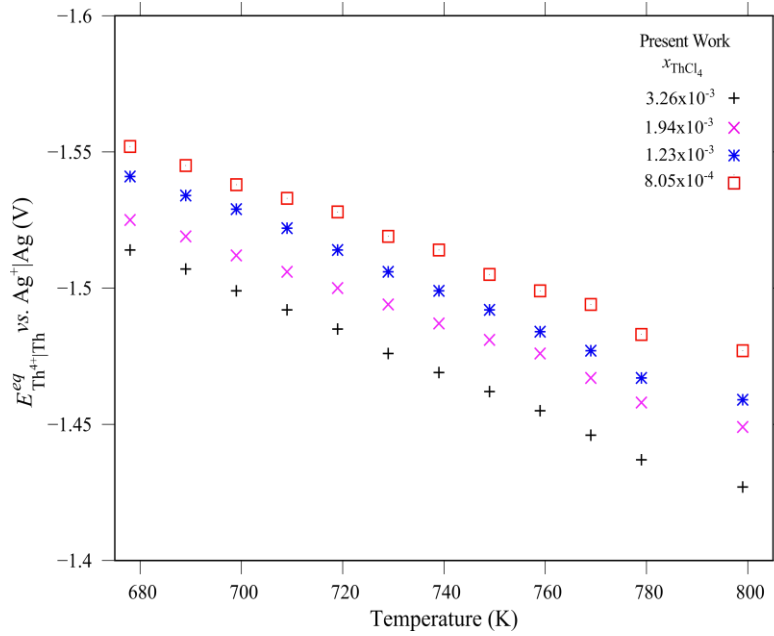


Figure 6.1 Equilibrium potential  $E_{Th^{4+}/Th}^{eq}$  measured against  $Ag^+/Ag$  reference electrode at various  $x_{ThCl_4}$  and temperatures in  $LiCl-KCl$  eutectic melt.

Table 6.2 Equilibrium potential of  $Th^{4+}/Th$  couple measured against  $Ag^+/Ag$  reference electrode ( $x_{AgCl} = 4.6 \times 10^{-3}$ ).

T/K	$x_{ThCl_4}$			
	$3.26 \times 10^{-3}$	$1.94 \times 10^{-3}$	$1.23 \times 10^{-3}$	$8.05 \times 10^{-4}$
$E_{Th^{4+}/Th}^{eq}$				
678	-1.514	-1.525	-1.541	-1.552
689	-1.507	-1.519	-1.534	-1.545
699	-1.499	-1.512	-1.529	-1.538
709	-1.492	-1.506	-1.522	-1.533
719	-1.485	-1.500	-1.514	-1.528
729	-1.476	-1.494	-1.506	-1.519
739	-1.469	-1.487	-1.499	-1.514
749	-1.462	-1.481	-1.492	-1.505
759	-1.455	-1.476	-1.484	-1.499
769	-1.446	-1.467	-1.477	-1.494
779	-1.437	-1.458	-1.467	-1.483
799	-1.427	-1.449	-1.459	-1.477

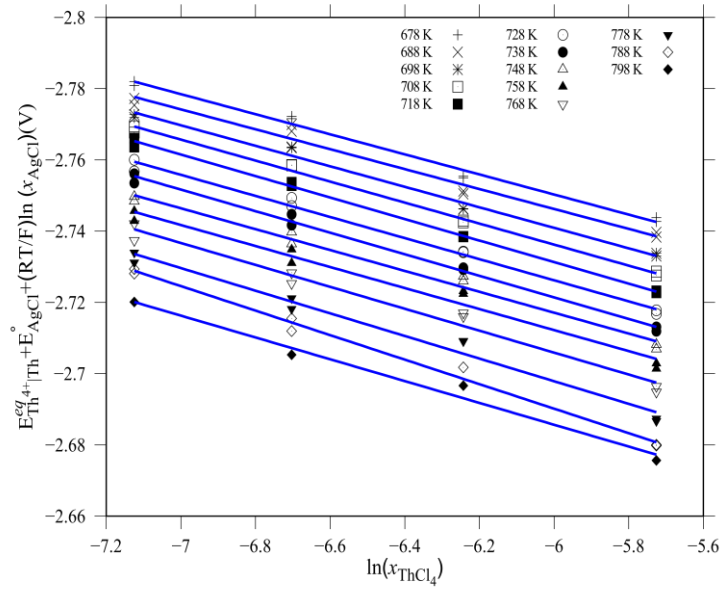


Figure 6.2 Variation of  $E_{Th^{4+}|Th}^{eq} + E_{AgCl}^{\circ} + \frac{RT}{F} \ln x_{AgCl}$  (vs.  $Cl^- | Cl_2$ ) vs.  $\ln x_{ThCl_4}$  (Method of Roy et al. [70, 71]) in LiCl-KCl eutectic melt.

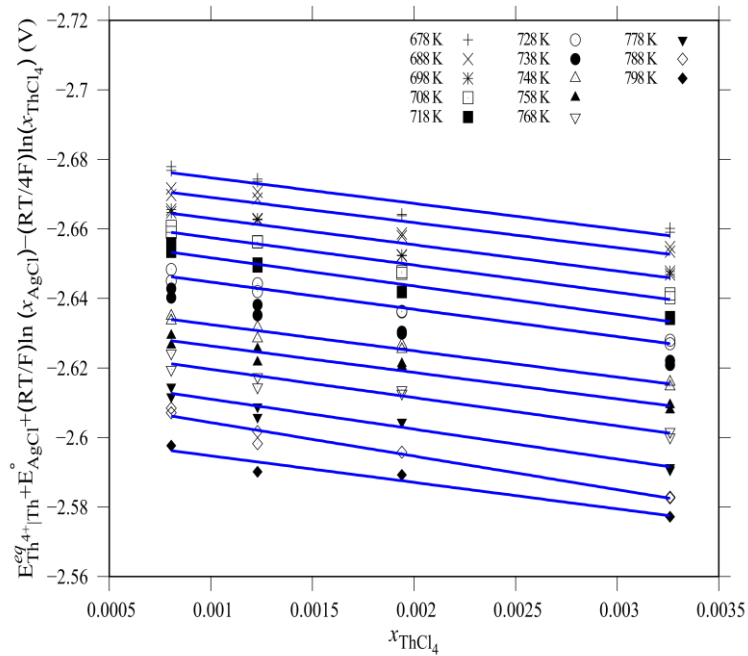


Figure 6.3 Variation of  $E_{Th^{4+}|Th}^{eq} + E_{AgCl}^{\circ} + \frac{RT}{F} \ln x_{AgCl} - \frac{RT}{4F} \ln x_{ThCl_4}$  (vs.  $Cl^- | Cl_2$ ) vs.  $x_{ThCl_4}$  (Method of Lantelme et al. [72, 73]) in LiCl-KCl eutectic melt.

$E_{\text{Th}^{4+}|\text{Th}}^\circ$  estimated by these two methods are tabulated in Table 6.3. Temperature dependence of  $E_{\text{Th}^{4+}|\text{Th}}^\circ$  obtained from methods of Roy *et al.* and Lantelme *et al.* are respectively given by Equations 6.1 and 6.2 respectively.

Table 6.3 Comparison of standard electrode potential of  $\text{Th}^{4+}|\text{Th}$  couple versus  $\text{Cl}^-|\text{Cl}_2$  estimated in the present work with literature data.

Cassayre <i>et al.</i> [7]		Yang <i>et al.</i> [15]		Martinot <i>et al.</i> [107]			
$T(\text{K})$	$E_{\text{Th}^{4+} \text{Th}}^\circ / \text{V}$	$T(\text{K})$	$E_{\text{Th}^{4+} \text{Th}}^\circ / \text{V}$	$T(\text{K})$	$E_{\text{Th}^{4+} \text{Th}}^\circ / \text{V}$		
693	-2.599	763	-2.733	673	-2.592 <sup>a</sup>	-2.664 <sup>b</sup>	-2.525 <sup>c</sup>
733	-2.577	775	-2.728	723	-2.533	-2.650	-2.498
773	-2.559	787	-2.722	773	-2.536	-2.638	-2.472
798	-2.534	804	-2.715				
823	-2.530	825	-2.704				
Present work							
$T/\text{K}$	$E_{\text{Th}^{4+} \text{Th}}^\circ / \text{V}$		$T/\text{K}$	$E_{\text{Th}^{4+} \text{Th}}^\circ / \text{V}$			
678	$-2.581 \pm 0.007^b$	$-2.682 \pm 0.002^c$	698	$-2.695^d$	$-2.698^e$	$-2.718^f$	
689	$-2.578 \pm 0.011$	$-2.676 \pm 0.002$	723	-2.671	-2.670	-2.713	
699	$-2.568 \pm 0.008$	$-2.670 \pm 0.002$	748	-2.651	-2.652	-2.705	
709	$-2.559 \pm 0.005$	$-2.665 \pm 0.001$	773	-2.624	-2.619	-2.684	
719	$-2.550 \pm 0.004$	$-2.659 \pm 0.001$	803	-2.606	-2.596	-2.669	
729	$-2.548 \pm 0.007$	$-2.653 \pm 0.001$					
739	$-2.539 \pm 0.006$	$-2.647 \pm 0.001$					
749	$-2.534 \pm 0.009$	$-2.640 \pm 0.001$					
759	$-2.530 \pm 0.012$	$-2.633 \pm 0.001$					
769	$-2.521 \pm 0.012$	$-2.628 \pm 0.001$					
779	$-2.507 \pm 0.012$	$-2.619 \pm 0.001$					
799	$-2.502 \pm 0.019$	$-2.614 \pm 0.002$					

<sup>a</sup> Method of Roy *et al.* [70, 71]

<sup>b</sup> Method of Lantelme *et al.* [72, 73]

<sup>c</sup> Method of Knacke *et al.* [68]

<sup>d</sup> By CP (Chapter 3)

<sup>e</sup> By SIV (Chapter 3)

<sup>f</sup> By CV (Chapter 3)

$$E_{\text{Th}^{4+}|\text{Th}}^{\circ} \text{ vs. Cl}^{-}|\text{Cl}_2 \text{ (V)} = -(3.042 \pm 0.017) + (6.838 \pm 0.241) \times 10^{-4} T \text{ (K)} \quad (6.1)$$

$$E_{\text{Th}^{4+}|\text{Th}}^{\circ} \text{ vs. Cl}^{-}|\text{Cl}_2 \text{ (V)} = -(3.120 \pm 0.010) + (6.435 \pm 0.136) \times 10^{-4} T \text{ (K)} \quad (6.2)$$

## 6.2 Data analysis and recommendations

Figure 6.4 shows graphical comparison of temperature dependence of  $E_{\text{Th}^{4+}|\text{Th}}^{\circ}$  reported in literature (presented in Table 6.3), and we make the following observations:

- a.  $E_{\text{Th}^{4+}|\text{Th}}^{\circ}$  reported by Yang *et al.* [15] falls in the potential region -2.733 to -2.704 V in temperature range 763-825 K. These values are more cathodic compared to data of Martinot *et al.* [107] estimated using the method of Knacke *et al.* [68] that lie in the potential region -2.525 to -2.572 V in temperature range 673-773 K.
- b. However, if Martinot *et al.* data are analysed by the methods of Roy *et al.* [70, 71] and Lantelme *et al.* [72, 73],  $E_{\text{Th}^{4+}|\text{Th}}^{\circ}$  lies in the range -2.592 to -2.539 V and -2.664 to -2.638 V in the same temperature range.
- c.  $E_{\text{Th}^{4+}|\text{Th}}^{\circ}$  estimated from the semi-integral voltammetry (SIV) and logarithmic analysis of chronopotentiometry (CP) in the present work falls in the potential range -2.698 to -2.596 V in temperature range 698-803 K. On the other hand,  $E_{\text{Th}^{4+}|\text{Th}}^{\circ}$  estimated from anodic voltammograms (CV) of thorium electrode in the present work lies in more cathodic potential region (from -2.718 to -2.669 V). Average variation in data is 21 to 68 mV in the same temperature range.
- d. Variation in  $E_{\text{Th}^{4+}|\text{Th}}^{\circ}$  estimated from electromotive force data measured in thesis (Table 6.2) by the methods of Roy *et al.* and Lantelme *et al.* is only 10 mV, and that estimated by the former method lies closer to data reported by Cassayre *et al.* [7].

- e. Using method of Roy *et al.*,  $E_{\text{Th}^{4+}|\text{Th}}^{\circ}$  estimated from Martinot *et al.* data (-2.592 to -2.536 V) and that in present work (-2.581 to -2.502 V) agree well with each other.
- f. Method of Lantelme *et al.* leads to more cathodic estimation of  $E_{\text{Th}^{4+}|\text{Th}}^{\circ}$  has seen from Martinot *et al.* data (-2.664 to -2.638 V) as well as that measured in present work (-2.682 to -2.614 V), and both estimations agree well with each other.

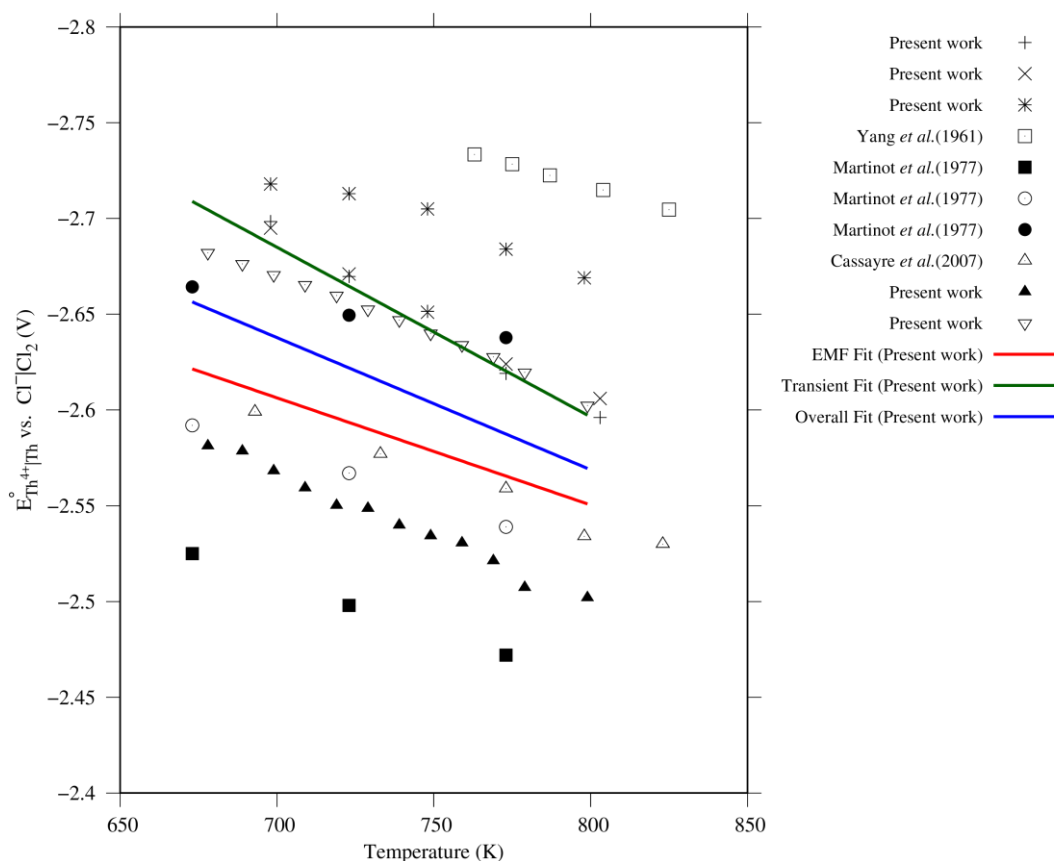


Figure 6.4 Temperature dependence of  $E_{\text{Th}^{4+}|\text{Th}}^{\circ}$  in LiCl-KCl eutectic melt reported by various authors and in the present work.  $E_{\text{Th}^{4+}|\text{Th}}^{\circ}$  of Martinot *et al.* [107] re-calculated using the method of Roy *et al.* and Lantelme *et al.* are also shown. Individual linear fitting of electromotive force and transient data along with the overall fit are also shown.

Based on above discussions,  $E_{\text{Th}^{4+}|\text{Th}}^{\circ}$  versus  $T$  obtained from electromotive force and transient measurements were independently least squares fitted to Equations 6.3 and 6.4. In case of former, all data except that from Yang *et al.* [15] were included in least squares fitting. In

case of latter, both Cassayre *et al.* [7] and that from transient technique in present work (discussed in Chapter 3) were included. Expressions for temperature dependence of  $E_{\text{Th}^{4+}|\text{Th}}^{\circ}$  are, respectively given by,

$$\text{EMF: } E_{\text{Th}^{4+}|\text{Th}}^{\circ} \text{ vs. Cl}^{-}|\text{Cl}_2(\text{V}) = -(2.998 \pm 0.189) + (5.594 \pm 2.571) \times 10^{-4}T \quad (6.3)$$

$$\text{Transient: } E_{\text{Th}^{4+}|\text{Th}}^{\circ} \text{ vs. Cl}^{-}|\text{Cl}_2(\text{V}) = -(3.305 \pm 0.204) + (8.857 \pm 2.713) \times 10^{-4}T \quad (6.4)$$

Linear least squares fits are shown in Figure 6.4. As seen from figure, emf data fit lies closer to Martinot *et al.* data (method of Roy *et al.*) and that estimated in present work (method of Roy *et al.*). Transient data fit lies close to that estimated using SIV and CP (discussed in Chapter 3). It is also seen that emf data fit also lies close to Cassayre *et al.* data [7], and transient data fit lies close to the present work (method of Lantelme *et al.*), and it also intersects Martinot *et al.* data (using method of Lantelme *et al.*).

In order to obtain final expression for temperature dependence of  $E_{\text{Th}^{4+}|\text{Th}}^{\circ}$ , we decided to give higher weightage to emf data fit than to transient data fit that is based on the fact that estimation of  $E_{\text{Th}^{4+}|\text{Th}}^{\circ}$  by electromotive force method is considered more reliable and accurate than that estimated using transient techniques. The overall fit expression of temperature dependence of  $E_{\text{Th}^{4+}|\text{Th}}^{\circ}$  combining Equations 6.3 and 6.4 is given by,

$$E_{\text{Th}^{4+}|\text{Th}}^{\circ} \text{ vs. Cl}^{-}|\text{Cl}_2(\text{V}) = -(3.121 \pm 0.195) + (6.900 \pm 2.628) \times 10^{-4}T \quad (6.5)$$

Equation 6.5 is also represented in Figure 6.4. It lies close to data of Cassayre *et al.* [7] and that estimated in thesis work (method of Lantelme *et al.*). Corresponding temperature dependence of  $\Delta_f G_{\text{ThCl}_4}^{\circ}$  is given by,

$$\Delta_f G_{\text{ThCl}_4}^{\circ} (\text{kJ mol}^{-1}) = -(1204.7 \pm 75.3) + (0.266 \pm 0.101)T \quad (6.6)$$

### 6.3 Estimation of $\gamma_{\text{ThCl}_4}^{liq.}$

For estimating  $\gamma_{\text{ThCl}_4}$  in LiCl-KCl eutectic melt, Equation 2.22 was used, which is discussed in Chapter 2. Thermochemical data of pure ThCl<sub>4</sub> liquid for  $\Delta_f G_{\text{ThCl}_4,liq.}^\circ$  were taken from Glassner [106], Martinot [107], Fuger [108], FactSage 6.4 database based on Barin and Kubaschewski [110] and Fuger and Brown [119]. In studies on Th<sup>4+</sup>/Th couple in LiCl-KCl eutectic melt by Yang *et al.* [15],  $\gamma_{\text{ThCl}_4}$  was reported in the range  $0.59 \times 10^{-3}$  to  $3.34 \times 10^{-3}$  in the temperature range 768-823 K, and was based on Glassner's expression on pure solid ThCl<sub>4</sub> valid in the temperature range 298-1043 K. Glassner had also obtained expression for pure ThCl<sub>4</sub> liquid valid in temperature range 1043-1195 K. The latter data was extrapolated to the present temperature measurement range 678-798 K, and is compared in Figure 6.5 with  $\Delta_f G_{\text{ThCl}_4,liq.}^\circ$  from Martinot [107], Fuger [108], FactSage 6.4 [109, 110] and Fuger and Brown [119] and  $\Delta_f G_{\text{ThCl}_4,s}^\circ$  from Glassner [106].  $\Delta_f G_{\text{ThCl}_4,liq.}^\circ$  of pure ThCl<sub>4</sub> liquid in temperature range 1043-1195 K obtained by Glassner is also shown.

We now refer to  $\gamma_{\text{ThCl}_4}$  estimated using the hypothetical supercooled liquid reference data (Figure 6.5) as  $\gamma_{\text{ThCl}_4}^{liq.}$ , and the temperature dependence of  $RT \ln \gamma_{\text{ThCl}_4}^{liq.}$  (or partial excess Gibbs energy  $\overline{\Delta G_{\text{ThCl}_4}^{ex}}$ ) is shown in Figure 6.6. For sake of comparison, we have also used  $\Delta_f G_{\text{ThCl}_4,s}^\circ$  data to estimate  $\gamma_{\text{ThCl}_4}$  although we refer to it as  $\gamma_{\text{ThCl}_4}^{liq.}$  in Figure 6.6.

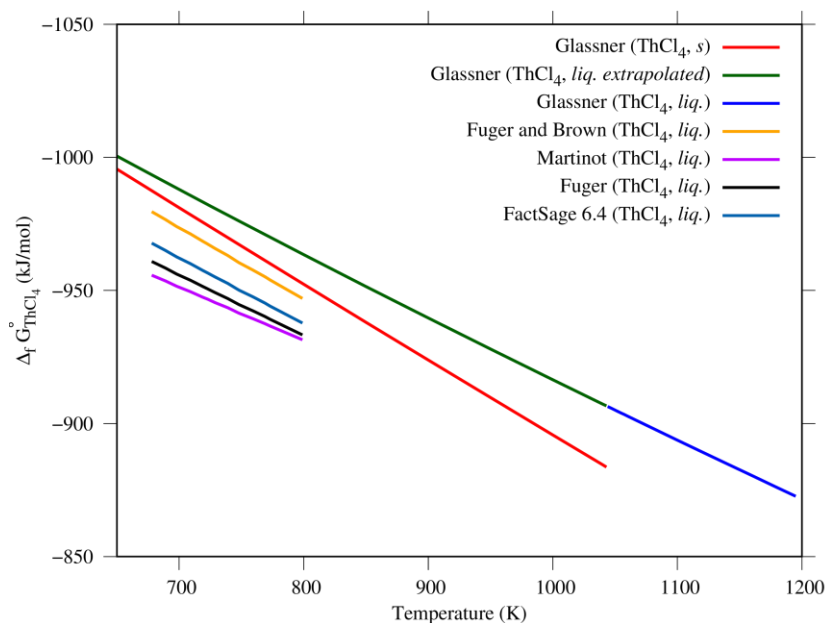


Figure 6.5 Variation of  $\Delta_f G_{\text{ThCl}_4, \text{liq.}}^\circ$  of pure  $\text{ThCl}_4$  liquid (hypothetically supercooled) as reference state versus  $T$  taken from different thermochemical data compilations [106-108, 110, 119],  $\Delta_f G_{\text{ThCl}_4, \text{s}}^\circ$  of pure solid  $\text{ThCl}_4$  from Glassner [106] is also shown.

There are two bands of data that are clearly seen. The first band is seen in the range -70 to -50  $\text{kJ mol}^{-1}$  in which  $RT \ln \gamma_{\text{ThCl}_4}^{\text{liq.}}$  estimated from  $\Delta_f G_{\text{ThCl}_4, \text{liq.}}^\circ$  data of Martinot [107], Fuger [108] and FactSage [109, 110] are observed whereas the second band appears in the range -45 to -35  $\text{kJ mol}^{-1}$  in which  $RT \ln \gamma_{\text{ThCl}_4}^{\text{liq.}}$  estimated from thermochemical data of Glassner [106] and Fuger and Brown [119] are observed. Data of both pure solid and liquid  $\text{ThCl}_4$  from Glassner's compilation were used for the estimation, and  $RT \ln \gamma_{\text{ThCl}_4}^{\text{liq.}}$  is seen to be closely matching with each other although it has a positive temperature dependence. Data estimated from Fuger and Brown shows that  $RT \ln \gamma_{\text{ThCl}_4}^{\text{liq.}}$  is temperature independent and is constant at around -45  $\text{kJ mol}^{-1}$ .

For establishing average temperature dependence of  $RT \ln \gamma_{\text{ThCl}_4}^{\text{liq.}}$ , we find that values estimated using Fuger and Brown [119] and Glassner [106] data are unlikely based on the current understanding of complexation of  $\text{Th}^{4+}$  in LiCl-KCl eutectic melt. Calculated  $\gamma_{\text{ThCl}_4}^{\text{liq.}}$  in

the temperature range 678-800 K varied from  $3.7 \times 10^{-4}$  to  $1.2 \times 10^{-3}$  and  $4.5 \times 10^{-3}$  to  $1.43 \times 10^{-2}$ , respectively, and that calculated using Martinot [107], Fuger [108] and FactSage [110] is in order of  $10^{-5}$ .

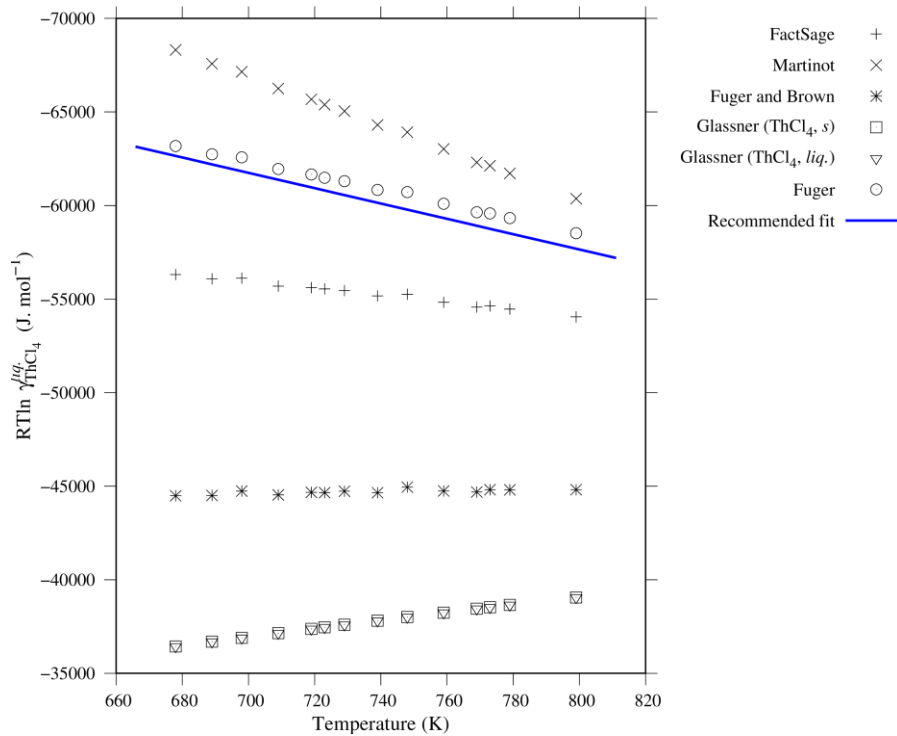


Figure 6.6 Variation of  $\gamma_{\text{ThCl}_4}^{\text{liq.}}$  in LiCl-KCl eutectic melt versus  $T$  estimated from various thermochemical compilations. The recommended linear least square fit is also shown.

It is recommend that  $RT \ln \gamma_{\text{ThCl}_4}^{\text{liq.}}$  estimated from Martinot [107], Fuger *et al.* [108] and FactSage [110] only should be used to calculate the average temperature dependence, and is given by the following expression obtained by linear least squares fitting:

$$RT \ln \gamma_{\text{ThCl}_4}^{\text{liq.}} (\text{kJ mol}^{-1}) = -(90428.5 \pm 12857.5) + (40.975 \pm 17.438)T \quad (6.7)$$

Least squares fit is shown in Figure 6.6, and lies very close to values estimated by Fuger's data [108]. Comparison of calculated  $\gamma_{\text{ThCl}_4}^{\text{liq.}}$  can be made with that reported by Dock [10]. In this work, electromotive force measurements in LiCl-KCl eutectic melt were carried out at

various  $x_{\text{ThCl}_4}$  ranging from  $1.74 \times 10^{-4}$  to  $6.65 \times 10^{-2}$  in the temperature range 723-929 K using

$x_{\text{AgCl}} = 1.319 \times 10^{-2}$  as reference. Temperature dependence of  $E_{\text{Th}^{4+}|\text{Th}}^\circ$  was reported as

$$E_{\text{Th}^{4+}|\text{Th}}^\circ = -3.009 + 6.776 \times 10^{-4}T \quad (6.8)$$

Dock's electromotive force data were analyzed using methods of Roy *et al.* [70, 71] and Lantelme *et al.* [72, 73]. However, it was seen that data at 773 K only could be used for the analysis.  $E_{\text{Th}^{4+}|\text{Th}}^\circ$  at 773 K was found to be -2.591 and -2.612 V, respectively using the two methods. These values are quite close to that reported by Cassayre *et al.* [7] (-2.559 V) and that reported in our earlier works using semi-integral voltammetry and chronopotentiometry (-2.619 and -2.624 V) at 773K.

Dock estimated  $\gamma_{\text{ThCl}_4}^s$  using pure solid  $\text{ThCl}_4$  as reference state, and also calculated  $\gamma_{\text{ThCl}_4}^{liq.}$  from

$\gamma_{\text{ThCl}_4}^s$  using the following relation:

$$\gamma_{\text{ThCl}_4}^{liq.} = \gamma_{\text{ThCl}_4}^s - \frac{\Delta_{\text{fus}}H_{\text{ThCl}_4}}{RT} \frac{T_{\text{fus}} - T}{T_{\text{fus}}} \quad (6.9)$$

Dock reported temperature and composition dependent expressions for  $\gamma_{\text{ThCl}_4}^s$ , and it ranged from  $0.569 \times 10^{-3}$  to  $3.298 \times 10^{-3}$  in the above temperature range 753-929 K. These values were similar to that reported by Yang *et al.* [15] suggesting that thermochemical data of pure solid  $\text{ThCl}_4$  (used as reference state for calculating  $\text{ThCl}_4$ ) were taken from Glassner [106]. Glassner's data estimates higher  $\gamma_{\text{ThCl}_4}^s$  in order of  $10^{-3}$ . Therefore, Fuger's and Barin and Kubaschewski's data (on which FactSage 6.4 databases are based) on  $\Delta_f G_{\text{ThCl}_4, liq.}^\circ$  are more reliable in estimating  $\gamma_{\text{ThCl}_4}$ , and consistent with currently accepted view of existence of high degree of complexation of  $\text{Th}^{4+}$  in chloride melts.

## 6.4 Conclusions

In the present work, we have presented thermochemical evaluation of thermodynamic properties of dilute solutions of ThCl<sub>4</sub> in LiCl-KCl eutectic melt. As part of this work,

1. From the variation of  $E_{\text{Th}^{4+}|\text{Th}}^{eq} + E_{\text{AgCl}}^{\circ} + \frac{RT}{F} \ln x_{\text{AgCl}}$  versus  $\ln x_{\text{ThCl}_4}$  and  $E_{\text{Th}^{4+}|\text{Th}}^{eq} + E_{\text{AgCl}}^{\circ} + \frac{RT}{F} \ln x_{\text{AgCl}} - \frac{RT}{4F} \ln x_{\text{ThCl}_4}$  versus  $x_{\text{ThCl}_4}$ ,  $E_{\text{Th}^{4+}|\text{Th}}^{\circ}$  was estimated in the temperature range 698-798 K. The former method for estimation of  $E_{\text{Th}^{4+}|\text{Th}}^{\circ}$  is recommended as it is estimated from the approximation  $x_{\text{ThCl}_4} \rightarrow 1$  or,  $\ln x_{\text{ThCl}_4} \rightarrow 0$ . The later method gives  $E_{\text{Th}^{4+}|\text{Th}}^{\circ}$  is essentially standard electrode potential at infinite dilution *i.e.*  $x_{\text{ThCl}_4} \rightarrow 0$  that tends to give more negative values of  $E_{\text{Th}^{4+}|\text{Th}}^{\circ}$ .
2.  $E_{\text{Th}^{4+}|\text{Th}}^{\circ}$  estimated from equilibrium (Chapter 6) and transient measurements (Chapter 3) was fitted to single temperature dependence expression (Eq. 6.5) by giving a higher weightage to data estimated by former method.
3. Temperature dependence of  $RT \ln \gamma_{\text{ThCl}_4}^{liq.}$  was established by choosing pure ThCl<sub>4</sub> in hypothetically supercooled liquid as reference state (Equation 2.21, discussed in chapter 2). Various thermochemical compilations were used to estimate  $\gamma_{\text{ThCl}_4}^{liq.}$  and the recommended expression for temperature dependence of  $RT \ln \gamma_{\text{ThCl}_4}^{liq.}$  is given by Equation 6.10, which suggests that  $\gamma_{\text{ThCl}_4}^{liq.}$  lies in the range  $1.5 \times 10^{-5}$  to  $1.7 \times 10^{-4}$  in the temperature range 678-799 K. In order to obtain the recommended fit,  $RT \ln \gamma_{\text{ThCl}_4}^{liq.}$  estimated using thermochemical data of Glassner was not used as the data predicts more negative  $\Delta \overline{G}_{\text{ThCl}_4}^{ex}$  at higher temperatures that cannot be substantiated.  $RT \ln \gamma_{\text{ThCl}_4}^{liq.}$  is more or less constant at all temperatures when Fuger and Brown data was used. These variations are not in agreement with the current understanding of ideality in molten salts at higher temperatures. The recommended fit for temperature dependence of  $RT \ln \gamma_{\text{ThCl}_4}^{liq.}$  closely matches with that estimated using thermochemical data of Fuger, which was also used by

Cassayre *et al.* for estimating  $\gamma_{\text{ThCl}_4}^{\text{liq.}}$ . Based on the current work, thermochemical data for liquid ThCl<sub>4</sub> by Fuger seems to be the most reliable data for estimation of  $RT \ln \gamma_{\text{ThCl}_4}^{\text{liq.}}$ .

## CHAPTER 7

### Electromotive force measurements on Cd-Th alloys in LiCl-KCl eutectic melt

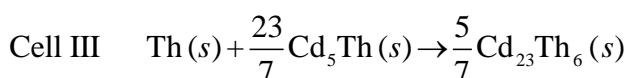
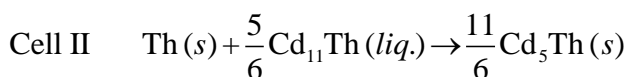
#### Results and discussions

This chapter discusses electromotive force measurements on Cd-Th alloys for determining  $\Delta_f G_{\text{Cd}_m\text{Th}_n}^\circ$  of Cd<sub>11</sub>Th, Cd<sub>5</sub>Th, Cd<sub>23</sub>Th<sub>6</sub> and Cd<sub>3</sub>Th intermetallics.  $\Delta_f H_{\text{Cd}_m\text{Th}_n}^\circ$  was estimated from linear least squares fitting of  $\Delta_f G_{\text{Cd}_m\text{Th}_n}^\circ$  vs.  $T$  and was compared with that from Miedema's model. Partial molar enthalpy and entropy of Th and Cd were estimated at 723 K and compared. The chapter concludes with discussion on the stability of these intermediates.

#### 7.1 Electromotive force measurements of Cd-Th intermetallics

Cell configuration for all emf runs for various composition of Cd-Th alloys have been described in Chapter 2. Reproducibility of emf at each temperature was checked by temperature cycling in both heating and cooling modes. Time taken for stabilization of emf in all the cell configuration depended on whether the two-phase alloys was solid or liquid. On an average initial stabilization of emf at low temperature was about 10h and subsequent attainment of equilibrium at higher temperature took about 2-3 h. This procedure was repeated at each temperature in heating and cooling cycles.

Overall cell reaction of cells I-IV are given by,



Corresponding emf at cells I-IV measured in the temperature range of 673-799 K are tabulated in Table 7.1 and graphically shown in Figure 7.1. Linear least squares fitting of

temperature dependence of emf ( $E_I$ ,  $E_{II}$ ,  $E_{III}$  and  $E_{IV}$ ) of Cells I-IV are given by Equations 7.1-7.4, respectively .

$$E_I \text{ (mV)} = (423.9 \pm 8.1) - (0.283 \pm 0.011)T \text{ (K)} \quad (7.1)$$

$$E_{II} \text{ (mV)} = (570.6 \pm 3.9) - (0.495 \pm 0.005)T \text{ (K)} \quad (7.2)$$

$$E_{III} \text{ (mV)} = (545.1 \pm 3.7) - (0.491 \pm 0.005)T \text{ (K)} \quad (7.3)$$

$$E_{IV} \text{ (mV)} = (270.3 \pm 1.9) - (0.138 \pm 0.003)T \text{ (K)} \quad (7.4)$$

Table 7.1 Electromotive force data of cells I, II, III and IV, superscription *h* and *c* refer to measurements in heating and cooling cycles, respectively.

Cell I		Cell II		Cell III		Cell IV	
<i>T</i> /K	emf (mV)						
673	236.51 <sup><i>h</i></sup>	682	231.26 <sup><i>h</i></sup>	673	214.11 <sup><i>h</i></sup>	684	176.09 <sup><i>c</i></sup>
673	236.91 <sup><i>c</i></sup>	684	231.67 <sup><i>c</i></sup>	682	208.92 <sup><i>c</i></sup>	686	175.18 <sup><i>h</i></sup>
698	226.37 <sup><i>h</i></sup>	697	226.71 <sup><i>c</i></sup>	688	206.55 <sup><i>h</i></sup>	698	173.99 <sup><i>h</i></sup>
698	227.41 <sup><i>c</i></sup>	698	225.28 <sup><i>h</i></sup>	693	204.42 <sup><i>c</i></sup>	702	173.35 <sup><i>c</i></sup>
703	223.16 <sup><i>h</i></sup>	703	222.35 <sup><i>h</i></sup>	698	201.84 <sup><i>h</i></sup>	709	172.65 <sup><i>h</i></sup>
703	223.94 <sup><i>c</i></sup>	713	218.44 <sup><i>h</i></sup>	709	196.67 <sup><i>h</i></sup>	712	171.38 <sup><i>c</i></sup>
713	221.68 <sup><i>h</i></sup>	723	211.49 <sup><i>h</i></sup>	718	192.84 <sup><i>h</i></sup>	713	172.26 <sup><i>h</i></sup>
713	221.74 <sup><i>c</i></sup>	727	210.77 <sup><i>c</i></sup>	722	192.26 <sup><i>c</i></sup>	723	171.02 <sup><i>h</i></sup>
723	218.32 <sup><i>h</i></sup>	733	206.44 <sup><i>h</i></sup>	723	190.14 <sup><i>h</i></sup>	723	170.44 <sup><i>c</i></sup>
723	218.25 <sup><i>c</i></sup>	744	202.13 <sup><i>h</i></sup>	732	186.96 <sup><i>c</i></sup>	733	169.21 <sup><i>h</i></sup>
748	211.91 <sup><i>h</i></sup>	748	200.54 <sup><i>c</i></sup>	734	185.15 <sup><i>h</i></sup>	734	168.85 <sup><i>c</i></sup>
748	212.12 <sup><i>c</i></sup>	754	196.58 <sup><i>h</i></sup>	744	180.21 <sup><i>h</i></sup>	748	166.96 <sup><i>c</i></sup>
763	207.76 <sup><i>h</i></sup>	763	192.59 <sup><i>h</i></sup>	748	178.63 <sup><i>c</i></sup>	754	166.21 <sup><i>h</i></sup>
763	209.97 <sup><i>c</i></sup>	773	187.47 <sup><i>c</i></sup>	754	175.63 <sup><i>h</i></sup>	763	165.96 <sup><i>c</i></sup>
773	205.49 <sup><i>h</i></sup>	784	183.26 <sup><i>h</i></sup>	763	170.96 <sup><i>h</i></sup>	773	164.44 <sup><i>c</i></sup>
773	205.85 <sup><i>c</i></sup>	788	180.65 <sup><i>c</i></sup>	763	170.19 <sup><i>c</i></sup>	764	165.33 <sup><i>h</i></sup>
		799	173.87 <sup><i>h</i></sup>	773	164.87 <sup><i>c</i></sup>	776	163.57 <sup><i>h</i></sup>
				789	156.54 <sup><i>c</i></sup>	789	160.53 <sup><i>c</i></sup>
				790	157.23 <sup><i>h</i></sup>	790	161.49 <sup><i>h</i></sup>
				799	152.15 <sup><i>h</i></sup>	800	159.64 <sup><i>h</i></sup>

*h*: Heating,  
*c*: Cooling

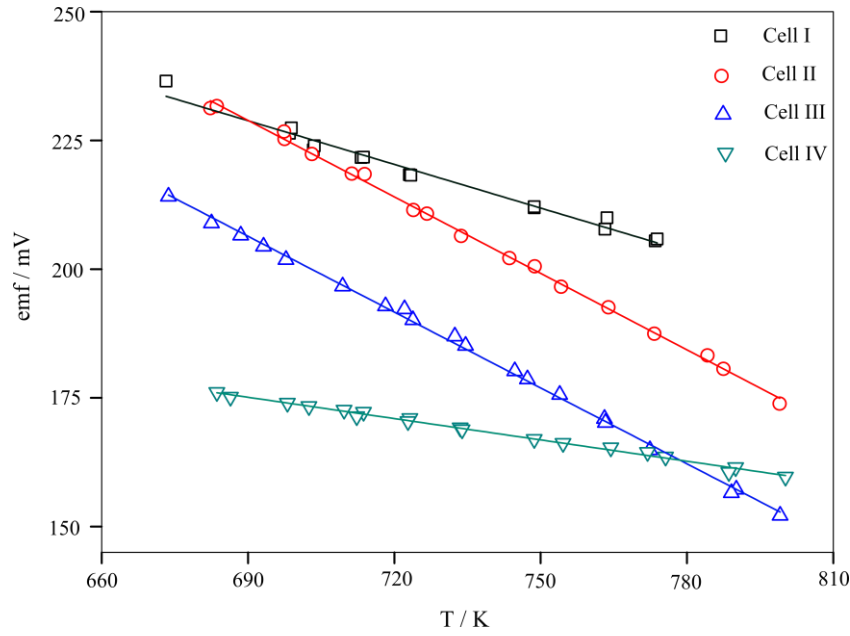


Figure 7.1 emf data for cells I-IV, respective linear least square fits are also shown.

## 7.2 Estimation of $\Delta_f G_{\text{Cd}_m\text{Th}_n}^\circ$ of Cd-Th intermetallics

$\Delta_f G_{\text{Cd}_1\text{Th}}^\circ$  using  $\alpha$ -thorium and liquid cadmium as reference states was calculated using Equation 2.29 (discussed in Chapter 2).  $\Delta_f G_{\text{Cd}_m\text{Th}_n}^\circ$  of  $\text{Cd}_5\text{Th}$ ,  $\text{Cd}_{23}\text{Th}_6$  and  $\text{Cd}_3\text{Th}$  intermetallic compounds were calculated using Equations 2.30, 2.31 and 2.32, respectively (discussed in Chapter 2). Temperature dependence of estimated  $\Delta_f G_{\text{Cd}_m\text{Th}_n}^\circ$  of four Cd-Th intermetallics are shown in Figure 7.2 and linear least squares fitting are given by following expressions:

$$\Delta_f G_{\text{Cd}_1\text{Th}}^\circ / \text{J mol-atom}^{-1} = (-13885.35 \pm 269.87) + (9.44 \pm 0.37)T(\text{K}) \quad (7.5)$$

$$\Delta_f G_{\text{Cd}_5\text{Th}}^\circ / \text{J mol-atom}^{-1} = (-32638.69 \pm 145.98) + (25.94 \pm 0.19)T(\text{K}) \quad (7.6)$$

$$\Delta_f G_{\text{Cd}_{23}\text{Th}_6}^\circ / \text{J mol-atom}^{-1} = (-41219.89 \pm 68.27) + (33.83 \pm 0.09)T(\text{K}) \quad (7.7)$$

$$\Delta_f G_{\text{Cd}_3\text{Th}}^\circ / \text{J mol-atom}^{-1} = (-44636.91 \pm 44.92) + (34.87 \pm 0.06)T(\text{K}) \quad (7.8)$$

In Figure 7.3 variation of  $\Delta_f G_{\text{Cd}_m\text{Th}_n}^\circ$  with Th composition (atom fraction of Th) in Cd-Th intermetallics is shown and compared with  $\Delta_f G^\circ$  of intermetallics of Fe-Th, Co-Th, Ni-Fe,

Cu-Th and Th-Zn systems. Variation of  $\Delta_f G^\circ$  with composition was observed to be in similar pattern for all systems.

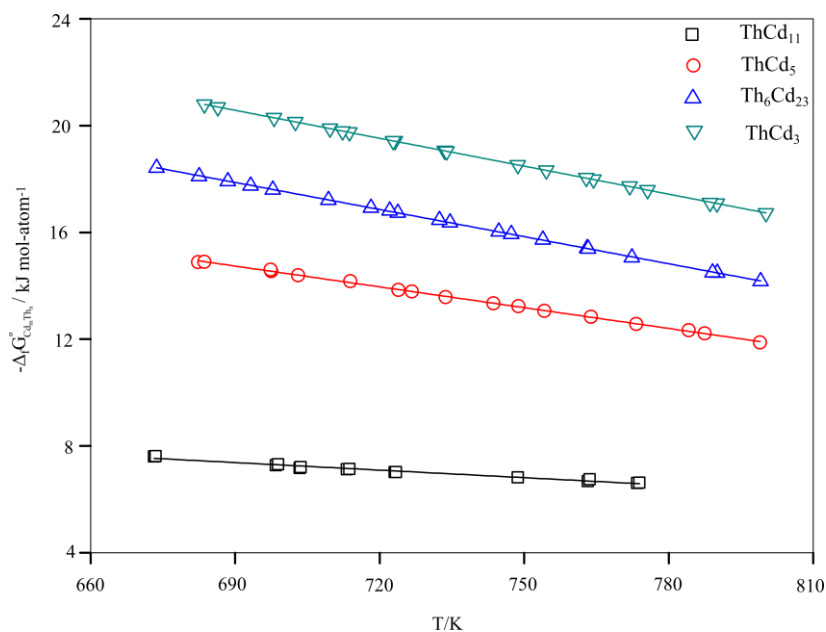


Figure 7.2 Temperature dependence of  $\Delta_f G^\circ_{\text{Cd}_m\text{Th}_n}$  of Cd-Th intermetallics.

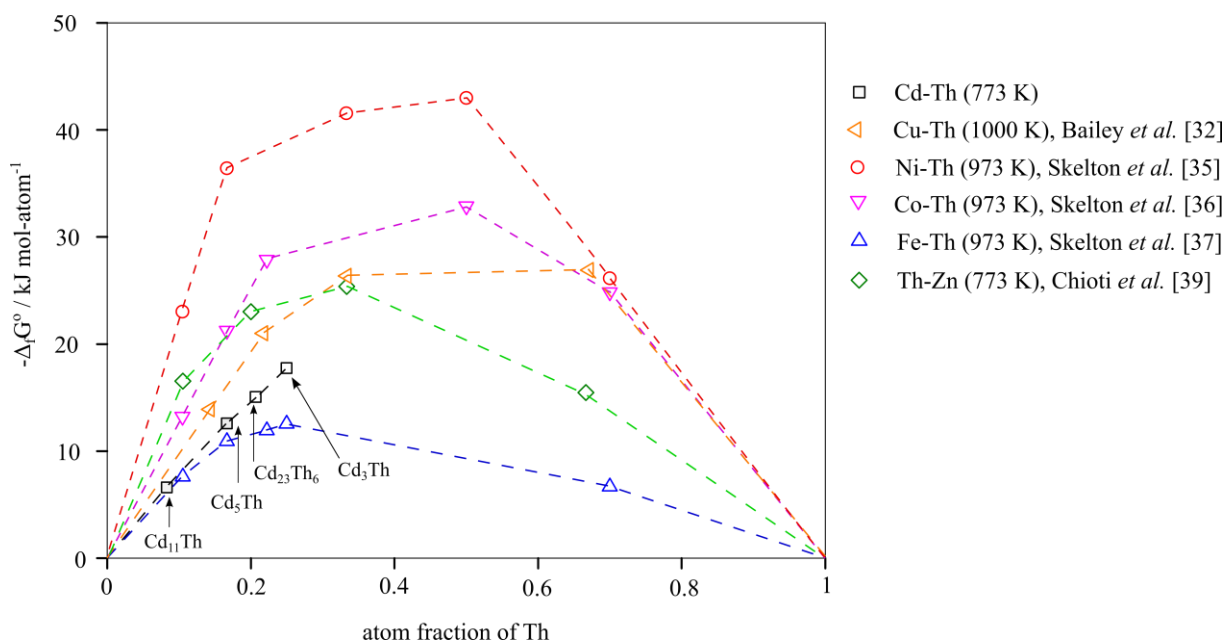


Figure 7.3 Comparison of  $\Delta_f G^\circ$  as a function of Th composition for intermetallics of Cd-Th, Fe-Th, Co-Th, Ni-Th, Cu-Th and Zn-Th systems [32, 35-37, 39].

$\Delta_f H_{\text{Cd}_m\text{Th}_n}^\circ$  and  $\Delta_f S_{\text{Cd}_m\text{Th}_n}^\circ$  of Cd-Th intermetallics were estimated from intercept and slope of the linear least squares fittings of  $\Delta_f G_{\text{Cd}_m\text{Th}_n}^\circ$  vs.  $T$ , respectively and tabulated in Table 7.2. Percentage of volume contractions ( $\Delta V \%$ ) which were computed from the lattice parameter data of Palenzona [52] for Cd-Th intermetallics are given in Table 7.2.

Table 7.2 Thermodynamic functions for the formation of Cd-Th intermetallics at 773 K.

Intermetallics	$\Delta_f G_{\text{Cd}_m\text{Th}_n}^\circ$ (kJ mol-atom <sup>-1</sup> )	$\Delta_f H_{\text{Cd}_m\text{Th}_n}^\circ$ (kJ mol-atom <sup>-1</sup> )	$\Delta_f S_{\text{Cd}_m\text{Th}_n}^\circ$ (J mol-atom <sup>-1</sup> K <sup>-1</sup> )	$\Delta V \%$
Cd <sub>11</sub> Th	-6.61±0.55	-13.88 ± 0.27	-9.43 ± 0.37	-1.68
Cd <sub>5</sub> Th	-12.57±0.29	-32.64 ± 0.15	-25.94 ± 0.19	-13.72
Cd <sub>23</sub> Th <sub>6</sub>	-15.06±0.14	-41.22 ± 0.07	-33.83 ± 0.09	1.85
Cd <sub>3</sub> Th	-17.73±0.09	-44.64 ± 0.45	-34.87 ± 0.06	0.24

$\Delta \bar{H}_{\text{Th}}$  and  $\Delta \bar{S}_{\text{Th}}$  of Th in Cd-Th intermetallics were calculated in the thesis. From linear fits of the data presented in Figure 7.1,  $\Delta \bar{S}_{\text{Th}}$  was calculated from the thermodynamic relation given by Equation 7.9 [120].

$$\Delta \bar{S}_{\text{Th}} = - \left( \frac{\partial \Delta \bar{G}_{\text{Th}}}{\partial T} \right)_p = zF \left( \frac{\partial E}{\partial T} \right)_p \quad (7.9)$$

$\Delta \bar{H}_{\text{Th}}$  was calculated from the Gibbs–Helmholtz relation given by Equation 7.10 [120].

$$\Delta \bar{H}_{\text{Th}} = -T^2 \left( \frac{\partial \left( \frac{\Delta \bar{G}_{\text{Th}}}{T} \right)}{\partial T} \right)_p = zFT^2 \left( \frac{\partial (E/T)}{\partial T} \right)_p \quad (7.10)$$

Partial thermodynamic quantities for Cd-Th intermetallics at 723 K which is near the mean of temperature range of measurement are summarized in Table 7.3. The activity of thorium in cadmium in Cd-Th two phase alloys was calculated from the emf data at each composition

according to the relationship given in Equation 2.21 (discussed in Chapter 2). Activity values are given in Table 7.3.

Table 7.3 Partial molar quantities for Cd-Th intermetallics relative to  $\alpha$ -Th (fcc) and liquid cadmium (hcp) at 723 K.

Two phase region	$\Delta\bar{H}_{\text{Th}}$ (J mol <sup>-1</sup> )	$\Delta\bar{S}_{\text{Th}}$ (J mol <sup>-1</sup> K <sup>-1</sup> )	$\Delta\bar{H}_{\text{Cd}}$ (J mol <sup>-1</sup> )	$\Delta\bar{S}_{\text{Cd}}$ (J mol <sup>-1</sup> K <sup>-1</sup> )	$a_{\text{Th}} \times 10^6$
Cd + Cd <sub>11</sub> Th	-161797.11	-109.105	-402.30	-0.34	1.02
Cd <sub>11</sub> Th + Cd <sub>5</sub> Th	-209811.71	-191.15	2335.61	5.92	6.70
Cd <sub>5</sub> Th + Cd <sub>23</sub> Th <sub>6</sub>	-203154.22	-189.47	812.61	5.37	16.5
Cd <sub>23</sub> Th <sub>6</sub> + Cd <sub>3</sub> Th	-100467.53	-53.25	-19523.12	-21.55	33.3

### 7.3 Comparison of $\Delta_f H_{\text{Cd}_m\text{Th}_n}^\circ$ data with estimation using Miedema's model

$\Delta_f H_{\text{Cd}_m\text{Th}_n}^\circ$  of Cd-Th intermetallics was calculated using Miedema's Model which is a semi-empirical approach based on electronegativity ( $\phi^*$ ), electron density at the boundary of the Wigner-Seitz atomic cell ( $n_{\text{ws}}$ ) of the alloying elements [121-124]. According to the rule for the metallurgical behaviour of transition metals in terms of the parameters  $\phi^*$  and  $n_{\text{ws}}$ , if  $\Delta\phi^* \geq 0.48\Delta n_{\text{ws}}$ , the two metals form intermetallic compound readily. For Cd-Th system  $\Delta\phi^*/\Delta n_{\text{ws}} \geq 0.48$ , so Miedema's Model is suitable for this system. Experimental  $\Delta_f H^\circ$  values were compared with theoretically calculated values by Miedema's Model. Good agreement was observed between experimental and Miedema's estimation.  $\Delta_f H_{\text{Cd}_m\text{Th}_n}^\circ$  values of Cd-Th intermetallics have also been compared with that of Fe-Th, Co-Th, Ni-Th, Cu-Th and Th-Zn systems reported by Bailey *et al.* [32], Skelton *et al.* [35-37] and Chiotti *et al.* [125]. Variation of enthalpy of formation of Cd-Th intermetallics with Th composition follows the same trend as observed in Fe-Th, Co-Th, Ni-Th, Cu-Th and Th-Zn systems, which is shown in Figure 7.4.

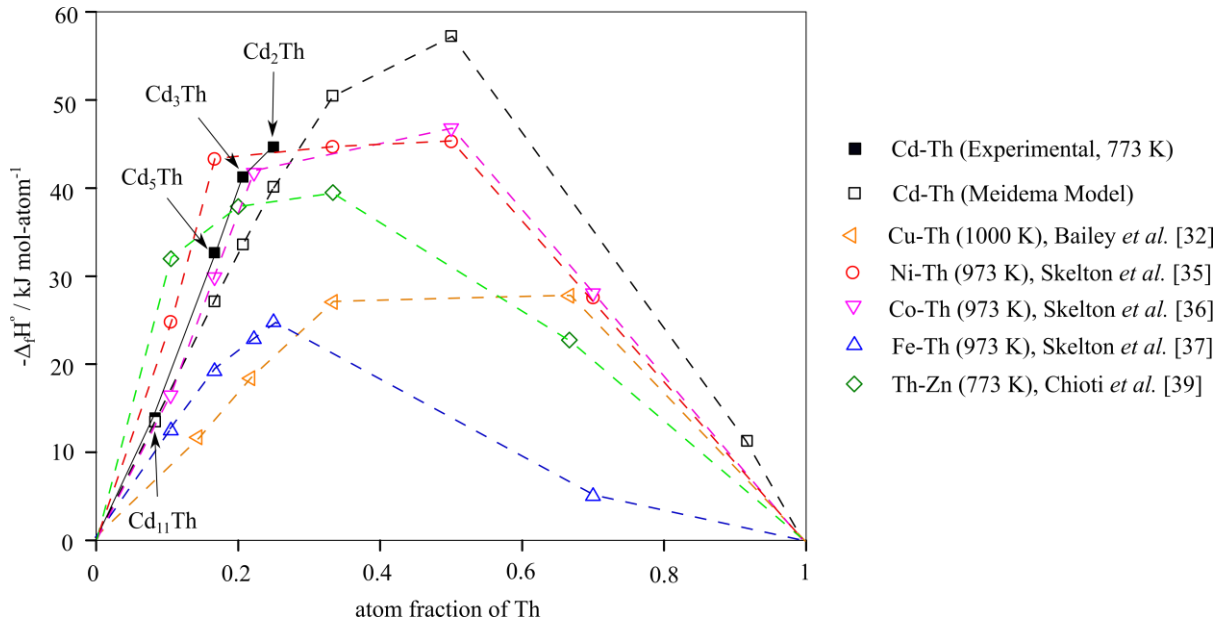


Figure 7.4 Comparison of experimental values of  $\Delta_f H^\circ_{\text{Cd}_m\text{Th}_n}$  with that of Miedema estimation and with experimental values of Cu-Th system [32], Ni-Th, Co-Th, Fe-Th systems, reported by Skelton et al. [35-37] and Th-Zn system [39].

## 7.4 Conclusions

This study provides thermodynamic functions of Cd-Th intermetallics at various temperatures. Following conclusions can be drawn based on experimental observations:

1. Estimated  $\Delta_f G^\circ_{\text{Cd}_m\text{Th}_n}$  of Cd-Th intermetallics was found to be in increasing order from cadmium rich side ( $\text{Cd}_{11}\text{Th}$ ) to thorium rich side ( $\text{Cd}_3\text{Th}$ ) which is a clear indicative of increasing stability when shifting from Cd rich side to Th rich side. Due to lack of experimental data of  $\Delta_f G^\circ_{\text{Cd}_2\text{Th}}$  and  $\Delta_f G^\circ_{\text{CdTh}}$  it was difficult to conclude about the intermetallic with maximum stability in Cd-Th system.
2. Small negative values of standard entropy of formation of Cd-Th intermetallics infer an absence of significant contribution of configurational entropy to the entropy of formation. Therefore it can be inferred that entropy of formation of Cd-Th intermetallics arise mainly from the difference between vibrational entropy of the intermetallics and vibrational entropy of Th and Cd metals.

3. Negative value of entropy of formation implies more ordered structure of the Cd-Th intermetallics compare to the constituent thorium, cadmium elements. An increasing order of negative values of entropy from  $\text{Cd}_{11}\text{Th}$  to  $\text{Cd}_3\text{Th}$  infers the most ordered structure of  $\text{Cd}_3\text{Th}$  and least ordered structure of  $\text{Cd}_{11}\text{Th}$ .
4. Variation of standard enthalpy of formation of Cd-Th intermetallics were found to be in similar trend with that of Th-Ni, Th-Fe and Th-Co systems.

## Chapter 8

### Conclusions and future outlook

#### 8.1 Conclusions

The present thesis described in Chapters 2-7 was devoted to five major investigations in LiCl-KCl eutectic melt:

- 1) Redox behaviour of  $\text{Th}^{4+}|\text{Th}$  couple in LiCl-KCl eutectic melts using various electrochemical transient techniques.
- 2) Determination of  $i_0$  of thorium under cathodic and anodic polarization conditions.
- 3) Elucidation of mechanism of cathodic deposition and anodic dissolution of thorium using electrochemical impedance spectroscopy.
- 4) Determination of  $\Delta_f G_{\text{ThCl}_4}^\circ$  of  $\text{ThCl}_4$  in LiCl-KCl eutectic melt using electromotive force measurements, comparison with literature data and making suitable recommendations.
- 5) Determination of  $\Delta_f G_{\text{Cd}_m\text{Th}_n}^\circ$  of Cd-Th intermetallics using electromotive force measurements

In 1), different electrochemical transient techniques were employed to study the reduction mechanism of  $\text{Th}^{4+}|\text{Th}$  couple in LiCl-KCl eutectic melt, and it was extended to estimate  $E_{\text{Th}^{4+}|\text{Th}}^{\circ*}$  of  $\text{Th}^{4+}|\text{Th}$  couple. In 2),  $i_0$  of thorium was determined at inert tungsten (cathodic), liquid cadmium (cathodic) and thorium (anodic) electrodes in the temperature range 698-798 K, and its temperature and composition dependence was studied. In 3), studies on  $\text{Th}^{4+}|\text{Th}$  couple already carried out in 1) was extended to investigations using electrochemical impedance spectroscopy that included validation of complex impedance data by K-K transforms and equivalent circuit fitting of data. In this work, theoretical equilibrium potential

of  $\text{Th}^{4+}|\text{Th}$  couple was also determined and compared with anodic dissolution data. This was further extended to 4) electromotive force measurements on  $\text{Th}^{4+}|\text{Th}$  couple in the eutectic melt to determine  $E_{\text{Th}^{4+}|\text{Th}}^\circ$ ,  $\Delta_f G_{\text{ThCl}_4}^\circ$  and  $\gamma_{\text{ThCl}_4}$  of  $\text{ThCl}_4$  in LiCl-KCl eutectic melt. Recommendations based on statistical analysis of data were also made. Finally, in 5), electromotive force measurements for determining  $\Delta_f G_{\text{Cd}_m\text{Th}_n}^\circ$  of Cd-Th intermetallics were carried out.

## 8.2 Challenges during experimentation

Several challenges were encountered during the course of measurements. They are briefly described below,

### i. Preparation of moisture and hydroxide free LiCl-KCl eutectic melt:

Presence of moisture and hydroxide (most probably LiOH formed due to high temperature hydrolysis of LiCl) in the eutectic melt either during cyclic voltammetric or emf measurements lead to distortions and observation of non-reproducible peaks of redox couple under study. Preparation of melts before actual experiments with  $\text{ThCl}_4$  was tested for its purity by running a cyclic voltammograms and estimating the residual current density in the potential range 0 to -1.6 V.

One of the major challenges in the present work was preparation of  $\text{ThCl}_4$  in chlorinated LiCl-KCl eutectic salt.  $\text{ThCl}_4$  was prepared by equilibration of Th metal with  $\text{CdCl}_2$  in LiCl-KCl eutectic inside argon atmosphere glove box. Purity level of glove box was maintained as low as possible during equilibration (oxygen impurity < 10 ppm, moisture < 10 ppm) to avoid oxidation of thorium metal and formation of thorium oxychlorides. In some of the experiments appearance of additional peaks were observed in cyclic voltammograms of LiCl-KCl- $\text{ThCl}_4$  recorded at inert tungsten electrode and shown in Figure 8.1. In Figure 8.1 A|A' couple was identified as  $\text{Th}^{4+}|\text{Th}$  (characterized in Chapter 3) and D|D' was identified as

$\text{Cd}^{2+}|\text{Cd}$  due to residual  $\text{Cd}^{2+}$  in the electrolyte, but B|B' couple and oxidation peak C could not be identified. Appearance of additional peaks may be due to moisture ingress in the electrolyte during preparation of  $\text{LiCl-KCl-ThCl}_4$  electrolyte or during measurements. Few lots of  $\text{LiCl-KCl-ThCl}_4$  electrolyte prepared earlier were not of very high purity and presence of moisture of possibly hydroxides was detected. Generation of reproducible electrochemical and thermodynamic data of thorium was very challenging due to vaporization of  $\text{ThCl}_4$  at 773 K. Breaking of alumina crucible containing  $\text{LiCl-KCl-ThCl}_4$  electrolyte, liq. Cd basket,  $\text{Ag}^+|\text{Ag}$  reference electrode while assembling electrochemical cell before measurements or during the course of measurements in some of the experiments were some the difficulties faced during the course of this study.

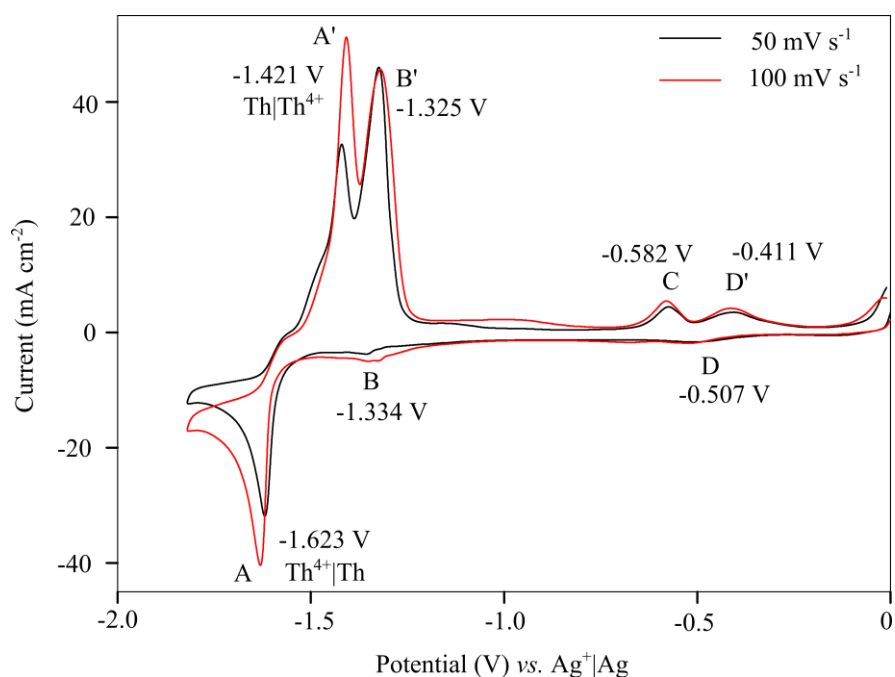


Figure 8.1 Cyclic voltammogram of  $\text{LiCl-KCl-ThCl}_4$  at inert tungsten electrode,  $T = 773 \text{ K}$ ,  $A = 0.25 \text{ cm}^2$ .

ii. Preparation, characterization and emf measurement on Cd-Th alloys:

Few difficulties were encountered during preparation, characterization and emf measurements on Cd-Th alloys due to oxidation of thorium, vaporization of cadmium during

preparation of Cd-Th alloys. During initial stages, few Cd-Th alloys were found oxidized during the equilibration of thorium and cadmium at 773 K. Emf measurements on CdTh<sub>3</sub>+ThCd<sub>2</sub> two-phase alloy was not successful due to non-reproducible emf tabulated in Table 8.1.

Table 8.1 Electromotive force data of the cell Th|Th<sup>4+</sup>||LiCl-KCl-ThCl<sub>4</sub>||⟨Cd<sub>3</sub>Th⟩<sub>s</sub>+⟨Cd<sub>2</sub>Th⟩<sub>s</sub>

<i>T</i> / K	emf (mV)		
	Run 1	Run 2	Run 3
673	-	-	305.22
683	175.57	145.35	286.41
698	161.31	133.42	-
703	-	-	261.41
718	148.44	157.11	249.74
723	-	-	232.79
733	159.29	161.53	232.92
753	179.39	175.58	-
773	203.60	174.61	-
793	187.36	179.25	-

### 8.3 Impact of present work

In this thesis work, a better understanding of electrochemistry of Th<sup>4+</sup> in LiCl-KCl was attempted with a combination of equilibrium potential and transient measurements. The present work has provided recommendations on  $E_{\text{Th}^{4+}|\text{Th}}^{\circ*}$  of ThCl<sub>4</sub> in LiCl-KCl eutectic melts (Chapter 3 and 6) and  $\gamma_{\text{ThCl}_4}$  of ThCl<sub>4</sub> (Chapter 6). These recommendations can be used by future researchers to benchmark their experimental data sets. In this work, thermodynamic data on Cd-Th intermetallics have also been generated. These data are not currently available in literature and can help in thermodynamic modelling of Cd-Th binary system using CALPHAD methodology.

## 8.4 Future outlook

The following studies can be taken up in future to further understand the redox and thermodynamic behaviour of  $\text{Th}^{4+}$  in LiCl-KCl eutectic melt

- 1) Electrochemical studies of thorium at other inert and reactive electrodes such as Bi can be carried out to generate basic electrochemical and thermodynamic data base on thermodynamic properties of thorium with liquid electrodes.
- 2) Estimation of exchange current density of  $\text{Th}^{4+}|\text{Th}$  couple can be estimated at higher concentrations of  $\text{ThCl}_4$  in molten LiCl-KCl eutectic to investigate its composition dependence.
- 3) Estimation of activity coefficient of  $\text{ThCl}_4$  in LiCl-KCl eutectic at higher concentrations of  $\text{Th}^{4+}$ .
- 4) Estimation of enthalpy of mixing of  $\text{ThCl}_4$  in LiCl-KCl melts using calorimetric methods.
- 5) Emf measurements on  $\text{CdTh}_2$  and  $\text{CdTh}$  intermetallics after addressing the problems as described above.

## List of errata in journal publications

“Electrochemical studies on the reduction behaviour of Th<sup>4+</sup> in molten LiCl-KCl eutectic”, Gurudas Pakhui, Manish Chandra, Suddhasattwa Ghosh, B. Prabhakara Reddy, K. Nagarajan, *Electrochim. Acta.* **2015**, 155, 372-382.

1. Page no. 376, Eq. 10:  $\tau$  in denominator should be replaced by  $t$ .
2. Page no. 377, Eq. 12 and 13: Ag|AgCl should be replaced by Ag<sup>+</sup>|Ag.
3. Page no. 379, Eq. 20:  $E_h$  should be replaced by  $E_{1/2}$  and  $m(t)$  in the denominator should be replaced by  $m_c(\infty)/2$ .

4. Page no. 379: In expression of  $\ln \left\{ \frac{m_c(\infty) - m(t) \left[ 1 + \exp \left\{ \frac{RT}{nF} (E - E_{1/2}) \right\} \right]}{i(t)} \right\}$  vs.  $E(t)$ ,  $RT/nF$  should

be replaced by  $nF/RT$ .

5. Page no. 380, Eq. 21:  $C_{Th^{4+}}^{1-\alpha}$  should be replaced by  $C_{Th^{4+}}$  and  $\alpha^2$  term should be added in denominator.

“Th<sup>4+</sup>|Th couple in LiCl-KCl eutectic: Anodic polarization of thorium and electrochemical impedance spectroscopy study at tungsten, cadmium and thorium electrodes”, Gurudas Pakhui, Suddhasattwa Ghosh, B. Prabhakara Reddy, *Electrochim. Acta.* 2019, 295, 354-366.

1. Page 363: In the line “ $R_s$  varies within  $3\Omega$  and.....”,  $3\Omega$  should be replaced by  $3m\Omega$ .

## REFERENCES

- [1] M.V. Smirnov, L.D. Yushina, "Cathode processes occurring in the electrodeposition of thorium from fused electrolytes", *Bull. Acad. Sci. USSR, Div. Chem. Sci. (Engl. Transl.)*, **5** (1956) 1321-1328.
- [2] M.V. Smirnov, L.D. Yushina, "Cathode processes during deposition of thorium from molten electrolytes", *Izv. Akad. Nauk, SSSR, Otd. Khim. Nauk*, **11** (1956) 1285-1293.
- [3] M.V. Smirnov, L.E. Ivanovski, "The reduction of Th<sup>4+</sup> ions in chloride melts by metallic thorium", *Zh. Fiz. Khim.*, **31** (1957) 802.
- [4] M.V. Smirnov, L.D. Yushina, *Izv. Akad. Nauk, SSSR, Otd. Khim. Nauk*, **2** (1959) 251-258.
- [5] L. Martinot, "Electrochemical behaviour of tetravalent thorium in molten (Li-K)Cl eutectic", *J. Radioanal. Nucl. Chem. Lett.*, **103** (1986) 357-363.
- [6] K. Liu, L.-Y. Yuan, Y.-L. Liu, X.-L. Zhao, H. He, G.-A. Ye, Z.-F. Chai, W.-Q. Shi, "Electrochemical reactions of the Th<sup>4+</sup>|Th couple on the tungsten, aluminum and bismuth electrodes in chloride molten salt", *Electrochim. Acta.*, **130** (2014) 650-659.
- [7] L. Cassayre, J. Serp, P. Soucek, R. Malmbeck, J. Rebizant, J.P. Glatz, "Electrochemistry of thorium in LiCl-KCl eutectic melts", *Electrochim. Acta.*, **52** (2007) 7432-7437.
- [8] P. Chiotti, S.J.S. Parry, "Separation of various components from uranium by oxidation-reduction reactions in a liquid potassium chloride-lithium chloride/zinc system", *J. Less Common Met.*, **4** (1962) 315-337.
- [9] P. Chiotti, C.H. Dock, "On lower valent thorium chlorides in fused chloride salts", *J. Less Common Met.*, **41** (1975) 225-239.
- [10] C.H. Dock, "Oxidation states of thorium in fused LiCl-KCl eutectic", Ph.D. Thesis, Library, Iowa State University, Ames, Iowa, (1965).
- [11] P. Chiotti, J.E. Fuller, C.H. Dock, M.C. Jha, "The binary systems ThCl<sub>4</sub>-Th and ThCl<sub>4</sub>-ThOCl<sub>2</sub>", *J. Less Common Met.*, **31** (1973) 365-376.
- [12] J.E. Fuller, "The thorium-thorium tetra chloride system", M. S. Thesis, Library, Iowa State University, Ames, Iowa, United States, 1968.
- [13] P. Chiotti, M.C. Jha, M.J. Tschetter, "Reaction of thorium and ThCl<sub>4</sub> with UO<sub>2</sub> and (Th, U)O<sub>2</sub> in fused chloride salts", *J. Less Common Met.*, **42** (1975) 141-161.
- [14] D. Inman, G.J. Hills, L. Young, J.O.M. Bockris, "Some thermodynamic aspects of molten salts: halides of uranium, zirconium, thorium, and cerium in alkali halide eutectics", *Ann. N. Y. Acad. Sci.*, **79** (1960) 803-829.
- [15] L. Yang, R.G. Hudson, C.-Y. Chien, "A study of equilibrium between metals and their polyvalent chlorides in LiCl-KCl eutectic melt", in: G. R. S. Pierre (Ed.), *Physical Chemistry of Process Metallurgy*, Vol. 8 of Volumes 7-8 of Metallurgical Society Conferences, Interscience Publishers, New York, 1961, pp. 925-943.

- [16] D. M. Gruen, R. L. McBeth, J. Kooi, W.T. Carnall, "Oxidation states of the elements and their potentials in fused-salt solutions : the actinide elements", *Ann. N. Y. Acad. Sci.*, **79** (1960) 941-949.
- [17] M.V. Smirnov, V.Y. Kudyakov, "Thorium valency in molten alkali halides in equilibrium with metallic thorium", *Electrochim. Acta.*, **28** (1983) 1339-1348.
- [18] V.Y. Kudyakov, M.V. Smirnov, N.Y. Chukreev, Y.V. Posokhin, "Formation of divalent thorium in a medium of fused potassium chloride", *At. Energ.*, **24** (1968) 551-556.
- [19] M.V. Smirnov, V.Y. Kudyakov, "Complexing in molten mixtures of thorium and alkali halides", *Electrochim. Acta.*, **28** (1983) 1349-1359.
- [20] M.V. Smirnov, L.D. Yushina, "Reversible potentials of metals in fused electrolytes, communication 1. reversible potentials of thorium in fused chlorides", *Bull. Acad. Sci. USSR, Div. Chem. Sci. (Engl. Transl)*, **8** (1959) 231-238.
- [21] M.V. Smirnov, V.Y. Kudyakov, Y.V. Nosokhin, Y.N. Krasnov, "Electrochemical behavior of thorium in molten sodium chloride and equimolar mixture of potassium chloride and sodium chloride", *At. Energ.*, **28** (1970) 419-420.
- [22] E. Hayek, T. Rehner, A. Frank, "Halogenide des zwei- und dreiwertigen thoriums", *Monatsh. Chem.*, **82** (1951) 575-587.
- [23] Y. Kanashin, V. Butorov, E. Novikov, I. Nichkov, S. Raspopin, *Elektrokhimiya.*, **8** (1972) 73.
- [24] R. Srinivasan, S.N. Flengas, "Electrode potentials of thorium tetrachloride in alkali chloride melts", *Can. J. Chem.*, **42** (1964) 1315-1322.
- [25] P.J. Tumidajski, S.N. Flengas, "Potential measurements of thorium tetrachloride in alkali halide solutions", *Can. J. Chem.*, **69** (1991) 462-467.
- [26] F.R. Clayton, G. Mamantov, D.L. Manning, "Electrochemical studies of uranium and thorium in molten LiF-NaF-KF at 500° C", *J. Electrochem. Soc.*, **121** (1974) 86-90.
- [27] P. Chamelot, L. Massot, L. Cassayre, P. Taxil, "Electrochemical behaviour of thorium(IV) in molten LiF-CaF<sub>2</sub> medium on inert and reactive electrodes", *Electrochim. Acta.*, **55** (2010) 4758-4764.
- [28] P. Chamelot, L. Massot, C. Hamel, C. Nourry, P. Taxil, "Feasibility of the electrochemical way in molten fluorides for separating thorium and lanthanides and extracting lanthanides from the solvent", *J. Nucl. Mater.*, **360** (2007) 64-74.
- [29] S. Delpech, S. Jaskierowicz, D. Rodrigues, "Electrochemistry of thorium fluoride in LiCl-KCl eutectic melts and methodology for speciation studies with fluorides ions", *Electrochim. Acta.*, **144** (2014) 383-390.
- [30] C.B. Alcock, "Thermodynamic data for uranium and thorium intermetallic compounds: A historical perspective", *J. Nucl. Mater.*, **167** (1989) 7-13.

- [31] C.B. Alcock, J.B. Cornish, P. Grieveson, "Knudsen effusion studies of compounds of uranium and thorium with elements of groups IIIb and IVb", IAEA, International Atomic Energy Agency (IAEA), 1966.
- [32] D.M. Bailey, J.F. Smith, "Thermodynamics of formation of Th-Cu alloys", Thermodynamics of nuclear materials: Proceedings of a symposium on the thermodynamics of nuclear materials, International Atomic Energy Agency, Vienna, 1974, pp. 355-365.
- [33] N. J. Magnani, W. H. Skelton, J.F. Smith, "Thermodynamics of formation of Th<sub>2</sub>Fe<sub>17</sub>, Th<sub>2</sub>Co<sub>17</sub>, Th<sub>2</sub>Ni<sub>17</sub>, ThCo<sub>5</sub>, ThNi<sub>5</sub>, ThCu<sub>4</sub>, and ThNi<sub>2</sub> from electromotive force measurements", Nuclear Metallurgy, P. Chiotti, Ed., U.S. Atomic Energy Commission Report, CONF-690801, 1969, pp. 727-742.
- [34] B. Prabhakara Reddy, R. Kandan, R. Babu, K. Nagarajan, P.R. Vasudeva Rao, "Thermodynamic studies on ThGa<sub>2</sub>", *J. Nucl. Mater.*, **294** (2001) 112-118.
- [35] W.H. Skelton, N.J. Magnani, J.F. Smith, "Thermodynamics of formation of Th-Ni alloys", *Metall. Mater. Trans.*, **1** (1970) 1833-1837.
- [36] W.H. Skelton, N.J. Magnani, J.F. Smith, "Thermodynamics of formation of Th-Co alloys", *Metall. Mater. Trans.*, **2** (1971) 473-476.
- [37] W.H. Skelton, N.J. Magnani, J.F. Smith, "Thermodynamics of formation of Th-Fe alloys", *Metall. Mater. Trans.*, **4** (1973) 917-920.
- [38] J.F. Smith, "Thermodynamic properties of binary thorium systems", *J. Nucl. Mater.*, **51** (1974) 136-148.
- [39] P. Chiotti, K.J. Gill, "Phase diagram and thermodynamic properties of the thorium-zinc system", *Trans. Met. Soc. AIME*, **221** (1961) 573.
- [40] V. A. Kadochnikov, A. M. Poyarkov, V. A. Lebedev, I. F. Nichkov, S. P. Raspopin, "Thermodynamic properties of thorium-antimony alloys", *Soviet Atomic Energy*, 1974, pp. 1174-1175.
- [41] A. M. Poyarkov, V. A. Lebedev, I. F. Nichkov, S. P. Raspopin, "Thermodynamic properties of thorium melts containing bismuth", *Soviet Atomic Energy*, 1974.
- [42] A.M. Poyarkov, V.A. Lebedev, I.F. Nichkov, S.P. Raspopin, "Thermodynamic properties of liquid alloys of thorium with aluminum", *Soviet Atomic Energy*, 1973, pp. 1138-1140.
- [43] N.J. Magnani, "A thermodynamic study of phase stability in the transition-metal rich phases of the thorium-iron, thorium-cobalt and thorium-nickel systems and the copper rich phases of the thorium-copper systems", Ames Laboratory, Iowa State University, Ames, Iowa, 1968.
- [44] J. Bates, M. Ader, J. Meisenhelder, W. Shinn, B.S. Tani, M. Krumpelt, "Phase relations in the thorium-cadmium system", *J. Less Common Met.*, **77** (1981) 205-213.
- [45] I. Johnson, K.D. Anderson, "Solubility of thorium in cadmium", U.S. Atomic Energy Commission Rep, 1960.

- [46] A. Brown, "MX<sub>2</sub> compounds of thorium and the polymorphism of thorium disilicide ", *Acta. Cryst.*, **14** (1961) 860-865.
- [47] G. Bruzzone, M.L. Fornasini, F. Merlo, "Rare earth intermediate phases with cadmium", *J. Less Common Met.*, **30** (1973) 361-375.
- [48] J. Dutkiewicz, "Cd-Th (Cadmium-Thorium)", *Binary Alloy Phase Diagrams, II Ed.*, T.B. Massalski, **2** (1990) 1032-1035.
- [49] J. Dutkiewicz, "The Cd-Th (Cadmium-Thorium) System ", *J. Phase Equilib.*, **14** (1993) 86-89.
- [50] M.L. Fornasini, "Crystal structure of (Ho-, Er-, Tm-, Lu-, Y-)Zn<sub>5</sub> and ThCd<sub>5</sub> intermetallic compounds", *J. Less Common Met.*, **25** (1971) 329-332.
- [51] M.L. Fornasini, A. Palenzona, P. Manfrinetti, "Crystal structure of the new thorium intermetallics ThIn and Th<sub>6</sub>Cd<sub>7</sub>", *J. Solid State Chem.*, **51** (1984) 135-140.
- [52] A. Palenzona, S. Cirafici, "The thorium-cadmium phase diagram", *J. Less Common Met.*, **77** (1981) 215-220.
- [53] Krishan Kumar, Suddhasattwa Ghosh, B. P. Reddy, K. Nagarajan, "Evaluation of exchange current density of U and Zr in molten LiCl-KCl eutectic", IGC-325, 2014.
- [54] D.L. Maricle, D.N. Hume, "A new method for preparing hydroxide-free alkali chloride melts", *J. Electrochem. Soc.*, **107** (1960) 354-356.
- [55] W.P. Davey, "Precision measurements of crystals of the alkali halides", *Phys. Rev.*, **21** (1923) 143-161.
- [56] J. T. Mason, M. C. Jha, P. Chiotti, "Crystal structures of ThCl<sub>4</sub> polymorphs", *J. Less Common Met.*, **34** (1974) 143-151.
- [57] A. Datta, N. Sivaraman, T.G. Srinivasan, P.R.V. Rao, "Liquid chromatographic behaviour of lanthanides and actinides on monolith supports", *Radiochim. Acta.*, **99** (2011) 275-283.
- [58] S. Vijayalakshmi, S. Annapoorani, R.U. Maheswari, Theme Meeting on Recent Trends in Analytical Chemistry (TRAC) Chennai, India, 2012.
- [59] K. Suriya Kumari, R. Umamaheswari, S. Annaporni, G. Pakhui, S. Ghosh, P. Venkatesh, B.P. Reddy, "Chemical analysis of impurities in cadmium with emphasis on pyroprocessing applications", IGC Report-346, 2018.
- [60] A.J. Bard, L.R. Faulkner, "Electrochemical Methods-Fundamentals and Applications", 2nd ed., John Wiley and Sons, New York, 1980.
- [61] J.R. Taylor, "An Introduction to Error Analysis : The study of uncertainties in physical measurements", 2nd ed., University Science Books, Sausalito, California, 1997.

- [62] B.A. Boukamp, "Kramers-Kronig test for Windows", <https://www.utwente.nl/en/tnw/ims/publications/downloads/KK-windows.zip>, 2018.
- [63] B. Boukamp, "A linear Kronig-Kramers transform test for immittance data validation" *J. Electrochem. Soc.*, **142** (1995) 1885-1894.
- [64] B.A. Boukamp, "Electrochemical impedance spectroscopy in solid state ionics: recent advances", *Solid State Ionics*, **169** (2004) 65-73.
- [65] E. Barsoukov, J.R. Macdonald, "Impedance Spectroscopy : Theory, Experiment, and Applications", 2nd ed., John Wiley & Sons, New York, 2005.
- [66] A.C. Gruner, W.T. Thompson, "The activity of AgCl in AgCl-LiCl-KCl melts", *Can. J. Chem.*, **53** (1975) 1084-1092.
- [67] S.N. Flengas, T.R. Ingraham, "Electromotive force series of metals in fused salts and activities of metal chlorides in 1:1 molar KCl-NaCl solutions", *J. Electrochem. Soc.*, **106** (1959) 714-721.
- [68] O. Knacke, J. Krahe, F. Muller, "Aktivitat von  $UCl_3$  in der eutektischen Schmelze LiCl-KCl", *Z. Physik Chem, Neue Folge*, **50** (1966) 91.
- [69] L. Yang, R.G. Hudson, "Equilibrium electrode potentials of some metal-chlorine galvanic cells and activities of some metal chlorides in LiCl-KCl eutectic melt", *Trans. Am. Inst. Min. Metall. Eng.*, **215** (1959) 589-601.
- [70] J.J. Roy, L.F. Grantham, D.L. Grimmett, S.P. Fusselman, C.L. Kruger, T.S. Storvick, "Thermodynamic properties of U, Np, Pu, and Am in molten LiCl-KCl eutectic and liquid cadmium", *J. Electrochem. Soc.*, **143** (1996) 2487-2492.
- [71] S.P. Fusselman, J.J. Roy, D.L. Grimmett, L.F. Grantham, C.L. Krueger, C.R. Nabelek, T.S. Storvick, "Thermodynamic properties for rare earths and americium in pyropartitioning process solvents", *J. Electrochem. Soc.*, **146** (1999) 2573-2580.
- [72] F. Lantelme, Y. Berghoute, "Electrochemical studies of  $LaCl_3$  and  $GdCl_3$  dissolved in fused LiCl-KCl", *J. Electrochem. Soc.*, **146** (1999) 4137-4144.
- [73] F. Lantelme, J.F. Equey, S. Mueller, M. Chemla, "Thermodynamic properties of iron and nickel chloride solutions in molten lithium chloride-potassium chloride", *J. Phys. Chem.*, **95** (1991) 905-908.
- [74] F. Lantelme, H. Alexopoulos, M. Chemla, O. Haas, "Thermodynamic properties of aluminum chloride solutions in the molten LiCl-KCl system", *Electrochim. Acta.*, **33** (1988) 761-767.
- [75] L. Yang, R.G. Hudson, "Some investigations of the Ag/AgCl in LiCl-KCl eutectic reference electrode", *J. Electrochem. Soc.*, **106** (1959) 986-990.

- [76] S. Vandarkuzhali, N. Gogoi, S. Ghosh, B. Prabhakara Reddy, K. Nagarajan, "Electrochemical behaviour of  $\text{LaCl}_3$  at tungsten and aluminium cathodes in LiCl-KCl eutectic melt", *Electrochim. Acta.*, **59** (2012) 245-255.
- [77] G. Mamantov, D.L. Manning, J.M. Dale, "Reversible deposition of metals on solid electrodes by voltammetry with linearly varying potential", *J. Electroanal. Chem.*, **9** (1965) 253-259.
- [78] H. Matsuda, Y. Ayabe, "Zur Theorie der Randles-Sevcikschen Kathodenstrahl-Polarographie", *Z. Elektrochem.*, **59** (1955) 494-503.
- [79] S.A. Kuznetsov, H. Hayashi, K. Minato, M. Gaune-Escard, "Electrochemical behavior and some thermodynamic properties of  $\text{UCl}_4$  and  $\text{UCl}_3$  dissolved in a LiCl-KCl eutectic melt", *J. Electrochem. Soc.*, **152** (2005) C203-C212.
- [80] S.A. Kuznetsov, H. Hayashi, K. Minato, M. Gaune-Escard, "Electrochemical transient techniques for determination of uranium and rare-earth metal separation coefficients in molten salts", *Electrochim. Acta.*, **51** (2006) 2463-2470.
- [81] J.G. Osteryoung, R.A. Osteryoung, "Square wave voltammetry", *Anal. Chem.*, **57** (1985) 101-110.
- [82] P. Chamelot, B. Lafage, P. Taxil, "Using square-wave voltammetry to monitor molten alkaline fluoride baths for electrodeposition of niobium", *Electrochim. Acta.*, **43** (1998) 607-616.
- [83] P. Chamelot, P. Palau, L. Massot, A. Savall, P. Taxil, "Electrodeposition processes of tantalum(V) species in molten fluorides containing oxide ions", *Electrochim. Acta.*, **47** (2002) 3423-3429.
- [84] M.S. Krause, L. Ramaley, "Analytical application of square wave voltammetry", *Anal. Chem.*, **41** (1969) 1365-1369.
- [85] J. Osteryoung, J.J. O'Dea, "Electroanalytical chemistry", (A. J. Bard Ed.) Marcel Dekker, New York, 1986.
- [86] L. Ramaley, M.S. Krause, "Theory of square wave voltammetry", *Anal. Chem.*, **41** (1969) 1362-1365.
- [87] R.A. Osteryoung, A. J. Osteryoung, "Pulse voltammetric methods of analysis", *Phil. Trans. Roy. Soc. London, Ser.*, **302** (1981) 315-326.
- [88] L. Nadjo, J.M. Saveant, D. Tessier, "Convolution potential sweep voltammetry", *J. Electroanal. Chem.*, **52** (1974) 403-412.
- [89] K.B. Oldham, G.D. Zoski, "Effect of semioperators on reversible cyclic voltammograms", *Anal. Chem.*, **52** (1980) 2116-2123.
- [90] M. Goto, K.B. Oldham, "Semiintegral electroanalysis: Shapes of neopolarograms", *Anal. Chem.*, **45** (1973) 2043-2050.

- [91] M. Goto, K.B. Oldham, "Semiintegral electroanalysis: Studies on the neopolarographic plateau", *Anal. Chem.*, **46** (1974) 1522-1530.
- [92] M. Goto, K.B. Oldham, "Semiintegral electroanalysis: The shape of irreversible neopolarograms", *Anal. Chem.*, **48** (1976) 1671-1676.
- [93] M. Grenness, K.B. Oldham, "Semiintegral electroanalysis: Theory and verification", *Anal. Chem.*, **44** (1972) 1121-1129.
- [94] P. Delahay, "New Instrumental Methods in Electrochemistry", Interscience Publishers, New York, 1954.
- [95] T. Berzins, P. Delahay, "Oscillographic polarographic waves for the reversible deposition of metals on solid electrodes ", *J. Am. Chem. Soc.*, **75** (1953) 555-559.
- [96] J.E.B. Randles, "A cathode ray polarography: part 11-the current-voltage curves", *Trans. Faraday Soc.*, **44** (1948) 327-338.
- [97] A. Sevcik, "Oscillographic polarography with periodical triangular voltage", *Collect. Czech. Chem. Commun.*, **13** (1948) 349-377.
- [98] M. Mohamedi, S. Martinet, J. Bouteillon, J.C. Poignet, "Comprehensive examination of the electrochemistry of indium in the molten LiCl-KCl eutectic", *Electrochim. Acta.*, **44** (1998) 797-803.
- [99] S. Ghosh, K. Kumar, A. Venkatesh, P. Venkatesh, B.P. Reddy, "Exchange current density and diffusion layer thickness in molten LiCl-KCl eutectic: a modeling perspective for pyroprocessing of metal fuels", *Nucl. Technol.*, **195** (2016) 253-272.
- [100] S. Ghosh, S. Vandarkuzhali, N. Gogoi, P. Venkatesh, G. Seenivasan, B.P. Reddy, K. Nagarajan, "Anodic dissolution of U, Zr and U-Zr alloy and convolution voltammetry of  $Zr^{4+}|Zr^{2+}$  couple in molten LiCl-KCl eutectic", *Electrochim. Acta.*, **56** (2011) 8204-8218.
- [101] A. Venkatesh, S. Ghosh, S. Vandarkuzhali, B.P. Reddy, K. Nagarajan, P.R.V. Rao, "Modeling the anodic behavior of U, Zr and U-Zr alloy in molten LiCl-KCl eutectic", *Nucl. Technol.*, **182** (2013) 98-110.
- [102] F. Kobayashi, T. Ogawa, M. Akabori, Y. Kato, "Anodic dissolution of uranium mononitride in lithium chloride-potassium chloride eutectic melt", *J. Am. Ceram. Soc.*, **78** (1995) 2279-2281.
- [103] O. Shirai, M. Iizuka, T. Iwai, Y. Suzuki, Y. Arai, "Recovery of neptunium by electrolysis of NpN in LiCl-KCl eutectic melts", *J. Nucl. Sci. Technol.*, **37** (2000) 676-681.
- [104] O. Shirai, T. Kato, T. Iwai, Y. Arai, T. Yamashita, "Electrochemical behaviors of PuN and (U, Pu)N in LiCl-KCl eutectic melts", *J. Phys. Chem. Solid.*, **66** (2005) 456-460.
- [105] O. Shirai, K. Uozumi, T.I. Arai, "Recovery of U by electrolysis of UN in LiCl-KCl eutectic melts", *J. Nucl. Sci. Technol.*, **3** (2002) 745-748.

- [106] A. Glassner, "The thermochemical properties of the oxides, fluorides and chlorides to 2500 K", Argonne National Laboratory, Lemont, 1957, pp. 201-274.
- [107] L. Martinot, J. Bohet, G. Duyckaerts, "Thermodynamic properties of dilute solutions of ThCl<sub>4</sub> in (Li-K)Cl and (K-K)Cl eutectics", *Inorg. Nucl. Chem. Lett.*, **13** (1977) 315-319.
- [108] J. Fuger, V.B. Parker, W.N. Hubbard, F.L. Oetting, "The Chemical Thermodynamics of Actinide Elements and Compounds, Part 8", "The Actinide Halides", IAEA, Vienna, 1983.
- [109] C. Bale, E. Belisle, P. Chartrand, S. Deckerov, G. Eriksson, A. Gheribi, K. Hack, I.H. Jung, Y.B. Kang, J. Melancon, A. Pelton, S. Petersen, C. Robelin, J. Sangster, P. Spencer, M.A.V. Ende, Factsage thermochemical software and databases 2010-2016, *Calphad*, **54** (2016) 35-53.
- [110] I. Barin, O. Knacke, O. Kubaschewski, "Thermochemical properties of inorganic substances", Springer-Verlag Berlin Heidelberg, 1977.
- [111] X. Wang, W. Huang, Y. Gong, F. Jiang, H. Zheng, T. Zhu, D. Long, Q. Li, "Electrochemical behavior of Th(IV) and its electrodeposition from ThF<sub>4</sub>-LiCl-KCl melt", *Electrochim. Acta.*, **196** (2016) 286-293.
- [112] R. Cumberland, M.S. Yim, "Estimation of Uranium and Plutonium exchange current densities on solid electrodes", in: Proceedings of the International Pyroprocessing Research Conference (IPRC)The Abbey Resort on Lake Geneva in Fontana, Wisconsin, hosted by Argonne National Laboratory, Chemical Sciences and Engineering Division, 2012.
- [113] R.M. Cumberland, M.-S. Yim, "Development of a 1D transient electrorefiner model for pyroprocess simulation", *Ann. of Nucl. Energy*, **71** (2014) 52-59.
- [114] M.A. Rose, M.A. Williamson, J. Willit, "Determining the exchange current density and Tafel constant for Uranium in LiCl-KCl eutectic", *ECS Electrochem. Lett.*, **4** (2015) C5-C7.
- [115] M. Bachtler, W. Freyland, G.A. Voyiatzis, G.N. Papatheodorou, "Electrochemical and simultaneous spectroscopic study of reduction mechanism and electronic conduction during electrodeposition of tantalum in molten alkali chlorides", *Ber. Bunsenges. Phys. Chem.*, **99** (1995) 21-31.
- [116] M. Matsumiya, R. Takagi, "Electrochemical impedance spectroscopic study on Eu<sup>2+</sup> and Sr<sup>2+</sup> using liquid metal cathodes in molten chlorides", *Electrochim. Acta.*, **55** (2000) 673-681.
- [117] J.E.B. Randles, "Kinetics of rapid electrode reactions", *Discuss. Faraday Soc.*, **1** (1947) 11-19.
- [118] J.R. Macdonald, "Impedance spectroscopy: emphasizing solid materials and systems", John Wiley and Sons Inc., New York, 1980.
- [119] J. Fuger, D. Brown, "Thermodynamics of the actinide elements", *J. Chem. Soc., Dalton Trans.*, **0** (1973) 428-434.

- [120] D.R. Gaskell, "Introduction to the Thermodynamics of Materials", 4th ed., Taylor & Francis, New York, 2003.
- [121] A. Dębski, R. Dębski, W. Gasior, "New features of Entall database: Comparison of experimental and model formation enthalpies", *Arch. Metall. Mater.*, **59** (2015) 1337-1343.
- [122] A.R. Miedema, "The electronegativity parameter for transition metals: Heat of formation and charge transfer in alloys", *J. Less Common Met.*, **32** (1973) 117-136.
- [123] A.R. Miedema, F.R.d. Boer, P.F.d. Chatel, "Empirical description of the role of electronegativity in alloy formation", *J. Phys. F: Met. Phys.*, **3** (1973) 1558-1576.
- [124] A.R. Miedema, F.R. de Boer, R. Boom, "Model predictions for the enthalpy of formation of transition metal alloys", *Calphad*, **1** (1977) 341-359.
- [125] P. Chiotti, M. Koizumi, Annual summary research report in metallurgy, Ames Laboratory, Iowa State University, 1960, pp. 28-30.